College of Instrumentation & Electrical Engineering, Jilin University

Academic Practice "Six in One" Training Project

English Proceedings

2018 (First Half)

CONTENTS

Intelligent guide eyeglasses

YuanXin; Sun Xiaoxu; ZhouDan
（*College of Instrumentation & Electrical Engineering, Jilin University*）

***Abstract*-In the air medium, ultrasonic range finder sensor because of its good performance, low price, convenient use, in the field of robot positioning system, automatic vehicle navigation, vehicle safety driving assist system, city traffic management and management of expressway monitoring system, as well as river, well and warehouse and material level detection used in. Because the ultrasonic wave propagation is not susceptible to interference, energy consumption slow, medium of communication in the longer distance, which are often used for ultrasonic distance measurement, such as the location and level measurement can be achieved by ultrasound. Therefore, in-depth study of ultrasonic generation and propagation, the development of high performance ultrasonic transducer and its transceiver circuit, the ultrasonic detection technology development has very important real sense. This article introduces the design of control based on single chip ultrasonic ranging principle: control by STC89C52 timer produces a certain frequency pulse, calculated from transmitting to receiving echo time, so as to obtain the measured distance, voice broadcast，vibration and LED lights.**

***Key words*-Ultrasonic wave Voice Gyroscope Wireless video**

I. INTRODUCTION

BECAUSE the ultrasonic measurement is a non-contact detection technology, which is not affected by the influence of light and the color light of measured object , etc. This machine is cleaner and more resistant to moisture, dust, high temperature, corrosive gases and other harsh environment than other instruments with the figure of less maintenance, no pollution, high reliability, long life. So uhrasonic ranging system is mainly used in the Reverse Sensor of a car, robot automatic obstacle avoidance walking, building construction site and some industrial field in level, depth, pipe length measurement and etc.so the research of ultrasonic ranging system is of great practical significance. The research and design of this subject can improve our ability of circuit design and deepen our understanding and application of SCM.

II. SYSTEM DESIGN

This project mainly studies a kind of intelligent blind guide glasses, including glasses body and blind guide glasses control box. The guide glasses control box includes main processor, ultrasonic sensor module, remote wireless control module, correction module. Voice and vibration warning module and LED warning module. After the operation, there are two ways to guide blind, one is in simple cases or when no one online support, we need ultrasound. Remote help can be provided in complex situations where online support is available.

In a simple case, the processor module captures the information dynamically according to the ultrasonic sensor module, and sends out information to the user through the voice and vibration prompting module .In a difficult case, through real time video frequency (V.F.), traffic will be transported to terminal. The person who receive directly from the terminal will guides the blind to walk, so the function of guiding the blind is complete. This working module will help the blind to avoid obstacles as well as facilitate travel and life. At night, the LED indicator light is switched on through the photosensitive sensor, so that other passers-by can understand the user's condition and avoid them in time.

Because most blind people still have a faint light sense .In order to protect their eyes and prevent the damage of ultraviolet light, we changed it to the pattern of sunglasses.

A. remote control service

The video frequency (V.F.) taken by Web Camera in the glasses will be transmit to terminal, then the blind person is guided by the real time road condition after the terminal is received.

The working principle of the wireless camera is the new monitoring camera, which is the wireless receiver is embedded into the network camera. It uses the WIFI channel with IEEE 802.11B/G standard protocol. WIFI is a wireless network composed of AP (Access Point. AP) and wireless network adapter. AP are usually called network bridge or access point. It is regarded as a bridge between the traditional wired LAN network and wireless local area networks, so any PC equipped with a wireless card can through the AP to share the wired local area network or even the wide area network resources. Its working principle is equivalent to a built-in wireless transmitter HUB or routing, and the wireless network card is CLIENT terminal equipment responsible for receiving signals transmitted by AP terminal equipment. The AP, like the wired network switches or routers, wireless stations can connect quickly and easily to the network.

The camera selected has two methods of working. One is watching the local video .Another is remote monitor and control .When the distance of terminal and camera is closed, we choose the first model. At this time, the camera itself is WIFI. Terminal connect the WIFI provided by the camera to receive the real-time condition of transportation.

When the distance is far, the second model (remote monitor and control) is chosed. Terminal has to connect other WIFI to receive the real-time condition of transportation.

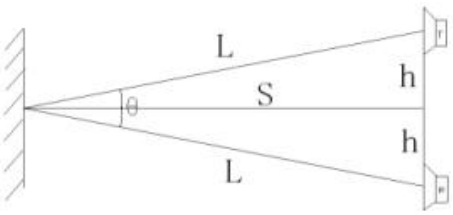

Fig. 1. Magnetization as a function of applied field.

B. microcontroller

This design is based on STC89C52 microcomputer system. Generally it should include: microcontroller, crystal oscillator circuit, reset circuit.STC89C52 microcontroller series has the advantages of small volume, light weight, simple structure, low cost and common control functions can be achieved easily. And the microcontroller can be applied in small embedded systems, so it was a wide range of applications.

C. Ultrasonic module

C1. principle of ultrasonic

There are many ways of ultrasonic distance measurement, such as phase detection, acoustic amplitude detection and transit time detection so on. Although the phase detection method has high accuracy, the detection range is limited and the acoustic amplitude detection method is susceptible to be influenced by reflected waves.

The ranking system uses the ultrasonic transit time detection method. Its principle is that: the system detect the time t of from ultrasonic emitted by transmitter sensor to the receiving sensor disseminated by the gas medium. This time is the transit time, and then find out the distance 1.We suppose the distance 1 as the measurement, and t as the differential time of flight, ultrasonic propagation speed of C. There are l=ct/2.Ultrasonic immediately stop the clock after the reflected wave is received by the receive . And then calculate the distance by the single chip.

The algorithm design of ultrasonic distance measurement is that the speed of ultrasonic transmission in the air is 340 meters per second (15 C).t2 is receiving ultrasonic time, t1 is Ultrasonic wave emission time. t2-t1 is that the absolute value of a time difference. Assumes t2-t1=0.03S, then there are 340m * 0.03S=10.2m.Because in this time of 10.2m, the distance of ultrasonic from the shooting distance to the returned back is following:

Because angle of θ/2 is small, it can be ignored. So

$$L \approx S 。 \quad (1)$$

The distance from ultrasonic waves generated to return because it encounter an obstacle as follows:

$$L=C*(t2-t1)/2 \quad (2)$$

Because ultrasonic is a kind of sound wave, the sound velocity of C is relative to air temperature, in general, every increase of 1 degrees Celsius temperature, velocity increase 0.6 meters per second.

When in use, if the temperature change is not big, it may be considered that the velocity of C is basically the same, the calculation from C to 340m/s. if the ranging accuracy is very high, it can be corrected by change hardware circuit to increase temperature in order to compensate circuit or in case of unchanged hardware circuit through the method of software of the improved algorithm.

C2. Use Component Selection

Because the precision and length of the measuring distance are not very high, it is reasonable that the precision is up to 2cm and the measuring distance is up to 5m, so the ultrasonic module can choose the HC-SR04 which is cheap and practical.

Fig .2. HC-SR04 Module physical map

D. voice model

The voice module is designed with NY3P035 chip, the chip contains a ROM. Microcontroller pulse signal sequence to the chip to lookup ROM address in order to make a sound.

The principle of the single chip microcomputer is to send a reset pulse to the RST (Rest) foot first , then send 10 pulses to the DATA foot . The chip works immediately to play the sound of the tenth section .If you need to play the fifth section of the sound , first send a reset pulse to the REST pin , and then send 5 pulses to the DATA foot . The chip works immediately to play the voice of paragraph 5 [4].

The chip patch package has simple hardware interface , low power consumption , cool and smooth sound color , extremely high cost performance [5], besides , it is more intelligent , accurate and effective in speech synthesis ,identifying text , numbers and strings , and the chip has greatly improved in voice synthesis effect and intelligent degree , and is a Chinese speech synthesis chip which is truly oriented to the application field of high - end industry[6] .

Voice prompt sound is transmitted to the blind by the headset. The headset is black flushbonading soft silica gel earphone .Voice can be clearly communicated to the blind, DB is not too high, try to reduce the damage to the long-term wear blind listening, direct contact with the ear is soft silicone, long-term wear will not bring back an uncomfortable sense. Reach the goal of humanization.

E. correct model

The MPU6050 sensor is the first 9 - axis motion processing sensor chip in the world . It is integrated with three - axis MEMS gyroscope, three - axis MEMS accelerometer , and an extensible data motion processor DMP (Digital Motion Processor) , and the output of the MPU6050 sensor is digital data[1] . It does not need A / D converter because it can transmit directly to the single - chip microcomputer for processing, thus reducing the energy consumption , error and the volume of the whole system [2].

By using the MPU6050 sensor , the change of three - axis acceleration and the three - axis angle in the glasses can be detected in real time , and the change of the characteristics is used for judging whether the glasses are right in front . If the glasses are right in front , the ultrasonic distance measuring module can work normally , otherwise , the buzzer will alarm prompt .Only when the blind put the glasses level, the buzzer will stop the alarm and the ultrasonic distance measuring module will work.

F. vibrator module

The realization of the vibration module is a vibration motor. The function of the vibration module is that when the outside world is noisy, the voice may not be heard. Vibration is used to remind blind people of obstacles. The vibration module is a miniature vibration motor with a 716 vibration hollow cup, which is a waterproof vibration motor and has a metal stainless steel shell.

The motor is not installed on the glasses .He is connected directly from the control chip and is in direct contact with the skin of the blind person , so that the motor can be placed in the ear or elsewhere , so as to achieve the effect of reminding .

When the processor calculates that the distance of the front obstacle is less than 30cm, the vibration motor will vibrate, which reminds the blind to be careful and careful.

G. LED reminding module

When it is dark, the LED lights emit yellow light, which can remind other pedestrians to take the initiative to avoid the blind. Yellow light is also more penetrating and can be seen by others when there is fog or poor visibility. More comprehensive protection of the blind, providing conditions for blind people to travel at night.

This module is implemented by using a photosensitive resistor. The LED does not glow when the light is felt, and the LED lights emit yellow light when the environment is dark.

H, ACPI

Charging is used directly to make sure the electricity , and the power supply time is long . After testing, a charging treasure with capacity of 10000mAh can be used to supply the operation of the whole system for more than 12 hours .

Ⅲ.SOFTWARE DESIGN

Software design is based on hardware design. First of all, the principle of hardware design should be clearly defined, and the categories of hardware design and software design should be distinguished. Software design should be clear about the real purpose of the design content, the design procedure should be simple and clear, reduce redundant information as far as possible, reduce the burden of CPU.

In order to facilitate the use and maintenance of the system, the program of the system adopts the modular design idea, the program is mainly composed of initialization and program control. The initialization part mainly includes the initialization of single-chip microcomputer. Sensor initialization and so on. Each module of the program is completed and then integrated together, then completed the whole program. This program is written in C51 language.

Ⅳ.TEST RESULTS

After many tests, the instrument can work normally in two models. Under remote control ,the mobile phone APP can receive the road condition information . When the glasses are in the horizontal state and the ultrasonic distance measuring module works, the voice chip can successfully prompt the distance of the front obstacle ,the accuracy is within 2 cm , the response period is within 2s , compliance with technical indicators. When the distance of the obstacle is less than 30cm, the vibration motor will vibrate, remind the blind to notice; When the environment is in a relatively dim state , the LED lamp is lit , and other pedestrians are reminded to actively avoid blind people by a dazzling yellow light. Thus the basic realization of the opening set index.

Ⅴ.SUMMARY

This design introduces an ultrasonic distance measuring system based on single chip microcomputer, and gives the design proposal of the corresponding software and hardware.

The system of smart glasses meet the required measurement accuracy, using ultrasonic ranging module STC89C52 design ,which is easy to operated, has fast response speed and low cost. Due to the use of a single 5V power supply, so mobility with voice output. In the place where requires high precision, because the ultrasonic propagation velocity in the air temperature is a little big, it is necessary to consider to transform the ultrasonic propagation velocity at different temperatures. Then through the method of temperature compensation should be corrected for the transmission speed, so that it has higher measurement accuracy, strong anti-interference ability,faster response characteristics[3].

Overall , through this design we has learned a lot, benefit greatly and also has a further understanding of the development and circuit design of the single - chip microcomputer .

Reference

[1] Zhuo Congbin. Design of falling detection and alarm system based on MPU6050 acceleration sensor. Electronic devices, 2015

[2] Qiu Yunping.MPU6050 module angle algorithm processing and application in embedded system. Journal of Jiangxi Institute of science and technology, 2014

[3] Xie Yuanyou. Design of simple light clock based on single chip microcomputer. Undergraduate thesis of Yibin University, 2014

[4] Yang long frequency. Design of DS18B20 multi point temperature measurement and speech broadcasting system. Graduation thesis of Xi'an University of Arts and Science, 2016

[5] Zhou Lin. Ultrasonic ranging speech broadcast paper. Chengdu University of Electronic Science and technology, 2010

[6] Wu Xiaolin . Ultrasonic range finder with language function. Electrical application , 2007

Intelligent Home Control System Based on Interaction between STM32 and Host Computer

Zhang Huaizhu; Ni Zhiwei; Ning Yang; Liu Wenshuai

（College of Instrumentation & Electrical Engineering，Jilin University）

***Abstract*-The theory and the algorithm of the artificial neural network are applied in the research of the technique and the composition, the gross mass fraction of element, the thickness of surface alloying layer as well as the absorption rate is built. The calculation results are in good agreement with the experimental results.**

***Keywords*-Double glow Artificial neural network Prediction model**

0 FOREWORD

THE smart home is an efficient, comfortable, safe, convenient and environment-friendly living environment that integrates the building, network communication, information appliances, automatic equipment, system integration, structure, service and management. Control system, computer network system and network communication technology in one of the home control system[1].

With the improvement of the national economy and the rapid development of science and technology, especially the rapid development and improvement of computer technology and sensor technology, intelligent modernization of family life has become possible. Computer science and technology have influenced and changed people's life from aspects of comfort, convenience and safety, subverting people's living habits and improving people's quality of life, so smart home control system came into being in such a form[2] .

The design of the hardware circuit structure is simple, divided into controller module, gprs communication module, human-computer interaction module, the relay output control module, curtain control module five circuit modules, Which controller based on the arm core, cotex-m3 technology 32-bit controller STM32F103R8T6. Human-computer interaction module uses OELD display to display data[3], independent keyboard as input device and curtain control with stepper motor module.

The structure of the dissertation is as follows:

The first part introduces the background of the design, the practical significance of designing the smart home system controlled by GPRS network communication, and clarifies the institutional arrangement of this article[4].

The second part studies the principle of gprs communication control and completes the overall scheme design of smart home system based on stm32 controller and GPRS network communication control.

The third part, complete the entire system hardware circuit design.

The fourth part, the completion of the system software system design.

The fifth part, the completion of the design of the system debugging, and analysis and solve the problems encountered in debugging.

1 SYSTEM OVERALL PROGRAM DESIGN

1.1 System Requirements Analysis

According to the task book requirements: This article is to design a smart home system based on the stm32 controller and GPRS network communication control[5]. The system technical indicators are:

1) frame count stm32 hardware system, combined with GPRS wireless network technology to achieve mobile short message control appliance switch operation

2) The system real-time collection of home environment temperature and humidity state, in the event of an exception, can notify the host SMS alarm.

3) System has a calendar clock, you can set the time to complete the timer switch appliances.

4) System automatically sampled stifled light intensity, automatic control of the window switch.

5) Human-computer interaction is good, with good user-friendly interface.

1.2 system options

1.2.1 telecommunications

The use of GPRS network to achieve wireless control. Currently with the popularity of mobile phones, mobile phones have become an indispensable part of people's lives. Have a cell phone GPRS network. According to statistics released by China Mobile Information Industry, coverage of China's GPRS network reached 98%. Therefore, GPRS wireless as a carrier of home control more conditions. And from the cost and technical difficulty of consideration, GPRS undoubtedly more advantages. Therefore, the program chose to GPRS network to achieve wireless communications[6].

1.2.2 monitor options

OLED LCD display. Taking into account the low power consumption and interactive friendly, LCD screen must be the first to be. The traditional character LCD, although it may meet the above two requirements. But compared to portability, the choice of OLED displays, will be more superior. OLED displays are generally SPI data communications.

1.2.3 temperature and humidity sensor program options

The use of temperature integrated temperature sensor, DHT11 is a temperature and humidity composite sensor with calibrated digital signal output. It uses a dedicated

digital module acquisition technology and temperature and humidity sensing technology to ensure that products with high reliability and excellent long-term stability.

1.3system design as a whole

By comparing the program to determine the design of the basic program. At the same time completed the design of the overall design.

2 SYSTEM HARDWARE CIRCUIT DESIGN

This article has completed the systematic plan comparison and the overall structure design. This chapter will complete the hardware design of the entire system. This chapter will be divided into five parts to introduce the system hardware circuit, respectively, the control unit module, human-computer interaction module, sensor module, the controller used to do the related introduction.

2.1Control Unit Module

The controller used in this design is a 32-bit controller based on the ARM core and cotex-m3 architecture technology.

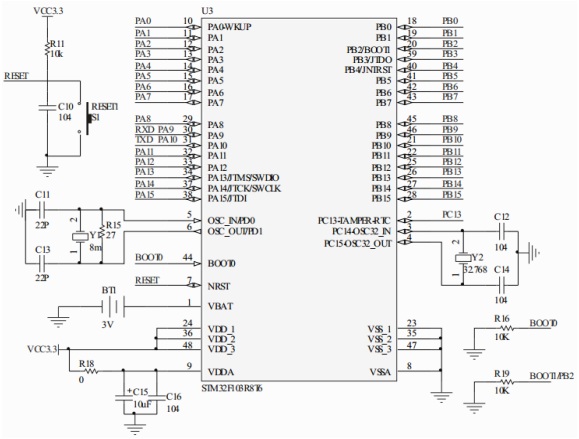

Figure 2.1 Control Unit

2.2 human-computer interaction module

Human-computer interaction module includes key setting circuit and OLED display circuit. The circuit shown in Figure 2.3

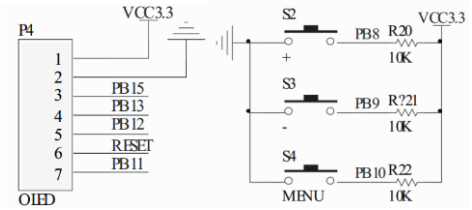

Figure 2.2 Human-computer interaction module

2.3 GPRS circuit design

GSM module, the key part of the system, is directly related to the realization of remote control functions. The module supports 900 ~ 1800 frequency band, including China Mobile and China Unicom. Compatible with TTL level, through the serial port control, can be connected directly with the microcontroller serial port. The circuit shown in Figure 2.3

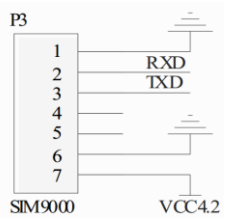

Figure 2.3 SIM900 schematic

2.4 temperature and humidity sensor circuit design

According to the DHT11 official data sheet, the sensor supply voltage range is 3.3V to 5.5V. It has a total of 4 pins. Respectively for the power supply, serial data bus, empty feet, grounding feet.

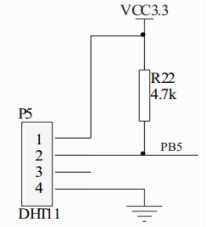

Figure 2.4 Temperature and Humidity Sensor Circuit Schematic

2.5 light intensity detection circuit design

Light intensity detection circuit shown in Figure 2.5, the photosensitive resistor and 10kΩ resistor in series, the voltage divider by the resistor R23 and capacitor C9 RC low-pass filter circuit, directly to the microcontroller AD acquisition channel PA0 for AD conversion

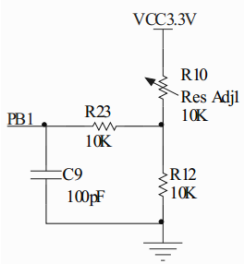

Figure 2.5 Schematic diagram of light intensity detection circuit

2.6 curtain control circuit design

Stepper motor is the electrical pulse signal into angular displacement or linear displacement of the open-loop control components. Under non-overload conditions, the motor speed and stop position depend only on the frequency and pulse number of the pulse signal, without being affected by load changes. That is, a pulse signal is applied to the motor and the motor rotates by a step angle[7].

The schematic diagram shown in Figure 2.6.

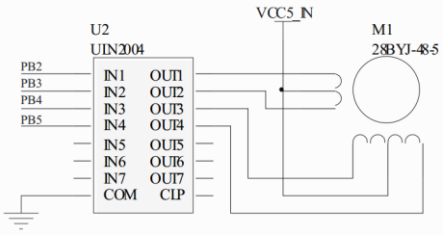

Figure 2.6 stepper motor drive schematic

3SOFTWARE DESIGN

3.1program structure analysis

The design of the software needs to be completed tasks are divided into:

1) Read text messages from SIM900 GPRS module, and judge, so as to switch on and off home appliances.
2) collect light intensity, automatically adjust the curtain switch to achieve automatic control of home lighting.
3)Collecting the temperature and humidity values, to determine the occurrence of an exception, trigger short message alarm to notify the host.
4) read the master calendar clock, switch the time for household appliances management.
5) to complete the key scan, the current operation of the message or data displayed on the LCD screen.

3.2 main program design

In order to meet the real-time temperature and humidity acquisition, the program uses a cyclic scan of the DHT11 sensor data read. The main program needs to complete the function as the first to complete the system initialization[8], so the whole program framework needs to be completed in the main program setup task is to initialize the various parts of the system, human-computer interaction.

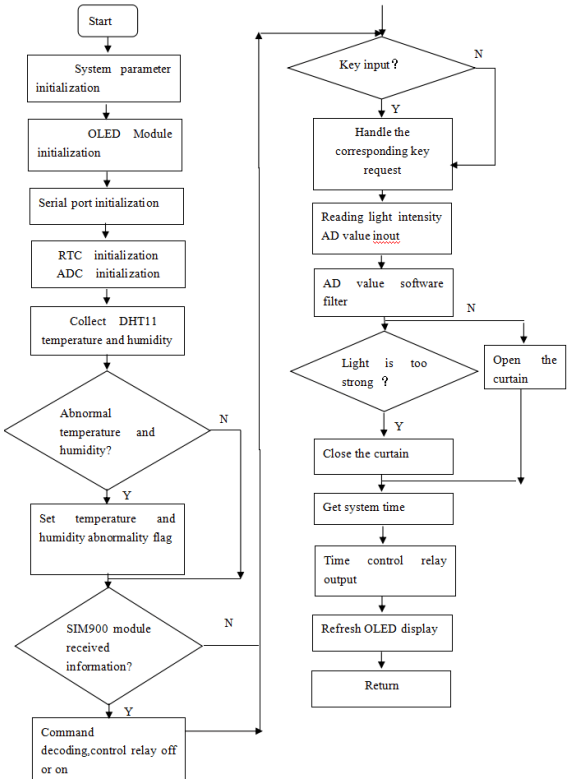

Figure 3.1 Main program flow chart

3.3SIM900 communication program design

As SIM900 module supports AT serial command set, access to SIM900, in fact, is on the microcontroller serial port access. Therefore, through the AT command, you can control the SMS SIM900 to send and read messages. The following is an introduction to AT commands involving sending and reading text messages:

AT+CMGF=?
AT+CMGS
AT+CMGR
AT+CMGD

The design SIM900 serial communication protocol for the 9600 baud rate, 8 data bits, no parity, a stop bit.

After the system is power on SIM900 first initialize, set the mode of short message, and receive short message reporting mode mode.

4.SYSTEM DEBUGGING AND RESULT ANALYSIS

System debugging process, found some problems, and finally through the process of repeated changes and debugging, constantly debug the parameters of the communication protocol and feedback control function, find the most reasonable experimental method, and find out the most suitable algorithm for this design ,and ultimately all the problems can be solved[9]. Through the actual test, this design of the smart home system based on stm32 controller and GPRS network communication control to receive short messages, and respond to effective commands to control the relay to achieve the switch control of home appliances, and can be based on light Intensity, the curtains to achieve automatic switch, and accurately respond to the time, set the time to open the relay. The design prototype to meet the design requirements of the mission statement. Therefore, it has a certain practical value and reference value.

5. PROGRAM SIMULATION DESIGN

System simulation using simulation software Proteus7.0. After entering the main interface of Proteus, double-click the microcontroller to draw the system hardware schematics and load the successful hexadecimal files.

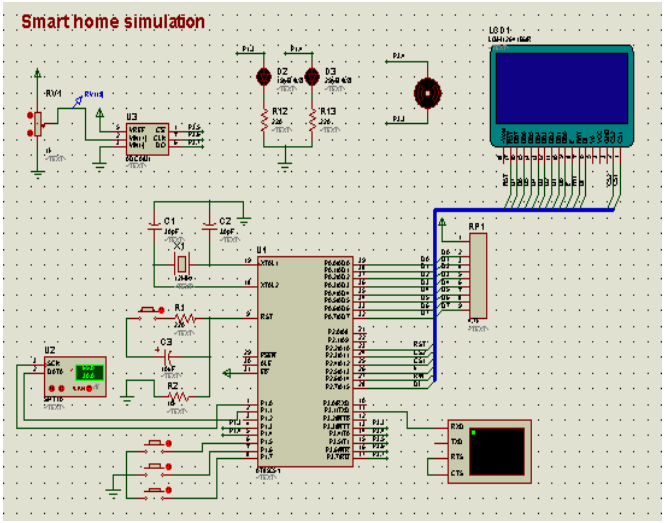

6 CONCLUSION

This paper has completed the research and design of smart home system based on stm32 controller and GPRS network communication control. Completed the prototype design and production. The system designed to meet the mission needs.

References

[1] United States] Stephen Prata. C Primer Plus (Fifth Edition) Chinese version. Beijing: People's Posts and Telecommunications Press, 2005-2-1
[2] Guo Tianxiang. The new concept of 51 SCM C language tutorial. Beijing: Electronic Industry Press, 2009-1-1
[3] Yan Weimin Data structure (C language version) Beijing: People's Posts and Telecommunications Press, 2011-2-1
[4] Zhang Yigang, Peng Xiyuan, SCM principles and application design, Power Industry Press, 2008.4.
[5] Pioneer studio, microcontroller programming examples. Tsinghua University Press, 2002.
[6] Qiu Lan, Zhang Xiaoyun translation, C language programming practical tutorial, electronic industry press, Beijing, 2001.7.
[7] Zhou Hong, Hu Wenshan, Zhang Liming, Lu Yi Yan, intelligent home control system China Electric Power Press, 2006.01
[8] Yang Guangxiang, STM32 microcontroller principle and engineering practice, Wuhan University of Technology Press, 2013-6
[9] Zhang Yang, Liu Jun, Yan Han-yu, atomic teaching you to play STM32, Beijing University of Aeronautics and Astronautics Press

An overview of fiber Prague grating (FBG) demodulation method

Tianze Wang; Shilong Liang; Zihang Qin
（*instrument science and engineering institute, jilin university*）

***Abstract*-Optical fiber sensing technology is developing rapidly along with the development of optical fiber communication technology. It has been widely applied in many fields such as power, bridge, medical treatment, mine and so on. The existing FBG demodulation products are difficult to be widely applied because of their high cost and large volume. Therefore, the key to the practicability of FBG sensors is to reduce costs and develop miniaturization, modularization and sensor demodulation system suitable for engineering applications. This paper first describes the basic principles, characteristics and development prospects of FBG sensing technology, and introduces the principles and components of the four demodulation methods, such as matched FBG tunable filter, tunable optical fiber F-P filter, and compares and analyzes their performance. The filter part of the moving average filtering, wavelet filtering, zero phase filtering, Savitzky-Golay filtering and filtering algorithm were summarized; for fitting part, five kinds of traditional power fitting algorithm of weighted average method, Gauss fitting and deconvolution method were outlined.**

***Keywords*-FBG demodulation filtering fitting**

I. INTRODUCTION

OPTICAL fiber sensing is a new sensing technology which has developed rapidly in recent years. It is called the three pillars of modern information technology together with communication technology and computer technology. The progress of modern information technology reflects the various aspects of the world economy and social life today, and is an important symbol to measure the development process of modern science and technology. Fiber Bragg grating (FBG) is one of the widely used passive fiber devices. With the continuous improvement of sensing technology and FBG fabrication process, the development of sensor network system with high accuracy, strong stability, low cost and easy reuse is the trend of sensing technology[1].

Optical fiber sensing technology with the development of optical fiber and optical communication technology and development, especially to light as the carrier and optical fiber as the medium, emergence of fiber grating sensing technology perception and transmission of the external signal to the optical fiber communication and optical fiber sensing and related field with a milepost type revolution. Fiber Prague grating (FBG) with its good stability, anti electromagnetic interference, low cost, small volume, high sensitivity, high reliability, wide measuring range and use can be made of various sensors and sensor networks, etc., are widely used in the detection of electromagnetic, mechanical, strain, temperature, radiation, torque, chemical composition the physical quantity, bridges, dams, nuclear industry, aviation and navigation, building structure and mining project monitoring system[2].

Fiber Bragg grating sensor in many fields of continuous rapid development, make it in the world wide attention and application. When the sensor is used to measure the physical quantity of the external environment, it can be multiplexed through a wireless optical fiber network. The fields involved in sensor networks include peripheral security, industrial process control, structural monitoring, and reconnaissance of dangerous substances. When compared with free space wireless communication, fiber optic network provides more secret, eliminates external electromagnetic interference, and avoids the loss of channels due to atmospheric conditions. With the increase in the demand for danger warning sensors, the dependence on their continuity is becoming more and more strong.

II . ANALYSIS OF COMMON FBG DEMODULATION TECHNOLOGY

The key of the FBG sensing demodulation system is the tiny offset of the detection center wavelength. Currently, the commonly used demodulation methods are matched grating filtering, non-equilibrium interferometry, tunable narrow-band light source and tunable filtering[3].

A. Matched grating filter method

The matched grating filtering method uses another FBG as reference gratings, and with heterodyne carrier technology, it changes with the wavelength of FBG under the action of driving elements. At the same time when the reference wavelength reflection grating and grating sensor, light is fully reflected through the measured wavelength offset sensing FBG maximum reflection power on the reference of the FBG, while driving the driving signal and the corresponding reflected wavelength of the sensing element, to obtain the changes measured by the driving signal, to realize demodulation signal using reference grating[4].

B. Nonequilibrium M-Z interferometer method

Unbalanced M-Z interferometer detection principle: light is composed of a wide spectrum light source, through the coupler incident into FBG, reflected by the FBG through another coupler into M-Z interferometer, the optical path difference of OPD interferometer. The wavelength change as the phase change, by detecting the changes of output light intensity of FBG

interferometer wavelength the amount of change, and then ascertain the measured signal size.

C． Tunable narrow band light source method

The principle of tuning narrow band light source method: the FBG array is scanned by the tunable narrow band laser that determines the wavelength to determine the center wavelength. The piezoceramic PZT is driven by sawtooth wave voltage or sine wave. The Bragg reflector laser is fixed with PZT. When the laser is scanned in a certain wavelength range, its wavelength will be consistent with a FBG wavelength. The light at this wavelength will be strongly reflected by the corresponding grating. The reflected signal enters the detector through the coupler, and the relationship curve between the wavelength and the FBG reflectivity is known by the digital oscilloscop

D． Tunable F-P filter method

Tunable F-P filter detection principle: the F-P cavity is fixed on the PZT, can be regarded as a narrow-band filter, reflected in a certain wavelength range of light into the F-P cavity, the sawtooth wave driving voltage regulating PZT, only certain wavelengths can meet the interferometric coherence conditions, produce coherent extreme, this scanning voltage PZT corresponding to FBG the reflection wavelength, and the measured physical quantity.

The advantages and disadvantages of the above four demodulation methods are shown in table 1

Table1

Performance comparison of different demodulation systems

Method	Advantage	Shortcoming
Matched grating filter method	The structure is simple、the cost is low the requirement of the reflection light intensity is low	high requirements for the detector he sensing grating has a small range of measurement
Nonequilibrium M-Z interferometer method	High resolution and high bandwidth, it can be used to form a distributed sensing system measurement	the measurement range is limited and easy to be disturbed. It is only suitable for dynamic
Tunable narrow band light source method	The resolution is high and the signal to noise ratio is high. the corresponding temperature resolution is about 0.2℃	the tunable range and stability of the laser are limited, the number of sensing gratings
Tunable F-P filter method	Small size, low price, good stability, the output is the corresponding signal of the wavelength. the ideal filtering effect can be achieved by changing the length and reflectivity of the F-P	High precision F-P filter is expensive and the filter loss is large

It can be seen from the above comparison that the tunable filtering method is a kind of demodulation scheme with better practicality and more mature technology. Therefore, the demodulation system is designed on the basis of the tunable method. The demodulation principle is shown in Figure 1

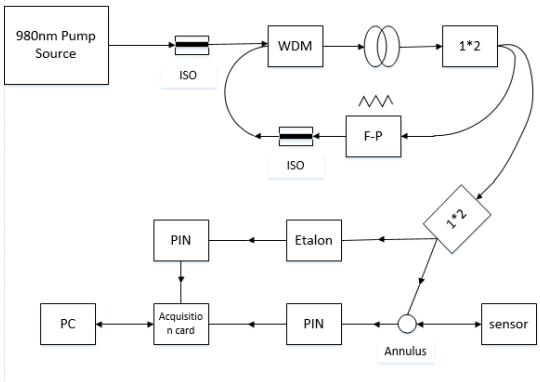

Fig.1 Schematic diagram based on tunable filter method

III. SIGNAL PROCESSING FLOW

In order to filter out noise and improve the accuracy of system demodulation, a FBG signal processing process based on virtual instrument is constructed, as shown in Figure 2. This process can be described as: firstly, the reflection spectrum of FBG signal using digital signal processing technique for denoising to improve the signal-to-noise ratio, then the coarse positioning peaks of the signal sequence, the approximate location for the peak, in order to reduce the workload and improve the accuracy of subsequent demodulation, followed by fitting the data signal, peak fitting curve is the center wavelength of FBG[5].

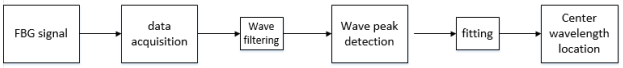

Fig.2 Processing flow of FBG reflection spectrum data

The process can reduce the noise of FBG demodulation system and improve the accuracy of wavelength detection. Due to the influence of noise and noise in the acquisition process, the peak point of reflection spectrum will be slightly shifted, which will seriously affect the demodulation accuracy of the sensing signal.

IV. AN OVERVIEW OF FILTERING ALGORITHMS

One of the main steps in this process is filtering. The system can use the hardware to filter noise, denoising, but the cost is high, and the use is not convenient, can also use the software filter, strong versatility and low cost, easy to realize, so this topic through software filtering, using digital signal processing method to eliminate the interference of noise[6].

This paper analyzes the traditional sliding average filtering, five point three times smoothing, median filtering, IIR digital filtering, FIR digital filtering, wavelet filtering, Savitzky-Golay smoothing filtering, zero phase filtering and other filtering methods.

A. Sliding average filtering

Set the length of the original data for M, the continuous N sampling data as a queue, each sampling time, the new data into the end of the line, give the first team data, always keep the queue N the latest data. Then the output of the N subsampled filter is N weighted average of the latest data. By setting different weights, the proportion of the new sampling data in the moving average can be changed. This method can effectively suppress high frequency small noise and periodic interference, and has high smoothness. But the effect of random pulse interference filtering is not good, and the sampling deviation produced by pulse interference can not be eliminated, and the sensitivity is low.

B. Five point three times smoothing filter

In this method, the least squares polynomial is used to smooth the discrete data for three times according to the least square rule, and the five point three smoothing formulas can be obtained.

$$\bar{y}_1 = \frac{1}{70}[69x_1 + 4(x_2 + x_4) - 6x_3 - x_5]$$

$$\bar{y}_2 = \frac{1}{35}[2(x_1 + x_5) + 27x_2 + 12x_3 - 8x_4]$$

$$\bar{y}_i = \frac{1}{35}[-3(x_{i-2} + x_{i+2}) + 12(x_{i-1} + x_{i+1}) + 17x_i]$$

$$\bar{y}_{m-1} = \frac{1}{35}[2(x_{m-4} + x_m) - 8x_{m-3} + 12x_{m-2} + 27x_{m-1}]$$

$$\bar{y}_m = \frac{1}{70}[-x_{m-4} + 4x_{m-3} - 6x_{m-2} + 4x_{m-1} + 60x_m]$$

In these equations, $i = 3,4.....m-2$, $\bar{y}_i$ is x_m after the smooth.

C . Median filtering

Median filtering is a nonlinear data processing method based on sorting statistics rules. It can filter the noise very well, and it is known that N equal distance sampling points are $\lambda_1 < \lambda_2 < ...\lambda_{n-1} < \lambda_n$ corresponding sampling data $y_1, y_{21}, ...y_{n-1}, y_n$. At the center of the sampling point, the M points are taken each before and after, which is expressed as:

$Y = \{y_{i-m}, y_{i-m+1}, ...y_i, y_{i+1}, ...y_{i+m}\}$

$\bar{y}_i = Median(Y)$ The value after median filtering is the value of the sampling point.

D. IIR digital filtering

IIR filter is a class of recursive linear time invariant systems with good amplitude frequency characteristics, but the phase frequency characteristics are nonlinear. The output value of the IIR filter is related to the input value and the output value of the filter. That is, the actual IIR filter needs feedback information, which causes the error caused by each operation will return to the input as part of the input signal, which is error accumulation.

E. FIR digital filtering

Compared with IIR, FIR can provide accurate linear phase. The FIR filtering principle uses the current and previous input sample values to determine the current output sample values. The accurate linear phase of filtered signal is at the cost of reducing the amplitude response characteristics, and the location is also offset compared with the original signal, but the offset is only related to the order of the filter. FIR has no feedback system, where phase requirements are not strict, FIR can be used to save resources. FIR can effectively improve the signal to noise ratio, but it can not filter the noise in the bandwidth of the filter.

F. Wavelet filtering

The application of wavelet transform to FBG signal processing, the basic principle is according to the specific signal prior conditions, coefficient of the signal and noise in different scales with different mechanism, the greatest extent to keep the signal coefficients but also reduce or even completely eliminate the noise coefficient, in order to obtain the best estimate of the noise free signal.The basic model of wavelet denoising is: hypothetical data containing noise $f_i = g_i + \varepsilon_i, i = 1,2,..., N(N = 2'')$ It is composed of the real signal g_i and the noise ε_i, which are independent of each other. The assumption satisfies the following conditions: (1) obeying the normal distribution; (2) unrelated; (3) the variance is a constant of three conditions. The measurement data are transformed by wavelet transform $w = \theta + \eta$, Wavelet de-noising can be simplified as $w = W(f), w_t = D(w,t), \hat{g} = W^{-1}(w_t)$

$W(\bullet)$ is a wavelet transform operator, $D(\bullet,\bullet)$ is a nonlinear filter operator, and $W^{-1}(\bullet)$ is a wavelet inverse transform operator.

G. Savitzky-Golay smoothing filter

Savitzky-Golay smoothing filtering is equivalent to low-pass filtering in time domain. The principle is based on polynomial function. According to the least square method, the data is optimally fitted through mobile windows, so that the noisy signal is smoothed. The polynomial function of fitting is:

$$f_i = \sum_{k=0}^{n} b_{nk} i^k = b_{n0} + b_{n1} i + b_{n2} i^2 + ...b_{nn} i^n$$

Square error and set up:

$$E = \sum_{i=-m}^{m} [f_i - x(i)]^2 = \sum_{i=-m}^{m} [\sum_{k=0}^{n} b_{nk} i^k - x(i)]$$

To minimize the error, that is, the derivative of the coefficients of E is 0:

$$\frac{\partial E}{\partial b_{n_r}} = 0, r = 0,1,2,..., n$$

We can get: $\sum_{k=0}^{n} b_{nk} \sum_{i=-m}^{m} i^{k+1} = \sum_{i=-m}^{m} x(i) i^r$

M is the number of data points required to fit the single side, the n is the polynomial order, the input data is x (I), and the fitting polynomial f can be obtained. M is the number of data points that are used to minimize the least square method on both sides of the current data point. The length of the mobile window is m *2+1 and must be greater than n.

H. Zero phase filtering

After the signal sequence is filtered by zero phase, the phase of the signal is not changed, that is, the phase response of the system function is 0. The principle of zero phase filtering is as follows: first, we extend the signal sequence, then send it to the filter, then filter the sequence inversion and send it to the filter again, and the resulting sequence is inverted again, so that we get the zero phase output sequence. If the input signal is x (n), the impulse response is the filter filter of the H (n),

and the expression of the zero phase filtering in time domain and the frequency domain expression of the output are as follows:

$$y_1(n) = x(n) * h(n)$$
$$Y_1(e^{j\omega}) = X(e^{j\omega})H(e^{j\omega})$$
$$y_2(n) = y_1(N-1-n)$$
$$Y_2(e^{j\omega}) = e^{-j\omega(N-1)}Y_1(e^{-j\omega})$$
$$y_3(n) = y_2(n) * h(n)$$
$$Y_3(e^{j\omega}) = Y_2(e^{j\omega})H(e^{j\omega})$$
$$y_4(n) = y_3(N-1-n)$$
$$Y_4(e^{j\omega}) = e^{-j\omega(N-1)}Y_3(e^{-j\omega})$$

From the above deduction, the final input and output can be expressed as: $Y(e^{j\omega}) = X(e^{j\omega})\left|H(e^{j\omega})\right|^2$, It can be seen that there is no additional phase between the output $Y(e^{j\omega})$ and the input $X(e^{j\omega})$, which can achieve zero phase shift filtering. It is noticed that the X sequence is multiplied with the square of the system function module, so the order of the filter is doubled, and the amplitude will decrease because of the square multiplication.

V. AN OVERVIEW OF THE FITTING ALGORITHM

To get the accurate center wavelength data points, we must accurately fit the signal waveforms to further determine the peak position. There are many commonly used fitting methods. In this paper, several widely applied fitting algorithms are compared.

A. Power weighted averaging method

The basic principle is that the horizontal and vertical coordinates of each point in the waveform data values were seen as the particle system in corresponding particle position vector and the quality of the size of the abscissa centroid can be obtained under the definition of the centroid weighted average algorithm, when the waveform steep or axisymmetric, coordinate and centroid position of a wave. The set weighting coefficient is equal to the reflected light power, and the center wavelength of the FBG reflection spectrum can be obtained by weighted average processing of the wavelength data.

B. Gauss polynomial fitting

The basic principle is to transform the waveform curve by using the Gauss function polynomial, and to fit the spectral peak function by the general polynomial. Since the reflection spectrum of FBG is approximately the Gauss function, we only need to get the FBG function corresponding to the FBG reflection spectrum, so we can see the central wavelength value corresponding to the reflection spectrum:

$$y = \mathrm{In}I$$
$$a = -4\mathrm{In}2/(\Delta\lambda_s)^2$$
$$b = 8\mathrm{In}2 * \lambda_s/(\Delta\lambda_s)^2$$
$$c = \mathrm{In}I_0 - 4\mathrm{In}2 * (\lambda_s/\Delta\lambda_s)^2$$

So posture:

$$I(\lambda) = I_0 \exp[-4\mathrm{In}2(\frac{\lambda-\lambda_s}{\Delta\lambda_s})^2]$$

May be expressed as:

$$y = ax^2 + bx + c$$

By using the method of general polynomial fitting, the values of a, B and C in the expression are obtained, and then the symmetry is known.:

$$\lambda_s = \frac{-b}{2a}$$

C. Three order spline fitting

The basic principle is to get the peak data by approximating the captured waveform through the formula

$$\Delta\lambda_B = 2\Lambda\Delta n_{eff} + 2n_{eff}\Delta\Lambda$$
$$f = p\sum_{i=0}^{n-1} W_i(y_i - f(x_i))^2 +$$
$$(1-p)\int_{x_0}^{x_{n-1}} \lambda(x)(f^n(x))^2 dx$$

In the sentence, Wi is the I element of weight. Lambda (x) is a piecewise constant function. P is a balance parameter. When P value is [0,1], it can be smoothed and approximates the fitting curve of data points. The P tends to 1, and the fitting is more approximate to the original data; the P tends to be 0, and the fitting is smooth. When the values of P are 1 and 0, they are three spline interpolation and linear fitting respectively.

D. Deconvolution method

The reflection spectrum signal is convoluted with the interference function in the F-P cavity, so the signal after the operation is larger than the original reflection spectrum, and the resolution is reduced. In order to improve the demodulation accuracy, the FBG reflection spectrum after operation can be processed by deconvolution. The disadvantage of the deconvolution method is to amplify the influence of high frequency noise.

E. Solution method of slope line intersection

The maximum value of optical power of FBG sensing signal is I0. Two thresholds I1, I2 and I2= alpha I0 are called high thresholds, I1= I1= I0 is low threshold, alpha is high threshold coefficient, beta is low threshold coefficient, optical power range I1-I2 can be determined. 4 threshold points can be obtained by the reflection spectrum curve. There are two points A, B, C and D on the left and right sides of the curve. When I1-I2 is within a certain range, the curve segments AB and CD can be approximated to a straight line. The equation of the linear AB and CD is obtained by the least square fitting, and the two line intersection point E is the position of the central wavelength.

VI. SUMMARY

This paper summarizes the current main methods of FBG demodulation system, describes the advantages and disadvantages of each method, the tunable F-P filter demodulation system and system block diagram and signal processing are given based on the basic principle of signal processing for review in the process of filtering and fitting filtering, fitting methods of. The demodulation function of the FBG system can be realized through the virtual instrument platform.

References

[1] B.Zhang, M. Kahrizi. High-Temperature resistance fiber Bragg grating temperature sensor fabrication [J].IEEE sensors journal, 7(4), 586-591,2007.

[2] J.Biqiang, Z. Jianlin, Q. Chxian. An optimized strain demodulation method based on dynamic double matched fiber Bragg grating filtering [J]. Optics and Lasers in Engineering, 49(3),415-418,2011.

[3] Yang Mu, Liu Xiuhong, Liu Wei, et al.. Applied research of optical fiber sensor in oil and gas pipe corrosion monitoring[J]. Laser & OptoelectronicsProgress,2014, 51(2): 020604.

[4] Benitez, D.; Gaydecki, P.A.; Zaidi, A.; Fitzpatrick, A.P. The use of the Hilbert transform in ECG signal analysis. Comput.[J] Biol. Med. 2001, 31, 399–406.

[5] Yang Gang, Xu Guoliang, Kwok junction, etc., high precision fiber Bragg grating wavelength demodulation system based on spectral zoning [J]. Chinese laser, 2015(4):98-103.

[6] Rao Yun Jiang, Wang Yiping, Zhu Tao and so on. Principle and application of fiber Bragg gratings. Beijing Science Press,2006.1～8.Yang Gang, Xu Guoliang, Kwok junction, etc., high precision fiber Bragg grating wavelength demodulation system based on spectral zoning [J]. Chinese laser, 2015(4):98-103.

Flipbook Design Based on KINECT Image Recognition

Jiyuan Li; Yuxuan Zhang
（instrument science and engineering institute, Jilin university）

***Abstract*-This thesis elaborates a design of a bookbinding machine based on Kinect image recognition. This design primarily serves disabled people, casualties, band conductors and other special groups who may not be able to read the book by hand. The biggest design feature is the use of Microsoft's Kinect system real-time capture user limb movements, and according to user action to determine their intentions, in order to accurately and timely issued a book instruction. At the same time, the design uses simple and efficient mechanical structure and vacuum suction principle to realize the book-turning movement, overcoming the shortcomings of the traditional book-turning machine with complex structure and complicated book-turning actions. The experimental results show that in the non-contact control mode, the bookbinding machine can realize the function of book-turning, the high accuracy of instruction recognition and the high success rate of book-opening. It has good application prospect.**

***Keywords*-bookbinding machine, image recognition, Kinect, Negative pressure adsorption**

INTRODUCTION

WITH the progress of the times and the development of science and technology, people's attention to vulnerable groups not only enriches their material life, but also deepens how to meet their spiritual needs[1,2]. However, in the present society, there are still some people who can not read books properly due to physical defects. Although they can be read using computers, electronic books and other electronic devices, these electronic devices can cause some harm to the user's eyes and are not economical. In addition, it is inconvenient to read paper books for bandaged wounded, band commanders and performers. In the face of the above problems, automatic book machine provides us with a solution. Therefore, the design and manufacture of a flipper great social value and market potential.

At present, domestic and foreign countries have had the design of the structure of the book, such as Japan's BOOKTIME5000 flip-flop, the United States Michael Donald Banks[3] Page Turner, Yueshan University Wu Yue[4], who research fully automatic adjustable page turning agencies and Dalian Jiaotong University Dong Yunmei[5] et al. However, the above bookbinding machines generally have the disadvantages of complex structure and high cost, meanwhile they lack the user-friendly design to obtain the user's instruction through the direct contact and the wearing of headgear, which can not really meet the needs of a specific group of people.

The paper-making machine developed in this paper makes up for the shortcomings of many traditional bookbinding machines mentioned above and makes full use of the current advanced computer technology to simplify the mechanical structure of the bookbinding machine and to optimize the way of obtaining user instructions, Experience, to achieve a low cost, high cost and other goals.

I. SYSTEM DESIGN

In this paper, Kinect image recognition based on the book machine can automatically recognize the user's body language, automatic page turning function. The system through the Kinect sensor returned a large number of data processing to determine the user body language, to achieve the user to open the book instructions to distinguish. The use of negative pressure adsorption principle, to achieve the book page adsorption, release and transmission and other activities. Among them, the suction force mainly depends on the fan system, and the suction pressure is absorbed by the system to absorb the book page and place it on the flip-flop stick, thus realizing the book-turning action. As shown in Figure 1, the bookbinding machine system uses a modular design, mainly composed of three parts: motion recognition part, the control system part, the mechanical structure part.

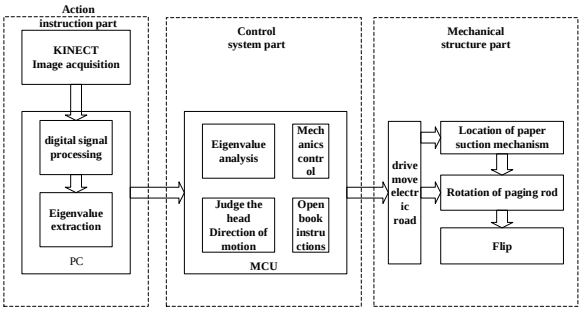

Figure 1: System block diagram

II. MOTION RECOGNITION SYSTEM DESIGN

A. Hardware introduction-Kinect

Kinect is a gesture sensing input device developed by Microsoft Corporation. It contains sensing devices such as color camera and depth sensor to meet the needs of people in work, interaction and entertainment. This powerful image data collector provides users with a wide range of image information such as color images, 3D depth images, and human skeletal motions using the in-depth machine learning of a random forest, and also thanks to its powerful Data acquisition,

Kinect has become the preferred gesture recognition front-end data acquisition cameras nowadays. In summary, Kinect somatosensory posture input device in the detection of image limb posture area extraction and processing than the average camera has a greater advantage. Therefore, this design uses Kinect as the front output device.

B.Motion capture principle

In order to correctly identify the user's intention to open the book, the design of the user's head mainly to determine the direction of rotation to accept the instruction to open the book. At the same time, in order to improve the fault-tolerant rate, in order to increase the user experience and prevent unnecessary judgments resulting in unnecessary book-opening, the motion recognition system uses two parameters to judge the head movement.

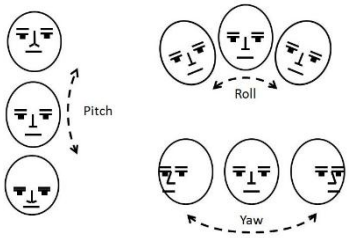

Figure 2: Head parameter diagram (provided by the Microsoft manual)

As shown in Figure 2, after processing the data collected by Kinect, we finally get three parameters: Pitch, Roll, Yaw. The core idea of the two-parameter decision method is to use the two parameters of Pitch and Yaw to form a mutual restraint relationship. Only when two parameters reach a certain condition, the instruction of turning the book-reading instruction will be triggered and sent to the lower computer through the serial port.

C.Face tracking

In order to obtain Pitch, Roll, Yaw three parameters, the system after obtaining the image data, you first need to locate the position of the face in the image, and then calculate the three parameters according to facial features. In 2012, Microsoft Asia Research proposed a Learn-based Descriptor (LE)[6,7,8] to solve the image problem and matching problem of face recognition.

Unlike other face descriptors, the LE descriptor is obtained by using unsupervised learning techniques to obtain an encoder from a training case, and then transforming the high-dimensional nonlinear data into low-dimensional linear data by using the dimensionality reduction algorithm to finally obtain a high judgment And easy to distinguish the face description and LE descriptors. The method uses unsupervised learning techniques to achieve a balance between constant force and judgment, that is, it has strong anti-interference ability and rapid face recognition and matching ability.

The obtained LE descriptor is processed by the resolver to determine the position of each standard point of the face and finally achieve face tracking.

III. MECHANICAL MOVEMENT SYSTEM DESIGN

A.Mechanical structure design

The main work is to realize the link book machine adsorption paper, and it is up to a certain height, and finally by the book book to achieve the action bar. This design uses the fan to produce negative pressure so as to achieve the purpose of absorbing paper. In order to adapt to different heights of paper and different materials of paper, the fan is placed on a movable bracket and close switch is formed to form a closed loop system, and the motor is used to realize the up and down movement of the bracket. When the horizontal section is higher than that of adsorbed paper book bar, book bar motor drives rotation to achieve the open book action.

B.*Mechanical description*

Referring to Fig. 2, the bookbinding machine consists of 9 components, each of which comprises a support plate (1), a stepper motor (2,3,6,9), a flip book (4), proximity switches Fan (7), fan bracket (10), vertical screw (11), roof beam (12), Kinect (13). The support plate 1 for supporting other components and books placed on both sides of the support plate 1 is set up vertical screw 11, by driving the stepping motor 2,6 can cause the screw rotation and drive fan bracket 10 up and down movement; fan bracket 10 mounted on the left end of the stepper motor 9, the stepper motor to rotate the track so that the fan 7 can move around; in the top of the vertical screw 11 for the top beam 12, top beam 12 placed Kinect image sensor 13; below the fan 7 And the stepper motor 9 are mounted below the proximity switches 5, 8, according to the state of the proximity switch to initialize the mechanical structure; the rear end of the support plate is fixed stepper motor 3, the output shaft of the stepper motor 3 Flip stick connected to the book 4, 3 stepper motor driven flip Flip stick 4 rotation, to achieve the book movement.

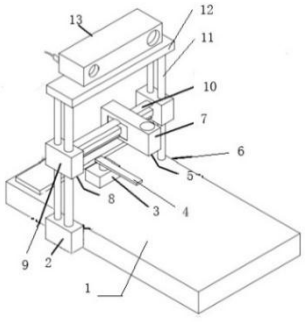

1. Support plate；2、3、6、9：Stepper motor；4. Book bar；5、8. Close switch；7. Fan；10. Fan bracket；11. Vertical screw；12. The top beam；13.Kinect

Figure 2: Flip-book machine mechanical structure

C.Mechanical movement description

In the initial state of the mechanical system, the stepping motor 8 rotates so that the book-turning rod is parallel to the upper end of the book; the fan moves leftward until it is shorted close to the switch 8, and the fan is at the leftmost position of the fan bracket at the end of the state; the fan bracket moves downwards Shorting the proximity switch 5, the fan brackets will stay at different heights depending on the thickness of

the book.

Book instructions issued. Right turn the book state, the fan starts, adsorption of paper, fan bracket upward movement, increase the height of the paper at one end. Fan bracket up motion stop, flip book counterclockwise rotation, driven paper to the right. The fan stops and the mechanical system is initialized again. In the case of a left-turn instruction, the mechanical system will move the fan to the far right before the fan starts, followed by the next steps.

V. CONTROL SYSTEM DESIGN

With reference to figure 1, the part of the control system mainly takes on the task of eigenvalue analysis, user intention judgment, mechanical structure control and communication. Among them, eigenvalue analysis and user intention judgement need a faster processor. Currently, the mainstream 32 bit processors generally meet the requirements. Besides, because the closed loop system is adopted in the mechanical structure control, the processor unit can not only output the control signal, but also accept the feedback signal. According to the above, 18 I/O ports are needed. In addition, the control unit needs to communicate with the host computer, so the serial interface is required. To sum up, considering the actual cost, processing speed and the number of I/O ports, the STM32F103ZET6 chip produced by ST is used as the micro control unit (Microcontrol Unit referred MCU).

VI. TEST RESULTS

In order to accurately reflect the practicability of the design, designers choose the good lighting room, and the bench book machine is arranged in the level of the number of spacious, practical test of book machine. The test includes left and right book book. The results of the test are shown in Table 1. Under the above conditions, left book book machine accuracy rate is 85%, the correct rate is 90% pages to the right. In summary, after the actual testing and inspection, this paper presents an automatic book machine solution can be established in accordance with the design scheme of motion capture, instruction judgment, flip and other functions. According to statistics, the correct rate of the book is 80%-90%.

Table 1 test results

Test direction	Average recognition （s）	Mean reaction time（s）	Correct rate
Left	1.115	10.075	85%
Right	1.105	10.855	90%

VII. CONCLUSION

This paper presents a Kinect image recognition based on the principle of negative pressure automatic flip machine solution. Through the action recognition, mechanical movement, the control system of three parts to achieve non-touch flip book. Practice has proved that the automatic book machine solution proposed in this paper can achieve a higher accuracy of the book, with high anti-interference ability, for a specific population has a high practical value and commercial potential.

References

[1] Wang Kan. Automatic book machine design [C] .// The 14th National Machinery Design Conference Proceedings .2008: 317-319.

[2] Banks M D. Page turner: US, US7750226[P]. 2010.

[3] Yi Yali, Wu Yue, Zhao San-ming, et al.Automatic adjustable page turning mechanism design [J] .Mechanical Research and Application, 2011 (6): 79-81.

[4] DONG Mei-yun, LI Pei-xing.Design and Movement Simulation of Foot-operated Flip-book Mechanism [J] .Journal of Dalian Jiaotong University, 2010, 31 (2): 24-27.

[5] Li Ni Ni.Application Research of New Technology in Computer Software Development [J] .Science and Technology Outlook, 2016, (05): 10.

[6] J. Shotton, A. Fitzgibbon and M. Cook, etc. “Real-time human pose recognition in parts from single depth images,” In Proc. of IEEE Conf.on CVPR, 2011, pp.1297-1304

[7] Cao Z, Yin Q, Tang X, et al. Face recognition with learning-based descriptor[C]// Computer Vision and Pattern Recognition. IEEE, 2010:2707-2714.

[8] High Zhiquan The two Kinect human motion capture based on [D]. of Nanjing University, 2017.

Design of Ground-Airborne electromagnetic environment simulating system using the three-dimensional coil

LI Zhuo-Wei; HE Kun; XU Li-Ning
(College of Instrumentation & Electrical Engineering, Jilin University)

***Abstract*—In order to simulate electromagnetic environment in field space and provide the means of physical simulation for motion noise resulting from Ground-Airborne electromagnetic exploration，a Ground-Airborne electromagnetic environment simulating system is designed. Parameters of coil assembly and schemes of emission current conforming to device's requirements are designed by modeling the space electromagnetic field and simulating the inner electromagnetic field distribution of three-dimensional coil. The results show that the Ground-Airborne electromagnetic environment simulating system is able to imitating the electromagnetic field which separation between receiver and transmitter is in the range of 1 to 10 kilometers and errors are all less than 10%.**

***keywords*—Three-dimensional coil Electromagnetic field Simulation system.**

I. INTRODUCTION

FREQUENCY-DOMAIN ground-airborne electromagnetic method is an emerging electromagnetic detection method. The method combines the advantages of airborne and ground-based frequency-domain electromagnetic method, proposing the working mode of ground-launched and air-received, which has advantages of fast speed, low cost and wide detection range, etc. In order to expand the effective detection depth of electromagnetic exploration, expand the scope of its application and implement multi-parameter measurement, the demand for detection accuracy is increasing day by day. At present, the accuracy of ground-to-air electromagnetic detection still fails to meet the researchers' expectations. One of the main factors limiting the development of this method is the motion noise. For frequency-domain surface-to-air electromagnetic method, due to the effects of the three dimensional vector electromagnetic field and geomagnetic field generated by the transmitter during the measurement and the magnetic noise level produced by the coils carried by the flight vehicle during the movement of the hoisting coil is difficult to decrease, this may cause great disturbance to the collected data. Therefore, the results of measurement include motion noise and poor data quality, which is not conducive to accurate inversion and interpretation. The current physical simulation of electromagnetic field is mostly confined to one and two dimensional level. In order to solve the influence of motion noise and electromagnetic interference on the precision of ground-airborne electromagnetic detection in the existing technology, a three-dimensional vector electromagnetic field simulation system is provided. Realizing the physical simulation of actual electromagnetic field during the field measurement in the laboratory, the basic experimental facilities are provided for the analysis and suppression of the electromagnetic detection motion noise in the ground-airborne frequency domain.

II. 3-D ELECTROMAGNETIC FIELD ANALYSIS

A. The formula of the source magnetic field response of the horizontal grounding conductor

The simulation analysis of three - dimensional electromagnetic environment was carried out, according to the theory of electromagnetic field and relevant theories of emission sources on layered earth are studied [1], the response formula of frequency domain and ground-airborne magnetic field of horizontal long traverse source is studied:

(1) Field level x component

(2) Field level y component

(3) Field level z component

$$H_x = -\frac{Ids}{4\pi}\cdot\frac{y}{R}\cdot\int_0^{\infty}(r_{TM}-r_{TE})\cdot e^{u_0(z-h)}\lambda J_1(\lambda R)d\lambda\Big|_{x'=-\frac{L}{2}}^{x'=\frac{L}{2}} \quad (1)$$

$$H_y = \frac{I}{4\pi}\int_{-\frac{L}{2}}^{\frac{L}{2}}\int_0^{\infty}[e^{u_0(z+h)}+r_{TE}e^{u_0(z-h)}]\lambda J_0(\lambda R)d\lambda dx' + \frac{I}{4\pi}\frac{x-x'}{R}\int_0^{\infty}(r_{TM}-r_{TE})\cdot e^{u_0(z-h)}J_1(\lambda\rho)d\lambda\Big|_{x'=-\frac{L}{2}}^{x'=-\frac{L}{2}} \quad (2)$$

$$H_z = \int_{-\frac{L}{2}}^{\frac{L}{2}}\frac{I}{4\pi}\cdot\frac{y}{R}\int_0^{\infty}[e^{u_0(z+h)}+r_{TE}e^{u_0(z-h)}\frac{\lambda^2}{u_0}J_1(\lambda R)d\lambda dx' \quad (3)$$

B. Calculation of magnetic induction intensity

Digital filtering and gaussian integral method [2] are applied to realize the numerical calculation of ground-airborne electromagnetic response, the matlab program is designed to calculate the response of the ground-airborne field in a one-dimensional layer, to obtain the numerical value (plural) of the three-dimensional electromagnetic field at any point. Take the magnetic field size of 2500m at the distance of the horizontal grounding conductor as an example:

Bx =

1.8262e-009 +4.5067e-011i

By =

4.9382e-010 +2.2847e-011i

Bz =

7.9855e-013 -2.6803e-012i

ans =

1.8262e-009 +4.5067e-011i

When the transmission current is 30A, the transmitting frequency is 1000Hz, and the flying height is 5m,x=1500，y=2000，z=-30, the intensity of the magnetic field is as high as the distance from the launch source center of 2500m. Because the scope of the study is the frequency domain, the result is complex, the amplitude is 1.8nT,Bx is 1.82nT,By 0.49nT,Bz is 2.6pT. Because the magnetic field is too small, the simulation should be scaled up. According to the similarity criterion of physical simulation[3], the reduction factor P is set to 100, that is, the physical simulation should be magnified 100 times.

III. ELECTROMAGNETIC SIMULATION SYSTEM DESIGN

A. Helmholtz coil magnetic field generator

Helmholtz coil has the ability to produce a certain range of uniform magnetic field and make simple characteristics, which makes it widely used in the teaching experiment of magnetic field and related scientific research [4-5].The helmholtz coil in the traditional sense is a coaxial circle with spacing equal to the radius of the coil, the two coils have the same number of turns and the same direction, with one copper wire in series, after loading the current, the two coils are aligned in the direction of the magnetic field along the axis, and then the uniform magnetic field parallel to the axis can be generated at the center point of the axis, as shown in figure 1.

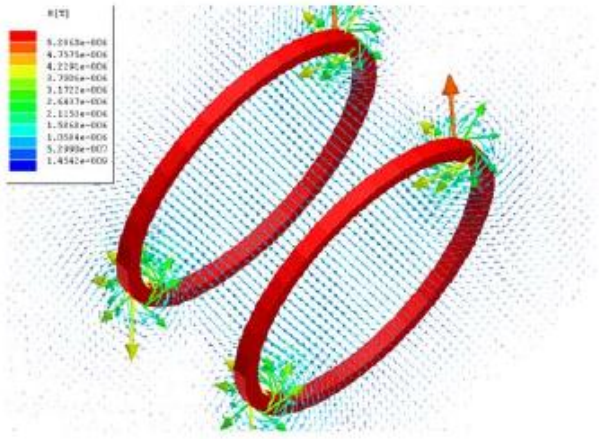

Fig.1 Diagram of circular Helmholtz coil magnetic field

Steps of Algorithm:

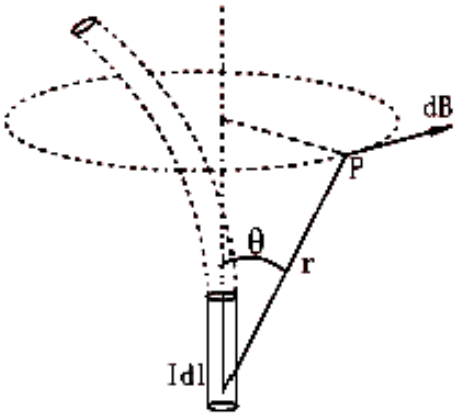

Fig.2 Biot-Savart law

According to the Biot-savart law [6], the magnitude of the magnetic induction intensity dB generated by the current element Idl at a point P in space is proportional to the size of the current element Idl, which is proportional to the sine of the Angle between the position vector and the current element Idl where the current element Idl is located, and inversely proportional to the square of the distance from the current element Idl to the P point. As shown in formula (4).

$$dB = \frac{\mu_0}{4\pi}\frac{I\,dl * r}{r^2} \tag{4}$$

μ_0 in the formula -- vacuum permeability.

The magnetic field formula of the current element is used to integrate the formula (4) according to the superposition principle, and the magnetic field distribution of any current can be obtained.

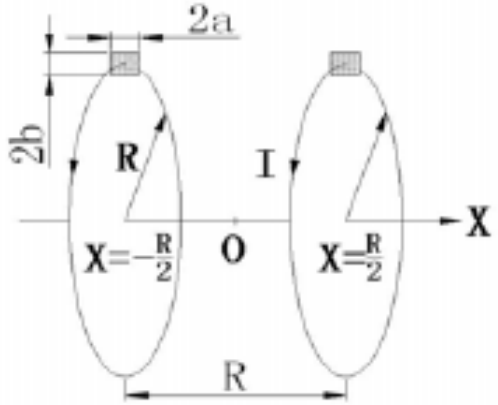

Fig.3 Helmholtz coils

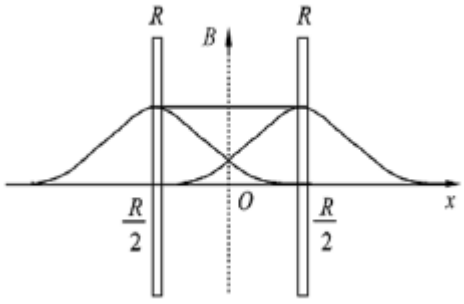

Fig.4 Superimposed magnetic field

Define the straight line of the center of the two circular coil as the X-axis, and the center point of the

line between the two circles is the coordinate origin O, the radius of the single turn helmholtz coil is R, and the two coils are on the plane of x = plus or minus L, and the current I in the same direction is connected to each coil. As shown in figure 3, the magnetic field distribution after superposition is shown in figure 4. The magnetic induction intensity of a pair of circular coils with radius R is obtained:

$$B = \frac{\mu_0 NIR^2}{2}\left\{\left[R^2+\left(\frac{R}{2}-X\right)^2\right]^{-\frac{3}{2}}+\left[R^2+\left(\frac{R}{2}+X\right)^2\right]^{-\frac{3}{2}}\right\}^{-1} \quad (5)$$

In the practical application, the copper wire wound in helmholtz is easy to be fixed as a rectangle, as shown in figure 5.

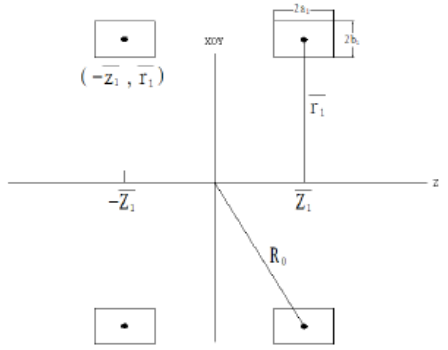

Fig.5 Diagram of coil wire spiral

According to the principle of superposition of magnetic field[7-8], the magnetic field can be decomposed into along vertical direction, the direction, north and south direction three magnetic field component, thus by making three axis perpendicular helmholtz coil to generate uniform magnetic field space combination can produce different artificial magnetic field vector.

How to control the size and direction of artificial magnetic field and its precision is the research direction of this paper.

B. Uniaxial square helmholtz coil

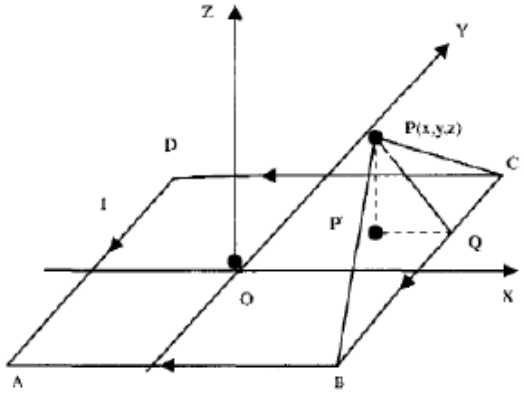

Fig.6 Rectangular coil

First, the magnetic induction intensity of the rectangular coil is discussed. The rectangular current-carrying coil is considered as a four-segment straight wire, which can be accurately solved by the formula (5). In the center of the rectangle current-carrying coil as the origin of coordinates, parallel to the horizontal edge to the right direction for the X axis direction, in the direction perpendicular to the paper face to Y axis is the direction, Z axis is perpendicular to the plane coil, and the Z axis is the direction and the direction of current form right hand spiral relationship.

Current I as shown in figure 6, AB = 2, BC = 2, the coordinates of the sites P (x, y, z), in order to calculate AB, BC, CD, DA edges at point P of the magnetic field strength at point P,,,, and every side along the x, y and z axis component of the magnetic field value, get the rectangle current-carrying coil at point P for the components in the magnetic induction intensity B:

$$\begin{aligned} B_X &= B_{ABX}+B_{BCX}+B_{CDX}+B_{DAX} \\ B_Y &= B_{ABY}+B_{BCY}+B_{CDY}+B_{DAY} \\ B_Z &= B_{ABZ}+B_{BCZ}+B_{CDZ}+B_{DAZ} \end{aligned} \quad (6)$$

C. Three axis square helmholtz coil design

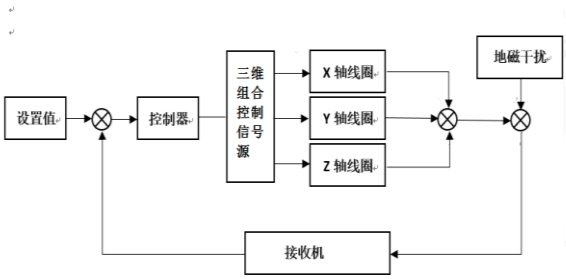

Fig.7 Block diagram of the three-dimension vector electromagnetic field simulating system

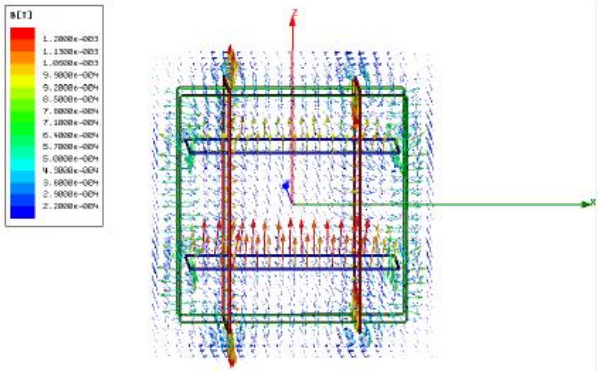

Fig.8 Magnetic field of distribution triaxial squire coil

As shown in figure 7, the three dimensional combination control signal source can launch a certain frequency, adjustable frequency square wave voltage signal, by changing the voltage size or series resistance to get fulfilment to the size of the current value of the three source respectively connected to the x, y, z axis, electricity, again through the receiver space magnetic field measurement. Figure 8 shows the magnetic field distribution of the three-axis helmholtz square coil.

Test equipment including test coil, a receiver, screen, mouse, test coil center for measurement point, place the test coil in magnetic field simulation of space used to test the size of the magnetic field, the receiver on the USB interface, will be transmitted to

the computer, the data collected through the program shows the time domain and frequency domain waveform.

D. Coil installation

The project application along the wooden rectangle frame - length, width and height (x, y, z) were 3.51 m, 4.33 m, 3.51 m, winding coil, which used a combination of square and rectangular coil, coil connection with terminal blocks, in order to load or unload; Each quarter of the coil is fixed by two solid wire slots, and the dog is fixed at the corner of the cuboid, as shown in figure 9.

Fig.9 Traixial squire coils device

Ⅳ.EXPERIMENTAL TEST

A. The test of the coil

First of all, our group tested the magnetic field when the three coils were separately energized (setpoint x=0, y=0, z=0).

Table 1 magnetic response chart of electrifying three coils separately

Energizing coil	ELECTRIC CURRENT(MA)	Magnetic field direction	Magnetic field size (nT)
x	50	x	419
x	50	y	16.9
x	50	z	80.6
x	25	x	221.7
x	25	y	6.45
x	25	z	7.25
x	10	x	70.96
x	10	y	3.22
x	10	z	2.42
y	50	x	11.3
y	50	y	269.3
y	50	z	8.06
y	25	x	5.64
y	25	y	146
y	25	z	7.5
y	10	x	4.06
y	10	y	52.42
y	10	z	4.06
z	50	x	15.3
z	50	y	18.5
z	50	z	445.8
z	25	x	8.06
z	25	y	9.67
z	25	z	200.88
z	10	x	3.22
z	10	y	4.03
z	10	z	87.9

It can be seen that in the case of changing only the current passing through the coil, the magnitude of the magnetic field generated in the three directions is also proportional to the current value, so we only need to use this table data as a reference and then according to the magnetic field. The principle of superposition can simulate the electromagnetic environment generated by the long-ground wire source in the field that you want to simulate.

B.Experimental results

We plan to simulate the field environment with Bx=200nT, By=300nT, and Bz=400nT. After comparison with the data in Table 1, we calculated that the currents that should pass through the three sets of xyz coils are 23.86 mA, 44.88 mA, and 44.86 mA. In the experiment, after the corresponding current flows through the three groups of coils in the device, there is still an error of about 10% between the magnetic field value and the theoretical value at the midpoint of the uniform space, and then the current value of the pass is fine-tuned several times. The experimental results obtained by the test are Bx=199 nT, By=298 nT, and Bz=404 nT. The error is less than 1%. So the final result is that we have realized the simulation of field magnetic field environment.

Ⅴ.CONCLUSION

This article presents a method based on three-axis Helmholtz coil magnetic field generator to generate artificial magnetic field of arbitrary direction and certain intensity. Through derivation and analysis, it is concluded that the square coil can obtain the ideal uniform magnetic field parameters. On the basis of modeling and simulation, various parameters that are in accordance with the actual project are designed, and the feasibility of the design method is further verified by the experimental data, and the initial design requirements are achieved.

References

[1] Misak N. Nabijian. Exploration Geophysics Electromagnetic Method Volume I [M]. Geological Publishing House, 1992-01.

[2] Hu Ruihua,Lin Jun,Sun Caitang,et al. Hankel transform combined with summation of Gaussian quadrature and continuous fractions and its application in geophysics[J]. Computational Geophysical and Geochemical Computing,2015(1):1-9

[3] Hu Bing, Yu Jingcun, Liu Zhenqing, et al. Study on influence of transient electromagnetic method on the detection of middle and low resistance shielding layers by physical simulation[J]. Journal of Engineering Geophysics, 2010, 07(6): 661-666.

[4] Sabaka T J, Olsen N, Langel R A. A comprehensive model of the quiet‐time, near‐Earth magnetic field: phase 3[J]. Geophysical Journal International, 2002, 151(1):32-68.

[5] Zhang Sanhui. College Physics (Electromagnetics)[M]. Beijing: Tsinghua University Press, 2008, 112-114.Caruso M J. Applications of Magnetoresistive Sensors in Navigation Systems[J]. Sensors and Actuators, SAE SP-1220, 1997:15--21.

[6] Cheng Shouyi, Jiang Zhishui. General Physics Volume II [M]. Beijing: Higher Education Press, 1988:221-223.

[7] Liu Jiliang, Li Desheng, Lin Enhuai, et al. Optimization Design of Square Helmholtz Coils [C]// China Institute of Instrumentation 2010 Academic Industry Conference. 2010.

UAV Landform Classification based on Raspberry Pi and TensorFlow

Gong Liangyu; Pan Chaoting; Zhang peng
（College of Instrument Science and Electrical Engineering Jilin University）

***Abstract*-The essay discusses the Raspberry Pi features and introduces the TensorFlow learning system.In view of the limitation of traditional satellite monitoring geomorphology classification such as unclear visibility of the fog weather and the restricted area of military, a UAV topography classification system based on Raspberry Pi and TensorFlow is designed. The system takes raspberry pi as the core, and aerials the landscape by connecting the camera to drone. The system has the advantages of real-time aerial photography, classification and identification of complex landforms, portability, improved processing speed and recognition rate.**

***Keywords*-Raspberry Pi TensorFlow Aerial photography Geomorphological classification**

I. PREFACE

WITH the continuous development of UAV landing recognition and visual technology, people are eager to study a method to classify the terrain by drones. The traditional satellite classification has certain limitations, especially due to some heavy fog weather, which brings great inconvenience to landform classification.

For the limitation of satellite observation, the author designed a drone terrain classification system based on Raspberry Pi and TensorFlow. By constructing a camera on a drone, a visual platform for a Raspberry Pi is built. By controlling the drone, the Raspberry Pi is used as the core to perform real-time image data collection on the current environment, and aerial views of the ground are taken. Data transmission and processing.

II. BACKGROUND INTRODUCTION

A.Review Stage

In the past few years, machine learning has made tremendous progress in solving these problems. Among them, we found that a model called deep convolutional neural network achieved ideal results in difficult visual recognition tasks. Researchers demonstrate steady progress in the field of computer vision by testing their results on ImageNet, a standard reference set in the field of computer vision. A series of models continuously demonstrated performance enhancements, of which Inception-V3 is the most advanced and outstanding. Running image recognition tasks on the latest model Inception-v3 is efficient and fast [1].

III.SYSTEM DESIGN

A.Experiment method

On board of unmanned aerial vehicle (uav) camera to make data acquisition system, and using the raspberry pie as control core, the collected data in real-time processing get geological features such as image data, then through the algorithm software TensorFlow data processing, the landscape classification of image classification neural network is established.

IV.HARDWARE DESIGN

A.Introduction of Raspberry Pi

Raspberry Pi (Chinese name "Raspberry Pi", abbreviated as RPi, (or RasPi / RPI) is designed for learning computer programming education, only credit card size micro-computer, and its system is based on Linux [2].

It is an ARM-based microcomputer motherboard with an SD/MicroSD card as a memory hard disk. There are 1/2/4 USB ports and a 10/100 Ethernet interface (A type has no network port) around the card main board. Keyboard, mouse, and network cable, as well as a TV output interface for video analog signals and an HDMI high-definition video output interface [3]. The above components are all integrated on a motherboard that is only slightly larger than a credit card. All the basic functions of a PC can be connected to a TV and a keyboard to perform functions such as spreadsheets, word processing, game playing, and high-definition video playback. . Raspberry Pi B only provides computer boards, no memory, power, keyboard, chassis or connection. [4]

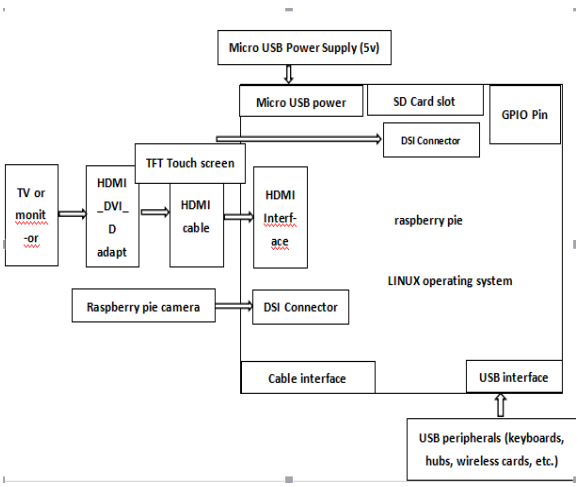

Fig. 1. Raspberry pie hardware resource interface and peripherals reference

B.Raspberry Pi Camera Takes Pictures

By comparing other cameras, the V2 Sony IMX219 camera was eventually selected. The connection between the camera and the Raspberry Pi can be directly connected through the soft cable. This camera captures 3280*2464 high-quality pixel resolution and supports 1080p30 and 720p60 with a diagonal of 4.6mm and effective back-illuminated CMOS image sensor with about 8.08 million pixels. Shooting can achieve all pixels at 30 frames/pixel. The function of the second still picture and dynamic picture is also excellent with the compatibility of the Raspberry Pi. Therefore, this camera is very suitable for high altitude landscape photography.

C.Data collection and capture

The image acquisition module decodes the streaming media data collected by the camera into a JEPG format image, uses two while loops, and the outer layer while determines whether the network port between the computer and the Raspberry Pi development board is connected. If the two are in the same network segment, the connection is indicated, and the inner while loop is entered. If the network segment is in a different segment, the connection is not connected. In this case, an error message should be sent.

Tasks to be completed within the inner while include verifying the correctness of the socket data packet. That is, check whether the first 4 bytes of the socket packet are in JPEG format. If not, the packet error is indicated and the packet should be discarded. If it is correct, it begins to receive data packets. If the length of the received data packet is less than the length of the displayed data packet during the receiving process, the received data packet should be saved, waiting for and received. The next correct data packet is concatenated to get the complete data packet. The working flow chart is shown in the following figure [5]:

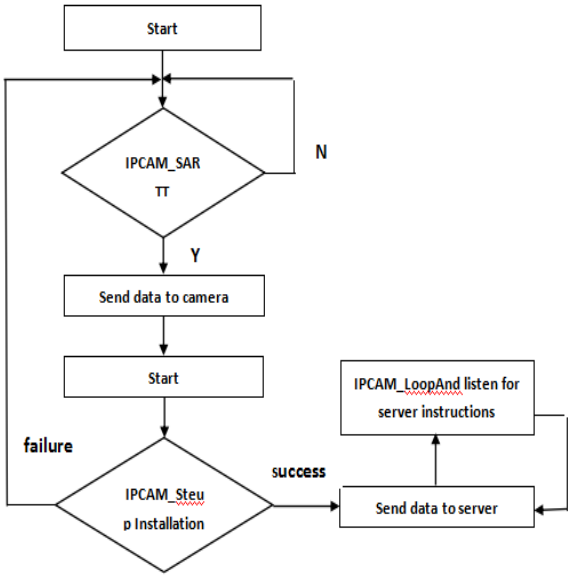

Fig. 2 working flow chart of the camera[6]

D.Data classification and processing

The collected image data is transmitted to the CPU, the image is read by the IPL library through TensorFlow software, and then OpenCV is used as an interface for reading the image.

Because the possible read samples of the image are too large, batches are read in batches to calculate the pixels of the image. Then define a network structure, measure the relationship between the value and Groundtruth, use feed-dict to fill the data, and finally serialize the image for storage [6].

Verification means: Compare the captured data with the image searched on the Google map, collect the data, and compare and process the relevant data.

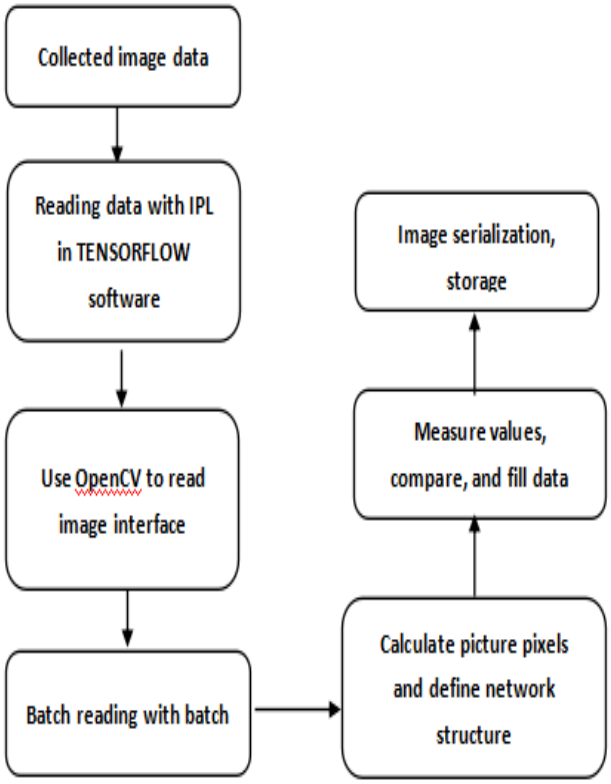

Fig. 3 Data processing flow chart

V.SOFTWARE DESIGN

A.TensorFlow introduction

TensorFlow is Google's second-generation artificial intelligence learning system based on DistBelief's R&D. Its name comes from its own operating principle. Tensor (Tension) means an N-dimensional array, Flow (Flow) implies calculation based on a data flow graph, TensorFlow flows from one end of the flow graph to the other. TensorFlow is a system that transfers complex data structures into artificial intelligence neural networks for analysis and processing [7].

TensorFlow can be used in a variety of machine learning and deep learning areas such as speech recognition or image recognition. Various aspects of DistBelief, a deep learning infrastructure developed in 2011, have been improved. It can be as small as a smartphone or as large as a few. One thousand data center servers run on various devices. TensorFlow will be completely open source and can be used by

anyone [8].

B.Raspberry pie interface

First, prepare the Raspberry Pi development board, the system image file and the 32G memory card to install the operating system, insert the SD card into the card reader and connect it with the computer, format the SD card with the SDFormatter.exe software, and then use Win32DiskImager.exe. Write the image and complete the installation of the system[9].

Connect the computer and Raspberry Pi through the network cable. The query shows that the dynamic IP of the Raspberry Pi is 192.168.137.64. The remote desktop is controlled by putty and tightvncserver. The following figure shows the RNC interface

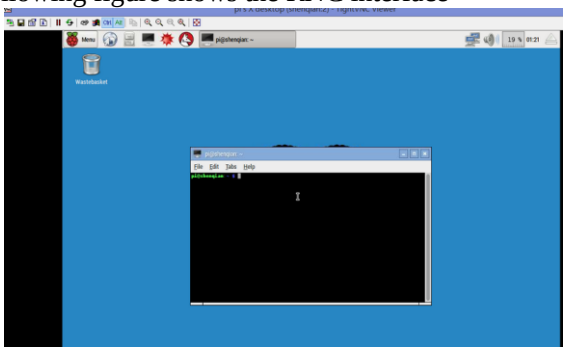

Fig. 4 Raspberry pie VNC interface map

C.Raspberry Pi Taking Photos

a.Install Raspberry Pi camera:

Defined in the terminal, using numpy and opencv to open the camera. The main order is as follows:

sudo apt-get update

sudo apt-get upgrade

sudoraspi-config

Select Enable Camera to Launch Raspberry Pi Camera.

b.Continuous photographs of Raspberry Pi:

Enter the command at the terminal:

Raspistill -t 600000 -tl 1000 -o image_num_%d_today.jpg

Taking a continuous shot.Among them,within 600000ms (10 minutes), a picture is taken every 10 seconds and named:image_number_1_today.jpg

D.Image recognition function:

We chose the Inception-V3 model of Google Image Database for image classification and processing.

As shown in the picture we want to identify a high mountain

Fig. 5 Mountain

The program runs as follows:

```
stone (score = 0.48543)
sky (score = 0.25685)
cliff, drop, drop-off (score = 0.13608)
promontory, headland, head, foreland (score = 0.01095)
ibex, Capra ibex (score = 0.00321)


Process finished with exit code 0
```

Fig. 6 Program run result diagram

From the results of the program, we can see that the initial recognition program identified almost no mountain, and the recognition rate was 0. The first two items were stone and sky. The third item was related to high mountains, but it did not meet our expectations. Recognition rate requirements, so we need to optimize the image recognition library, train the neural network, improve the recognition rate.

The second recognition result is as follows:

```
alp (score = 0.48543)
sky (score = 0.25685)
cliff, drop, drop-off (score = 0.13608)
promontory, headland, head, foreland (score = 0.01095)
ibex, Capra ibex (score = 0.00321)


Process finished with exit code 0
```

Fig. 7 The program runs the result chart again

It can be seen that after the optimization training, the program identified the stone as high mountains, the recognition rate and accuracy have been improved, but it has not yet reached our expectations, the second sky is not what we need, need to be carried out again After optimization, the total recognition rate has been gradually improved, as shown in the following table (some of the training processes are omitted):

Training times	Recognition rate
1	13.608%
2	62.151%
4	73.465%
8	78.629%
16	82.412%
32	87.836%

Fig. 8 Training results table

The final recognition result:

```
alp (score = 0.48543)
valley,vale (score = 0.25685)
cliff, drop, drop-off (score = 0.13608)
promontory, headland, head, foreland (score = 0.01095)
ibex, Capra ibex (score = 0.00321)


Process finished with exit code 0
```

Fig. 9 The program finally runs the result graph

The final recognition rate reached 87.836%, in line with our expectations.

Another example is to identify a picture of a lake:

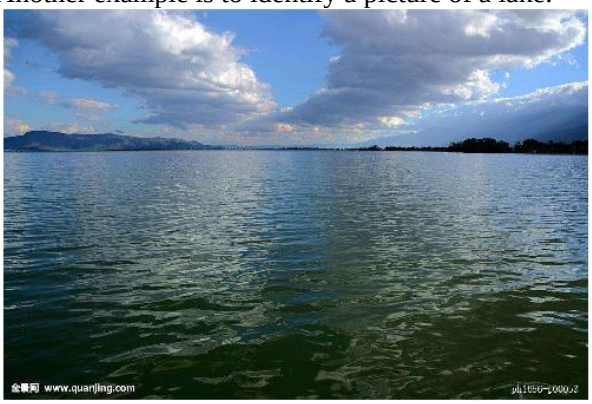

Fig. 10 Lake

The program runs as follows:

```
lakes (score = 0.89431)
breakwater, groin (score = 0.02393)
desert (score = 0.02306)
city (score = 0.00952)
pier (score = 0.00274)


Process finished with exit code 0
```

Fig. 11 Program run result diagram

From the results of the program, we can see that the program identified 89% of the pictures as lakes, which also achieved our expected recognition rate.

VI.CONCLUSION

Through this project, we successfully successfully deployed the camera and the Raspberry Pi, and successfully achieved the camera's camera and continuous camera function, and the resolution reached 3280*2464. In software, through programming, optimization of neural network training improved. The recognition rate of topography and landscape pictures completed the expected results. But at the same time, there are also deficiencies, such as the transmission speed and the processing speed is relatively slow, can not achieve 100% real-time identification; at the same time there are still deficiencies in the program, in some of the more complex image recognition, the recognition rate Not ideal. And these will also be our future direction.

References

[1] Li Nannan. Research on terrain feature recognition technology for drone landing sites[D]. Shenyang Institute of Aeronautical Engineering, 2010.

[2] Wang Jiangwei, Liu Qing, Fun Raspberry Pi [M]. Beijing: Beijing University of Aeronautics and Astronautics Press, 2013: 1-80

[3] Zhang Jun, Li Xin. Handwritten character recognition under TensorFlow platform[J]. Computer Knowledge and Technology, 2016,(16): 199-201

[4] Li Longqi, Fang Hairdressing, Tang Xiaoteng. Raspberry Pi platform under the real-time monitoring system development [W]. Haojiang College Newspaper, 2014.

[5] Li Wensheng. Based on Raspberry Pi embedded Linux development teaching exploration [M]. Electronic Technology and Software Engineering, 2014.

[6] Zhang Huaizhu, Yao Linlin, Shen Yang, Yao Xinyi. Design of Low-altitude Observation System of Crops Based on Raspberry Pi[J]. Journal of Jilin University(Information Science Edition), 2015, 33(06): 625-631.

[7] Liu Yan. Research on vehicle-mounted monitoring system based on ARM-Linux[D]. Changsha: Central South University. 2009

[8] Wang Jinqing. Design and Implementation of Remote Wireless Intelligent Vehicle Monitoring System[D]. Beijing: National University of Defense Technology, 2008.

[9] Liu Fan, Liu Pengyuan, Li Bing, Xu Binbin. Design of deep learning model for video target tracking under Tensorflow platform [J]. Progress in Laser and Optoelectronics

[10] Zhang Wei. Design and Implementation of Smart Home System Based on Machine Learning [D]. Jilin University, 2016.

[11] Zhang Hong. Embedded USB Image Acquisition System Based on ARM[D]. Chengdu: Xihua University. 2009

Design of High Precision Three Component Magnetic Field Measurement Device Based on Giant Magnetoresistance Sensor

SHANG XIN-Lei; YAN Su; MA BIN-Yuan;YU LONG-Ze
(College of Instrument Science and Electrical Engineering, Jilin University)

***Abstract*-The measurement of geomagnetic field is one of the most important probes in the field of geophysical exploration. This paper mainly introduces the design method and technology of high precision three component magnetic field measurement device based on giant magnetoresistance sensor. [1][2][3]The magnetic measurement device adopts MSP430F149 as the main control chip, and combines the four modules of GMR sensor, signal conditioning circuit, acquisition circuit and host computer to measure the geomagnetic field. The GMR sensor probe using giant magneto impedance effect measurement of magnetic field sensor, the amplifier circuit built-in preliminary amplification of the electrical signal is converted to the magnetic signal; signal conditioning circuit of sensor signal before amplification filtering, acquisition circuit will use LTC2508 32 as the core chip of the analog signal to digital. The PC software is designed using LabVIEW front panel to the signal processing of the main control chip came and the corresponding display. After testing, the results show that the design has high accuracy in measuring the geomagnetic field and is easy to be industrialized. It has a certain reference value and development value for geomagnetic field measurement in geophysical exploration.**

***Key words*-giant magnetoresistance sensor; high precision analog to digital conversion; LabVIEW upper computer panel; geomagnetic field measurement; magnetic method geophysical prospecting**

INTRODUCTION

TO measure the magnetic field is one of the most important geochemical field of geophysical exploration, but for more accurate measurement of surface to surface magnetic field with high precision is always a big problem. At present, there are many geomagnetic field measuring instruments in the market, but most of them are simple in principle, single in function and more mechanized. [3][4][6]With the rapid development of science and technology and the importance of the measurement of geomagnetic field to the importance of national defense, the accurate measurement of geomagnetic field is one of the urgent problems we need to solve. Based on the principle that modularization is easy to general-purpose, it is necessary to design a magnetic measuring device that is easy to operate and can repeat the measurement of the geomagnetic field.

Giant magnetoresistance sensor is a high-tech product which integrates magnetic thin film, semiconductor integration and nano technology. It is widely applied. Meanwhile, giant magnetoresistive sensor also has many advantages such as measuring the surrounding geomagnetism and its variation. [4][5]With the development of the national economy, GMR sensor has been developed rapidly in the application, is widely used in aerospace magnetic azimuth sensor, nuclear submarines and aircraft automatic navigation, military and so on in the field of 3D electronic compass, more suitable for the project to measure the magnetic field is weak magnetic field. Based on the above viewpoints, this paper designed a high precision of three component magnetic field measuring instrument based on GMR sensor, can be measured with high accuracy of geomagnetic field, were collected simultaneously with the 32 bit analog-to-digital conversion chip LTC2508 - 32, so as to ensure the high precision measurement of the geomagnetic field.

I. RESEARCH CONTENT

This design needs to realize the function of measuring high precision of the earth's magnetic field, the normal work of the GMR sensor HMC1042 and HMC1041z powered by 3.3V power, through amplifying and filtering circuit conditioning for low voltage signal from the sensor to the use of 32 bit analog-to-digital conversion chip LTC2508 32 and its peripheral circuit analog to digital conversion the whole process is controlled by MSP430F149, the corresponding timing, and establish communication between PC and the main controller by means of serial communication, the data in order to the computer and data processing software. The main work flow is as follows:

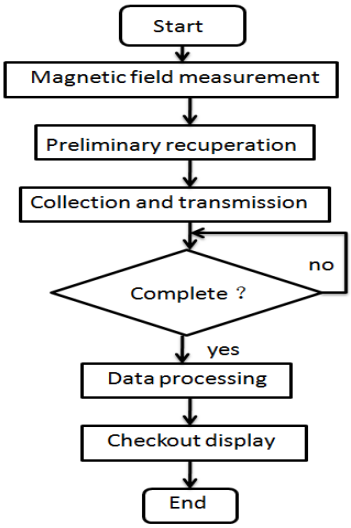

Fig.1 Workflow diagram

II. SYSTEM DESIGNING PROCESS

The overall framework of the system's functional design is shown in Figure 2.

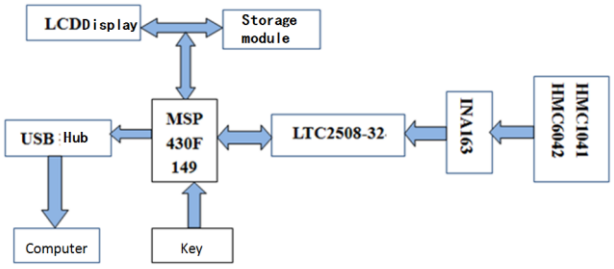

Fig.2 Overall framework of the system

The system is mainly composed of giant magnetoresistance sensor module, signal acquisition and conversion module, control module and other modules.

A. Giant magnetoresistance sensor module:

The vertical structure of the probe consists of a HMC6042 and a HMC1041z, and after correction for the good verticality, magnetic field measurement space at any point can use the vector synthesis principle for measuring the three-dimensional component of the magnetic field of the point, and the synthetic vector in a given probe coordinate system, avoid the space coordinates of the constraints multi degree of freedom, so as to improve the measurement accuracy. The range of magnetic field measurement is + 60000nT, and the output voltage is 1 volts. HMC6042 is a high-precision nonlinear output voltage type element, so it needs to be nonlinear correction when it is used. The temperature drift of HMC6042 is small, and the influence on the observation value can be ignored. Its drift and compensation work is completed by the Set/Reset set up in the built-in compensation calibration circuit, enabling it to measure accurately under the premise of normal work.

B. Modulation and acquisition module:

The conditioning circuit is made up of a built-in amplifying circuit and an external amplifying circuit made up of IN163. It completes the preliminary amplification and amplification of the signal, so as to achieve the purpose of analog-to-digital conversion.

The acquisition circuit is made up of three 32 bit acquisition boards, which are made up of LTC2508-32 and peripheral circuits. The acquisition and quantification and conversion processing of 3D magnetic vector are completed by controlling the acquisition time sequence and processing process by MSP430F149. Because LTC2508-32 has good linear characteristics and no loss of code, and has synchronous function of configurable digital filter, it looses the requirement of anti aliasing filter, and can achieve no delay output, so as to ensure the real-time performance of the timing. Besides, LTC2508-32 also has a wide common mode input range. With the help of external crystal oscillator and reference voltage of 3.3V and 4.096V, the high accuracy of acquisition is ensured, which makes the collected magnetic field data more reliable.

C. Main control module:

The main controller chip MSP430F149 is used to realize full duplex transmission and reception by using synchronous asynchronous transmitter and receiver in synchronous signal conversion circuit, so as to ensure the real-time transmission of the collected data.

III. EXPERIMENT ANALYSIS

The schematic diagram of the design of the giant magnetoresistance probe module circuit is shown in Figure 3 below.

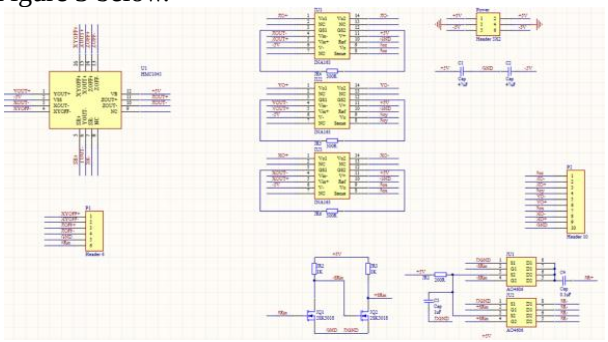

Fig.3 Schematic diagram of giant magnetoresistance probe

The designed probe PCB is generated as shown in Figure 4 below:

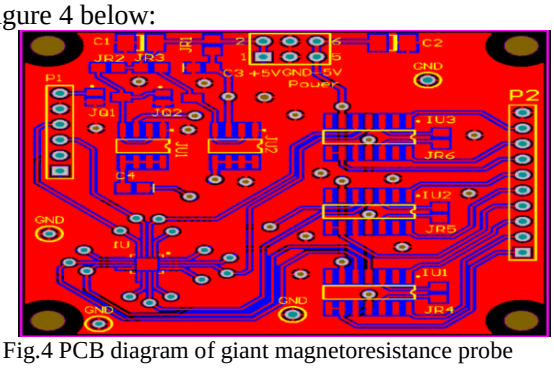

Fig.4 PCB diagram of giant magnetoresistance probe

The experimental comparison test data are shown in Table 1 as follows:

Table1 Experiments datas

Magnetic field measurement value （nT）	Known magnetic field value（nT）	relative error
54667.2	54669.6	-0.004%
54683.9	54679.2	0.009%
54682.6	54684.3	-0.003%
54653.8	54652.4	0.003%
54676.8	54675.0	0.003%
54668.4	54664.9	0.006%
54672.4	54671.6	0.001%
54676.8	54679.6	-0.005%
54669.3	54670.4	-0.002%
54664.9	54665.1	-0.0003%

As can be seen from table 1, the relative error is maintained at about 0.005%. It can be seen that this device has high relative measurement precision.

IV. CONCLUSION

This paper presents a high accuracy of three component magnetic field measurement of GMR sensor based on the model and the feasibility of each module design of magnetic field measurement device is validated, compared to the actual value of the magnetic field data, the design of the measuring device has the advantages of high accuracy, easy operation and other characteristics, the future will be applied to the actual project will have the high practical application value.

References

[1] Joao M.A. Rebello,Fumio Kojima,Tomasz Chady,Hiroyuki Nakamoto,Satoru Takenawa. Hysteresis Characteristic and Repeat Accuracy of Magnetic Type Tactile Sensor[J]. Studies in Applied Electromagnetics and Mechanics,2014,38.

[2] Joao M.A. Rebello,Fumio Kojima,Tomasz Chady, Hiroyuki Nakamoto, Satoru Takenawa. Hysteresis Characteristic and Repeat Accuracy of Magnetic Type Tactile Sensor[M].IOS Press:2014-06-15.

[3] C.P.O Treutler. Magnetic sensors for automotive applications[J]. Sensors & Actuators: A. Physical,2001,91(1).

[4] Octavian Postolache,Artur Lopes Ribeiro,H. Geirinhas Ramos. GMR array uniform eddy current probe for defect detection in conductive specimens[J]. Measurement,2013,46(10).

[5] N. Biziere,C Fermon,G. Le Goff. Hyper frequency behavior of the GMR effect in a single spin valve sensor[J]. Journal of Magnetism and Magnetic Materials,2007,316(2).

[6] Shengbin Hu,Baoxi Xu,Hongxing Yuan,Yunjie Chen,Jun Zhang,Rong Ji. Investigation of temperature rise in GMR sensor and disk induced by laser irradiation[J]. Journal of Magnetism and Magnetic Materials,2006,303(2).

Design of Triaxial Magnetic Field Measurement Device Based on Linear Hall Elements

Shang Xinlei; Dong Zhiwei; Liu Yi; Tang Shengliang
(College of Instrument Science and Electrical Engineering, Jilin University)

***Abstract*-There are many ways and methods to measure magnetic field. This paper mainly introduces a three axis magnetic field measurement device based on Hall sensor. The 32 bit AD acquisition chip has the characteristics of high accuracy. The device uses stm32f103zet6 as the main control chip, combined with three axis Hall sensor module, conditioning module, AD acquisition module, host computer, etc., to achieve magnetic field measurement of three components of a point, and display it on the master computer.After testing, this design has a high precision for the measurement of magnetic field, and has certain reference significance and development value in the field of magnetic field measurement.**

***Key words*-Hall sensor 32 bit AD Three axis magnetic field Master computer**

INTRODUCTION

IN order to study and develop magnetic logging while drilling more easily, it is necessary to establish an artificial magnetic field model and use appropriate devices to measure the three components of the magnetic field.

The research of three-dimensional magnetic field measurement mainly focuses on Teslameters for low-frequency or static measurement. Although the accuracy is high, it is difficult to meet the dynamic requirements of magnetic field measurement. The generally measurable range is not very large, and the measurement instrument for medium-high frequency is more common. Dimensional or two-dimensional magnetic fields, three-dimensional high-frequency measuring instruments are still in the experimental research stage[1]. Hall sensor can measure the magnetic field range can be 10 ^ 2nT ~ 10 ^ 10nT, which can be applied to the measurement of magnetic field triaxial component values[2], it is very suitable for this device.

The device design introduces a three-axis magnetic field measuring device based on Hall sensors, using stm32f103zet6 as the main control chip, combining three-axis Hall sensor module, conditioning module, AD acquisition module, etc., can achieve three levels of one point. The components are measured with high accuracy, wide range, and high resolution.

I. RESEARCH CONTENT

A. research content

The magnetic field vector distribution measurement system was studied and moved using a three-axis positioning device, and a linear Hall device was used to construct a three-axis Hall sensor, and a signal conditioning circuit was used to amplify and filter. After the AD conversion, the magnetic field strength triaxial data was obtained.

The micro-controller chip performs data processing on the measured magnetic field strength, and reasonably performs digital filtering on the data.

The measured system data is stored and transmitted to the host computer through the communication module.

B.The difficulties to be solved

--Solve specific problems of Hall sensor and modulation circuit implementation of magnetic field measurement.

--Use a reasonable AD chip and use correct control and digital filtering to achieve high accuracy.

--Detect undetectable areas with a reasonable detection layout.

II. DESIGNING PROCESS

A.System overall design

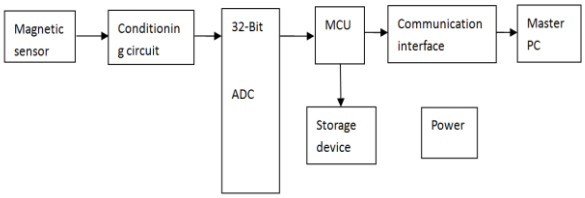

Fig.1 Design block diagram

Magnetic field sensor: A three-axis differential structure consisting of six Hall sensors SS495A1, which can measure a three-dimensional component of a point and output a differential signal, improving the accuracy of the measurement. Its magnetic field measuring range is ±670 gauss, output V level voltage, can not use the amplifying circuit. SS495A1 is a high precision linear output Hall element. The device features: internal temperature compensation circuit and correction of the resistance by the laser, so that the zero temperature drift is ±0.04% / ℃, the sensitivity drift is +0.02-±0.03% / ℃; the output voltage is -0.064T ~ +0.064T range is 0.5v ~ 4.5v (typical), it can directly interface with the microcontroller; 0T is 2.5v ± 0.075V; sensitivity is 3.125 ± 0.094; Linearity error is -1.0% range); operating temperature range is -40℃ to +150℃; operating voltage range is 4.5v to 10.5v and operating current is 7mA (typ).

Conditioning circuit: use the chip with analog switch function, so choose DG412 is a single-chip CMOS device, built-in four independent optional switch. It is designed with an enhanced LC2MOS process, featuring low power, high switching speed, and low on-resistance.The on condition of the DG412 switch is

that the associated control input is logic high. When turned on, each switch has the same conductivity in both directions, and the input signal range can be extended to the supply voltage range. All switches are open-closed and suitable for multiplexer applications. The design itself has a low charge injection characteristic that minimizes transients when switching digital inputs.

32-bit AD chip: Adopt Linear's latest AD chip LTC2508-32, is a 32-bit, 1Msps, SAR ADC with integrated pin configurable digital filter, optimized for low-bandwidth, high-precision applications, have Good linearity, no missing code. ±0.5ppm INL (typ), 145dB dynamic range (typ) at 61sps, 131dB dynamic range (typ) at 4ksps, guaranteed 32-bit, no missing codes, configurable digital filter with synchronization , Relaxed anti-aliasing filter requirements, dual output 32-bit SAR ADC, 32-bit digital filtered low noise output, 14-bit differential + 8-bit common-mode 1Msps no delay output, wide input common-mode range, guaranteed operation to 85℃ , 1.8V to 5V SPI-compatible serial I/O, low power: 24mW (at 1Msps), 24-pin 7mm x 4mm DFN package.

In addition to the LTC2508-32 chip, a crystal oscillator, 2.5V, 3.3V, 4.096V reference voltage, frequency factor selection switch, and other peripheral circuits were added, and software filtering was added during acquisition to make the entire module more fully functional.

Microprocessor: The stm32f103zet6 is a 32-bit ARM-based powerful microprocessor with 512K bytes of flash memory, with a maximum operating frequency of 72MHz. It has a variety of peripheral interfaces such as clocks, timers, AD and DA, and rich communication interfaces.

Communication interface: The Universal Asynchronous Transmitter Transmitter (USART), which adds a synchronous serial signal conversion circuit using the master chip stm32f103zet6, is a universal serial data bus used for asynchronous communication, enabling full-duplex transmission and reception.

Host computer: The host computer adopts MATLAB GUI interface, has a large number of toolboxes, rich functions, and is very convenient for data processing. From the perspective of doing GUI, MATLAB's visualization capability is very powerful, including a variety of three-dimensional, two-dimensional drawings, the interface is simple and clear.

B.software design

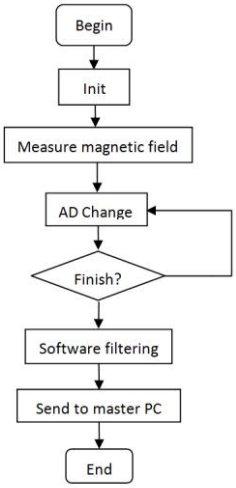

Fig 2 Software flow chart

III. EXPERIMENT ANALYSIS

A.T-probe's detection angle of space

There is a cylinder in front of the space to block, the traditional straight probe can only measure the area at both ends, can not detect the area behind the cylinder, and the use of T-type probe structure, the measurement sensor installed at the ends of the arrow, you can measure the left and right ends of the rear Area, to achieve a dead-end measurement.

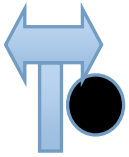

Fig 3 A schematic diagram of T probe measurement

B.For uniaxial magnets near and away from the curve

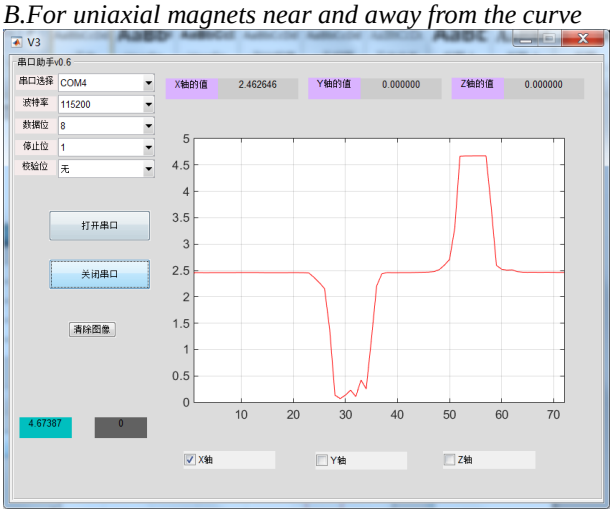

Fig 4 Uniaxial magnetic field measurement

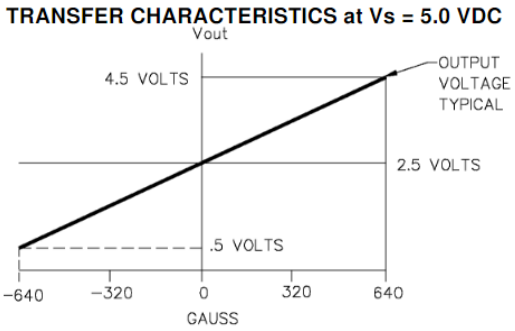

Fig 5 The relationship between voltage and Gauss value

From Fig. 4 and Fig. 5, it can be seen that when the positive and negative poles of the magnet are approached from a distance, the magnetic field intensity will show a changing trend, and the upper position machine can display the current magnetic field value and the maximum and minimum values, which conforms to the design requirements of the experiment.

C. Magnetic field strength and actual value error table

Table 1
Measurement error table

Known magnetic field value（Gs）	Voltage value（V）	Measured magnetic field value（Gs）	mistake（%）
0	2.5010	0.1	0.1
100	2.8124	100.4	0.4
200	3.1250	199.7	0.3
300	3.4375	299.8	0.2
600	4.3750	600.2	0.2
-100	2.1875	-100.4	0.4
-200	1.8750	-199.7	0.3
-300	1.5625	-300.1	0.1
-600	0.6250	-598.8	0.2

As It can be seen from the table that the effective number of the voltage measured by the device can reach 0.0001V, and the magnetic field resolution is 0.1Gs. At the same time, the error between the measured magnetic field value and the actual value is less than 0.5%, and the accuracy is high, which accords with the design requirements.

IV. CONCLUSION

The hardware and software design of the magnetic field measuring device of the Hall sensor realizes a high-precision and real-time measurement of the magnetic field. The device meets the requirements of precision, low power consumption and convenience.

If a traditional straight-line probe is used, it is difficult to measure the dead zone and it takes more time to measure the area. This design perfectly solves this problem. At the same time, the three-axis probe uses two Hall's differential structure to improve the measurement accuracy, and then with the 32-bit AD chip, making the measurement results greatly improved, in line with the design requirements.

References

[1] Lu Wendong, Xiao Lizhi, Ji Hongpeng, Liu Dongming. Introduction to key technologies of MWD logging tool while drilling[J]. Logging Technology, 2007, (02): 107-111.

[2] Li Xin, Xiao Lizhi, Hu Haitao. Investigation characteristics of NMR logging tool while drilling[J]. Chinese Journal of Spectrology, 2011,(01):84-92.

[3] Shang Xinlei, Wang Lin, Lin Jun, Fu Lei, Wang Xiaoguang, Chen Chen “Low Noise Wide Bandwidth Inductive Magnetic Sensor” Journal of Central South University (Natural Science Edition), 2015, (09): 3295-3301.

[4] Kang Huaguang et al.“Emulation Technology Fundamentals” Higher Education Press.

[5] www.opendv.com

Visual Measurement Technology of Automobile Drive Axle Housing Size Parameters

Cui Chang Kui; Li Hao Xuan; Tang Run Ze
（College of Instrumentation &Electrical Engineering, JiLin University）

***Abstract*-Measurement is an important method for human understanding of the world, and it is an important foundation for scientific development. With the development of the manufacturing industry, large-scale, high-precision, on-site measurement, and even dynamic measurement requirements have been proposed for measurement tasks. As a non-contact measurement method, vision measurement has the advantages of convenient measurement process, being insensitive to the shape of the measured object, fast measurement speed, etc. It has been widely used in mechanical manufacturing, online product testing and remote measurement and control[1] . Vision measurement technology uses images as an information carrier and is closely integrated with computer technology. It has the characteristics of non-contact, rapid measurement, and high precision, and has been widely used in various measurement tasks. Structural light vision measurement belongs to the category of computer vision measurement. It has attracted a large number of scholars to study it in recent years and has been widely used in many fields. In this paper, vision measurement technology is used to measure the drive axle housing of the vehicle, and an algorithm program for different processes is written. A complete calculation and measurement method is proposed.**

***Keyword*-Computer Vision；Measurement；Algorithm**

0 INTRODUCTION

MEASUREMENT is an important method for human understanding of the world, and it is an important foundation for scientific development. With the development of the manufacturing industry, large-scale, high-precision, on-site measurement, and even dynamic measurement requirements have been proposed for measurement tasks. Traditional three-dimensional technology can not meet this requirement. In this context, visual measurement has been produced and has become an important research direction. Vision measurement technology uses images as information carriers and is closely integrated with computer technology. It has the characteristics of non-contact, rapid measurement, and high precision, and has been widely used in various measurement tasks[2]. Structural light vision measurement belongs to the category of computer vision measurement. It has attracted a large number of scholars to study it in recent years, and has been widely used in many fields.

In China, the start of machine vision is relatively late, and the concentration of the industry is not very high. In the beginning, some agents are mainly agents of foreign brands. Now, many dealers have begun to launch free-brand products, but in the industry, Distribution, channel distribution, and mature automation products have significant differences. The relatively mature automated product quality and technical content of domestic machine vision are relatively low, and the market is far from saturated

1. OVERALL SYSTEM DESIGN

The function that needs to be realized in this design is to use a structured light sensor to perform non-contact measurement of the axle housing. The overall scheme is divided into three parts.

(1) The sensor part; the sensor system includes sensors, controllers, and acquisition structures.

(2) Algorithm: The algorithm part includes data reduction algorithm, data reduction algorithm, plane fitting algorithm, and three-dimensional fitting algorithm.

(3) The upper computer part: includes the user interface.

2. SENSOR DESIGN

According to the projection mode of the optical measurement system, the structured light projection method can be divided into the following types: point structure light projection method, line structure light projection method, multi-line structure light projection method, grid structure light projection method, surface structure light projection method [3].

The point structure light has the characteristics of rapid, real-time and strong, but the amount of information it obtains is not enough to meet the requirements of this measurement. The line structure light is generated by the projection system to produce light narrow plane slit light when measuring. When intersecting with the measured object, a bright light streak is generated on the surface of the measured object. The light streaks are modulated due to the different surface depths of the object to be measured. Multi-line structured light is measured by multiple beams encoded by a computer at the same time. The grid structure light is actually a set of interlaced functions in the spatial frequency domain, and the recognition effect is relatively good, but the recognition range is limited. The surface structure light is projecting the surface structure light of various modes onto the object to be measured. At this time, if the surface of the object is viewed from different directions in the projection optical axis, a surface structure light stripe is generated due to the unevenness of the shape [4].

The sensor model used in this design is the LJ-G200 produced by KEYENCE. The controller uses the LJ-V7000.

Taking into account the size of the measured object,

the spot diameter of the sensor has become an important consideration. Figure 1 shows the spot diameter of the sensor used for this test. The controller's instruction format and response command format are shown.

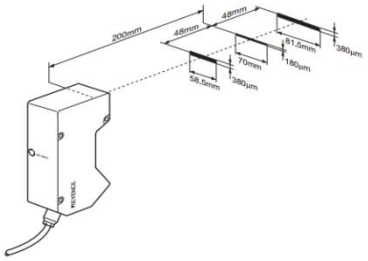

Figure1 sensor spot diameter

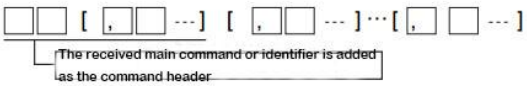

Figure2 incoming command format

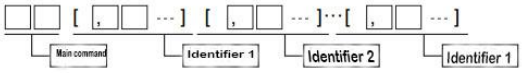

Figure3 response command format

3 ALGORITHM DESIGN

The algorithm part includes data reduction algorithm, data reduction algorithm, plane fitting algorithm, three-dimensional fitting algorithm

3.1 Data Recovery Algorithm

The sensor scans the data format and stores it in csv format. Some of the data are shown in Figure 4.

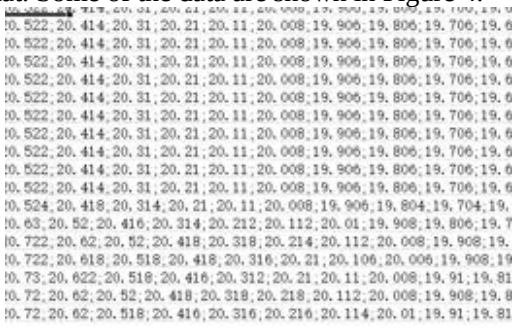

Figure4 part of the data

The process of data processing is shown in Figure5.

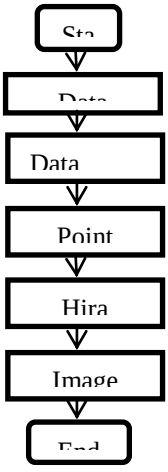

Figure5 data processing

2.2 Data Reduction Algorithm

Due to the large amount of data collected during the experiment, the computational process is bloated, takes a long time, and for a poor operating environment, there is a situation that can not be run, so for the above situation, this paper proposes a noise removal based on The data is reduced as shown in Figure 6 [5].

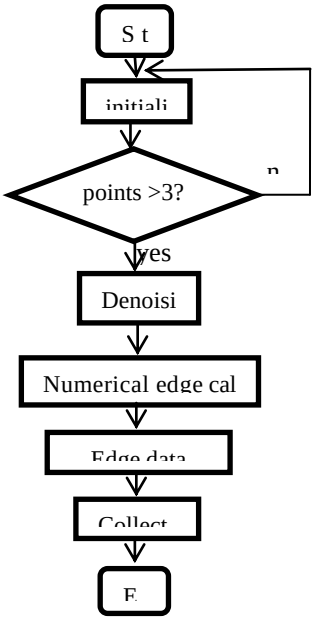

Figure6 data reduction algorithm

2.3 Plane fitting algorithm

In the calculation of distance and length, point-by-point calculations will lead to a substantial increase in the calculation process, so the use of the plane distance to calculate the specified distance, plane fitting using the least squares fit [6].

2.3.1 Least Squares Method

Least square method (also known as the least square method) is a mathematical optimization technique. It finds the best function matching of the data by minimizing the square of the error. The least squares method can be used to easily obtain unknown data and minimize the sum of squared errors between these obtained data and actual data [7].

Quadratic equation (1) on the plane:

$$a_{11}x^2 + a_{22}y^2 + 2a_{12}xy + 2a_{13}x + 2a_{23}y + a_{33} = z \quad (1)$$

For equal-precision N sets of data (x_i,y_i), i=1,...,N; x_i,y_i are accurate if the predicted value is zi. When estimating the parameters using the least squares method, it is required that the bias weighted sum of squared of the observed values zi is the smallest. Denote by functional error δ(2)

$$\delta = \sum_{i=1}^{N} \sum_{j=1}^{N} [z_{i,j} - (a_0 + a_1 x_{i,j} + a_2 y_{i,j} + a_3 x_{i,j}^2 + a_4 x_{i,j} \cdot y_{i,j} + a_5 x_{i,j}^2)] \quad (2)$$

The values of a0, a1, a2, a3, a4, and a5 affect the size of δ. To find the minimum value for δ, it is natural to find partial derivatives for a0, a1, a2, a3, a4, and a5, respectively. Actually, it is a functional code. Extreme problems. Final collation available Figure 7 Matrix representation [8]

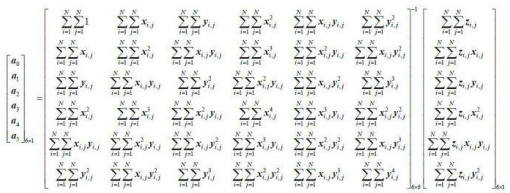

Figure7 matrix representation

2.4 Three-dimensional fitting algorithm

The three-dimensional algorithm is implemented using the fit function and curve fitting toolbox in the MATLAB language. The schematic diagram of completion is shown in Fig. 8. Since the fit function and curve fitting toolbox are MATLAB program functions, no further description is given here [9].

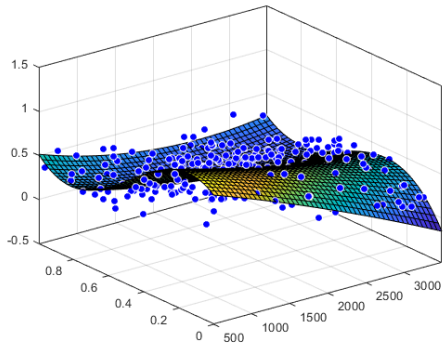

Figure8 Three-dimensional fitting plane

4. UPPER COMPUTER PART DESIGN

Because C # language and windows system good phase, so this uses C # to write the graphical interface. The graphical interface is shown in Figure 9.

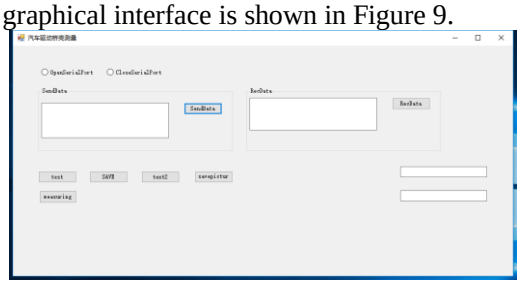

Figure9 PC interface

The upper computer industry has the serial port settings, including this interface for serial port settings, including: terminator, baud rate, data bits, parity bits, stop bits, and flow control. Serial port sending, serial port receiving data, data saving function, data processing button, image display button, result display window. The image processing part is mixed programming by C# language and MATLAB language.

5 EXPERIMENTS AND ANALYSIS

According to the above hardware and algorithm software design, measurement is performed on an analog measurement device to explore the degree of completion of the algorithm and the processing speed of the host computer. The original data shown in Figure 4 above, click on the host computer data processing, display graphics and measurement results.

The processing time of MATLAB data is displayed as 1.314855 seconds, and the processing time reaches the initial design requirement.As shown in Figure 10

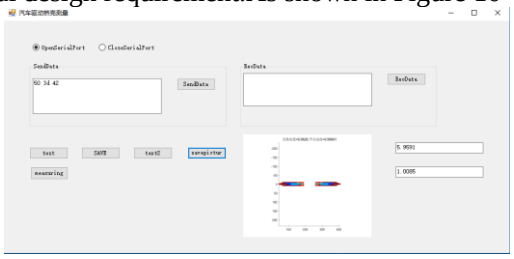

Figure10 data processing completed PC interface

6 CONCLUSION

The article proposes a set of detailed and complete algorithms for data processing, proposes streamlining of redundant data, speeds up the processing speed in a lower operating environment, and does not have much influence on the operation results.

Line-based structured light measurement technology based on active vision has significant advantages over traditional passive vision measurement techniques in measuring range, measurement accuracy, and active control, and has become the mainstream method in the field of visual measurement. Line structured light measurement is a technology driven by application requirements. With the advancement of science and technology, people's requirements for measurement accuracy, measurement efficiency, and comprehensive processing performance have been continuously improved, leading to the emergence of new problems in line structure light measurement. Although line-structured light measurement technology has been proposed for more than a decade now, there is still a long way to go in terms of improving test performance.[10]。

References

[1] Zhang Dashan. Research and application of structure motion measurement algorithm based on high-speed vision [D]. University of Science and Technology of China, 2017.

[2] Zhan Dong. The key technology of line structure light vision measurement and its application in rail transiinspection [D]. Southwest Jiaotong University, 2016.

[3] Jie Zexiao, Liu Jingxiao. On-site calibration technology for ultra-large-scale line-structured optical sensors[J]. 2015, 42(12): 290-296

[4] Hu Lihua. Monocular vision measurement theory and method for large objects [D]. Taiyuan University of Science and Technology, 2015.

[5] Yuan Xiaocui, Wu Lushen, Chen Huawei. Feature retention point cloud data reduction [J]. Optics and Precision Engineering, 2015, 23 (09): 2666-2676.

[6] IA Xiao-yong, XU Chuan-sheng, BAI Xin. The establishment of the least squares method and its thinking method[J]. Journal of Northwest University(Natural Science Edition), 2006(03):507-511.

[7] GUO Bin, WANG Bin, LIANG Xueping, YAN Chao, GUO Yuming. Non-linear least square method for fitting fault

plane parameters and its MatLab implementation[J]. Earthquake in Sichuan, 2016(03):29-33

[8] Zhu Yanhua. Analysis of Least Squares Fit Parameters[J]. Education in Times, 2012(19):151+154.

[9] Zhang Hu. Three-dimensional reconstruction of two-dimensional images in machine vision [D]. North China University of Technology, 2006.

[10] LN Naiguang, SUN Peng, GENG Xiaoping, HAN Jiandong. Research on key technologies of three-dimensional vision measurement of structured light[J]. Journal of Beijing Information Science and Technology University, 2010, 25(01): 1-5.

Design of High Precision Digital Cymometer based on FPGA

Qian Chenghui; Wang Pengfei; Wang Yulin; Yu Sijia
(College of Instrumentation and Electrical Engineering, Jilin University)

***Abstract*-A digital frequency meter with gate time of 1s based on FPGA is designed, which is used to measure the frequency of sinusoidal wave signal with high precision. The device can also measure the time interval and the duty cycle of the pulse signal, which is based on the programmable logic device (FPGA) and the embedded single-chip computer (STM32). The high-precision measurement of signal frequency is realized by using the method of equal precision frequency measurement. The absolute value of the relative error of the digital cymometer to the frequency measurement of sinusoidal signal is not more than 0.01%. The absolute value of relative error of time interval measurement for the same frequency square wave signal is not greater than 1%，and the absolute value of relative error for duty cycle measurement of pulse signal is not greater than 1%.**

***Key words*-FPGA digital frequency meter Prediction model**

INTRODUCTION

FREQUENCY measurement is a classical topic in the field of measurement science and technology[1]. There are many kinds of frequency measurement methods. Direct measurement method, periodic measurement method and equal precision measurement method. Direct measurement method measures the number of pulse within gate time by generating a gate with a fixed time. The frequency of the measured signal is obtained by conversion[2], the periodic measurement method is to measure the period of the pulse signal firstly, and the frequency of the measured signal is obtained by using the conversion relation of the frequency is the reciprocal of its period[3]. The conversion relationship between these two methods is simple. It is easy to design and realize, but it is obvious that the frequency measurement accuracy of direct frequency measurement method is higher than that of periodic frequency measurement method for low frequency signal because of the existence of ±1 counting error.

The above two methods can't meet the requirements of wideband and high precision measurement [4]. By using equal precision frequency measurement method, we can solve the problem above. The method of equal precision frequency measurement is to count the measured signal and the high frequency standard signal by using two counters respectively, when the gate time is guaranteed to be an integer multiple of the period of the signal to be measured. The counting error of the pulse signal is changed into the counting ±1 error of the high frequency standard signal, and the equal precision measurement is realized. Based on this, a method of equal precision frequency measurement is provided in this paper. Combined with programmable logic device (FPGA) and embedded single chip computer (STM32), the characteristics of high timing accuracy of FPGA and high speed of operation of STM32 are brought into full play, and the functions of time interval measurement and duty cycle measurement are developed to realize the measurement of high precision, wide frequency band and large amplitude signal.

I. DESIGN PHILOSOPHY

A. Equal precision frequency measurement principle

It is necessary to use two counters and a high frequency standard clock signal with known frequency in the process of using the equal precision frequency measurement method. The principle of the measurement is as follows: first, the preset gate signal is given, when the rising edge of the pulse signal to be tested comes, synchronous trigger circuit is used to synchronize the preset gate signal with the signal to be tested. When the actual gate signal is opened, the rising edge of the gate signal is aligned with the rising edge of the signal to be tested. In the actual gate time, a counter is used to count the test pulse signal. Count the standard signal with another counter. After, when the rising edge of the signal to be measured comes, the gate closes and the two counters stop counting. Combined with the frequency of the standard high frequency signal and according to the conversion relation of the equal precision measurement frequency, the frequency of the signal to be tested can be obtained. The measuring principle is as shown in figure 1[5].

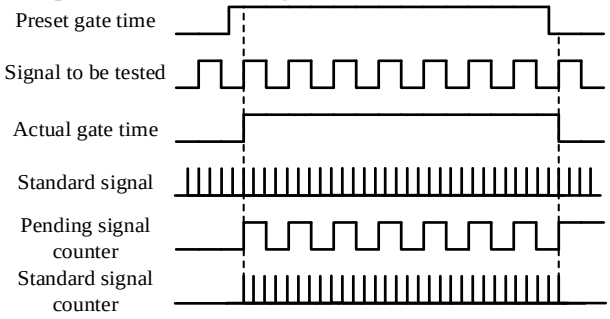

Fig.1. Principle diagram of equal precision frequency measurement method

Assuming the gate time is T, the count of the signal to be measured is *N1*, the counter of the standard signal is *N2*, the frequency of the standard signal is *f0*, and the frequency of the signal to be tested is *fx*, then

$$N_1 = T \times f_x \quad (1)$$

$$N_2 = T \times f_0 \quad (2)$$

Therefore, the frequency of the pulse signal to be measured is:

$$f_x = \frac{N_1}{N_2} f_0 \quad (3)$$

Combining the whole derivation process with figure 1, we can find that the actual gate time is not a fixed value, but a value related to the pulse signal to be measured and is exactly an integer multiple of the period of the signal to be tested. Therefore, there is no ±1 error in counting the measured pulse signal[6]. However, the actual gate time is not synchronized with the standard signal, so there is still ±1 error in counting the standard pulse signal. So according to the formula (3), will have

$$\Delta f_x = \frac{f_0}{N_2}\Delta N_1 - \frac{N_1}{N_2^2} f_0 \Delta N_2 + \frac{N_1}{N_2}\Delta f_0 \quad (4)$$

In the formula, $\Delta N1 = 0$, $\Delta N2 = \pm 1$, so the error of the frequency measurement is as follows

$$\delta = \frac{\Delta f_x}{f_x} = \frac{\Delta f_0}{f_0} \pm \frac{1}{N_2} \quad (5)$$

By formula (5), it can be seen that the frequency measurement error is only related to the error of the standard signal and the value of the *N2*, but not to the frequency of the signal to be measured. In this paper, the phase-locked loop inside the FPGA is used to produce a standard signal with a frequency up to 200 MHz. Therefore, the frequency stability is extremely high, and the error can be neglected basically, that is $\Delta f0/f0 = 0$. Assuming that the true frequency of the signal to be measured is *fx'*, then

$$f_x' = \frac{N_1}{N_2 \pm \Delta N_2} f_0 \quad (6)$$

$$\delta = \frac{|f_x' - f_x|}{f_x} \times 100\% \quad (7)$$

Simultaneous formula (3), (6), (7), then

$$\delta = \frac{\Delta N_2}{N_2} \times 100\% \le \frac{1}{N_2} = \frac{1}{T f_0} \quad (8)$$

As can be seen from formula (5) and (8), the longer the gate time is and the higher the frequency of the standard signal is, the smaller the measuring error of the equal precision measurement method is[7]. The frequency doubling of the external clock signal from the FPGA internal phase-locked loop to 200MHz, the gate time is 1 s, so the accuracy is 5 ×10-7.

B. Time interval measurement principle

When measuring the time interval, using the XOR gate to perform the two square wave signals input to FPGA firstly. When the two signals are in different levels at the same time, the XOR gate outputs a high level, whereas the output is low. So that, the high level duration of the pulse signal generated by the operation results is the time interval between the two square wave signals. In the gate time, the standard signal is counted by a counter during the high level duration of the signal after the gate. The frequency of the counting result divided by the standard signal is the time interval between the two signals. The measurement principle of the time interval is shown in figure 2.

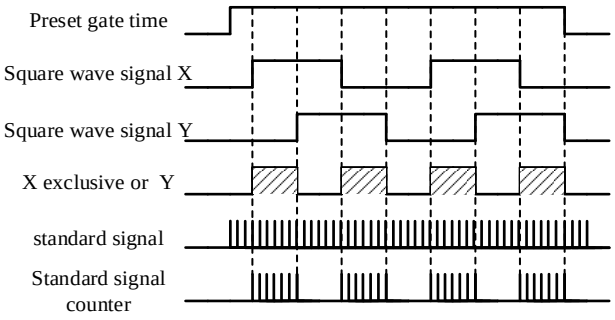

Fig.2. Principle diagram of time interval measurement

C. Duty cycle measurement principle

The principle of duty cycle measurement is similar to the principle of time interval measurement. The difference is that only input one pulse signal, and the high and low level time of pulse signal in a period of one cycle need to be counted in a gate time. The duty cycle is a high-level duration meter numerical divided by the total count.

Ⅱ. CONCEPTUAL DESIGN

The system can measure the frequency, duty cycle and time interval of the signal inputted. But the FPGA, as a digital logic device, can only processes the digital signal. Therefore, a broadband amplifier circuit and a hysteresis comparator are designed to form the input analog signal into a digital signal and input it to the FPGA for counting. The overall design scheme is shown in figure 3.

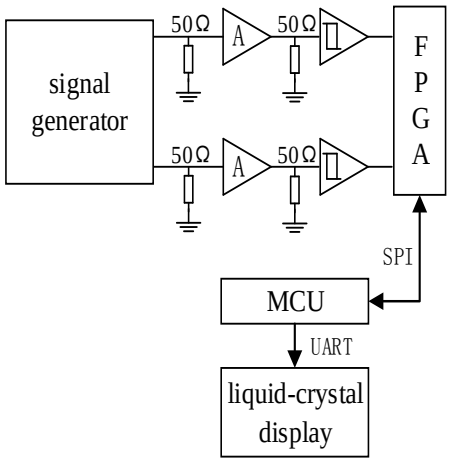

Fig.3. System block diagram

The signal to be measured is generated by the signal generator and transmitted to the two-stage cascade wideband signal amplifier after 50Ω matching. The signal is amplified 100 times, and the amplified signal is transmitted to the high-speed hysteresis comparator after 50Ω matching. The analog signal is shaped into a pulse signal and transported to the FPGA to count. After counting, the counting result is sent to the single chip microcomputer through the SPI bus, and the measurement result is calculated by the single chip microcomputer according to the principle formula of measurement. After rounding the result, the data is printed to the TFT LCD screen for display. Because the amplitude of the input signal varies in a large range, the output signal may appear positive and negative

symmetrical amplitude clipping distortion after amplification by the wideband amplifier. However, because the threshold median of the latter stage hysteresis comparator is set to 0 level voltage and the threshold width is 17mV, the output signal of the comparator still retains the characteristics of input frequency, duty cycle and time interval.

A. Design of hardware circuit

The hardware circuit consists mainly of a broadband amplifier and a high speed hysteresis comparator. The schematic diagram of the broadband channel amplifier is shown in figure 4.

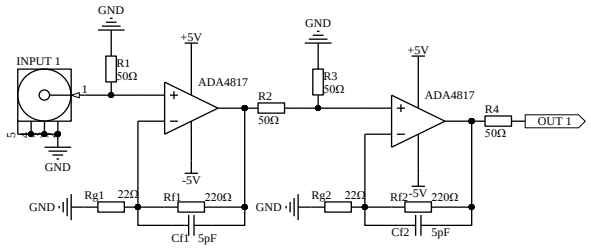

Fig.4. Broadband amplifier circuit

The wideband amplifier uses a broadband, low noise voltage feedback type operational amplifier chip ADA4817, and it has a 1.05GHz bandwidth with 870V/μs slew rate, and with a high voltage pendulum ratio of 4nV/√Hz[8]. Under the condition of 10 times amplification per stage, the amplifier cascade amplifies by 100 times. The parasitic capacitance of the chip is 0.1pF. Considering that the feedback resistor can form a pole with the parasitic capacitance of the pin in high frequency, it is easy to cause the operational amplifier to oscillate in the high frequency region, so it parallels a 5pF capacitor on the feedback resistor *Rf*. The open loop gain in the high frequency region is reduced and the OPA oscillation is avoided. Because the frequency band of the signal to be tested is up to 100 MHz, the signal is input by the SMA RF connector.

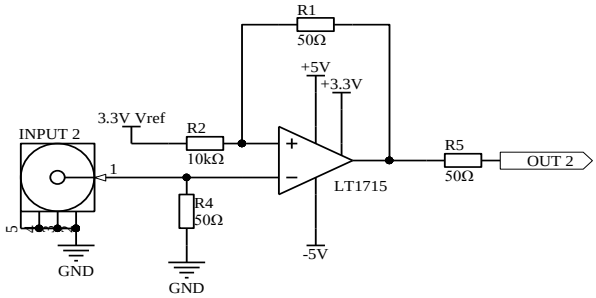

Fig.5. High speed hysteresis comparator circuit

The circuit schematic diagram of hysteretic comparator is shown in Fig. 5. LT1715 is used for high-speed comparator chip. The comparator can compare 150 MHz signal and has independent input and output power supply function.

Circuit using inverse hysteresis comparator, and generates a 3.3V reference voltage by linear regulator chip AMS1117-3.3[9] in the inverse end as a reference voltage. The power supply input is ±5V, you can compare the bipolar signal output by +3.3V power supply, ensure the output signal is a unipolar digital signal, transfer into FPGA[10]. According to the working principle of the comparator threshold voltage, *VTH* is

$$V_{TH} = \frac{R_1 V_{REF}}{R_1+R_2} + \frac{R_2 v_o}{R_1+R_2} \quad (9)$$

Because the output high voltage is *VOH* = 3.3V and low voltage is VOL = 0V, the higher threshold voltage is *VT*+ = 32.8 mV, and the lower threshold voltage is *VT*- = 16.4 MV, so the return voltage is as follows

$$\Delta V_T = V_T{}^+ - V_T{}^- = 16.4\text{mV} \quad (10)$$

B. Design of software

The software function part includes the FPGA counting sequential logic part and the calculation and display part by using STM32. The counting logic circuit of FPGA is shown in figure 6.

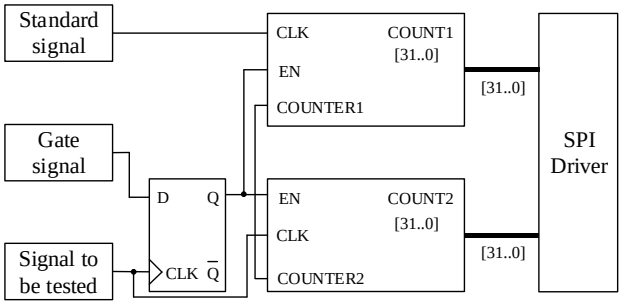

Fig.6. FPGA logic circuit diagram

The actual gate signal is an enabling signal of two counters. After synchronizing the gate signal and the signal to be measured by D flip-flop. The rising edge of the actual gate signal is aligned with the rising edge of the signal to be tested. Through two 32bit counters, the standard signal and the signal to be measured are counted, and the counting results are fed into the SPI driver through the internal parallel bus. The calculation value is sent to the single chip computer by SPI bus.

STM32 program flow chart is shown in Fig. 7. STM32 completes the data, operation and display functions. When the MCU receives the SPI interrupt from FPGA, it begins to receive data, which contains the frequency, time interval and duty cycle data flag bits. The valid data is taken out according to the mark bit and the operation result is displayed on the LCD screen.

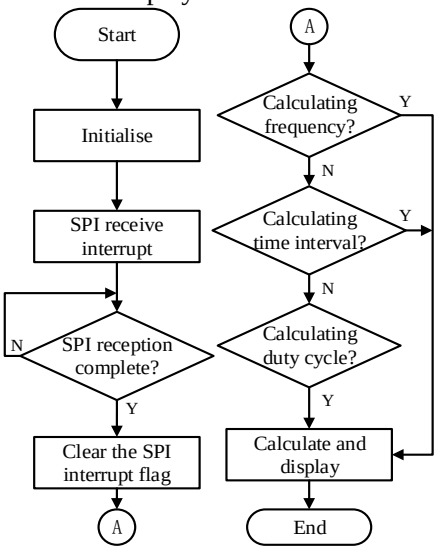

Fig.7. Flow chart of MCU program

III EXPERIMENT

A Frequency measurement experiment

Frequency measurement of sinusoidal wave: frequency range is 1 Hz ~ 100 MHz, effective value range is 10 mV ~ 1 V. Changing the frequency and amplitude of input signal and record the result in Table Ⅰ. From Table Ⅰ, we can see that change the frequency and amplitude of signal will affect the accuracy of frequency measurement. However, the relative error of the whole measurement is not more than 0.01%. Because of the temperature drift of the external crystal oscillator used in FPGA, the standard pulse signal is jitter, which affects the measurement accuracy, but the overall precision is better than 0.01%.

TABLE Ⅰ

Experimental data of frequency measurement and error

effective value	10mVrms	100mVrms	1Vrms
Frequency	Result(Hz)	Result(Hz)	Result(Hz)
	Error	Error	Error
1 Hz	0.999969	0.999995	0．999922
	0.0031%	0.0005%	0.0078%
1 MHz	100005	1000000	1000005
	0.0005%	0	0.0007%
100 MHz	100001368	100000247	100001740
	0.00137%	0.000247%	0.00174%

B Time interval measurement experiment

Square wave time interval measurement with same frequency: frequency range is 100 Hz ~ 1 MHz, peak to peak value is 50 mV ~ 1 V, the frequency and amplitude of each input signal are the same, changing the frequency, amplitude and time interval of the input signal. The results of time interval measurement are recorded in Table Ⅱ. It can be seen from Table Ⅱ that the change of frequency and amplitude of input signal will affect the measurement accuracy of time interval, but the overall relative error of measurement is less than 1, which meets the design requirements. Figure 8 is the final design of physical map of this system.

TABLE Ⅱ

Experimental data of time interval measurement and error

Frequency	Input Voltage	Time Interval	Result	Error
100 Hz	1Vpp	2ms	1.986ms	0.700%
1 kHz	200mVpp	200μs	199.156μs	0.422%
1 MHz	50mVpp	200ns	199.152ns	0.424%

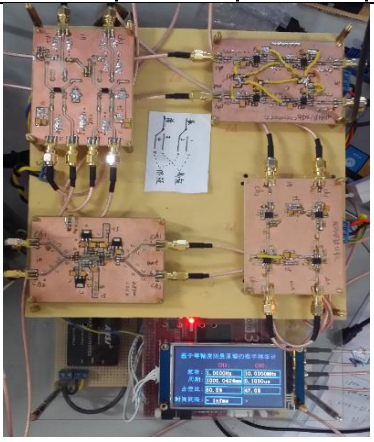

Fig.8. System physical diagram

C Duty cycle measurement experiment

Pulse duty ratio measurement: frequency range is 1 Hz ~ 5 MHz, the peak to peak value ranges is 50mV ~ 1V, the test process of fixed input signal peak 50mV, the change of the input signal frequency and duty ratio, time interval measurement results recorded in Table Ⅲ. From the experimental data and error calculation results in Table Ⅲ, it can be seen that changing the frequency of input signal will bring errors to the measurement of duty cycle, but the overall relative error is less than 1%, which meets the design requirements.

TABLE Ⅲ

Experimental data of duty cycle Measurement and error

Duty Ratio	10%	50%	70%	90%
Frequ-ency	Result(Hz)	Result(Hz)	Result(Hz)	Result(Hz)
	Error	Error	Error	Error
1 Hz	10.024%	50%	70.0071%	89.579%
	0.24%	0	0.0101%	0.468%
1 MHz	9.9951%	50%	69.995%	89.999%
	0.049%	0	0.00714%	0.00111%
5 MHz	10.074%	50.083%	70.235%	90.624%
	0.74%	0.166%	0.336%	0.693%

Note: The peak value of the fixed input signal during the test is 50 mV.

Ⅳ CONCLUSION

The high frequency wideband operational amplifier and high-speed hysteresis comparator circuit constitute a double amplification and comparison circuit. Amplify the pulse signal, the sinusoidal, and rectangular waves with different amplitudes by 100 times, the shaping circuit is composed of a high-speed comparator input level always receives the signal amplitude medium, using hysteresis comparator circuit form improved circuit the stability of the system. With simple circuit to measure the relative error within 100 MHz sine wave does not exceed 10-4. FPGA as the main chip, VHDL described as "precision frequency measurement" logic circuit of high-speed parallel processing, with the help of embedded microcontroller STM32's internal resources, improve the efficiency of the system. The method accords with the development trend of stable, high efficiency, low power consumption and low cost of instrument system nowadays, has certain practical significance and practical value. The works in The Electronic Design Competition of Jilin University in 2017 has won the first prize of the school level.

References

[1] Hu Wenjing, Zhang Baiguo, Liu Xiang, etc. FPGA implementation of High Precision Frequency Measurement based on range Self-tuning [J]. Application of electronic technology. 2012(1):73-76

[2] Wang Hui. Implementation of high speed and high precision frequency measurement system based on FPGA [J]. Sensor world, 2006(1):27-29.

[3] Ning Zehong, Xu Dawang, Dong Zhanyong. Frequency measurement technique based on frequency conversion [J]. Journal of Measurement Science and Instrumentation. 2013, 4(2):146-149.
[4] Hao Tongguan, Cheng Ming. Design of constant Precision Cymometer based on FPGA Nios Ⅱ [J]. Electronic measurement and instrument. 2009, 46(2):56-58.
[5] Zhou Songjiang, Wang Lihua, Gao Shihao, Zhang Heng. Design of Equal Precision Multifunctional Frequency Meter based on FPGA [J]. instrumental technique. 2017(03):1-3+7.
[6] Yan Xilan, Xie Jingming, Xiong Maohua. Research and Design of High Precision Digital Cymometer based on
[7] FPGA and VHDL [J]. Computer Optical disk Software and Application. 2014(15):91-94.
[8] Mao Zhide, Lv Weishan. Design of equal precision frequency meter based on FPGA [J]. Electronic measurement technology. 2006, 29(4):85-86.
[9] Wideband, ultra-low-noise, voltage-feedback operational amplifier with shutdown (Rev.E)[S].2008.
[10] AMS1117-3.3 Datasheet[S].2012
[11] Liao Yan, Chen Lixue, Lai Chunhong, etc. Design of Isoprecision Cymometer IP Core based on FPGA [J]. Application of electronic technology. 2007,33(12):21-23

Study on suppression of voltage spike in high frequency electromagnetic transmitter

Li Gang; Yanyu Chen; Luyao Tang; Yu Sheng
(College of Instrumentation and Electrical Engineering, Jilin University)

***Abstract*-In this paper, the reasons of voltage spike in high-frequency electromagnetic transmitter are analyzed. Based on the traditional full-bridge inverter circuit, an analysis method of suppressing voltage spike is explored. The parameters of the buffer circuit are optimized, and the voltage spike of the high-frequency electromagnetic detection transmission bridge is reduced. The simulation results verify the performance of the proposed method. And an efficient, stable electromagnetic transmitter can be designed.**

***Keywords*-Electromagnetic Transmitter; Inverter; Voltage Spikes; Suppression; Snubber Circuits**

I INTRODUCTION

WITH the development of science and technology in human society, the use of electromagnetic methods for geological exploration, resource exploration, urban construction, and military exploration has become a general trend. The secondary field signal is generated by the artificial field exciting the underground material, and the information such as the structure and composition of the underground material are obtained by receiving the secondary field signal. However, as a full-bridge inverter circuit, due to the high-speed switching-off and the presence of inductance in the main circuit of the full-bridge, there is a large voltage spike in the output side of the transmitter, which is not only a great threat to the switch but also a serious EMI problem. To a great extent, the quality of the transmitted waveform is reduced, so that the established primary field loses its stability, and errors in repeated measurement or sweeping work are introduced to make the detection result lose consistency[1].

In this paper, the generation of voltage spikes is analyzed in detail, and voltage spikes are suppressed by designing a reasonable absorption circuit and rational layout of the circuit layout and the selection of component.

II CAUSE OF HIGH FREQUENCY VOLTAGE SPIKE

In this paper, the MOS tube is used as the switch of the full-bridge inverter circuit. Under the drive of the special drive circuit, the MOS tube can be divided into two states: open and open. The voltage spikes are mainly generated during the high-speed switching of MOS transistors. Since the MOS transistors are turned on and off, the following half-bridges are used to explore the causes of high-frequency electromagnetic emission spikes[2].

Figure 1 shows the main circuit of one phase of the inverter full-bridge circuit. The main structure is the DC side supporting capacitor, the switching transistor MOS tube, the load, and the diode[3].

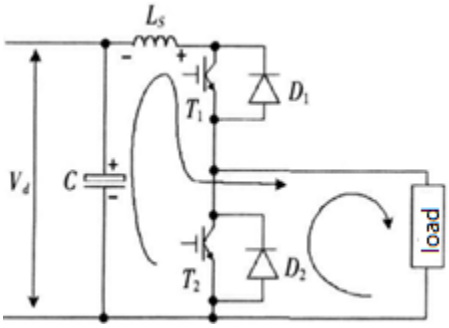

Fig.1 Typical main loop structure of inverter circuit

Assume that the circuit is an ideal circuit (L_s=0), when the switch T_1 is turned off, because the load is inductive load, the current can not be mutated, as shown in the figure, the current through the freewheeling, so that the voltage of both ends of T_1 rise and become $V_d + V_{D_2}$ (freewheeling diode forward conduction voltage)[4].The forward voltage of the diode is usually negligible in large voltage circuits, and the impact on the peak voltage is less.

In fact, the bridge circuit is not an ideal circuit ($L_S \neq 0$), L_s mainly including the parasitic inductance of the DC side capacitor, the stray inductance of the main circuit, and the parasitic inductance of the switching device. Due to the high-speed switching of the switch tube, the current of L_s at both ends occurs changes. This twill excite large voltage spikes at both ends (directions shown in the figure as follows)[5].

In the high-frequency electromagnetic emission full-bridge circuit, it can reach 2~3KA/μ. Although the inductance of the main loop can be very small, it can still generate a large voltage spike.

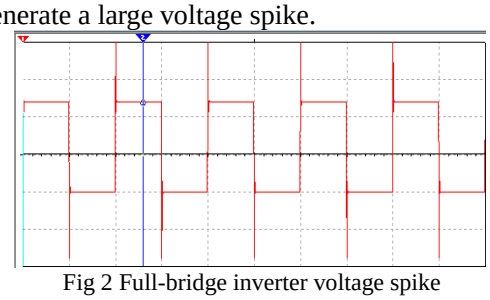

Fig 2 Full-bridge inverter voltage spike

According to the circuit simulation, we can see that the amplitude of the voltage spike exceeds the amplitude of the signal by more than double[6].

III VOLTAGE SPIKE ABSORPTION CIRCUIT

Voltage spike absorption circuit, also called snubber circuit. Absorption circuit does not necessarily improve the conversion rate of the entire system, but it has a significant inhibitory effect on the spikes in the circuit. There are three commonly used absorption circuits:

1) C-type absorption circuit, which can absorb the spike voltage in the switching state of the switch by connecting the high-frequency capacitor in parallel with the bus end of the switching device.However, as the power level increases, the parasitic inductance on the bus may be damped and oscillated, which is not suitable for high-power transmitters[7].

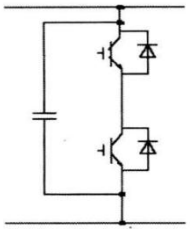

Fig 3 C-type buffer circuit

2) RC type buffer circuit.

Compared with the C-type snubber circuit, the RC-type snubber circuit works better, but the same applies only to low-power inverters.

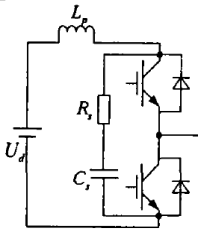

Fig 4 RC buffer circuit

3) A typical RCD buffer, when the switching device is turned off, the absorption capacitor is charged, so the voltage rise is limited, the voltage rises slowly, until the capacitor charge is greater than the DC side bus voltage, through the resistance discharge to the power supply, feedback energy.The buffer circuit has a significant suppression effect on voltage spikes and is suitable for high-power inverter circuits. The only disadvantage is that the circuit losses are too high and the conversion rate is low[8].

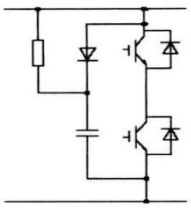

Figure 5 RCD buffer circuit

4) RCD clip clamp snubber circuit

This buffer circuit not only can suppress the peak, the circuit loss is small, is often used in the high-power high-frequency circuit, it is the ideal buffer circuit.

When the energy in the switch L_s turns off, the energy is conserved in C_s ,by the law of energy conservation,we can get that:

$$\frac{1}{2}L_S I^2 = \frac{1}{2}C_S \Delta U^2$$

Among them, the peak voltage generated when the switch is turned off is the ΔU , In order to guarantee the overvoltage energy of the switch tube before it is turned off, the RC time constant is less than 1/3 of the switching period, so there is

$$R_S \le \frac{1}{3C_S f_s} .$$

IV INVERTER FULL-BRIDGE CIRCUIT SPIKE SUPPRESSION SIMULATION

Multisim software is used to simulate the circuit design. The simulation process assumes that the main loop bus inductance is 200nH and the switching frequency is 10 kHz. According to the calculation simulation circuit parameters designed, the values of the inductor and capacitor are,

$$C_s = 5\mu F \;\; R_s = 5\Omega .$$

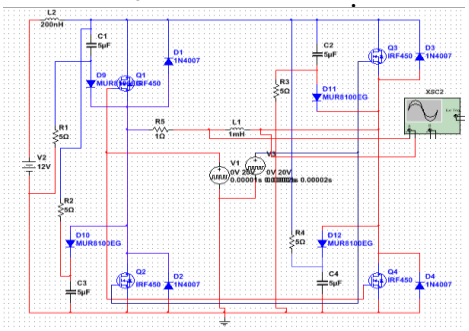

Fig 7 Full-bridge inverter circuit with buffer circuit added

The simulation results are shown in Figure 8.

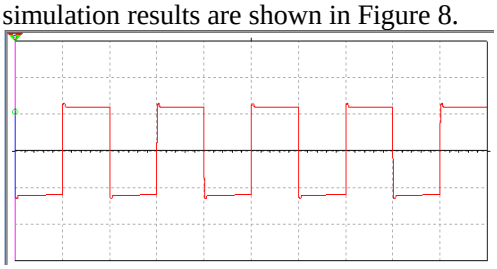

Fig 8 spike diagram after adding a buffer circuit

The above figure shows that after adding the RCD snubber circuit, the voltage spikes are greatly reduced.

V CONCLUSION

In this paper, the causes of high-frequency emission spikes are analyzed in detail, and the method of suppressing voltage spikes is found. The main analysis is to suppress the voltage spikes by adding buffer circuits. By comparing the characteristics of various snubber circuits, the circuit simulation of RCD limiting clamped snubber circuit was carried out, and its parameter calculation formula was given. This study can reduce the voltage spikes in high-frequency electromagnetic detection bridges. Provides an efficient, stable, and compliant primary field signal for electromagnetic detection systems.

References

[1] Chen Jiabiao.Design and Implementation of RCD Clamp

Flyback Converter[J].Communication Power Technology,2002.10

[2] Zhang Xiaobin.Simulation and experimental research of RCD snubber absorption circuit[J]

[3] Ning Dalong. Gate RCD active voltage equalization circuit for IGBT series devices[N].Electrical Engineering Journal,2013.2

[4] Liu Bin. Research on IGBT turn-off voltage spike suppression for high-power inverter power supply[J].Ship Science and Technology,2009.12

[5] Liu Guowei.Research on RCD clamp circuit in flyback converter[J]

[6] Wang Juan.Mechanism analysis of IGBT voltage surge in full-bridge inverter circuit[M].Hohai University, 2006.6

[7] Zhou Jing.Research and implementation of full-bridge high-frequency inverter circuit[M].Electronic Test,2009.7

[8] Tian Songya.Simulation of IGBT working process in bridge inverter circuit[M], 2006.7

External Triangle Thread Detection Based on Digital Image Processing Technology

CHEN zhi-yu; SUI xue-ming; HE gui-shan; LIU ming-yang
(School of Instrtument Science and electrical engineering, Jilin University)

***Abstract*-A contactless detection system for the external triangle thread with the digital imaging processing technology and visual measurement technology was presented. The system used image manipulation method to measure geometrical parameters,including binary image production, edge detection, contour hunting and the thread geometrical parameter calculation. Sizes of a external triangle thread detected by suggested method were given, and the feasibility and correctness of the method were validated theoretically and practically.**

***Key words*-digital image processing; visual measurement; thread; edge detection**

0 THE PREFACE

VISUAL measurement based on digital image processing technology is currently a very popular technology, including industrial, military, medical and many other fields have used this technology[1]. The traditional thread detection method has low work efficiency and the accuracy of the obtained result is not high. Therefore, it is a trend to apply visual measurement technology to thread inspection[2]. This detection method first uses the camera to take a picture of the thread, and then sends the picture to the computer. The processing of the image is completed by a thread parameter detection program, such as denoising, enhancing the image, binarizing the image, etc., and then threading the image to the edge. Detection and extraction, the edge of the information extracted from the thread parameters, determine the thread is qualified, the entire detection process without the participation of people, the computer automatically completed, with high efficiency, high precision, low cost characteristics[3].

1 SYSTEM STRUCTURE AND WORKING PRINCIPLE

The system consists of a bracket, a bolt fixture, a CCD camera, a light source, and a computer. The specific working principle is that the image acquisition environment is set up by a bracket, a bolt fixture, and a light source, and then the image is captured by a CCD camera and transferred to a computer. The image is digitally processed to obtain the outline image of the thread. There is a one-to-one linear relationship between the thread outline image (indicated by the number of pixels) and the actual size (in millimeters), ie the measurement ratio between the two is constant K. It is determined by the magnification ratio of the objective lens and the magnification ratio of the CCD device. A certain algorithm calculates the geometric parameters of the thread image and multiplies it by the proportional constant K to calculate the true geometrical parameter of the thread. Finally, it compares with the standard size to judge whether it is qualified or not[4].

2 IMAGE ACQUISITION AND PROCESSING

Using SJM-500 industrial camera, USB driver, like the original size of 2.2 * 2.2um, resolution of 640 * 480. We need to extract the outline of the thread, do not need to know the surface characteristics of the thread, so choose the backlight illumination, as shown in Figure 1. The thread detection system program is written in MATLAB. The main flow of thread image digital processing is image filtering, image enhancement, edge detection, image measurement, thread size parameter calculation, display, and output[5].

2.1 Image filtering

Because outside noise and electromagnetic interference will cause the image captured by the camera to contain noise, the noise is usually randomly generated, and therefore has irregularities in distribution and size[6]. In order to make the image closer to the real situation, image denoising is needed, that is, filtering.

The method of image filtering depends on the characteristics of the noise itself. In general, the method of neighborhood averaging is used to reduce noise in the spatial domain. In the frequency domain, since the spectrum of noise is often in the high frequency range, various forms of low pass are used. Filtering method to remove noise.

In the spatial domain, the smoothing of the image often adopts mean filtering or median filtering. Mean filtering implements a neighborhood operation through a template operation. That is, the result of a certain pixel is not only related to the gray level of this pixel, but also the pixel of its neighboring region. Value related. The description of a template operation in mathematics is a convolution operation. The idea of the smooth template is to remove the mutation point by one point and several points around it, so as to filter out certain noise, but the image has a certain degree of ambiguity, and reducing the image blur is one of the major problems in image smoothing processing. It depends on the nature of the noise itself. The main problem of the mean filter is that it may blur the sharp discontinuity in the image, but the nonlinear filter algorithm can both eliminate the noise and keep the details of the image, so the median filter is the simplest nonlinear filter, it uses an odd number The template window of points, which overlaps the center of the window with the pixels to be processed in the image, reads the gray value of each corresponding pixel under

the template, sorts the gray scale from big to small, and finally takes the median of the sequence to replace the template center. Pixel value[7]. Figure 2-1 is the original image, Figure 2-2 is the mean filter, Figure 2-3 is the median filter, you can see from the figure, the average filter after the template becomes larger is more blurred, and the median filter after the image is uniform The edge is more obvious.

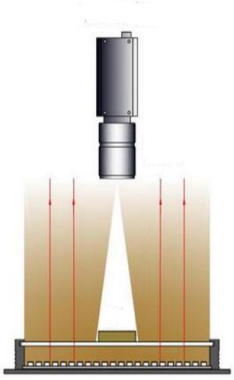

Fig.1 Backlighting schematic

Fig.2-1 Original image

Fig. 2-2 3*3 mean filter Fig.2-3 Median filter

2.2 Image enhancement

The top hat transform is the difference between the original image and the result of the open operation of the image. This transform was originally named because it uses an upper flat cylindrical or parallelepiped shape (like a top hat) as a structural element. The low-hat conversion is the difference between the closed operation result of the image and the original image. The high and low cap conversion is defined as:

Top Hat Transform: That (f) = f- (f○b)

Low Hat Conversion: Bhat(f)=(f·b)-f

An important use of high and low hat shifts is to correct the effects of uneven light, high hats are used for bright objects on dark backgrounds, and low hats are used for the opposite. Therefore, the high-low cap conversion can be used to enhance the digital image, because the high-hat transform has some characteristics of high-pass filtering, emphasizing the target's grayscale peak, enhancing the edge information of the image, and the low-hat transform can find the valley value in the image. , highlighting the boundaries between the connected objects, so the combination of high and low cap conversion can make the image foreground and background grayscale further stretched, highlighting the relevant goals and details, and play an image enhancement role. The original image plus the results of the top hat transform, and then subtract the low-hat transform, can effectively improve the contrast of the image and improve the edge detection effect.

2.3 Image edge detection and extraction

The edges of the image are the basic features of the image. The so-called edge refers to the collection of those pixels whose stepwise changes in the surrounding pixel gray level or roof changes. The edges are widely present between the object and the background, between the object and the object, between the primitive and the primitive. Therefore, it is an important feature that image segmentation depends on. The edge of the object is the difference in the characteristics of the image within the local area, and it is reflected in the discontinuity of the image (such as the mutation of the gray level, the mutation of the texture structure, etc.). Large-scale discontinuities become boundaries. The types of edges can be divided into two types: one is called a step edge, and the gray values of pixels on both sides are significantly different; the other is called a roof-like edge, and it is located in the gray value from increasing to decreasing[8]. Turning point. Edge detection is to outline the outline of each object with edge points, so as to analyze whether the image contains some objects that need to be identified. If a pixel falls on the boundary of an object in the image, its neighborhood will become a grayscale change band. Two of the most useful features for this change are the rate of change and direction of the gray scale, which are each represented by the magnitude and direction of the gradient vector. Because the edge point is generally located at a position where the gray value in the image changes drastically, that is, where the gray value derivative is larger or larger, the classical edge extraction method is to examine the change of the gray level of each pixel of the image in a certain area. The detection of edges using the variation of the edge's proximity to the first-order or second-order directional derivatives is called the edge detection local operator method. The edge feature extraction operator subtracts the original image feature value from the transformed image feature value through the translation transformation, and the edge feature of the image is highlighted after the transformation. The purpose of the edge detection is to extract the boundary of the thread. After comparing operators such as Roberts, canny, and sobel, we decided to use the Sobel operator for edge detection. The Sobel operator weights the influence of the pixel position, so the effect is good, and it has a smooth effect on noise, and can remove some The pseudo-edge provides more accurate edge direction information, as shown in Figure 4.

Fig.3
Enhanced

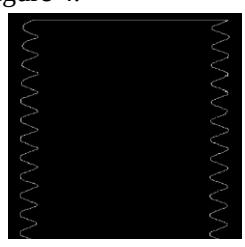

Fig.4
Sobel operator edge detection

3 PARAMETER CALCULATION

3.1 System calibration

After digitizing a two-dimensional graph, the computer will have a matrix of M rows and N columns. The matrix represents each pixel in the image and the coordinate system is established so that each pixel has its own coordinate point. The row coordinates in this coordinate system are from From top to bottom, the column coordinates increase from left to right. In this way, the coordinates of a point represent a pixel and they are discrete. Due to system imaging and lens magnification, the ratio of actual size to direct pixel is not constant, not a fixed value, but if the experimental system is fixed, this ratio can be obtained by calibration. In actual operation, a target with a length of L1 can be used to obtain its image, and after processing such as filtering, binarization, and edge detection, its pixel size L2 is obtained, and the system measurement ratio K=L2/L1.

3.2 Thread parameter measurement

Assuming that the bolt to be tested is placed horizontally, the coordinates of the four vertices are M1, M2, P1, and P2. The distance between M1, M2, and P1 and P2 is determined. The distance is the long side of the rectangle bounded by the bolt, and the short is the external. For the short side of the rectangle, calculate the midpoint coordinates G1 and G2 of the two short sides. From the two midpoints, you can get the linear equation of a parallel line of the thread axis, as follows:

$$Y - M1*Y = \frac{M2*Y - M1*Y}{M2*X - M1*X}(X - M1*X) \quad (1)$$

The thread diameter d is the diameter of an imaginary cylinder tangent to the external thread root or the female thread crest.

When the slope of this parallel line is present and not 0, the parallel line is moved upwards and stops moving when it is tangent to the upper thread bottom. The tangency condition is that the pixel value of the intersection point is (0, 0) becomes (255, 255). Calculate the equation of the parallel line at this time Yl=k*X+bl. Similarly, move the parallel line downwards when it is tangent to the bottom of the thread. It stops moving, and the tangency condition is that the pixel value of the intersection point changes from (0, 0) to (255, 255), and then the equation of this parallel line Y2=k*X+b2 is calculated, so that the two parallel The distance between the lines is the trail of the thread. The formula for the trail is as follows:

$$d = \frac{|b1 - b1|}{\sqrt{1 + k^2}} \quad (2)$$

The major thread diameter D is the diameter of the imaginary cylinder tangent to the male thread crest or the female thread. Let b3=b1+30, Y3=k*X+b3, move this line downward, and stop moving when it is tangent to the top of the thread crest. The tangency condition is that the pixel value of the intersection point is (0 , 0) becomes (255, 255), calculate the equation of this straight line Y3=k*X+b3 at this moment, make b4=b2+30, Y4=k*X+b4 again, move this straight line up again It will stop moving when it is tangent to the crest of the thread below. The tangency condition is that the pixel value of the intersection point changes from (0, 0) to (255, 255), and then the equation of the line at this time Y4=k*X+b4. In this way, the distance between two parallel lines is the major diameter of the thread,. The formula for the major diameter is as follows:

$$D = \frac{|b3 - b4|}{\sqrt{1 + k^2}} \quad (3)$$

Pitch measurement:

The pitch is the axial distance between the corresponding points on two adjacent teeth of the thread. We have obtained the linear equations Yl=k*X+bl and Y3=k*X+b3. Now we need to find a scan line that intersects the thread, so let b=(b1+b3)/2, The linear equation of the scan line is Y=k*X+b. This scan line intersects with the thread to obtain a series of intersections p1, p2, p3, p4, as shown in Figure 5. The distance between p1 and p3 is the pitch P1. The distance between p2 and p4 is the pitch P2, and in turn, the value of three pitches is taken and the final pitch P is obtained using the formula P=(P1+P2+P3)/3.

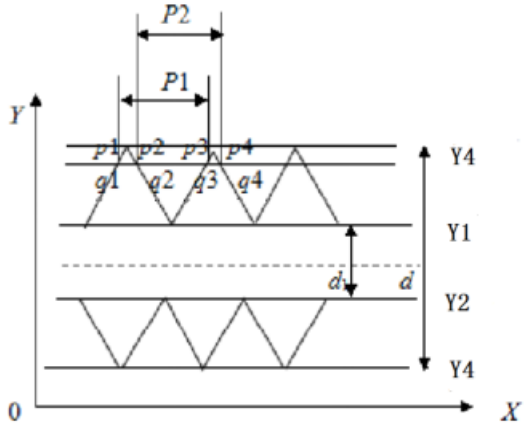

Fig.5 Measurement schematic

Tooth angle measurement:

The profile angle α is the angle between the two sides of the thread profile in the axial section of the thread. As shown in Figure 6.

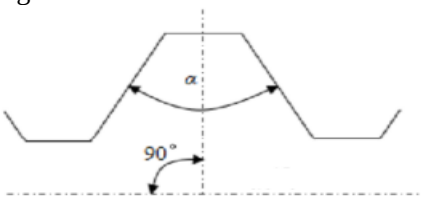

Fig.6 Thread Form Angle

In the process of finding the pitch, we get a series of intersections of the scan line Y=k*X+b and the thread line so that b'=b+3. Scan the thread line with the scan line Y=k*X+b' Get a series of intersections q1、q2、q3、q4. Knowing the coordinates of p1 and q1, we can find the equation of the line where these two points lie. The formula is as follows:

$$Y - p*Y = \frac{q*Y - p*Y}{q*X - p*X}(X - q*X) \quad (4)$$

Similarly, the straight line equations of p2 and q1 are obtained. The angle between two straight lines is the angle of the tooth profile and can be obtained by the following formula:

$$\partial = \arctan\left(\left|\frac{q1*Y-p1*Y}{q1*X-p1*X}-\frac{q2*Y-p2*Y}{q2*x-P2*x}\right| \Big/ \left(1+\frac{q1*Y-p1*Y}{q1*X-p1*X}*\frac{q2*Y-p2*Y}{q2*x-P2*x}\right)\right) \quad (5)$$

Find the value of the three profile angles α and use the formula α=(αl+α2+α3)/3 to find the value of the final profile angle α.

4 Experimental results

The thread identified in this experiment is an ordinary triangular thread. In the experimental setup, the main optical axis of the CCD cannot be guaranteed.

The thread axis is completely vertical and there will be a certain angle. In practice, according to the CCD, a right-angled edge of the triangular ruler is closely attached to the experimental plane of the thread, and the angle of the CCD is adjusted by another right-angled edge until the right-angled edge is imaged at a point on the CCD photosensitive surface. The smaller angle of the included angle has negligible effect on the result.

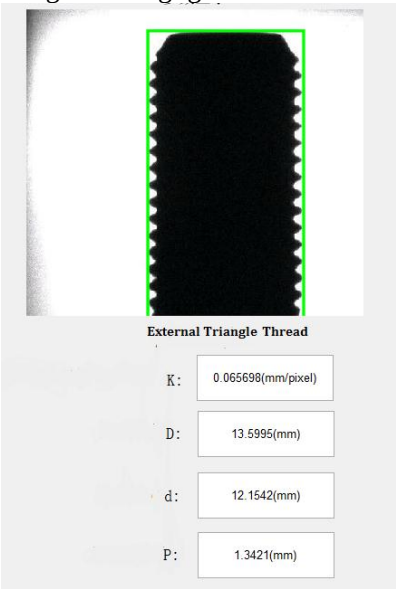

Fig.7 Measurement results

5 Error Analysis

In the actual manufacturing process of the camera, the distance between the pixels on the camera imaging surface is not uniform. In addition, the focus adjustment process is manually performed and can not be guaranteed to be accurate. All these factors will eventually lead to The measurement results are inaccurate or have errors[9]; the surface of the thread is uneven, and the boundary forms a two-dimensional surface. When taking a picture of the thread, the bolt and the camera must be parallel. If not, the photographed thread profile is easily deformed. The result of the subsequent thread geometry calculation is too different from the actual value. In binarizing the image, the selection of the threshold is the use of the histogram. The final determined threshold also depends on the accumulation and experience of some knowledge, so when selecting the threshold, , we must carefully analyze, do more experiments, to eliminate the error caused by the algorithm to a minimum[10]. In actual experiments, there are other factors that interfere, but the error caused by the above factors is the most obvious.

6 Conclusion

The design proposes a scheme based on digital image processing technology to automatically detect the large diameter, small diameter, profile angle, and pitch of the thread on the bolt through the photograph, and judge whether the bolt is qualified. Based on the image processing of matlab, the defect detection of the thread is extremely consistent with the requirements of industrial production, and the theoretical depth also has certain dig ability, which has important practical application value. Looking at the current industrial production, how to improve efficiency and accuracy is the key, so this design also has a high frontier.

Refernces

[1] Dou Huajun. Analysis based on digital image processing technology [J] Digital Technology and Applications. 2013. 12(12): 231-232.

[2] Li Hongjun, Han Yi. Digital image processing technology and its application, Computer Measurement and Control, 2002, 10(9) 620-622.

[3] LIN Xiaofeng,SHI Shaoli.Application of CCD Camera in Measurement of Workpiece Size[J].Optical Instruments,2002,9(3):11-13.

[4] Chen Lihong.Simplified algorithm for calibration and correction of CCD camera[J].Journal of Zhejiang University,2003 37(47):406-409.

[5] Sun Xuezhu, Fu Weiqiao, Liu Qing et al.Optical system design of high-precision CCD size automatic detection system[J].Optical Technique,1995,9(5):4-23.

[6] Zhang Shaojun, Ai Jiaojian, Li Zhongfu, Li Changjiang, Li Qingli. Measurement of geometric dimensions using digital image processing techniques [J]. Journal of University of Science and Technology Beijing, 2002, 24(3): 284-287.

[7] Rafael C. Gonzalez, Richard E. Woods. Digital Image Processing [M]. 2007.

[8] Waghule D. R, Ochawar, R. S. Overview on edge detection methods [C]. International Conference on Electronic Systems, Signal Processing and Computing Technologies, 2014: 151-156

[9] ZhangYunhui, Tan Qingchang, Tian Yuanji. Research on the Influencing Factors of Image Measurement System Accuracy [J]. Microcomputer Information, 2008 24 (24) :271-273.

[10] ChenXiangwei, Research on key technologies for computer vision inspection of mechanical parts[D]. Changchun: Jilin University, 2005.

The Study of Automatic Tracking and Object Grasping System of Quadrocopter

TENG Fei; LIU Hong-nan; LIU Tao; XIA Hong-jian
(College of Instrument and Electrical Engineering, Jilin University)

***Abstract*-In order to realize the quadrocopter's automation and informatization in transportation, we designed and realized a quadrocopter which could track and grasp target automatically and then carry it to the specified place. By applying the control theory of quadrocopter, we make it be able to judge its position in real time using computer vision technology, and adjust its attitude angel with the PID controller. Thus, we finished automatically tracking and target identification using camera and drove a manipulator to accomplish target grasping and releasing. The result shows that the quadrocopter could keep its flying height at 1m, and fly at the speed of 20cm/s. The machine could recognize and grasp a cylindrical target of which the radius is 4cm and the length is 8cm. The whole process can be finished in 50 seconds.**

***Key word*-Quadrocopter Automatic tracking Object extracting Computer Vision PID Controller**I.

INTRODUCTION

DUE to its simple structure, good maneuverability and low cost, the quadrotor unmanned aerial vehicles are widely used in civilian and military applications such as surveillance and reconnaissance [1]. In recent years, quadrocopters have been considered the best platform in the field of drone applications and experiments [2]. At present, many research institutes at home and abroad have successfully developed quadrotor unmanned aerial vehicles with autonomous flight in a simple constraint environment [3]. However, due to automation control technology and other reasons, the drone's autonomous transport of goods is still one of the major issues in current research. At present, the manipulation of drones and the loading and unloading of items need to be completed manually, which may greatly reduces work efficiency. In view of this, this paper proposes a scheme based on computer vision processing and PID control algorithm to automatically control the autonomous tracking and object grasping system of quadrocopters. To a certain extent, it makes up for the lack of autonomy of the drone in transport. By using computer vision technology, the system can process image information to obtain the current position of the aircraft, the target object and the delivery point. It can also control the attitude of the aircraft through the PID controller, while controlling the opening and closing of the robot to achieve the grasping and delivery of objects, so as to complete the task of autonomous tracking and transport.

II. DYNAMICS MODELING AND ALGORITHM ANALYSIS

2.1 Dynamics Modeling of Quadrocopter

The theory of treating the propeller blades as a rotating wing is called standard strip analysis. During the flight, the propeller is subjected to aerodynamic forces, which mainly include lift(represented by F) and resistance(represented by f). The lift is perpendicular to the direction of air flow, and the resistance is parallel to the direction of air flow [4]. Because of its light weight and small rotors, the quadrotor is very susceptible to various physical effects such as outside air flow, making it difficult to obtain a reliable and effective physical model [5]. Therefore, the secondary factors in the analysis process are ignored in this paper and the *quadrocopter* is simplified [6]. The simplified diagram is shown in Fig. 1, and the approximate mathematical model is obtained as follows:

$$F = C_T \rho S R^2 \Omega^2 \tag{1}$$

where:

C_T represents the aerodynamic coefficient

ρ represents the air density

S represents the propeller blade area

R represents the propeller blade radius

Ω represents the propeller angular velocity when the aircraft is flying

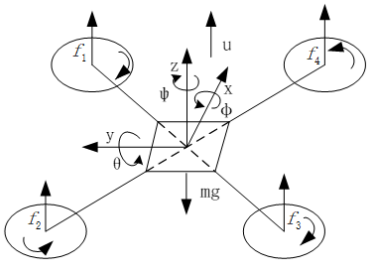

Fig. 1. Simplified diagram of the quadrocopter

Formula (1) is the tension of a single rotor during the flight of the aircraft.

When the aircraft performs a rolling motion, the resultant moment generated by the motors 1 and 4 and the resultant moment generated by the motors 2 and 3 interact to synthesize a rolling moment(represented by T_Φ) acting on the aircraft, that is:

$$T_\Phi = [(F_1 + F_4) - (F_2 + F_3)] \cdot d \tag{2}$$

where:

F_x represents the lift provided by motor x

d represents the vertical distance between the midpoint of the two adjacent motor shafts and the axis of gravity of the aircraft

When T_Φ is greater than zero, the aircraft tilts to the left, and when it is less than zero, the aircraft tilts to the right.

When the aircraft performs a pitching movement, the resultant moment generated by the motors 1 and 3 and the resultant moment generated by the motors 2 and 4

interact to synthesize a pitching moment(represented by T_θ) acting on the aircraft, that is:

$$T_\theta = [(F_1 + F_3) - (F_2 + F_4)] \cdot d \quad (3)$$

When T_θ is greater than zero, the aircraft tilts backward and when it is less than zero, it tilts forward.

2.2 PID Control Algorithm

The proportional-integral-derivative(abbreviated as PID) controller consists of a proportional unit P, an integral unit I, and a differential unit D. It is based on the control deviation e(t) between the given value r(t) and the actual output value y(t), that is:

$$e(t) = r(t) - y(t) \quad (4)$$

Then the proportionality, integral and differential coefficient are used to construct the control value through linear combination to the deviation, and the object is controlled [7].

The time domain differential equation of the PID controller is

$$u(t) = K_p[e(t) + \frac{1}{T_i}\int e(t)dt + T_d \frac{de(t)}{dt}] \quad (5)$$

where:

K_p represents the proportionality coefficient

T_i represents the integral time constant

T_d represents the derivative time constant

e(t) represents the deviation

u(t) represents the control value

The schematic of the PID control algorithm is shown in Figure 2.

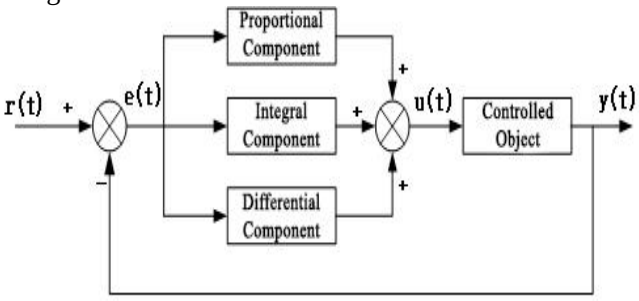

Fig 2. Schematic of PID control algorithm

Formula (5) describes the analog PID controller, which needs to be converted into a digital PID controller in the field of computer control. After discretizing the formula (5) by the backward difference method, we can get:

$$u_k = K_p[e_k + \frac{T}{T_i}\sum_{i=0}^{k} e_i + \frac{T_d}{T}(e_k - e_{k-1})] \quad (6)$$

where:

T represents the sampling period

u_k represents the control value

In this paper, the PID control algorithm is adopted for the fixed-height flight and tracking flight control of the aircraft. Therefore, r(t) in fig. 2 is the desired height or position coordinate of the aircraft, and the feedback value is the actual height or position coordinate of the aircraft. u(t) is the Pulse Width Modulation (abbreviated as PWM) wave duty cycle that controls the speed of the four motors of the aircraft. The controlled object is the four motors of the aircraft.

2.3 Open Source Computer Vision Library

Open Source Computer Vision Library (abbreviated as OpenCV) is an open source working library for implementing computer vision related technologies. It provides interfaces for multiple languages. The program has a high degree of modularity and can be packaged into functions or libraries. The function interfaces of image processing are all encapsulated in a simple and universal way. The basic visual recognition process can be realized and the algorithm is universal [8]. For a quadrocopter, which requires a high real-time performance, it is not enough to use an ordinary camera and simple image processing technology. However, using computer vision technology to process the image can quickly obtain the position information of the aircraft so that the real-time control of the attitude of the aircraft can be realized [9]-[11]. Therefore, the image processing of this system is based on OpenCV.

In this paper, the recognition process of target objects and delivery points mainly includes three parts: image acquisition, image recognition and target positioning. The feature patterns of target objects and delivery points in this system are designed as circular black spots. First, the Logitech C525 camera captures the image, and then grays and binarizes the image through a program, and performs morphology transformations to remove noise from the image. Compare the center point of the processed image with the target center point, so as to obtain the current aircraft position information. The image processing flow chart is shown in figure 3.

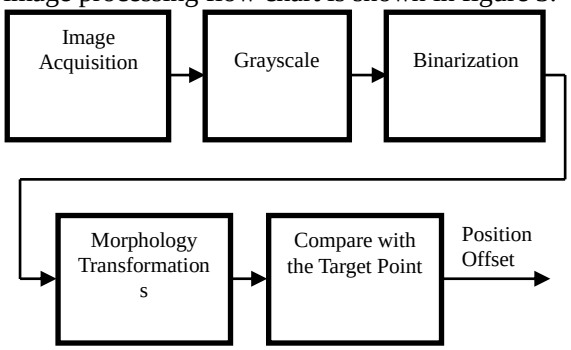

Fig 3. The flow of image processing

III. SYSTEM DESIGN

3.1 System Design Block Diagram

The system block diagram of the quadrocopter is shown in figure 4. The system consists of five parts: the frame and power system, the main controller section, the height data acquisition section, the image acquisition and processing section, and the object capture section.

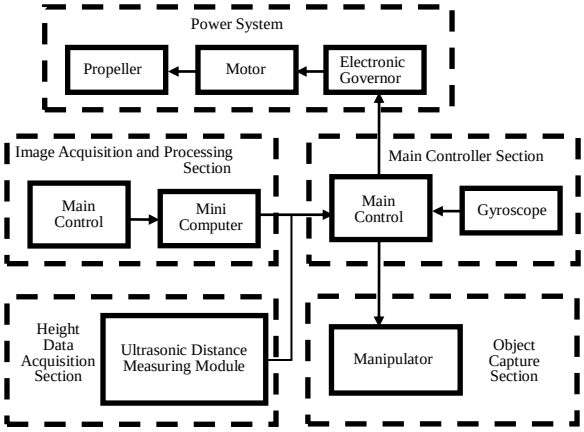

Fig 4. The system block diagram

3.2 Frame and Power System

The aircraft frame uses a Tarot 650 four-axis rack with a wheelbase of 650mm and has a large mounting space. The rack is equipped with an electrically powered tripod for robotic gripping of objects. The power system is composed of four groups of electronic governors, motors and propellers; the electronic governor converts the DC power to the three-phase AC to drive the motor according to the input signal. The motor adopts Sunnysky brushless disc type 4110 motor with KV value of 400, which can provide sufficient power and high reliability. The propeller uses 15 inch carbon fiber propellers.

3.3 Main Controller Section

The main controller section consists of the main controller and the MPU6050 gyroscope. The main controller uses the STM32F407VET6 chip. This chip has rich peripheral resources and various communication interfaces. It integrates single-cycle DSP instructions and floating point unit (abbreviated as FPU), which improves the computing performance of the chip. The quadrocopter is a hard real-time system. Therefore, it has a higher requirement for the speed of operation of the main controller. The chip we choose has powerful data processing capabilities, which can meet the requirements of this system. The MPU6050 chip integrates a 3-axis gyroscope and 3-axis accelerometer. It provides 16-bit accelerometer data at 400 kHz [9], and comes with a digital motion processor (abbreviated as DMP). Therefore, the chip can quickly acquire the attitude parameters of the aircraft and output it as Euler angles.

3.4 Height Data Acquisition Section

The height data acquisition section uses the ultrasonic distance measuring module US-100. The module can realize non-contact distance measurement from 2 to 450 cm. It comes with a temperature sensor to correct the distance measurement results, while having GPIO and serial communication. The internal watchdog makes it stable and reliable [10].

The ultrasonic ranging module can calculate the distance traveled during the interval between sound emission and return. After correction such as temperature compensation, it sends out height data through the serial port. The formula for calculating the height is as follows:

$$H = \frac{\upsilon \cdot \Delta T}{2} \tag{7}$$

where:

H represents the height of the aircraft

υ represents the speed of sound propagation in the air

ΔT represents the time interval between acoustic emission and reception

3.4 Image Acquisition and Processing Section

The image acquisition and processing section consists of the Logitech C525 camera and the mini computer ZOTAC PI320.

The Logitech C525 camera has an 8-megapixel resolution. The automatic focusing and automatic dimming can reduce the impact of the vibration of the aircraft and the change of light intensity on the image acquisition. The image acquired by it has high resolution and strong anti-interference, so it can meet the requirements of the system.

The mini computer ZOTAC PI320 adopts Intel Atom Z3735F processor, four cores and four threads, clocked at 1.33HGHz. It has a great advantage compared to single-chip microcomputer in dealing with a large amount of data. With 3 USB interfaces, it is convenient to connect the external equipment and communicate with the main controller. It uses a 5 V DC power supply to take power directly from the aircraft. It is compact and easy to carry on the aircraft.

3.5 Object Capture Section

The Object Capture Section uses an acrylic material manipulator. The structure of the manipulator is simple and easy to disassemble. It only has a servo with a weight of 9g. The maximum effective clamping distance between the two jaws is 160mm. The reaction speed is fast. In addition, it is lightweight and easy to carry on the aircraft.

3.6 Software Flow Chart

The software design is divided into two parts. The first is the control of the Fixed-Height Flight, the Automatic Tracking flight, and the control of the manipulator's opening and closing movements. The second is the extraction of the trajectory center line and the recognition of the target objects and delivery points. The program flow chart is shown in Figure 5.

3.7 Fixed-Height Flight

The ultrasonic distance measuring module feedbacks the current altitude value of the aircraft to the main controller through the serial port, and the main controller controls the flying height of the aircraft through a PID control algorithm. Formula (6) is a positional PID control algorithm. The actual PID control algorithm used in this paper is an incremental PID control algorithm. Incremental PID control algorithm has the characteristics of small overshoot and fast regulation [11]. In the control process, it only outputs the increment of the relevant control variable (represented by Δu(k)), that is, the amount of change corresponding to the position of the actuator. Therefore, the aircraft will not cause serious accidents because of sudden increase or decrease of control variables. The expected and actual values of the flight altitude of the

aircraft are used as the input and feedback of the PID controller, respectively. The formula is as follows:

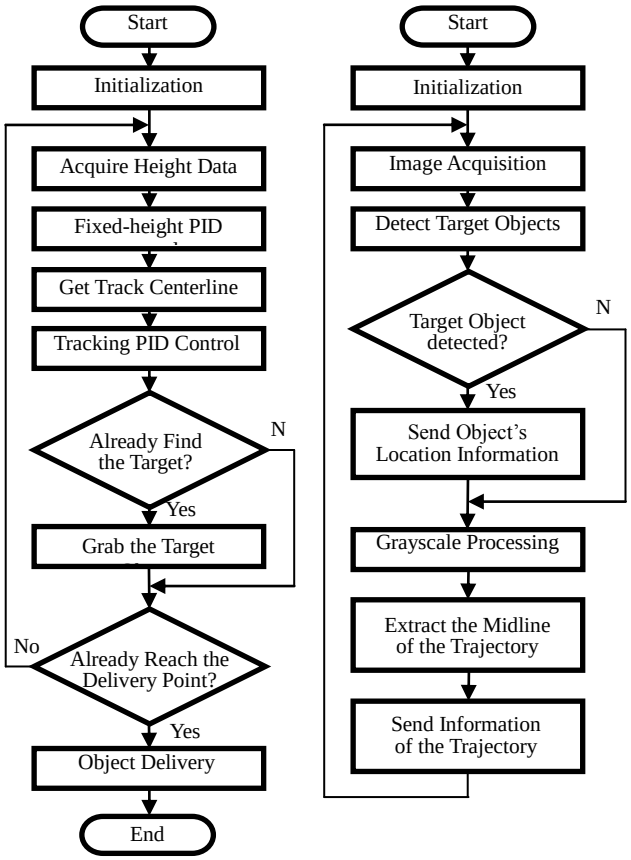

Fig 5. The software flow chart of Flight Control(left) and Image Processing(right)

$$\Delta u(k) = K_p(e_k - e_{k-1}) + K_i e_k + K_d(e_k - 2e_{k-1} + e_{k-2}) \quad (8)$$

This formula can be used to obtain the increment of the aircraft throttle value. Therefore, the formula for calculating the output throttle value(represented by U_k) is as follows:

$$U_k = U_{k-1} + \Delta u(k) \quad (9)$$

Finally, by mapping u to four PWM wave duty cycles controlling four motor speeds, the height of the aircraft can be controlled.

3.8 Automatic Tracking Flight

The mini computer sends the midline information of the trajectory to the main controller through the serial port. The main controller realizes the automatic tracking flight of the aircraft through the PID control algorithm.

In order to realize the aircraft's automatic tracking flight, it is necessary to comprehensively control the pitch, roll, and yaw movements of the aircraft. Therefore, three PID controllers are required to control the three kinds of movements. To achieve better control of the aircraft, a cascade PID controller solution is adopted, as shown in figure 6. The inner loop is speed control, and the outer loop is position control.

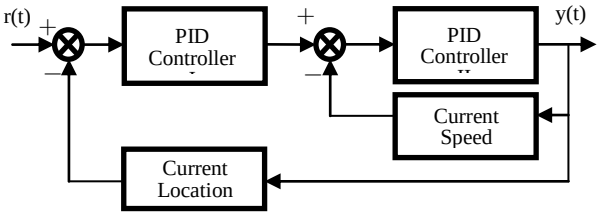

Fig 6. Cascade PID controller

3.9 Identification of Target Objects and Delivery Points

In the system, computer vision technology is used to complete the recognition of target objects and delivery points, including image acquisition, image recognition and target positioning. The characteristic patterns of target objects and delivery points in the system are designed as circular black spots. First of all, an image is acquired by a Logitech C525 camera. The image is then grayed and binarized, and the morphology transformations are performed to remove the noise in the image. Comparing the processed image center point with the target center point, the current aircraft position information can be obtained. The image processing flow chart is shown in figure 7.

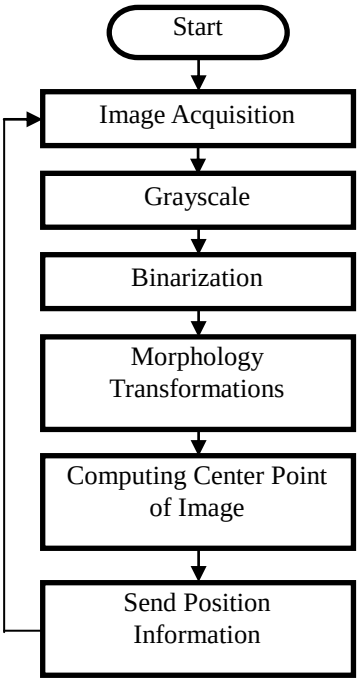

Fig 7. Image processing flow chart

3.10 Manipulator Opening and Closing Control

The aircraft flies along the trajectory, hovering over the object at a fixed point after identifying the object. After the aircraft descends a certain distance according to the instructions of the main controller, the main controller sends an instruction to the manipulator to control the robot to close and grasp the object. After the aircraft grabs the object, it rises to its original height and continues to fly until it recognizes the delivery point. Finally, the main controller controls the manipulator to open to release the object. The program flow chart for controlling the manipulator is shown in figure 8.

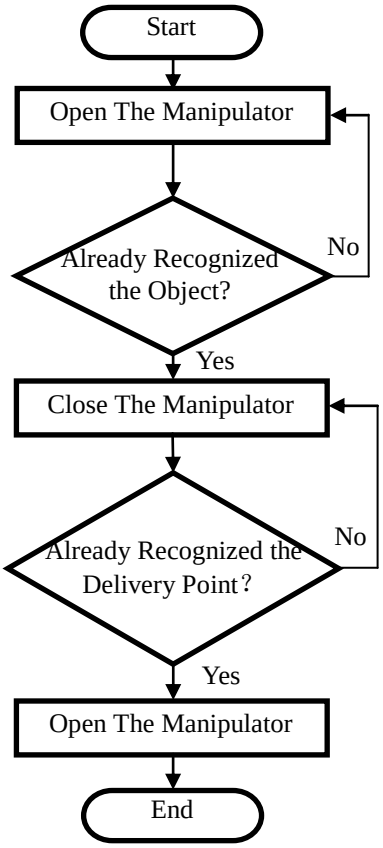

Fig 8. Program flow chart for controlling the Manipulator

IV. EXPERIMENTAL RESULTS AND ANALYSIS

4.1 Experimental Results of Fixed-Height Flight

This system has been adjusted many times to determine the appropriate PID parameters. In the end, the aircraft can quickly reach the desired altitude and stabilize under the adjustment of the PID controller, while the overshoot is small and the steady-state error is small. During the flight, the aircraft transmits the aircraft altitude data to the upper computer in real time via Bluetooth. The height curve drawn in the upper computer is shown in figure 9.

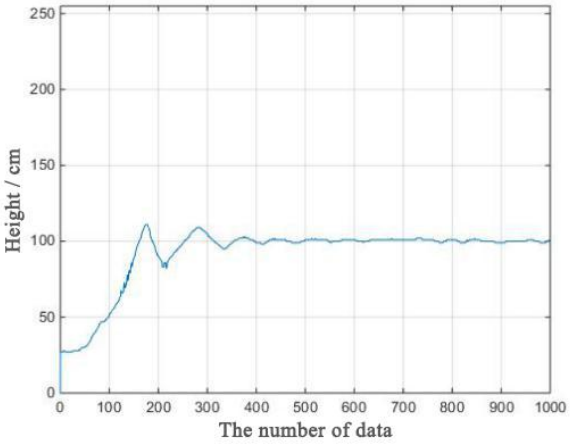

Fig 9. Curve of flight height

4.2 Experimental Results of Automatic Tracking

The camera module collects ground image information and transmits the image to the microcomputer. The microcomputer performs real-time processing on the image and calculates the current position deviation of the aircraft from the centerline, and then sends the position deviation to the main controller. The main controller regulates the position of the aircraft through the PID controller so that the aircraft can be quickly and accurately positioned above the centerline. After the flight is stabilized, the offset data calculated by the microcomputer each time is recorded and analyzed. The deviation of the aircraft from the centerline is shown in Table 1:

Table 1. Position deviation data of tracking

Experiment Number	Left Maximum Deviation (cm)	Right Maximum Deviation (cm)
1	5	4
2	4	6
3	3	3
4	3	4
5	4	2

According to the data in the table, the maximum deviation from the centerline after the aircraft has stabilized is no more than 10cm. Considering that the camera shake during the flight will also cause the image of the centerline to shift in the camera, it can be said that the aircraft can complete the automatic tracking flight and accurately locate the object within the offset range of no more than 10cm. So that the aircraft can successfully complete the capture of the target object.

V. CONCLUSION

Combined with ultrasonic sensors and camera image acquisition modules, the automatic tracking and object grasping system of quadrotor incorporates computer vision technology to achieves the function of stably flying and automatic tracking at a certain height and accurately positioning and capturing the target object, as well as the ability to accurately deliver objects to delivery points. It greatly expanded the capabilities of the quadrocopter aircraft and enabled the automation and informatization of drones in transportation. It provides a theoretical basis intelligence and informationization of drones for the future.

References

[1] LIU Yi-sha, YANG Sheng-xuan, WANG Wei, An Active Disturbance-Rejection Flight Control Method for Quad-Rotor Unmanned Aerial Vehicles[J]. Control Theory & Applications, 2015, 10:1351-1360.

[2] PAN Hai-zhu, Adaptive Navigation Control for Quadrotor Unmanned Aerial Vehicles[J]. Computer Simulation, 2012.

[3] Wang Lifei, Parameters Tuning of PID Controller[D]. China University of Petroleum, 2008.

[4] He Jiaji, Modeling the Quad-Rotor and Control Strategy Research[D]. Northeastern University, 2012.

[5] LIN Wei-cai, Design and Implementation of Four-Rotor Aircraft Controller[D]. Nanchang University, 2014.

[6] koo et al.Nonlinear Control of a Helicopter Based Unmanned Aerial Vehicle Model [C].Proc.37th IEEE Conf. on Decision and Control，1-25.1998.

[7] WANG Li-mei, Application Research of Open Source Computer Vision Library[J]. Public Communication of Science & Technology, 2013,(09):224-225.

[8] KANG Hai, ZHAO Kun, LIU Shu-lin, Design of Flight Attitude Recording System Based on MPU6050 module[J]. Electronic Design Engineering, 2015,(10):188-190.

[9] Qin Xiaowen, Wen Zhifang, Qiao Weiwei, Image Processing Based on OpenCV[J]. Electronic Test, 2011,(07):39-41.

[10] TENG Jun, WANG Di-lin, WEN Han-yun, Visual C++ Image Processing Method Based on OpenCV[J]. Modern Computer, 2012, (11):70-72.

[11] LIU Yu-hong, Research on Flight Control for Quad UAV Based on STM32F4[D]. Anhui University of Technology, 2015.

[12] YU Wen-qian, Design of Ultrasonic Distance Meter Based on US-100 Module[J]. Shandong Industrial Technology, 2015,(04):147+194.

[13] MEI Zhen, ZHAO Xilin, The Intelligent Car Speed Regulation System Based on the Incremental PID[J]. Journal of Hubei University of Technology, 2015,(02):72-76.

[14] SUN Yi-li, ZHEN Zi-yang, WANG Xin-hua, Quad-Rotor Helicopter Target Tracking Based on Computer Vision[J]. Electronic Design Engineering, 2016,24(18):159-161+165.

Research on Diesel Vehicle Environmental Monitoring System based on Vehicle Networking

Liu Jie; Sun Minjian;Chen Zifan; Yu Chengxin
(School of Instrument Science and electrical engineering, Jilin University)

***Abstract*-A wireless monitoring and transmission system for diesel engine exhaust gas (NOX) is designed with MSP430F149 single chip microcomputer as the core. The system takes nRF24L01 chip as wireless transmission module, which can realize the real-time collection, wireless transmission and communication with the host computer of NOX concentration in exhaust gas of diesel vehicle. Using LabVIEW to build man-machine interface, you can conveniently and real-time monitor the exhaust gas data. Compared with the GB exhaust emission data standard, when the exhaust emissions exceed the standard, the system will give the owner tips, warnings or related penalties. The system combines diesel vehicles and exhaust emission supervision departments, monitors diesel vehicle exhaust emissions, and further monitors and manages the over rated vehicles, and conforms to the environmental protection travel policy advocated by the state.**

***Key Words*-exhaust gas concentration detection; wireless transmission; upper computer display; exhaust emission monitoring**

INTRODUCTION

A large part of the source of air pollution is vehicle exhaust emissions, of which diesel vehicle exhaust emissions are particularly serious. With the enhancement of people's awareness of environmental protection, the government has paid more attention and investment in the field of environmental monitoring and the emission standards have become more stringent.In April 2016 the newly promulgated national Ⅴ vehicle emission standards stipulated that the factory diesel vehicles must meet the standards before they leave the factory[2].Therefore, we need to monitor the exhaust emissions of diesel vehicles in real time and send the information to the traffic environmental protection agency for supervision.Diesel exhaust pollutants include: carbon monoxide, hydrocarbons, nitrogen oxides, sulfur dioxide, soot particles, odor, etc., the main component of nitrogen oxides, so that vehicle exhaust NOX monitoring has become the top priority.In summary, our car-based diesel environmental monitoring system is very necessary for research, but also has a wide range of targeted groups, to change the vehicle annual inspection can not be achieved real-time monitoring of the status of the exhaust to ensure environmental protection Regulatory efforts[1].

1. SYSTEM HARDWARE DESIGN

A. System Hardware Design Overview

System hardware includes: sensor module, analog-digital conversion module, microprocessor, RF module and LCD module[5].Send the intersection of one-chip computer and the intersection of nitrogen and the intersection of oxygen and the intersection of sensor and the intersection of simulation and the intersection of voltage and signal digital sensor get the intersection of data and data, send data to the intersection of receiver and one-chip computer through nRF24L01 wireless module, send the data to upper computer again by serial communication.

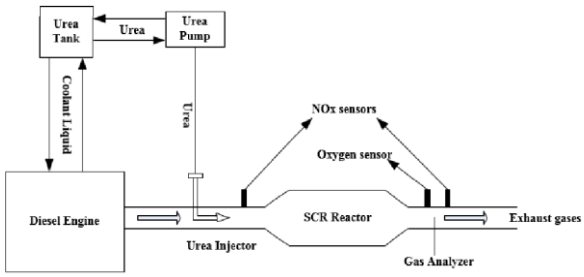

Figure 1. Algorithm flow chart of NOx sensor downstream SCR for monitoring

B. Microprocessor overview

Adopting the low-power 16-bit reduced instruction set MSP430F149 from TI Company of the United States as the core of system control, its low power consumption mode is very suitable for wireless node design.Microprocessor is mainly to coordinate the operation of the entire system, including the handling of 5WK9-6614H-type NOX sensor information collected and RF module transmit and receive information[6].

C. Nitrox Sensor Overview

A 5WK9-6614H NOX sensor was used to monitor the concentration of nitrogen oxides in the target gas[2].The NOX sensor has two working chambers: the first chamber contains an oxygen pump electrode and the second chamber contains an auxiliary electrode and a measuring electrode.In the first chamber, O2 is pumped out of the first chamber by applying a voltage to the oxygen pump electrode while converting NO2 to NO and into the second chamber;the auxiliary electrode in the second chamber is used to remove excess oxygen, while the measuring electrode is responsible for reducing NO to nitrogen and oxygen. According to the chemical reaction equation, the concentration of NOX can be obtained by measuring O2.

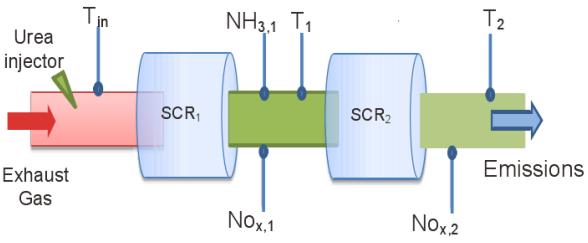

Figure 2. Monitoring activation conditions model

D. GPRS Overview

The nRF24L01 module is a radio frequency transceiver operating in the 2.4GHz-2.5GHz ISM band[3]. It can control the working mode, communication channel, output power and transmission speed of the wireless module through the lower computer program.During communication, nRF24L01 low-speed communication with the microcontroller, and wireless high-speed communication between the sender and the receiver, this can reduce the average communication current consumption, is very suitable for low-power energy-saving design.

2. EXHAUST GAS DETECTION MATHEMAICTICAL MODEL

NOX emission overrun monitoring: According to the collected parameter data, through the following steps of data calculation:

--First, Pe=（2π*Me*n）/60000=Me*n.

Pe: Effective power,KW;Me: Measured effective torque,N.m;N: Rotating speed,r/min.

--Second,Exhaust mass flow rate (kg / h) = Intake mass flow rate (kg / h) * 1.3

--Third,NOX emission mass (kg/h) = ((exhaust mass flow/29)*NOX concentration value)*46

29:Air molar mass;46:NOX molar mass.

--Forth,NOX specific discharge (g/(kw.h)) = (NOX emission quality (kg/h)*1000)/Pe

The actual measured NOx emissions from the engine were compared with the regulated NOX emission limits.

3. ERROR ANALYSIS

The error sources of the measurement system mainly include the following aspects: NOX sensor measurement error, exhaust gas outlet temperature, transmission signal interference, and the influence of single-chip AD conversion[7].

(1)NOX sensor measurement error: Because this experiment is to measure the O2 concentration to get the NOX concentration through conversion, two measurement errors will occur when measuring the O2 concentration and performing the conversion. It is necessary to perform error analysis and processing on this error.

(2)Exhaust outlet temperature effects:As the sensor in the exhaust port position, the location of temperature up to several thousands of degrees Celsius, in the case of high temperature if long-term work may lead to changes in measurement accuracy. K-type thermocouple temperature sensor can be used, the measurement range of 0 ~ 1300 ℃. With its measured system environment where the temperature, through the MAX6675 temperature sensor measurement data to compensate and correct.

(3)Transmission signal interference:In the data transmission and two-machine communication, due to external factors and noise on the signal interference, the signal can be processed by filtering.

4. SYSTEM SOFTWARE DESIGN

The lower computer program is written by IAR Embeded Workbench software, which can realize the functions of A / D acquisition, data processing and wireless communication[4].

The upper computer software selects LabVIEW to design on the one hand, uses the VISA function serial port to receive the data from the receiving end monolithic integrated circuit, can display the density change trend graph and the data in real-time on the dual-channel, and has the threshold value to set the function, the density exceeds the limit warning function.When the program exits, it can automatically generate the date format of the document, with the time format of the data to build easy to query data network. On the other hand, MATLAB is used to design, calculate and display the data of nitrogen and oxygen emissions, and compared with the international exhaust emission standards to monitor whether the exhaust gas exceeds the standard.

5. SYSTEM TEST

A.Communication system test

This experiment mainly includes the collection of the exhaust gas and the data communication[8]. Because the data is processed by the host computer and the two-machine communication, the communication system must be tested.The results show that the wireless communication module in the open environment has a longer transmission distance than the obstacle. In the open space, the more appropriate transmission distance is 50m, in the case of obstacles, the more appropriate transmission distance is 25m. In the actual measurement, the wireless module can be selected according to the need, and the wireless module with the power chip and the external antenna can be used where the signal is weak, so as to achieve the purpose of controlling the cost while meeting the requirements of the system in general.

B.Dual-communication test

In order to reduce the impact of communication distance on the measurement, the wireless communication distance is less than 0.1m, the data transmission rate is 1Mbps, and the number of transmitted data is 1000. Finally, it is concluded that the wireless transmission data will have a certain delay and packet loss. The larger the delay is, the smaller the packet loss rate will be.

C.NOX sensor linearity, stability test

By gradual gradual loading, the measured concentration of the NOX sensor measured at 10%, 20%, 50%, 80% of the measured value and the concentration measured by the gas emission analyzer. The gas emission analyzer measured as abscissa, NOX sensor measured concentration values for the vertical axis, the NOX sensor measurement accuracy and

stability calibration.

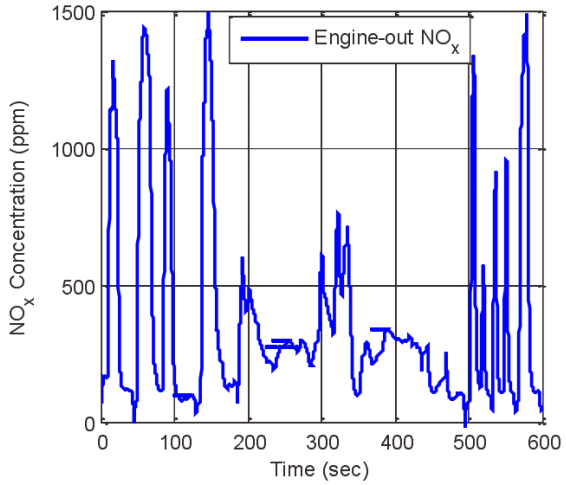

Figure 3. NOx concentration in steady upstream and downstream SCR

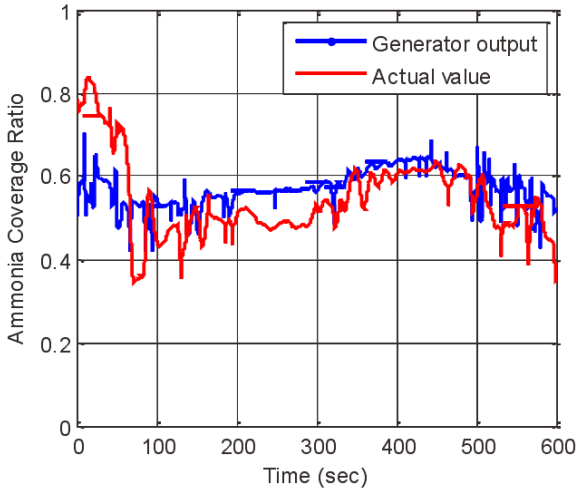

Figure 4. Subfunction "NOx sensor plausibility check"

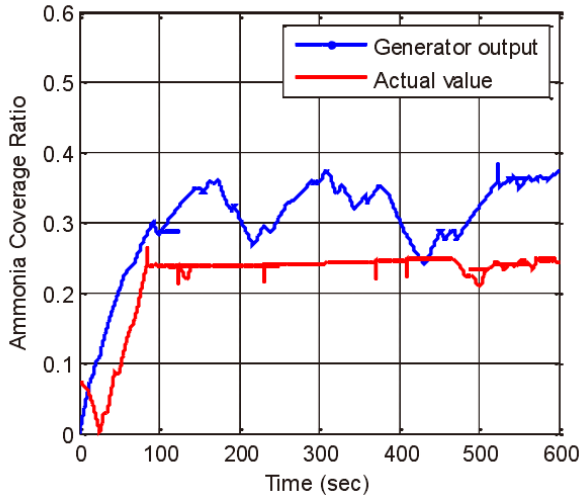

Figure 5. Basic module relation of the algorithm

6. CONCLUSION

The method is simple and low in cost, and provides a targeted and feasible solution for real-time monitoring of exhaust emissions[9]. The sensor itself has certain computing power and storage capacity, and can perform more complex tests according to changes in the physical environment , Through wireless communication transmission, can carry out collaborative monitoring. Combined with software and hardware, the complex vehicle exhaust emissions into intuitive data display, more convenient for vehicle owners to understand the vehicle information and environmental protection department supervision. In line with China's "national V" standard, the basic national policy of sustainable development in our country has relied on technology. It is convenient for the environmental protection regulatory authority to monitor the vehicle's superovulation from the source of exhaust gas pollution.

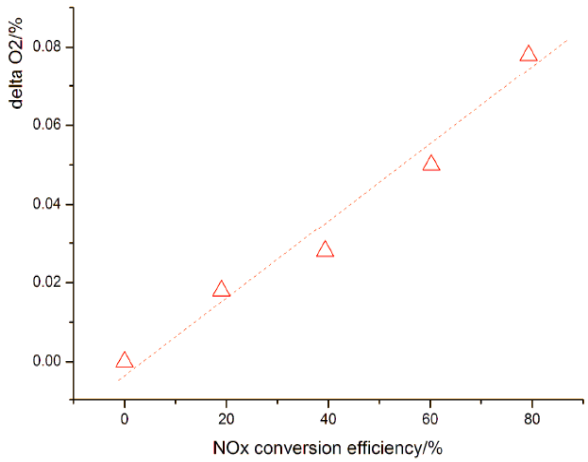

Figure 6.Model of the Monitoring test module

References

[1] Cai Yongxiang, Jinhua standard, Yu Fangping "SCR-based engine Ⅳ OBD system design"

[2] Liu Jiawei, Jilin University "Research on Diagnostic Strategy of Key Functional Modules of Diesel Engine SCR System OBD"

[3] Wang Jianhai, Fang Mao-dong, Yan Fu-wu, "Gasoline Vehicle Diagnostic System Basic Principles and Applications"

[4] Bi Haibo Beijing Jiaotong University "Heavy CNG engine locomotive diagnostic system research report"

[5] Deng Chenglin, Zhang Wei, Bu Jianguo, Automotive Engineering "Fault Management of State-Owned Diesel Engine OBD System Using SCR Technology"

[6] Chen Jiwei, Chen Xiaoju Zhejiang Vocational and Technical College of Electrical and Mechanical Technology "Wireless long-distance data acquisition and transmission device based on GPRS"

[7] Hu Wei, Xiong Xiaomeng, 2011 Western Auto Industry Academic Forum and Sichuan Proceedings of the 10th Automotive Academic Conference "Design of OBD Function Module for Diesel Urea-SCR System"

[8] Siebenbrunner,P.&R.Fischperer,&J.Bachler,De-NOx-Systems-Requirements for Software Development and Calibration for 2010 and beyond.[C]SAE International.April 14,2008

[9] Oliveira,L.&C.F.M Rossin.Optimizing the On Board Diagnostic System to Monitor for Reduction of the SCR

Catalyst Conversion Efficiency using the NOx Sensor,[C]SAE International.March 19,2010

Research on Establishment of a Chaotic System Model Based on Sinusoidal Signal Detection in Low SNR Environment

Yanchen Ge; Wenxuan Liu; Fu Liu
（instrument science and engineering institute, jilin university）

***Abstract*—Noise has always been a main problem when it comes to weak signals detection. In this paper, a new method using chaotic system is put forward, which has a unique characteristic of shifting between chaotic state and large periodic state due to the initial parameters. We will first discuss the detailed function of duffing oscillator, then with theoretical analysis and matlab simulations, proper parameters like are restoring force, damping coefficient and driving force are determined, which are later proved effective in performing an extraction of signal in a lower SNR environment. Gaussian White Noise is specially selected as a typical noise.**

***keywords*—Chaotic system Weak signal detection Duffing equation White noise Parameters**

I. INTRODUCTION

WEAK signal detection has important significance in practical applications, without which any kinds of exploration activities will be hard to process. However, with the increasing popularity of electronic devices, electromagnetic interference has become more and more common and powerful, making it difficult to distinguish tiny signals from it. Traditionally, people will try to suppress the noise to get a better SNR, but such method, after years of, would be quite difficult to make any more progress. Recently a brand new method based on chaotic system, instead of suppressing the noise like traditional method, aims to detect the signal directly.

Such method relies much on the modelling of the chaotic system, which is also the main goal of the paper. Duffing equation, as aa equation successfully describes many non-linear systems, can also be applied under such circumstance. Based on duffing equation, we will discuss on the selection of its parameters.

According to the Fourier series, any periodic signal can be decomposed into sinusoidal signals of different frequencies, making the sinusoidal signal an ideal test signal. Also, the Gaussian White Noise can be an excellent representative of all the noise.

II. DETECTION PRINCIPLE

Because the chaotic system is extremely sensitive to the initial conditions, a weak signal can have a great influence on the system state whereas noises of certain type have little effect on the system. Therefore, we can make the collected signal an input of the system. If the state of the system changes, the signal we want exists, and if not, it does not.

Duffing function has a form as followed

$$\ddot{x} + \underbrace{k}_{Damping\ Coefficient}\ \underbrace{\dot{x} + ax^m + bx^n}_{Restroing\ Force} = \underbrace{\gamma\cos(t)}_{Driving\ Force} + \underbrace{h\cos(t)}_{Test\ Signal} + \underbrace{zs}_{Noise}$$

In case the test singals have various frequcies,when signal is small,the frequency dose not affect the detection[1], we will take $t = \omega \cdot t$, then

$$\frac{\ddot{x}}{\omega^2} + \frac{k}{\omega}\dot{x} + ax + bx^3 = \gamma\cos(\omega t)$$

ω is the angular frequency of driving force.

In the equation, three parameters, k, γ and $ax^m + bx^n$ are undetermined and may have influence on the system.

III.SELECTION OF DAMPING COEFFICIENT

In order to determine k alone, we can temporarily set other parameters fixed as followed

$$a = -1, b = 1, m = 1, n = 3$$

The Melnikov function, as an analytical method to solve the chaotic system, has been proved efficient through years. It can find the relationship between the ratio of the amplitude and the damping coefficient of the drive power and the frequency [2].

The original form of Duffing function is

$$\ddot{x} + \epsilon \cdot k \cdot \dot{x} - ax^m + bx^n = \epsilon \cdot \gamma\cos(t)$$

When $\epsilon = 0$, the function can also be written as

$$\begin{cases}\dot{x} = y \\ y = x - x^3 - \epsilon \cdot k \cdot y + \epsilon \cdot \gamma \cdot \cos(\omega t)\end{cases}$$

Melnikov function forms as

$$M(t_0) = \int_{-\infty}^{+\infty} f(q^0 \Lambda g(q^0(t), t + t_0)dt$$

in which $f(x) = \begin{pmatrix} y \\ -x + x^3 \end{pmatrix}$,

$g(x) = \begin{pmatrix} 0 \\ -ky + \gamma \cdot \cos(\omega t) \end{pmatrix}$

leading to an inequality

$$\left|\frac{4k \cdot \cosh\left(\frac{1}{2}\pi\omega\right)}{3\sqrt{2\pi} \cdot \gamma \cdot \omega}\right| < 1$$

which can further be expressed as

when $\frac{\gamma}{k} > 0$, if $\frac{\gamma}{k} > \frac{4\cosh\left(\frac{1}{2}\pi\omega\right)}{3\sqrt{2\pi}\cdot\omega}$, the system becomes chaotic

when $\frac{\gamma}{k} < 0$, if $-\frac{4\cosh\left(\frac{1}{2}\pi\omega\right)}{3\sqrt{2}\pi\cdot\omega} < \frac{\gamma}{k}$,the system becomes chaotic

A. Relationship Between Damping Coefficient and Angular Frequency

We will first find the relationship between damping coefficient and angular frequency through the Melnikov Function as mentioned above, which is

$$\frac{k}{\gamma} = \frac{3\sqrt{2}\pi\cdot\omega}{4\cosh\left(\frac{1}{2}\pi\omega\right)}$$

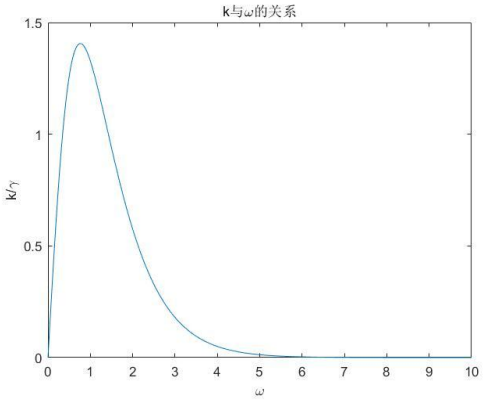

Fig. 1. Relationship between k and ω.

From the picture, we can see the function has a crest.

According to the inequality $\frac{k}{\gamma} < \frac{3\sqrt{2}\pi\cdot\omega}{4\cosh\left(\frac{1}{2}\pi\omega\right)}$, with every k selected, the range of frequency that can cause chaos is also determined. Smaller the k is, larger range the ω can have to produce a chaotic situation. Bigger the k is, smaller range the ω has, but also means a higher accuracy of specific ω. In practical applications, the frequency of the test signal is usually known, thus we should select k as big as possible. Other limits will be discussed in other to determine a smaller range of k.

B. The relationship between damping coefficient and chaos

To make duffing function solvable, according to mathematical derivation, k should be within the range of 0~2.

After several simulations with different k selected, we found that k somehow has influence on the chaotic states. The 'Quality' of the chaotic area will affect the final result. This 'Quality' will be evaluated in the following aspects. First, the periodic state between two chaotic state can't be too small, otherwise the addition of the test signal will make the system jump through the current chaotic area to the other chaotic area, not showing any of the periodic states, thus can't tell if the signal exits. Also, the chaotic area can't be too much, leaving no space for the system to enter the periodic area. If so, there is no way to tell whether the signal exits. Finally, the boundary should be easy to extinguish. an overly blurred boundary would make it hard to decide between chaotic state and periodic state[3].

In order to show the different states under different driving forces, a method called bifurcation diagram is put forward to facilitate the research, using which we can see exactly how the different k value changes the system state.

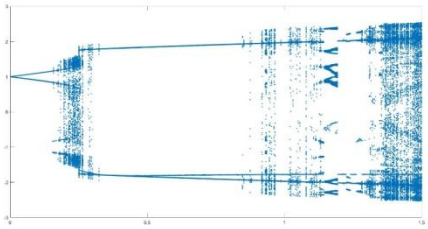

Fig. 2. k=0.1

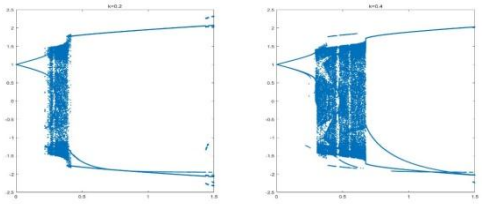

Fig. 3. k=0.2 k=0.4

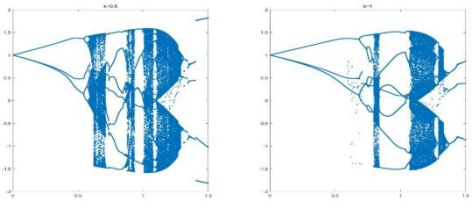

Fig. 4. k=0.8 k=1.0

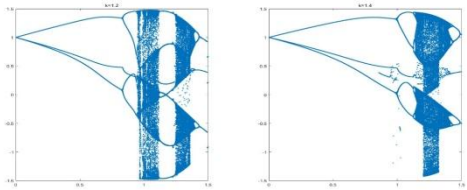

Fig. 5. k=1.2 k=1.4

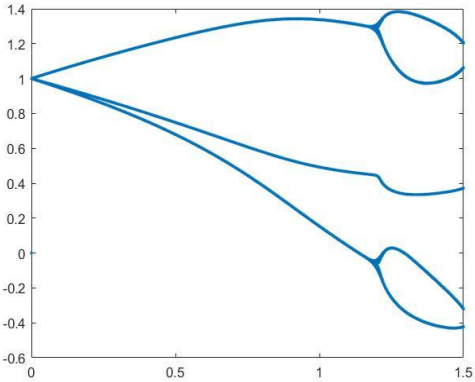

Fig. 6. k=1.6

TABLE I
Bifurcation Diagram With Different k Selected

k	System States
0.1	blur boundary between chaotic and periodic states.
0.2-0.5	distinctive boundary with reasonable states' areas.
0.5-1.5	periodic areas are too small; inverse period-doubling bifurcation exists.
1.5-2.0	no chaotic area exists

When k is between 0.2 and 0.5. the bifurcation diagram shows an ideal system for signal detection. When k is between 0.6 and 1.5, multiple chaotic area exits with small area of periodic states. When k is larger than 1.5, chaotic state no longer exists for the damping is too large for the system to become unstable[4].

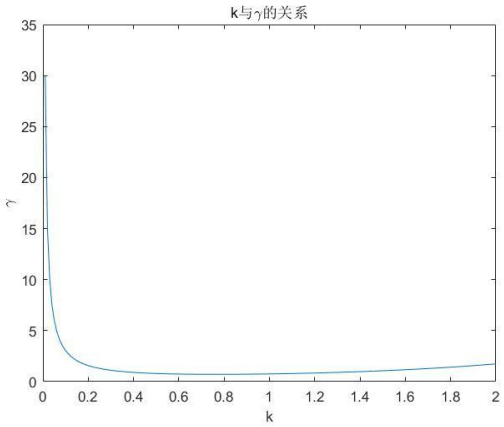

Fig. 7. Relationship between k and γ

When k is smaller than 0.1, k and γ are no longer in linear relationships, making the γ drops rapidly as k decreases. Eventually, this will cause the chaotic areas disappear.

An experience relationship between the amplitude of driving force would be appropriate when it is 15~20 times larger than the noise. Combining with the conclusion above that k is almost linear to γ, k should be larger when comes to a larger noise.

In summary, k should be selected in between 0.2 and 0.5 proportional to the noise power.

IV. Selection of Restoring Force

A. Rules of Restoring Force Selection

Restoring force is another important composition of the equation[5]. A potential energy hamilton equation is introduced to find the best answer of restoring force.

A general form of restoring force in a chaotic system is

$$f(x) = \sum_{i=1}^{N} a_i x^i$$

The stationary state of system potential energy hamilton equation is

$$\phi(x) = \sum_{i=1}^{N} \frac{a_i}{i+1} x^{i+1} - \frac{1}{2} = 0$$

After mathematical derivation, several rules are put forward to the selection of restoring force[6].

(1) The real root size of the stationary state potential energy hamilton equation solution and the corresponding x-variation range in each phase diagram is one to one.

(2) When the stationary state potential energy hamilton equation has a positive real root and a negative real root, the phase trajectory of the corresponding chaotic system can exhibit periodic motion.

(3) When the equation has only one positive real root or one negative real root, the phase trajectories of the corresponding chaotic systems will diverge, the phase diagram will become chaotic. And the signs of the roots will depend on the signs of stationary state potential energy hamilton equation.

(4) The stationary state potential energy hamilton equation's the highest-order coefficient and the highest-term power of the Hamiltonian equation must be an odd number. There are no strict restrictions on the power and the total number of terms for other terms.

According to the rules above, we narrow down our selection to $-x + x^3$ and $-x^3 + x^5$. $-x + x^3$ will be called first restoring force and $-x^3 + x^5$ as second restoring force in short.

We then put these two terms into the stationary state potential hamilton equation to find the root of the equation, verifying if they fits the rules above.

（1）As for the first restoring force, we have

$$-\frac{1}{2}x^2 + \frac{1}{4}x^4 - \frac{1}{2} = 0$$

solutions are

$$\begin{cases} x_1 = -1.6529 \\ x_2 = 1.6529 \\ x_3 = -0.8556i \\ x_4 = 0.8556i \end{cases}$$

With a positive and a negative root, this form meets the rules.

（2）As for the second restoring force, we have

$$-\frac{1}{4}x^4 + \frac{1}{6}x^6 - \frac{1}{2} = 0$$

solutions are

$$\begin{cases} x_1 = -1.4661 \qquad x_2 = 1.4661 \\ x_3 = 0.6546 - 0.8678i \\ x_4 = 0.6545 + 0.8678i \\ x_5 = -0.6545 - 0.8678i \\ x_6 = -0.6545 + 0.8678i \end{cases}$$

which also includes a positive and a negative root, thus meets the rules.

B. Comparison of System Sensitivity Under Two Kinds of Restoring Forces

If both form can be used, the sensitivity of both becomes the second condition[7].

With ω=1 and driving force set to cos(t), the phase diagram of the system using two restoring forces are shown as followed:

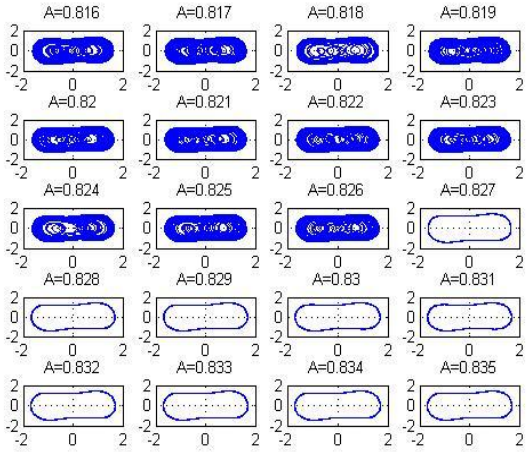

Fig. 8. Finding the critical state with the first restoring force

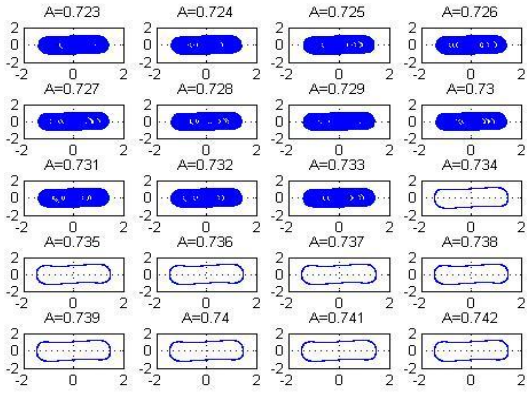

Fig. 9. Finding the critical state with the first restoring force

We can now see that the critical value of driving force amplitude with the first restoring force is 0.826 whereas the second restoring force as 0.733. Set the test signal's amplitude step by step as 0.0001→0.0002→0.0005→0.0008.

With the first restoring force, the phase diagram shows the system changing from chaotic state to chaotic state following by another chaotic state, and finally comes to a periodic state.

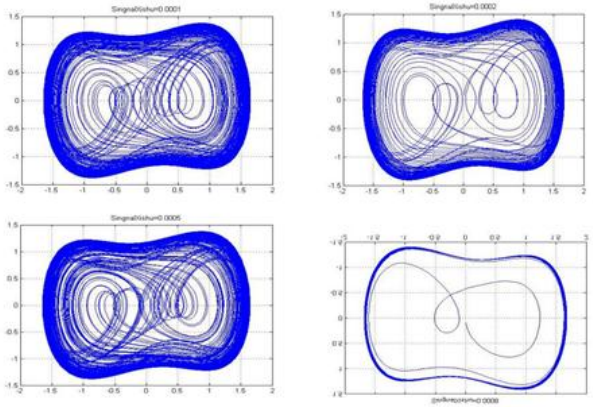

Fig.10.Phase diagram with the first restoring force

With the second restoring force, the phase diagram shows the system changing from chaotic state to chaotic state following by periodic state and so on.

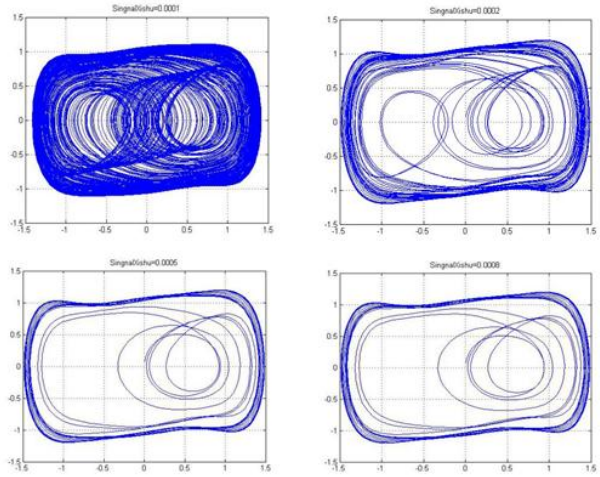

Fig.11. Phase diagram with the second restoring force

This shows the second restoring force changes earlier than the first restoring force, which further indicates a higher sensitivity[8].

V. Selection of Driving Force

A. Effect of Noise On Detection

The chaotic system has insensitivity to noise but strong sensitivity to weak signals at the same frequency, therefore has the ability to detect weak signals. In practical application, the collected signals include three types of noise in addition to the required weak signals: Gaussian white noise, power frequency harmonics, and impulse noise. Power frequency harmonics and impulse noise are easier to remove thus can be ignored. Among the three types of noise, Gaussian white noise has the most serious impact on chaos detection.

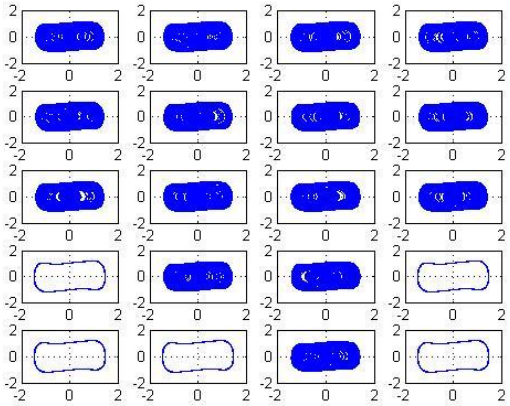

Fig.12. Changes of the system under the effect of noise

In the simulation process, we found that when the chaotic system is at its critical value, the power change of Gaussian white noise sometimes makes it into a large-period state, resulting in misjudgment. This kind of misjudgment is actually something we do not want to see. Therefore, it is necessary to study the reasons for this misjudgment[8].

First of all, because Gaussian white noise has the characteristic of wide frequency band. According to the characteristics of weak signal detected by chaotic system, it can be speculated that the added Gaussian

white noise contains weak signals with the same frequency as the chaotic system, leading the chaotic state into a periodic state. Secondly, the simulation time also affects this misjudgment. If the simulation time is not long enough, the periodic state appearing in the initial simulation may be regarded as a large-period state. In fact, with the extension of the simulation time, a chaotic state will eventually appear.

In this paper, under the condition of the power amplitude as 0.8265, we have done 100 simulation experiments by changing the input noise power and observing the chaotic system's changes. The results shown in the following table.

TABLE II

The Misjudgment Rate With Different Noise Under γ = 0.8265

Noise Power（σ2）	Misjudgment Rate
10-1	0%
10-2	0%
10-3	0%
10-4	2%
10-5	41%
10-6	5%
10-7	0%
10-8	0%

From the data in Table II, it can be seen that the noise power has a nonlinear influence on the misjudgment rate. Different noise powers cause the chaotic system to have an indeterminate state, that is, whether the system is in a chaotic or large-period state is unknown. When the power is 10-5, the chaotic system in a critical state is particularly sensitive to noise and is prone to misjudgment. The chaotic system does not monotonously increase with the reduction of the noise power intensity. On the contrary, the system might have a biggest misjudgment rate for a low power noise other than a bigger on, ie, there is a peak in the false positive rate.

B. Determine the driving force using phase diagram

From the bifurcation diagram, we already determined the approximate range of the amplitude of driving force. Now we use phase diagram to further gain a higher accuracy.

Phase diagram is a kind of drawing that can easily distinguish the state of the system. Drawing the phase diagram around the estimated threshold value of the driving force of the system can clearly show how the system reacts to the driving force[10].

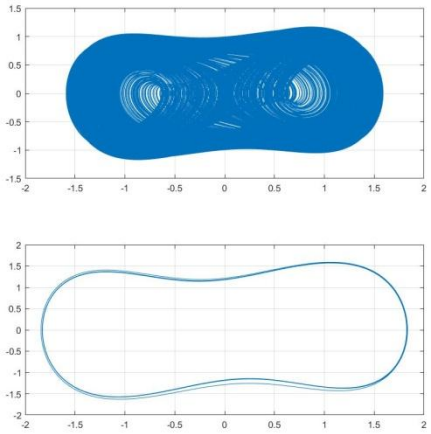

Fig.13. Phase diagram of duffing system under different states

Set the driving force before the system enters the chaotic state. Then, with the test signal mixed in, the system will become chaotic, by which we will know the test signal exists. In this model, γ is set to 0.733 as the threshold value.

According to the conclusion mentioned above, that the noise will affect the system in some way after all. We then make the noise at a level at which the noise will cause the minimum misjudgment rate.

During the simulation, we assume that the signal and noise have already been amplified to a proper power.

Here we use a test signal with an amplitude of 0.001, then put it in the noise to form a system of -40dB SNR.

We then set another group of data without any test signal.

As shown in Fig.14, in which the both diagrams are chaotic, the system doesn't receive any test signal. On the contrary, in Fig.15, the system suddenly enters the periodic state, which proved the validity of the model.

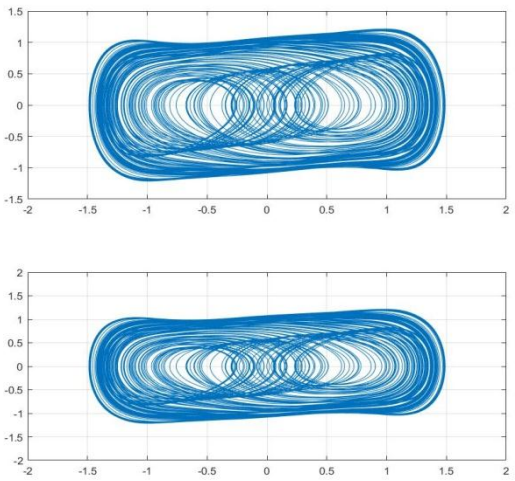

Fig.14. System with noise only

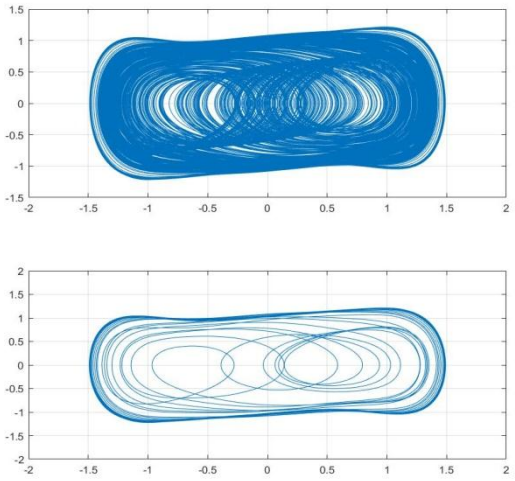

Fig.15. System with a test signal and noise

VI.CONCLUTION

With the chaotic system model based on Duffing equation,by selecting and adjusting the three parameters of damping coefficient,restoring force and driving force amplitude,it can be successfully used for the detection of weak sinusoidal signals with a higher SNR as well as better noise tolerance.However,the mutual influence between the three parameters and the influence of other types of signals remain to be discussed.

References

[1]. Greenspan, Bernie;Holmes, Philip.Repeated Resonance and Homoclinic Bifurcation in a Periodically Forced Family of Oscillators[J].SIAM Journal on Mathematical Analysis,1984,Vol.15,No.1

[2]. Fuxin Guo. Study of Signal Measuring Based on Chaos Theory[D]. Jilin University, 2005.

[3]. Nan Li, Mingyan Liu. Dynamic Characteristic Research and Weak Signal Detection of Fractional Order Duffing System[J].School of Information Engineering,2017,17(21):248-257.

[4]. Yongjian Li. Study on the Detection Method of Weak Vibration Signal Based on Duffing Chaos System[D]. Nanjing University of Aeronautics and Astronautics,2009.

[5]. Yue Li, Baojun Yang. Detecting Chaotic Systems of Periodic Signals in Strong Noise Background[J].Chinese Science Bulletin,2003(01):19-20.

[6]. Xueping Zhao, Yue Li, Baojun Yang. The discussion to the resilience items in the Duffing type system used for detecting events[J].Progres s in Geophysics, 2006(01):61-69.

[7]. Ying He. Research and application on the weak signal detection Chaos Duffing oscillator system[D].Chang'an University, 2010.

[8]. Jin Tian,Zhang Hua. Statistical approach to weak signal detection and estimation using Duffing chaotic oscillators[J]. SP Science China Press, 2011, 54(11)

[9]. Danhui Zhai, Qinjun Li, Ping Yang. Research on the Influence of Noise to Weak Signal Detection Based on Duffing equation[J],Computer Measurement and Control,2010,18(01):61-63.

[10].Jian Fan, Wenli Zhao, Wanqiang Wang. Research on chaotic detection performance of weak periodic signal based on Duffing oscillator[J]. Acta Phys. Sin., 2013, 62(18): 54-59.

Research on Multifunctional Guided Walking Stick System

Wang Zhihong; Zhang Yuehan; Yu Xuan; Wang Zhenzhen
（instrument science and engineering institute, jilin university）

***Abstract*-The multi-functional guide stick system successfully achieves real-time blind guidance, bringing convenience and sympathy to blind people's lives. The designed guiding sticks include three modules: measuring obstacles, voice broadcasting and communication. The obstacle detection module controls the height of obstacles by stepper motors and ultrasonic sensors through the STC89C51 single chip microcomputer, the distance and orientation of dynamic obstacles, and the distance of static obstacles; The voice broadcast module controls the Bluetooth headset through the STC80C51 MCU to achieve music playback, weather, time broadcast, and obstacle data broadcast functions. The communication module controls the GPS module through the STM32F103 microcontroller to obtain the latitude and longitude, the SIM card module sends latitude and longitude short messages and weather information, and the simulation 110 alarm. The three SCMs communicate through the serial port, in which the STM32 SCM of the communication module sends the weather information to the 51 SCM of the testing part. The obstacle detection part integrates the weather information and the obstacle information, and sends them to the broadcast module to broadcast the obstacle information. Weather and other data.**

***Keywords*-Ultrasonic Ranging; Location Avoidance; Bluetooth; GPS; Analog 110 AlarmI.**

I NTRODUCTION

THE blind group has always been a vulnerable group that needs to be cared for in the society. The inconvenience of going out is a big problem for the visually impaired. At present, there are many kinds of guide canes in the market, but most of them are simple in principle, single in function, relatively mechanized, and have many problems, which brings a lot of inconvenience to patients who often go out of sight. Moreover, with the rapid development of society, roads have become wider, more vehicles have been added, which pose a threat to the life safety of visually impaired patients, and improving the quality of life for blind people is an issue that we urgently need to address. Based on a simple and practical, low-cost point of view, it is necessary to design a smart cane that integrates GPS automatic positioning, multiple ultrasonic detection obstacles, and the ability to broadcast time and weather and obstacle data through a Bluetooth headset. This design integrates obstacle detection module, voice broadcast, and communication to achieve 0~180o dynamic obstacle angle detection, 0~60o static obstacle angle detection, 0~10m height and distance detection; and communication, analog 110 alarm, GPS positioning The information is uploaded to the mobile phone, which broadcasts system information, music, and audiobooks through Bluetooth headsets.

II.DESIGN SYSTEM

According to the system requirements, the design system is mainly composed of ultrasonic obstruction module, voice broadcast module, and communication module. The functional framework is shown in Figure 1.[1]

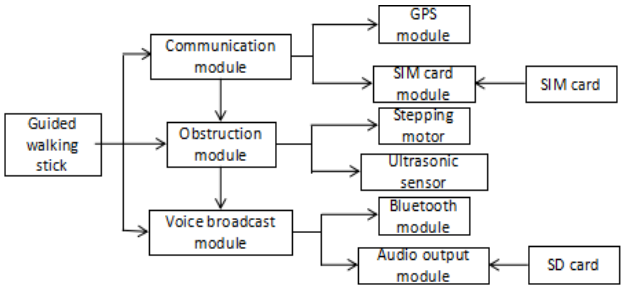

Fig.1 A functional framework for the design of a guide stick based on multiple sensors

III.ULTRASONIC DISTANCE MEASURING MODULE DESIGN

Ultrasonic sensors are currently a popular means of distance measurement. Compared with infrared ranging, ultrasonic ranging distance, the choice of output methods and other advantages. With the development of science and technology, the technology has been rapidly developed, performance has been continuously improved, functions have been continuously enhanced, varieties have been increasing, and the scope of application has also been continuously expanding, and is more suitable for obstacle avoidance. Based on the above points of view, this article designed a guide stick, accurately measures the distance between obstacles, and added a number of ultrasonic sensors to avoid dead angles, multi-position obstacles to obstacles, effective obstacle avoidance.

This module uses the STC89C51 master control, which controls the KS109 ultrasonic sensor [2] ranging, and controls the 9BYJ-48-5V stepper motor (ULN2003 driver) [3] for scanning auxiliary measurement angle.

When measuring the distance and azimuth of dynamic obstacles, stepping motor 1 uses ultrasonic sensor 1 to measure distance once every 10o. When the motor rotates 180o forward, the minimum value is taken as the shortest distance. The stepping motor

rotation angle is recorded when the distance is recorded. 180o empathy.

When measuring the height of the obstacle, the ultrasonic sensor 2 is used to measure the distance once every 10o, and the stepper motor 2 is rotated 90o in the forward direction, and the maximum and minimum values are taken. The height of the obstacle is calculated by the variance.

When measuring the distance of a static obstacle, an ultrasonic sensor 3 is used to operate.

Statistics above three data sent to the voice broadcast module.

The schematic diagram of the ultrasonic ranging module is shown in Figure 2 below.

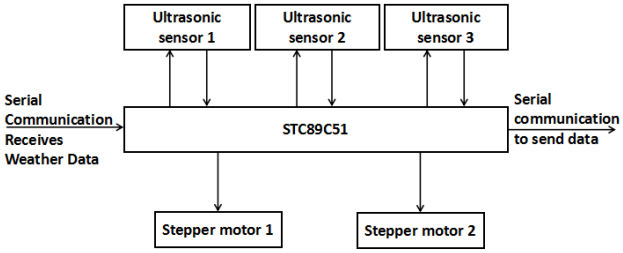

Fig.2 Ultrasonic distance measuring module block diagram

The ultrasonic sensor responds to the STC89C51 control via the I2C interface. Different beam I2C control commands are used to perform static and dynamic obstacle measurements. Through the delay, the ultrasonic sensor only performs the distance measurement when the stepper motor rotates 10 °.

The baud rate is changed to match the baud rate of the voice broadcast module and the communication module, so that it can conveniently receive the weather data of the communication module, and send the weather data together with the test data to the voice broadcast module.

The hardware connection is shown in Figure 3 below. The KS109 ultrasonic sensor requires four pins, where VCC is used to connect the +5V power supply, GND is used to connect the power ground, and SDA/TX is the data line of the I2C communication. It is connected to the P2.0 pin of the STC89C51. SCL/RX cited The pin is the clock line for I2C communication and is connected to the P2.1 pin of the STC89C51. Both the SCL and SDA lines require a 4.7K resistor from the host to pull up to VCC. Among them, the SDA and SCL pins used in the three KS109 ultrasonic sensors used in the module can be connected to a bus drawn from the P2.0 and P2.1 pins of the STC89C51, respectively. Two ULN2003 chips drive two 29BYJ-48-5V stepper motors via pins C1, C2, C3, and C4. The B1, B2, B3, and B4 pins are connected to the P1.0-P1.7 pin of the STC89C51 at a time. .

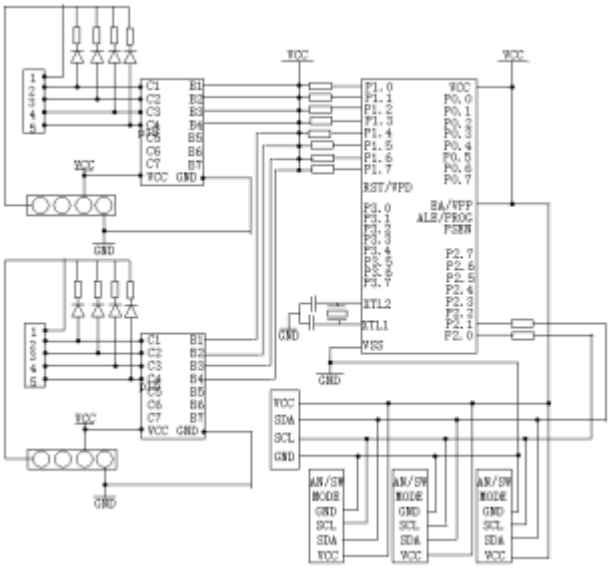

Fig.3 Circuit diagram for obstacle detection

IV. VOICE BROADCAST MODULE DESIGN

The voice broadcast module selects STC90C51 as the controller, music and audiobooks use SD card storage, time acquisition is completed with DS1302 clock module, BY8001 audio output chip as the audio signal output, using CSR Bluetooth module and BY8001 audio output chip and Bluetooth headset Connect, and finally output audio, block diagram shown in Figure 4.[5]

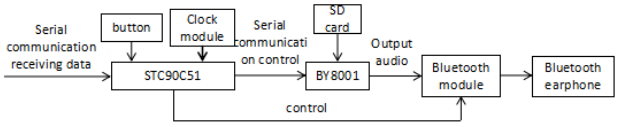

Fig.4 Voice module block diagram

The module receives the obstacle data and weather information from the STC90C51 control and obstacle detection module through serial communication. Press to select the type of audio signal to be output. When button 2 is pressed, BY8001 audio output module receives the control command of STC90C51 and outputs the corresponding audio signal; when button 1 is pressed, STC90C51 reads the current time value from the DS1302 clock module. The BY8001 audio output module receives the STC90C51 control command and outputs the audio signal of the corresponding weather and time information. When the button 3 is pressed, the STC90C51 controls the BY8001 to read the MP3 format file in the current folder of the SD card and output the corresponding audio signal. . The STC90C51 controls the Bluetooth module to receive the corresponding audio signal and transmit it to the Bluetooth headset for playback. [4]

The flow chart of this module is shown in Figure 5.

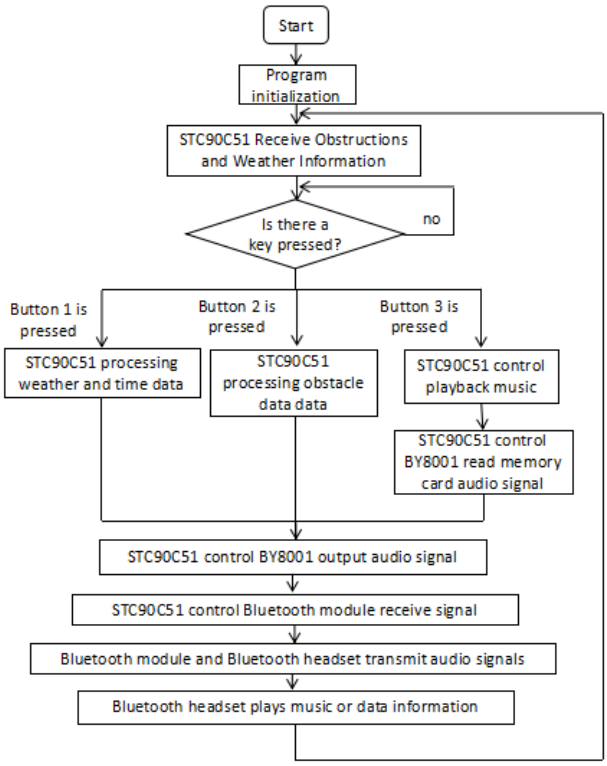

Fig5. Voice broadcast module flow chart

V.COMMUNICATION MODULE DESIGN

Functions that need to be implemented in the communication module include serial port sending that simulates one-touch alarms, sending longitude and latitude messages, and weather information. Based on the above requirements, the selection of module S1216 and module SIM900A is completed. The function of the S1216 module is to obtain local latitude and longitude information in real time. The function of the SIM900A module is to make calls, send short messages and receive short messages and read them.

The block diagram of the communication module is shown in Figure 6.

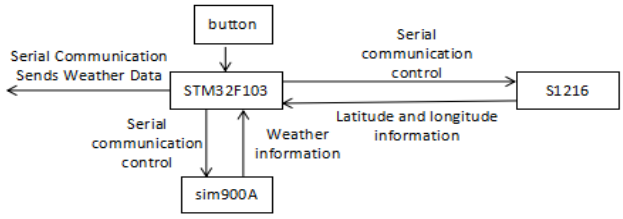

Fig 6. Circuit diagram for gps detection

The function of analog alarm is realized as follows: Writing a key interrupt in STM32, when the key is pressed, that is, when the pin p1 changes from high level to low level, the interrupt is triggered, and the control in the interrupt is sent as "AT+*****" The *****" AT command is sent to the SIM900A module. After receiving the AT command, the SIM900A module immediately calls the mobile phone number reserved in the program to successfully simulate the alarm. [6]

The method for sending latitude and longitude short messages is as follows: According to the reference data, you can use the command "MNEA_GNRMC_Analysis" to extract the latitude and longitude information. Therefore, in the STM32 set the p2 pin low-level trigger interrupt, when the p2 button is pressed, trigger this interrupt, the interrupt first send "MNEA_GNRMC_Analysis" to the S1216 module to read the latitude and longitude information, this information is interpreted and cached to the array During the delay, edit the text message again, and then send the message in a time-delay format such as "AT+CMGS="**********"", "SMS content", and "1A" (in hexadecimal). The sending instruction sends the edited latitude and longitude information message to the reserved mobile phone number. [7]

The method for sending weather information is as follows: In the STM32, an interrupt triggered by the low-level trigger of pin p3 is set, a fixed format information is sent to the SIM card in the SIM900A in advance, and an interrupt is generated in the STM32 by the key control. AT + CMGR = 1 "+ CMGR", the short message is read, the array is buffered in the STM32 MCU, and then sent to the STC80C51 MCU in the form of serial communication.

VI.EXPERIMENTS AND ANALYSIS

A Experiment

The practicality and stability of the entire system were tested. The experiment conducted an overall analysis of the guide stick.

This experiment simulates an experimental environment using a standard carton as the measured object. To measure the stability of the device, the experiment was set up to measure the experimental data every 1m, and the measurement distance was 1m to 10m. The obtained data is transmitted to the voice broadcast module through the communication between the single-chip microcomputers, and the data is obtained in the Bluetooth headset by pressing button two.

Next test the other functional modules:

(1) Simulate one-touch alarm: After the button is pressed, after about 10 seconds, the reserved mobile phone number receives the SIM card number call in SIM900A;

(2) Send latitude and longitude short messages: press the key two times, after about 10 seconds, the mobile phone number is reserved to receive text messages;

(3) Weather and time information broadcast: After the button 1 is pressed, the Bluetooth headset starts broadcasting weather and time information;

(4) MP3 music and audio books play function test: Press button 3 to start playing music or audio books stored on SD card, press button 4 to pause processing, press buttons 5 and 6 to press the previous song and next song processing , Press the buttons 7 and 8 to make volume and volume down.

B Analysis

After being measured in the ultrasonic distance measuring module, the measurement error within 8m

is 1.26%, and the measurement error from 8m to 10m is 2.37%. The data obtained from the Bluetooth headset is consistent with the data obtained from the obstacle detection module. As a result of the test, the effect is stable.

The communication module simulates a key alarm to receive the call. The content of the latitude and longitude message is: 43604724N 125113400E. The latitude and longitude information of the Baidu measurement site is: 43882304N125307140E. Using the online map to input the above two coordinates, it can be seen that the difference between the two sites is about 130 meters.

The communication module simulates a key alarm to receive the call. The content of the latitude and longitude message is: 43604724N 125113400E. The latitude and longitude information of the Baidu measurement site is: 43882304N125307140E. Using the online map to input the above two coordinates, it can be seen that the difference between the two sites is about 130 meters.

The weather and time data heard in the Bluetooth headset in the voice broadcast module are correct, and music and audio books can also be heard.

The experimental results show that each module realizes the measurement of obstacle distance, height, and azimuth of the system, simulates the alarm 110, uploads the GPS positioning information to the guardian's mobile phone, time, weather broadcast, and the function of playing music and audio books.

VII.CONCLUSION

In this paper, a multi-purpose guide stick is designed to gather the functions of obstacle detection, communication and voice broadcast together to realize the measurement of the distance, height and azimuth of the obstacle. The simulation 110 alarm, GPS positioning information upload To the guardian's mobile phone, time, weather broadcast, music and audio books, and other functions.

References

[1] KS109 Technical Specification. Guidance Technology Co., Ltd.

[2] Zhao Guoli.Design of Stepper Motor Control System Based on Single Chip Microcomputer[J].Industry and Technology Forum,2014,13(10):79-80.

[3] Liu Chun, Chen Zhibiao, He Guijiao. Research on Multifunctional Intelligent Guidance Cadenza System[J]. Wireless Network Technology, 2017(7):44-45.

[4] Qiu Hongchao,Liu Jiaoyu,Xiao Jie,Fang Lin.Design of Range Finder with Voice Broadcasting[J].Industrial Control Computer,2016,29(04):160-167

[5] Zhuang Peidong, Ma Guoqing, Ding Qun.Research and Application of Voice Broadcast Ranging System[J]. Electrical Measurement & Instrumentation, 2007, 44(502):40-4

[6] Electronic Enthusiasts Forum http://bbs.elecfans.com/jishu_1387474_1_1.html

[7] Li Chi,Duan Zhimin,Cong Peitian,Zhang Qi.Design of Network Multipoint Remote Data Monitoring System Based on STM32 and SIM900A[J].Microcomputerics & Applications,2016,35(24):105-108.

Novel color-changing light-absorbing display and its control technology

Lin TingTing[1]; Teng Fei[1]; Yang ShuJia[1]; Liu Yi[1]; Xia HongYin[2]
(1. College of Instrument Science and Electrical Engineering, Jilin University; 2. College of Chemistry, Jilin University)

***Abstract*—LED display has always been a research hotspot in the field of display, but it has low operating efficiency and high power consumption. It has always been a short board for applications and problems to be solved. In view of the inherent defects of LED displays, this article uses the electro-acid/electrochromic discoloration materials studied by the Supramolecular Materials and State Key Laboratory of the College of Chemistry of Jilin University as the raw material for display panels. It discusses how to use the new type of light-absorbing display materials to make displays and How to use MCU and FPGA to realize the drive and control of the new display screen, and the results verify the feasibility of the display screen manufacturing process and the feasibility of the control technology.**

***Key words*—Electro-acid-base material Display screen MCU FPGA.**

INTRODUCTION

ELECTRO-ACID/ALKALINE discoloration materials have enormous potential application value in display, information storage, sensors, optical communication and other fields. It is a research hotspot in recent years, with low energy consumption, large color contrast, high safety, and low operating voltage. Such advantages, in the future of social life, this material will be widely used, such as various signs in the city, billboards, can also be applied to electronic paper, smart glass, information storage, security materials, monitors, and smart Sensor. These advantages of new materials will all promote social progress and people's living standards.

Institute of Supramolecular Materials and State Key Laboratory of Chemistry, Jilin University, has developed a new type of electro-acid/alkaline color-changing material[1]. This kind of material is stable in structure, excellent in quality, and low in price, and can be maintained even under no voltage application. The color development for a long time, so the dot matrix display based on the material[2], has changed the traditional LED display operating efficiency is low, high power consumption of the shortcomings[3,4], this material requires only 1% ~ 5 of the energy consumption of ordinary circuits %, fast response time, good stability, and high contrast ratio. This article mainly introduces the production of a new type of display screen and a corresponding control system[5].

II. NEW DISPLAY MATERIAL WORKING PRINCIPLE

The discoloration process of the new light-absorbing material dot matrix screen is mainly based on the theory[6] of "electro-acid/alkaline discoloration" and electrochromic phenomenon (referred to when the material A undergoes an oxidation-reduction reaction and is converted into a material B with completely different spectral properties when subjected to electrical stimulation. When subject to counter-voltage stimulation, substance B is reversibly converted back to substance A. Substances A and B mentioned here may be two different redox states of the same substance, and may also be two different substances.

The main materials used here are fluorescein and 2,5-dimethoxyphenylhydrazone. The acid-base response material was applied to the electrochromic device, and the electrical stimulation was used instead of the chemical acid/base stimulation to achieve the redox reaction and its reverse process[7]. In addition, the new light-absorbing material has a memory effect. The memory effect mainly refers to the fact that the electrochromic material can still remain in an oxidized or reduced state after the operating voltage is removed. This memory effect is a unique property of the electrochromic material compared with display materials such as LCD, LED, and the like[15].

A.Feasibility test

Experimental raw materials:

Fluorescein,2,5-dimethoxyphenylhydrazine, tetrabutylammonium hexafluorophosphate (TBAPF6) and other raw materials are from Aladdin. Tetrabutylammonium hexafluorophosphate was recrystallized three times with ethanol and vacuum dried overnight. The chromatographic pure acetonitrile used in electrochemical tests was first stirred with CaH2 at room temperature overnight, and distilled under nitrogen protection conditions to remove the front fraction.

Test instrument:

Shimadzu RF-5310PC fluorescence photometer (Shimadzu Corporation, Japan), Bio-Logic SP-150 electrochemical workstation, Varian Mercury 300 MHz nuclear magnetic resonance apparatus, Shimadzu UV-2550 dual-channel UV-Vis spectrophotometer (Shimadzu Corporation, Japan).

Test Methods:

Cyclic Voltammetry: The test solution was tetrabutyl with 2,5-dimethoxyphenylhydrazine (n-BQ)/fluorescein (Flu) (1.0x10-3M/1.0x10-3) and 0.1 M. Ammonium hexafluorophosphate solution in acetonitrile is an acetonitrile solution containing

2,5-dimethoxyphenylhydrazine (1.0 x 10-3 M) and 0.1 M tetrabutylammonium hexafluorophosphate, or containing fluorescein (1.0 x 10-3 M) and 0.1 M tetrabutylammonium hexafluorophosphate in acetonitrile, the solvent is anhydrous chromatographic grade. Working electrode is glassy carbon electrode (surface area is 7 mm2, Shanghai Chenhua), auxiliary electrode is platinum wire electrode (Shanghai Chenhua), reference electrode is Ag electrode (Shanghai Chenhua), ferrocene Make a reference.

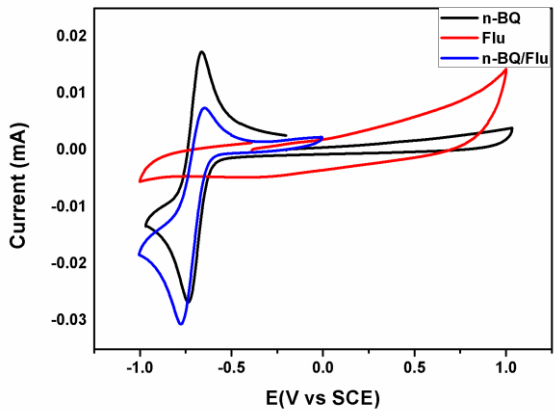

Fig.1 Cyclic voltammograms of 2,5-dimethoxyphenylhydrazone, fluorescein and their mixed systems

Preparation of test solution: containing 2,5-dimethoxyphenylhydrazine/hydroquinone/fluorescein (2.0x10-5 M/2.0x10-4 M/5.0x10-5 M) and 0.1 M Tetrabutylammonium hexafluorophosphate in acetonitrile.

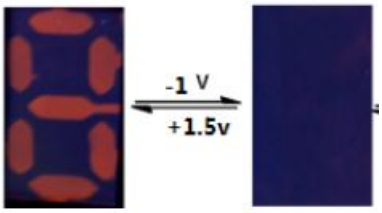

Fig.2 The principle of discoloration of electrochromic materials

As shown in the figure, the display screen does not develop color when no voltage is applied, and when the screen is stimulated with a voltage of 1.5V, the display screen is colored (red); when the screen is stimulated with a voltage of -1V, the display screen is discolored, and the display screen is realized[9,10].

B.New display production process

(1) Material properties

The main component of the ITO film is indium tin oxide. In the case of a thickness of only a few thousand angstroms, the ability of indium oxide to pass through is high and the tin oxide has a high conductivity. The ITO glass used in the new type of light-absorbing display is a conductive glass with high transmittance. Because ITO has a strong water absorption, it absorbs moisture and carbon dioxide from the air and reacts with chemicals and deteriorates. Therefore, it must be protected against moisture during storage. The ITO layer is prone to ion exchange reaction in the active valence ion solution to form other reactive substances that have poor conductivity and permeability. Therefore, in the process of processing, the active valence ion solution is avoided for a long time. The ITO layer consists of many fine crystal grains. The crystal grains will crack and become smaller during the heating process, thus increasing more grain boundaries. When the electrons break through the grain boundary, they will lose some energy, so the ITO layer of the ITO conductive glass is at 600 degrees. The following will increase the resistance as the temperature increases.

(2) Cutting of ITO glass

The ITO glass (40*40) was cut with a glass knife, rinsed with dichloromethane and absolute ethanol for about 15 minutes, and blown dry with nitrogen to ensure that it was in an anhydrous condition.

(3) Production of New Type of Dot Matrix Screen

An 8*8 lattice circuit template was drawn on the computer, and an 8*8 dot matrix was etched on the ITO glass using a laser printer. Make chemical devices and inject the prepared electrolyte[8].

III. DISPLAY DRIVE CIRCUIT AND CONTROL PRINCIPLE

The new type of color-changing light-absorbing display screen is filled with electro-acid-base color-developing material, which is different from the traditional LED common cathode or common anode. Its anode is respectively connected with the control end, and its cathode is a high-transmittance conductive ITO glass. Some point on the screen is lit and needs to pass through the corresponding control end. According to the new material coloration principle above, applying a positive voltage of 1.5V can make the display color, and applying a negative voltage of -1V can fade the display. When no voltage is applied, the display will remain unchanged for a long time.

Based on the above principle, if the display screen is required to display the setting content, it is necessary to control the coloring, fading, and maintaining state of each point through the controller, which requires designing a corresponding controller to realize the drive and display of the new type display screen.

Ⅳ.OVERALL SYSTEM DESIGN

The SCM control system is mainly composed of STM32 as the main control CPU[11], taking into account the control of the new lattice display screen requires more control ports, so the use of FPGA for auxiliary control[12,13].

In addition to the STM32 controller, the hardware circuit of the display controller consists of three parts: the human-machine dialogue window consisting of the LG12864 and the control keyboard, the bipolar programmable voltage source, the FPGA-controlled

switch selection logic control unit, and the block diagram of the controller. As shown in Figure 3.

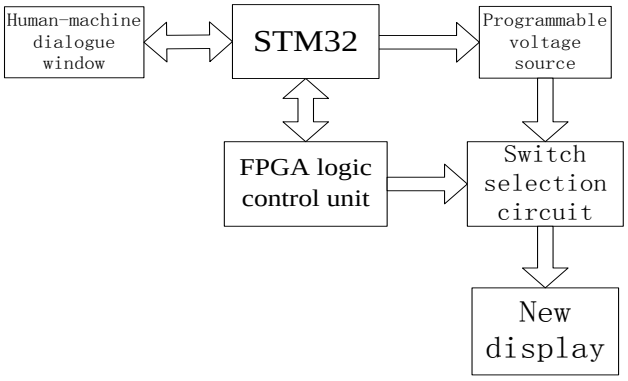

Fig.3 System structure frame diagram of new display

A.Human-machine dialogue window

The man-machine dialogue window consists of an LG12864 LCD display and keyboard. It sends commands to the STM32 control module through a keyboard scan and is displayed on the LG12864 liquid crystal display after processing[19]. This enables real-time information transmission and user-friendly operation.

The menu display is based on the LG12864 display. The contents of the display include the voltage provided by the system, the power-on time, the characters to be displayed, and the color or fade function. The LG12864 does not contain fonts internally, and it requires its own mode and the left and right half screens are controlled independently. The left half screen pixels are 64*64 pixels and the right half screen pixels are 64*64 pixels. The left and right half screens need to be driven separately[17,18].

Through the keyboard input command, the LG12864 display visually displays the input data. At the same time, the STM32 controls the voltage source according to the input data and transfers the data to the FPGA logic control unit to realize human-machine dialogue.

B.Bipolar Programmable Voltage Sources

Based on the new type of display screen, the forward voltage is applied to develop color, the reverse voltage is applied to fade, and remains unchanged when no voltage is applied, and the color fading voltage is affected by the environment. According to the electrochemical test results of the new material, the material can achieve color fading within the voltage range of -3v~+3v, but the color fading response effect is different. Therefore, it needs a controllable voltage source to adjust the voltage so that the display reaches the best color rendering state.

Because the display screen needs to adjust the voltage range is not large, step voltage is 0.1v, while the output resolution of 8-bit DAC0832 is 1/255, when the reference voltage is 5v, the minimum step is 0.02v, can meet the design requirements, The DAC0832 is simple and inexpensive, so the DAC0832 digital-to-analog converter is used to implement the bipolar programmable voltage source design.

Use STM32 as the control chip[14], connect with the digital-to-analog converter DAC0832 data interface, and make DAC0832 work in single buffer mode. Input the given value through the keyboard, and convert the digital quantity into analog quantity with the digital-analog converter DAC0832, and output the control voltage. The analog voltage value output by the DAC0832 is amplified by the op amp LM358, and the bipolar output of the programmable voltage source is achieved by controlling two DAC0832 and LM358.

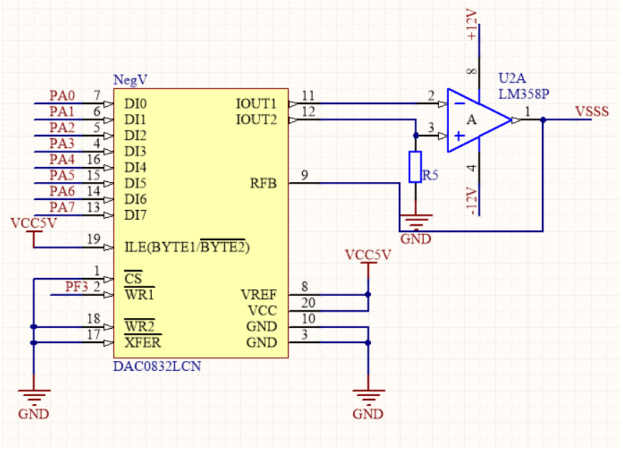

Fig.4 Programmable voltage source control circuit

C.SPI Communication Between STM32 and FPGA

Communication part In order to realize the reliable communication between STM32 and FPGA, must guarantee that both sides have the same data format and baud rate, this design adopts STM32 serial peripheral interface SPI to receive the data information, realize the data transmission SPI with FPGA The communication protocol between the host and the slave is: The master transmits 16 bits of data to the slave. The first 6 bits represent the key typed characters on the keyboard, followed by 2 bits representing color/fade, and the last 8 bits represent the color or fading delay. The transfer of SPI data is actually done through a shift register. The host shifts the data from its own shift register, while shifting the data from the shift register of the slave and removing its own data. Simply to understand, just like to paste two registers together, and then perform a loop left or loop right (SPI transmission can choose to send high or low first), until the exchange of data between the two registers. The clock signal SCLK controls the transmission rate.

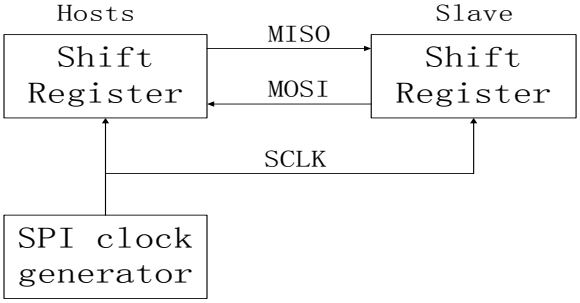

Fig.5 SPI communication schematic

D.Switch Selection Circuit Under FPGA Control

The switch selection circuit module is mainly

composed of ADG442 analog switches. As shown in FIG. 7 , the ADG442 includes four independent SPST switches, which are turned on at a logic high level, and the ADG442 switches have fast switching time, low power consumption, low leakage current, and conduction. The resistance is small.

The control signal of FPGA module comes from SPI communication with STM32, mainly adopt VerilogHDL programming, receive the 16 data transmitted by main controller through SPI, process and process. FPGA output control port is divided into fading control a port, color control b port, a port and b port are connected to the control switch on and off ports of the ADG442, and the on-off of the color port voltage and the fading port voltage are achieved by controlling the switch on and off. s Choice.

FPGA processing includes character processing[16], color fade processing, and fade-fade delay time processing. According to the processing result, the high and low levels of a port and b port are assigned, and then the ADG442 four-way analog switch is controlled to achieve the corresponding new display screen. Color, fade, and hold.

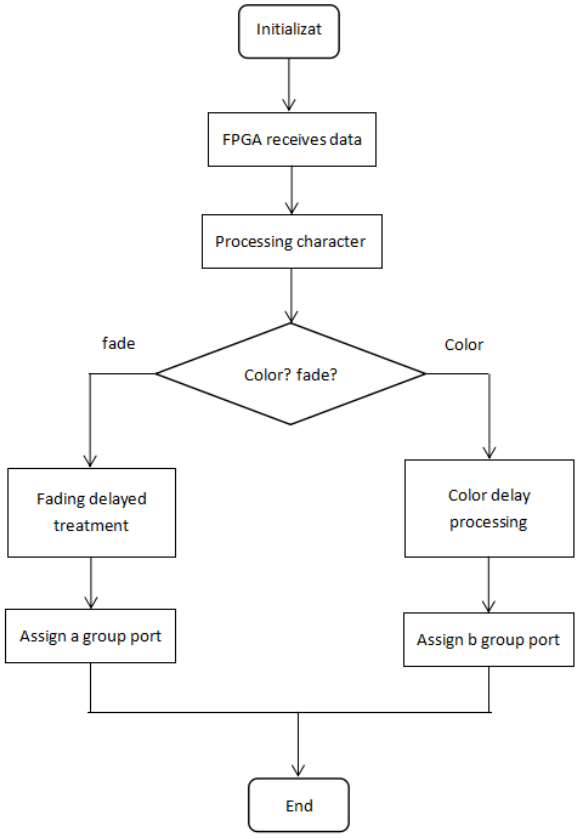

Fig.6 FPGA to receive data processing flow chart

In an actual circuit, each two independent switches are respectively connected to a lattice point and a positive and negative power supply. As shown in FIG. 8 , under the control signal of the FPGA control module, if the “color” is displayed, the positive voltage is connected. The switch is closed and positively charged; if it is "faded", the switch connected to the negative voltage is closed and negatively charged; if neither "coloring" nor "fading" is required, no power is applied so as to achieve lighting of the dot matrix. , fading or keeping.

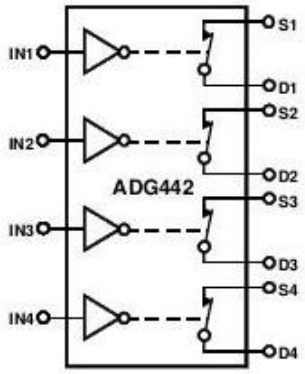

Fig.7 Functional Block Diagram of ADG442 Analog Switch

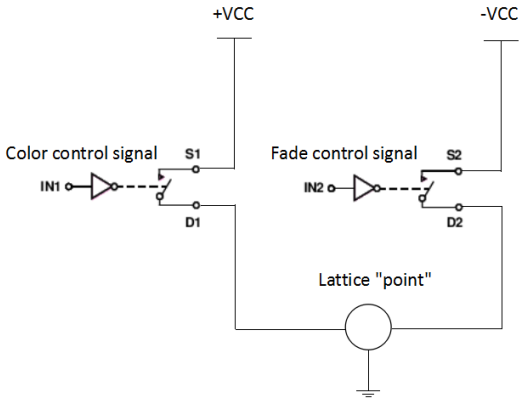

Fig.8 Lattice circuit connection diagram

Ⅴ.TEST RESULTS

A. Programmable voltage source voltage output result

In order to verify the reliability and practicality of the programmable voltage source, the output of the voltage source was tested. The test results are shown in the following table:

Table1 Setting/actual output voltage comparison table

setting/v	1.3	1.4	1.5	1.6	1.7	1.8
actua/v	1.22	1.32	1.42	1.50	1.60	1.69
setting/v	-0.7	-0.8	-0.9	-1.0	-1.1	-1.2
actua/v	-0.66	-0.78	-0.86	-0.95	-1.02	-1.15

According to the above table, it can be seen that there is a certain pressure drop on the line, so it needs about 0.1v compensation when setting the forward voltage.

B. "8" display debugging results

After the system is connected to the power supply, the output voltage is adjusted by controlling the keyboard. When a forward voltage of 1.5V is applied, the lattice points are colored. When a reverse voltage of -1v is applied, the lattice points are faded. If the voltage is not applied, the original state is not maintained. change. As shown in FIG. 8 , the required parameters are set on the control platform to set the display character as “1” or “7” as an example. The

application of the forward voltage time is 15s and the reverse voltage application time is 40s; when the system is running In the status of color, the highlighted “1” or “7” is successfully displayed on the display, and the character “1” or “7” remains unchanged after the power off; the display fades when switching to the fade operation status. , restore the original "blank" state.

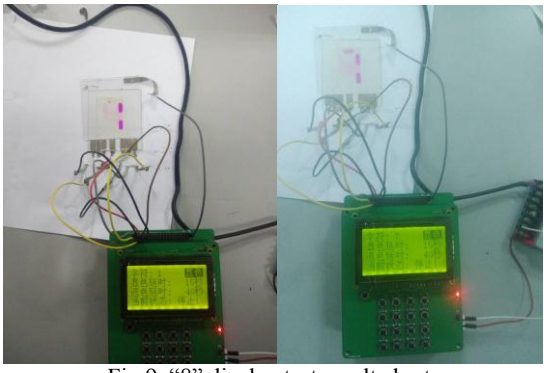

Fig.9 “8” display test result chart

Ⅵ.CONCLUSION

This article demonstrates the feasibility of this new display screen manufacturing process and the feasibility of control technology. At the same time, the control technology described in this article can provide a normal working environment for the new display screen, enabling the display screen to achieve normal color development and fading. , for the application of this material to achieve a forward-looking basic research.

References

[1] Zhang Yumo. Electro-acid/base theory and its application in organic electrochromic materials [D]. Jilin University, 2015.

[2] J. Cummings, C. Cai, L. Kondic. Towards an optimal model for a bistable nematic liquid crystal display device[J]. Journal of Engineering Mathematics, 2013, 80(1).

[3] Wang Xin, Lu Yang, Wei Jie, Guo Jinbao. Research progress of bistable liquid crystal display technology[J]. Information Recording Materials, 2011, 12(06): 25-33.

[4] Xia Meng. Design and Implementation of LED Display Based on ARM and CPLD[D]. Nanjing University of Aeronautics and Astronautics, 2009.

[5] Zhang Guanglei, Du Yanliang. Smart materials and structural systems[M]. Beijing: Peking University Press, 2010.

[6] Mortimer R J. Electrochromic materials [J]. Annual Review of Materials Research, 2011, 41:241-268.

[7] Chan J CH, Lam WH, Wong HL, Wong WT, Yam V WW. Tunable Photochromism in air-stable, robust dithienylethene-containing phospholes through modifications at the phosphorus center[J]. Angewandte Chemie International Edition, 2013, 52(44): 11504-11508.

[8] Kiri P, Hyett G, Binions R. Solid state thermochromic materials [J]. Advanved Materials Letters, 2010, 1(2): 86-105.

[9] Yen H-J, Lin H-Y, Liou G-S. Novel starburst triarylamine-containing electroactive aramids with highly stable electrochromism in near-infrared and visible light regions[J]. Chemistry of Materials, 2011, 23(7):1874-1882.

[10] Raymo F M, Tomasulo M. Electron and energy transfer modulation with photochromic switches [J]. Chemical Society Reviews, 2005, 34:327-336.

[11] Zhai Rina. Real-time control circuit design of LED dot matrix screen based on ARM[J]. Guangxi Education, 2015(23): 176-178.

[12] Lu Xinyun, Chen Wei, Zhang Jun. Design and Implementation of LED Dot Matrix System Controller Based on FPGA[J].Liquids & Displays, 2014,29(06):926-932.

[13] Zhou Peng, Li Yuanyuan. Design of LCD LCD Dynamic Display Driver Based on FPGA[J]. Electronic Quality, 2014(11):34-36+42.

[14] Li Chao. Research on LED Display Control Technology Based on ARM[D]. Nanjing University of Science and Technology, 2009.

[15] Huang Ziqiang. Bistable technology in flat panel display: status quo and progress (1) [J]. Modern Display, 2009(04):5-10.

[16] W.Kurdthongmee.Design and implementation of an FPGA-based multiple-colour LED display board[J]. Microprocessors and microsystems,2005

[17] L.Svilainis.LED brightness control for video display application[J].Displays,2009

[18] Blue LED based white light generation: Issues and control[J].Industry Applications Conference,2002

[19] L.Svilainis.LED PWM dimming linearity investigation[J].Displays,2008.

Anti snoring pillow design based on DSP voice recognition technology

Chen Chao; Zheng Yiming; Zhao Hang
（instrument science and engineering institute, jilin university）

***Abstract*—The direct cause of snoring is due to sleeping position and other issues caused by the narrowing of the respiratory tract, the air can not pass smoothly. However, existing anti-snoring pillows focus on preventing snoring through magnetic field or traditional Chinese medicine, but in fact these methods do not have a mature technical system and a complete theoretical basis. Not only does not apply to all people, and the effect is not high, the price is very expensive. Therefore, a system is designed to automatically change the user's sleeping position according to the snoring situation of the user by changing the shape of the air bag placed in different parts of the pillow so as to prevent snoring.**

On the basis of consulting the relevant literature at home and abroad, the mechanism and characteristics of snore sound are analyzed in detail. By comparing with the speech signal, the feasibility of using snoring sound to process snoring sound is analyzed. On the basis of DSP technology, a snore recognition algorithm was established based on DSP technology, and the snore time domain, frequency domain feature and MFCC eigenvalue were extracted, and then the algorithm was transplanted to TMS320F28335. The DTM pattern recognition method was used Snoring for identification testing. DSP and then test the results with the PWM waveform-driven pump control air bag deflation to adjust sleeping position, so as to achieve the effect of assisting sleep. After the actual test the system works well.

***Keywords*—DSP Technology Signal Processing Voice Recognition Dynamic Time Warping (DTW)**

0 FOREWORD

THE anti-snoring pillow extracts the characteristics of the time domain and frequency domain of the snoring sound, establishes the snoring recognition algorithm and transplants it into the DSP, and processes the click signal through the DSP to detect whether the sleeping person is snoring and judges the result of the recognition to charge the air bag. Ventilate to adjust the sleeper's sleeping position to prevent snoring.

I. THE ESTABLISHMENT AND IMPLEMENTATION OF SQUEAK RECOGNITION ALGORITHM

A. Implementation

The voice recognition belongs to pattern recognition. Firstly, the collected snoring acoustic signal is pre-processed, and the MFCC model of the snoring acoustic signal is extracted by extracting the time-frequency and frequency domain characteristic parameters of the input snoring acoustic signal. The squeak feature vector sequence is obtained through the Dynamic Time Warping (DTW) recognition algorithm. The distance between the humming templates in the template library is used to find a template with a similar degree. The input signal can be considered as the same as the template signal, and then the recognition result of the humming signal is output.The DSP judges the result of the recognition, generates a PWM waveform to drive the DC motor airbag, adjusts the inflation and deflation state of the airbag, and changes the sleeping state of the sleeping person to improve the sleep quality.

B. Barking time and frequency domain features

Audio feature parameter extraction is to extract information from the audio signal that is useful for sound perception and can accurately represent this audio signal. "The characteristic parameters of the audio signal are sometimes in the domain and in the frequency domain. The sound can be obtained by sampling the sound signal. Time domain information, but if performing voice recognition, often requires frequency domain analysis "The purpose of frequency domain analysis is to transform complex time domain waveforms into thousands of harmonic components to study if the frequency structure of the sound is obtained.

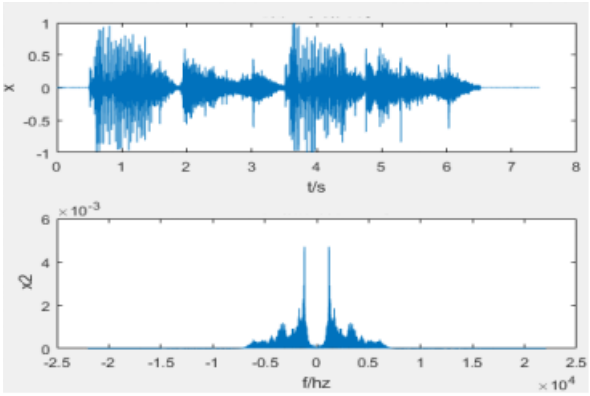

Fig. 1. Barking time and frequency domain feature maps

C. Hum pretreatment

Under normal circumstances, the internal and external noise of the system will not be processed before the feature extraction, it is not conducive to the extraction of signal useful components, causing inconvenience to the signal analysis and calculation.

Therefore, the original signal must be preprocessed.The hum noise frequency domain signal mainly consists of high frequency components. In order to improve the recognition effect of the humming sound, it is necessary to pre-emphasize the high frequency part of the snoring sound.The signal is pre-emphasized, usually after digitizing the sound signal, passing it through a first-order high-pass filter, ie a pre-emphasis filter.Its transfer function is shown in Equation (1).[1]

$$H(z)=1-\frac{u}{z} \quad (1)$$

Among them, u is the weight coefficient, ranging from 0.9 to 1, with a value of 0.9.

Since the sound number is a random signal, it has non-stationary characteristics, but in a very short time (10-30ms), the audio signal can be regarded as a quasi-steady state process.Therefore, the audio signal should be windowed and framed. The number of frames is usually about 33-100 frames/sec.In order to make frame-to-frame smoothness excessive, framing generally uses alternate segmentation methods. The length of the overlapped signal segment between the previous frame and the next frame is the frame shift. In general, the length of the frame shift does not exceed the length of the frame

1/2. The frame division is implemented by weighting the fixed-length movable window, that is, using the window function w(n) to multiply the original signal s(n) to form the windowed signal sw(n) as shown in equation (2).

$$H(n)=\begin{cases}0.54-0.56\cos\left[2\pi n/(N-1)\right], 0\le n\le N-1\\ 0, \quad n=other\end{cases} \quad (2)$$

There are many noises in the collected snoring signals. In the process of identifying them, to ensure the recognition rate and to reduce the storage and processing time of the data, it is required to correctly recognize the start and end positions of the snoring sound. Therefore, endpoint detection is required for hum. The parameters commonly used in endpoint detection include short-term energy, zero-crossing rate, cepstral distance, pitch difference, and energy spectrum variance. The system adopts a dual threshold detection method based on short-term energy and short-term zero-crossing rate.

Short-term energy: In the sound signal collected by mic, the energy of the click signal is much greater than that of the noise signal, so the start and end points of the click signal can be distinguished by the difference in energy. The short-term energy of the n-th frame audio signal x(m) is represented by E(n), as shown in equation (3).

$$E(n)=\sum_{m=0}^{N-1}\chi^{2}(m) \quad (3)$$

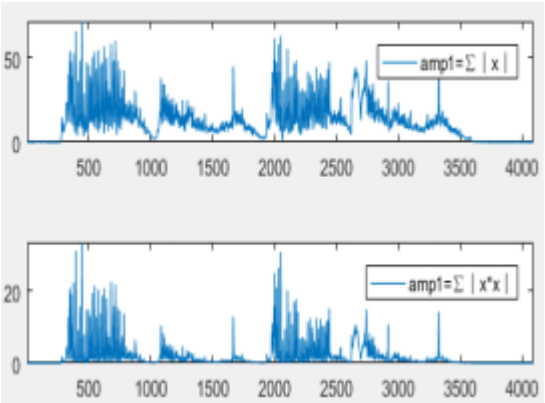

Fig. 2. Bark amplitude, short-term energy diagram

Short-term zero-crossing rate: The short-time zero-crossing rate indicates the number of times a sound signal waveform passes through the horizontal axis (zero level). For continuous sound signals, zero-crossing means that the time domain waveform passes through the time axis; and for discrete signals, if the adjacent sample value changes sign, it is called zero-crossing. The short-term zero-crossing rate of the sound signal x(m) is represented by Z, as shown in equation (4).

$$Z=\frac{1}{2}\sum_{m=0}^{N-1}\left|\mathrm{sgn}\left[x(m)\right]-\mathrm{sgn}\left[x(m-1)\right]\right| \quad (4)$$

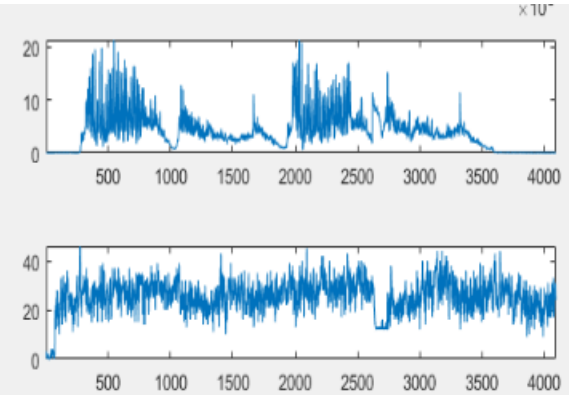

Fig. 3.Short-term energy, zero rate diagram

Double-threshold detection method based on short-term energy and short-term zero-crossing rate.Short-term energy and short-term zero-crossing rate of the double-threshold endpoint detection method is to set short-term energy and short-term zero-crossing rate of two threshold characteristics to end-point detection of the sound signal. Using a double threshold detection method to process a sound signal, if the short-term energy and the zero-crossing rate of a certain signal are small or all zero, it can be considered as a useful signal segment; the rest is useless noise.

D. Humming frequency domain analysis

Frequency domain analysis of the click signal is performed using a fast Fourier transform. The basic idea of the fast Fourier transform method is to use the periodicity and symmetry of the complex exponential function, make full use of the intermediate operation results, and greatly reduce the computational workload. It is to decompose a long-term sequence x(n) into a relatively short time series. The sub-time series can be further decomposed into smaller sub-time series, recursively until finally the simplest sub-time series is obtained. To a number up; then use the Fourier transform formula to Fourier transform the simplest sub-time series obtained finally, and then combine the Fourier transform results of each sub-time series according to certain rules, and finally get Fourier transform of the original time series.

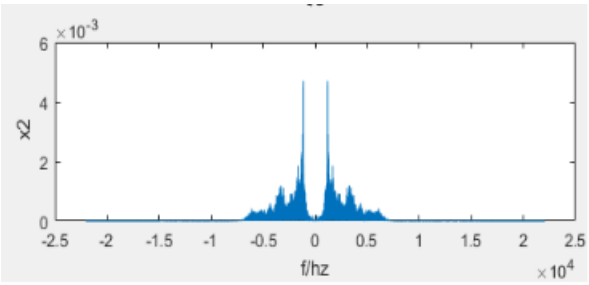

Fig. 4.Humming frequency domain feature map

E. Barking MFCC feature extraction

Melt frequency cepstrum coefficients are used to extract the MFCC eigenvalues of squeak. Melt cepstrum coefficient (MFCC) is a main characteristic parameter of speech recognition based on the auditory characteristics of the human ear, which has a nonlinear relationship with Hz frequency. Studies have found that the cochlea plays the role of a filter bank in the human auditory system, enabling the human ear to have good recognition performance and noise immunity. At low frequencies, the filtering is performed on a linear scale; at high frequencies, the filtering effect is on the logarithm.

Scale up. This makes the MFCC's computational accuracy decrease as the frequency increases. Based on this characteristic, the Fourier transform of the short-term audio signal uses a triangular filter bank that is evenly spaced on the Mel scale to obtain approximately equal frequency resolution.

Mel scale is defined as: $2595\lg\left(1+\frac{f}{700}\right)$

There is a strong correlation between the signals output by the filter bank. Therefore, it is necessary to perform a cepstrum transformation to reduce the correlation. Discrete Cosine Transform (DCT) is used here to obtain cepstrum coefficients.[2]

F. Barking recognition and detection

In isolated speech recognition, the simplest and most effective method is to use the DWT dynamic time warping algorithm. This algorithm is based on the idea of dynamic programming (DP) and solves the problem of template matching with different lengths of pronunciation. It is earlier and more common in speech recognition. A classic algorithm. This algorithm is often used in acoustic target recognition, especially in embedded systems where the amount of memory is relatively small. This system uses the DTW algorithm for snoring recognition. A brief introduction to this algorithm will be given below.

Each entry in the template library is called a reference template.

Usually a reference template is represented as:

{R(1), R(2),,,R(m),,R(M)},

m is the time sequence number of the training sound frame, m-1 is the starting signal frame, m-M is the end signal frame, so M is the total number of signal frames included in the template, and R(m) is the feature vector of the m-th frame. An input target signal to be identified is called a test template, which can be represented as {T(1), T(2),,,T(n),,,T(N)}, where n is the timing index of the target acoustic signal. N-1 is the starting signal frame, and n-M is the end signal frame. Therefore, N is the total number of signal frames included in the template. T(n) is the feature vector reference template and test template of the nth frame. Generally, the same type of feature vector, the same frame length, the same window function and the same frame shift are generally used. Of course, the end point detection algorithm is used to determine the start point and the end point no matter in the stage of training and establishing the template and the identification stage.

Assume that the test and reference templates are denoted by T and R respectively. To compare the similarity between them, the distance D(T, R) between them can be calculated. The smaller the distance, the higher the similarity. In order to calculate this distortion distance, it should be calculated from the distance between each corresponding frame in T and R. Let n and m be the frame numbers arbitrarily chosen in T and R, and D(T(n), R(m)) to represent the distance between the two feature vectors. The distance function depends on the distance metric actually used. Euclidean distance is usually used in DWT algorithm, if N-M can be calculated directly, otherwise T(n) and R(m) should be considered for alignment.Alignment can use linear expansion method, if N<M can linearly map T For a sequence of M frames, calculate its distance from {R(1), R(2),,,R(M)}" but this calculation does not take into account the fact that the sound segments are in different situations. Durations can produce long or short changes, so the recognition effect cannot be optimal. "So it's more about using dynamic programming (DP)."

If each frame number of the test template n is plotted on the horizontal axis in a two-dimensional rectangular coordinate system, each frame number of the test template is plotted on the vertical axis in a two-dimensional rectangular coordinate system. Marking, drawing a number of vertical and horizontal lines to draw a number of vertical and horizontal lines through these frame numbers representing the frame number, each intersection point (n, m) in the grid represents a frame in the test pattern and one of the templates. The intersection of frames. The DP algorithm can be attributed to finding a path through several grid points in the grid. The grid points passed by the path are the frame numbers for distance calculation in the test and reference templates. The path is not randomly selected, and the speed of any language is first. It is possible to change, but the order of its parts cannot be changed, so the path chosen must start from the lower left corner and end from the upper right corner.[3]

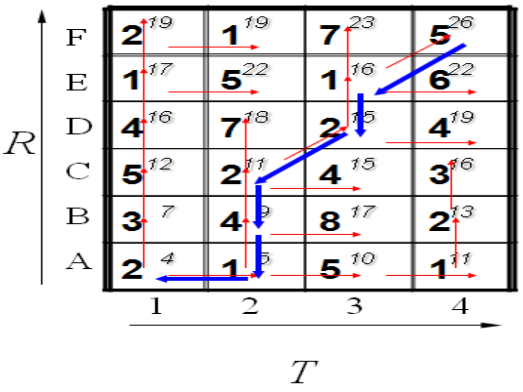

Fig. 5.DTW algorithm search path diagram

II. SYSTEM HARDWARE DESIGN IMPLEMENTATION

A. Hardware system overall design

The whole system is designed based on DSP. The DSP judges the recognition result through relevant above-mentioned algorithms. Through the PWM internal PWM peripheral, it drives the DC motor air pump through PWM pulse wave. The air pump adjusts the size of the airbag through charging and deflation to change Sleepers sleep in order to improve sleep. And use the LCD screen to display system operating status and buzz recognition results.

B.DSP signal processor

This system DSP signal processor chooses TMS320F2812. The TMS320F2812 operates at up to 150 MHz (clock cycles of 6.7 ns), processing data faster and efficiently. With a rich GPIO port, you can control the GPIO port to achieve the call to each module circuit. With PWM built-in, it can generate PWM pulse waveform for DC motor air pump driving. On-chip 36 K word SRAM can handle a large amount of complex data processing; on-chip RAM is reliable, not susceptible to external disturbances and does not cause external electromagnetic interference, and some on-chip memories can be accessed in one instruction cycle Two times, the instruction is more efficient and the simulation efficiency of the system is improved. And on-chip 128K ×16-bit Flash memory, no external expansion of Flash, simplifying the hardware structure.

C.Humming acquisition module

The buzz acquisition chip selects TLV320AIC23 audio processing chip. The TLV320AIC23's analog-to-digital converter and digital-to-analog converter (DAC) are integrated inside the chip. Adopt advanced oversampling technology. 16-bit, 20-bit, 24-bit, and 32-bit sampling data can be provided at sampling rates from 8kHz to 96kHz. The output signal-to-noise ratio of ADC and DAC can reach 90dB and 100dB respectively. Simultaneously. The TLV320AIC23 also has very low power consumption (23mW in playback mode and 15μW in power saving mode). The above advantages make the TLV320AIC23 a very ideal audio codec, and it complements TI's DSP series.

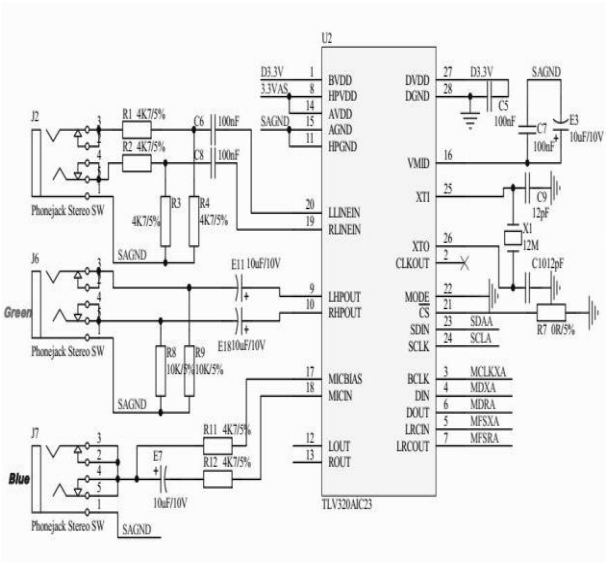

Fig. 6. Bark sound acquisition module circuit diagram

D. Motor drive module

Using the TMS320F2812 internal PWM module to generate two independent EPWM1A waveforms and EPWM1B waveforms Two PWM signals with deadband directly from the pin to generate motor drive using two NPN and two PNP transistors. The air pump can be controlled to change the size of the airbag.

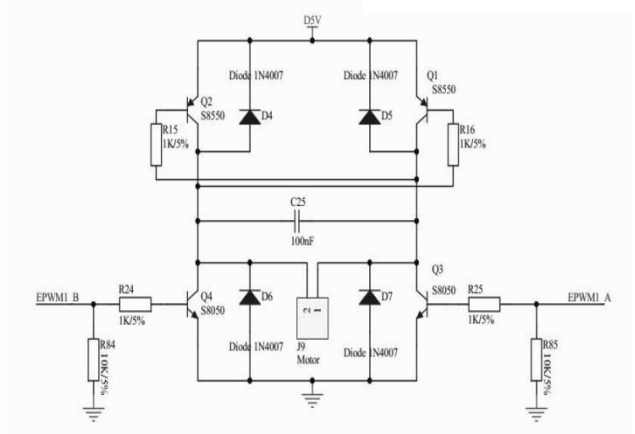

Fig. 7.PWM DC pump module circuit diagram

E.LCD module

1602 liquid crystal is a dot-matrix LCD module designed to display letters, numbers, symbols, etc. It consists of a number of 5X7 or 5X11 dot matrix character bits. Each dot character can display one character. Each bit has an interval between dot lines. Each line also has an interval, which can be used as a character spacing and line. The role of spacing. With its English words displayed, it can be used to simply display DSP work status and click recognition results.

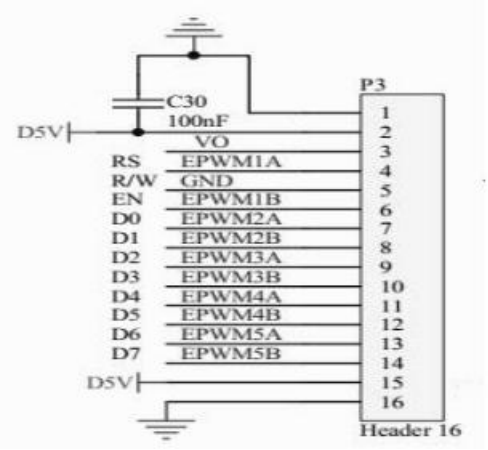

Fig8.LCD module circuit diagram

III. Test Results

The accuracy of the system was tested by humming the MP3 player to simulate the hum in the actual state. After 50 test results, the system can accurately identify 30 snoring sounds, and can drive the air pump to deflate and change the airbag size. Therefore, the system as a whole can meet the design requirements.

IV. Conclusion

The immediate cause of snoring is narrowing of the respiratory tract due to problems such as sleeping position, and the air cannot pass smoothly. The existing anti-snoring pillows focus on the prevention of snoring through magnetic fields or traditional Chinese medicines. However, in reality, these methods do not have a mature technical system and a complete theoretical basis. Not only does it not apply to all people, but it also has poor efficacy and the price is very high. The system can automatically change the sleeping position of the user according to the user's snoring conditions and change the shape of the airbag placed in different parts of the pillow, thereby improving sleep.

References

[1] Li Yunhuan. Research on Traffic Information Detection Technology Based on Voice Recognition[D]. Chang'an University, 2014

[2] Hu Zhifeng. Research on Train Early Warning Based on Embedded Sound Recognition Technology[D]. Southwest Jiaotong University, 2007.

[3] Xia Huida. Research on Sound Target Recognition in Battlefield Based on DSP[D].North University of China,2006.

[4] Zhou Xiaowu. Design and Research of Embedded Real-time English Speech Recognition System[J]. Electronic Design Engineering, 2017, 25(08):187-190.

[5] Dong Hu. Home service robot control system based on embedded speech recognition[J]. Microcomputer Applications, 2017, 33(04): 15-19.

[6] Zhong Chenfan. Design and Development of Speech Recognition System Based on LD3320 Chip[D]. Nanjing University, 2015.

[7] Yang FN. Research and design of embedded speech recognition system [D]. Wuhan University of Technology, 2014.

[8] Wang Zhiguo. Research on key technologies of embedded human-machine speech interaction system [D]. University of Science and Technology of China, 2014.

[9] Cui Jinzhong, Zhou Yuanbin, Chen Leibiao. Implementation and Optimization of Embedded Speech Recognition System Based on DHMM[J]. Journal of University of Electronic Science and Technology of China, 2013, 42(06): 930-934.

[10] Chen Yu. Research and design of home appliance keyword speech recognition system based on embedded.

[11] Sheng. Design and Implementation of Embedded Speech Recognition System

[12] Zhang Yingzhen. Development of embedded speech recognition system and its application in smart furniture

[13] Liu Min. Research on Speech Recognition Technology of Embedded Platform

[14] SHAO Xuebin. Automobile air conditioning control system based on speech recognition

[15] Wang Huan. Research and implementation of voice control terminal for embedded non-specific human vehicle electrical appliances

[16] Yan Xian. Research and Design of New Voice Interactive Smart Home Monitoring System

[17] Jia Jing. Design of embedded speech recognition module based on STM32

[18] Liu Junchuan, Zhang Yuru, Wen Kai. Remote control for household appliances that can identify non-specific voice commands

Design of high-accuracy digital voltmeter based on C8051F350

Longhao Guo; Shaonian Yang; Mingyue Li
(College of Instrumentation and Electrical Engineering, Jilin University)

***Abstract*-In view of the low resolution of the traditional digital voltmeter, this design uses a dual single chip system to improve the measurement accuracy through the initial measurement and the precision measurement. The single chip microcomputer STM32 system uses the built-in ADC to do rough measurement and the 24V range is divided. The internal DAC output is used to compare the voltage between the sub files, the sub circuit processing and the output differential voltage are precisely measured by the C8051F350 SCM system and displayed by the LCD5110 LCD screen. The design accuracy is up to 0.1mV.**

***Key words*-C8051F350 High-accuracy Voltmeter**

0. INTRODUCTION

A digital voltmeter is a voltage measuring instrument that transforms a continuous analog voltage signal into a discrete digital signal and is displayed through a visual interface. This new digital measurement technology compared to the traditional analog voltage meter, has the advantages of high measuring precision, good stability, fast response and so on, and the measured values are stored in digital form, to facilitate the visualization of measurement data, to avoid the traditional voltage meter visual error produced in the process of reading[1]. Based on the above features, the digital voltmeter has been widely used in the related fields, such as automatic instrument, automatic measurement, electronic electrical measurement and so on.

Digital voltmeter is common, the data processing unit uses a 8 bit processor, the maximum resolution is only 0.0196 (5/) V, not on the weak voltage change below the resolution of the effective recognition and measurement, which will affect the accuracy of digital voltmeter measurement in a certain extent, especially the measurement of micro voltage[2]. The design uses a dual single chip system, with a rough measurement and a precision measurement to achieve the measurement accuracy of 0.1mV.

I. SYSTEM TOTAL DESIGN

The design adopts dual MCU system, uses STM32 system to do rough measurement and divides the 24V range, and then the differential voltage obtained from the sub file is measured by C8051F350 SCM system. The actual voltage value is further calculated and displayed through LCD5110 LCD screen. The precision is 0.1mV.

The 12 bit successive approximation A/D conversion module, which is integrated within the STM32 single chip microcomputer, can be used to judge the profile of the measured voltage[3]. By calculation, the maximum resolution of A/D conversion theory can only reach 0.006V (24/ =0.0058), which does not conform to the index. If you want to meet the index, you have to score a 0.5V per 0.5V (0.0001*), and in actual use, the 12 bit A/D of A/D has a 1 bit runout in the end[4]. In order to stabilize the measurement, the gear must be continued to be subdivided. If we continue to subdivide the stalls, there will be a lot of errors and too many sub files, so we do not choose the STM32 for the A/D processing. The reference voltage is 3.3V commonly used, can be the following.

$$\frac{3.3}{2^n} < 0.0001$$

n is the AD digit required for the precision measurement[5]. N>15 can be solved.So this design uses C8051F350 microcontroller as the precision measurement of the processing unit, the internal sigma-delta A/D integrated 24 bit conversion module, the output is 10 times per second, PGA=1, A/D can stabilize the collected 16, in the reference voltage of 3.3V, the highest precision can reach 0.05mV (3.3/ = 0.00005), conformity index, measurement the process can be completed to measure. The precision of the reference voltage is 3.3V, so we divide the 24V per 3V.

The design adopts dual MCU system, in which STM32 MCU system includes A/D conversion, MPU and D/A conversion, C8051F350 MCU system includes A/D conversion, MPU and display circuit. The peripheral circuit includes the signal receiving circuit, the alarm circuit and the file position processing circuit. When the system works, first by receiving a signal acquisition circuit of DC voltage signal and 0~24V voltage signal into 0~2.4V signal attenuation, attenuation of the alarm circuit outrange judgment, if not excessive process is STM32 MCU control system A/D converter to attenuate the signal of coarse grading, and control of the built-in D/A output gear interval 0.3V shift voltage signal. The shift voltage signal and the attenuation signal are input into the gear processing circuit for differential amplification of a gain of 10 and a differential voltage signal of the output range of 0-3V. The A/D converter in the C8051F350 microcontroller system processes the differential voltage signal accurately, and calculates the actual value of voltage and controls the display circuit according to the gear data and the measured data obtained from the STM32 microcontroller port[6]. The frame diagram of the system is shown in Figure 1.

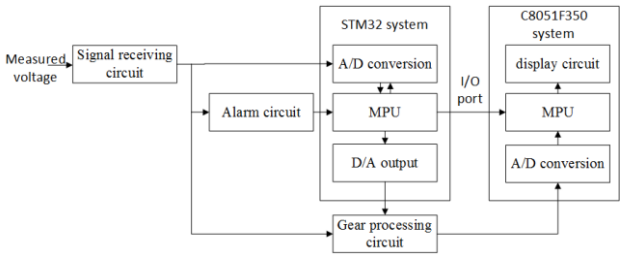

Fig.1 System structure block diagram

II. DESIGN OF STM32 SCM SYSTEM

2.1 ADC collection

The rough measurement circuit adopts STM32 microcontroller as the processing unit of the voltage coarse measurement circuit, and has 12 bits successive approximation A/D converter internally. The highest resolution of the 3.3V is 0.8mV ($3.3/2^{12}=0.0008$) and the conversion rate is 1MHz[7]. The initial voltage signal of the 0-2.4V is enough to be divided into 0.3V. In the realization method, only through the simple software design, the digital conversion of the measurement simulation can be completed, and the result of the voltage measurement can be obtained.

2.2 Gear judgment circuit

According to the results of rough measurement, the STM32 single chip microcomputer is used to judge the results of the rough measurement. The PD.0-PD.4 port is used as the output port of the data signal of the file, and the measured data signal is transmitted to the C8051F350 single chip microcomputer[8]. The roughing result is obtained through the 12 bit D/A conversion in STM32 and the output to the stall processing circuit through the PA.4 port.

2.3 STM32 MCU system program

This project is STM32 SCM system with STM32 MCU A/D conversion function, realize the rough measurement of the signal acquisition and calculates the gear gear data signal, circuit will shift the output data signal to the C8051F350 singlechip, shift voltage signal into analog gear signal through the D/A module in the STM32 monolithic machine[9]. The program flow of the roughing circuit is shown in Figure 2.

In the rough test, we first initialize the ADC1, make PA.1 as the analog input port, set the ADC frequency division factor to 6 frequency division, the frequency is 12MHz, and set ADC1 to work in independent mode, single conversion mode and single channel mode, and calibrate A/D at the same time. After the acquisition of A/D, the internal program of the MCU compares the voltage values and divides each 0.3V. The output voltage signal is D/A function of STM32, which is converted from D/A function to analog signal according to the result of gear shift. It is used as the reference end of differential input for A/D precise measurement. When the D/A is initialized, the PA.4 is used as the output side, without the use of the trigger function, the waveform generation is not used, and the output cache is closed.

The A/D conversion in STM32 MCU uses the PA.1 port as the input port of the acquisition signal, and the PD.0-PD.4 port is used as the output port of the stall data signal. The D/A conversion uses the PA.4 port as the output port of the file voltage signal.

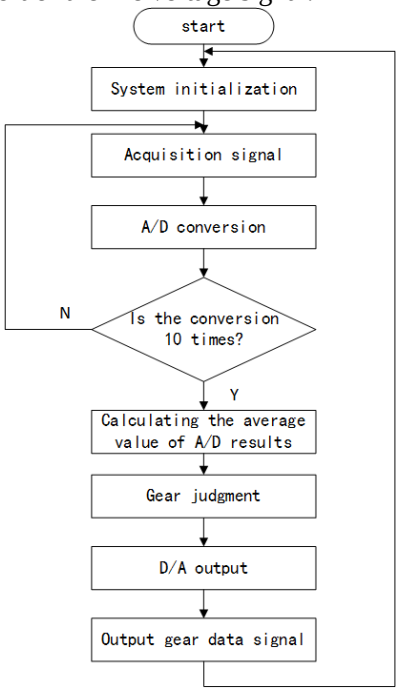

Fig.2 Program flow chart of rough measurement circuit

III. DESIGN OF C8051F350 SCM SYSTEM

3.1 ADC collection

This design uses C8051F350 microcontroller as a microcontroller and has 32 bits data processing capability. Compared with the traditional 8 bit MCU, C8051F350 has 24 bit sigma-delta A/D converter internally, and outputs 10 times / sec. When PGA=1, the theoretical maximum resolution reaches 20 bits, see Table 1. According to the experiment, the number of stable and non jumpy digits can be up to 16. Under the reference voltage of 3.3V, the maximum accuracy can reach 0.05mV ($3.3/2^{16}=0.00005$), and the differential voltage in the 0-3V range can be measured, which is in line with the index. Through the software design, the measurement of the differential signal and the final result can be calculated.

3.2 display circuit

LCD5110 LCD is the classic LCD module produced by Nokia. It has the advantages of simple interface, fast speed and small driving voltage, and is especially suitable for battery powered portable mobile devices. In this design, the actual voltage value obtained by the LCD5110 liquid crystal display circuit is shown.

3.3 C8051F350 MCU system program

The precision measurement part uses the A/D conversion function of C8051F350 microcontroller to realize the accurate measurement of the differential signal, and calculates the actual voltage value according to the gear data information. The actual voltage value is encoded by the microcontroller and is displayed by 5110 LCD. The process flow of the precision circuit is shown in Figure 3.

In the C8051F350 microcontroller, the system clock is set as the standard 24.5MHz, the output word frequency is 10Hz, the baud rate is 115.2kHz, and a consortium is defined to store the AD value of 24 bits to facilitate processing and later calculation. The AD is set as a differential mode output, input from the AD2 and AD0 ports, and the average value filter is performed on an average of ten times, and the voltage value is displayed once a second[10].

In the precision measurement circuit, the A/D conversion is used as the input port of the AD2 and AGND ports as the differential voltage signal, and the P1.0-P1.4 port is used as the receiving port of the data signal of the gear. After the actual voltage value is coded, the P0.0-P0.4 port is used as the output port of the coded signal.

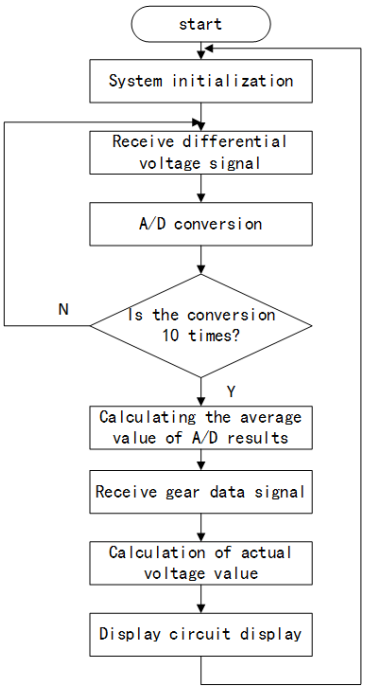

Fig.3 Program flow chart of precision measurement circuit

IV. Peripheral Circuit Design

4.1 Signal receiving circuit

Signal receiving circuit adopts a CHV-25P/50 module with a closed-loop Holzer Yu wave voltage sensor direct acquisition of DC voltage signal, avoid detecting circuit and digital voltmeter interference between the circuit, and the voltage of 0-24V attenuation is 0-2.4V, then the collected signal attenuation after sent to the STM32 MCU in the A/D.

4.2 Alarm circuit

As a signal receiving circuit of the digital voltmeter, the DC voltage signal collected by the signal receiving circuit is judged by the comparator. If the alarm is over, then the LED lamp is lit, and the low level signal is output, and STM32 is forbidden to collect A/D. If the voltage signal is within the range, the alarm circuit outputs the high level signal, and the A/D module in the STM32 is enabled.

4.3 Gear processing circuit

As a digital voltage meter's gear processing circuit, the differential signal between the gear signal and the initial voltage signal is processed by a differential amplifier circuit with a gain gain of 10 and a voltage follower, and a differential signal can be generated for the precise circuit, as shown in Figure 4.

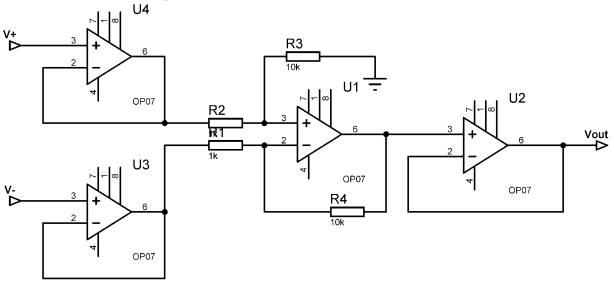

Fig.4 The gear processing circuit diagram

In the diagram, V+ input the initial voltage signal, the V- input voltage signal and the Vout output the differential voltage signal after the amplification.

V. Experiment

In order to test the accuracy of the self-made digital voltmeter system for voltage measurement, the system itself is used as an experimental equipment to simulate the experiment. In the case of maintaining the D/A output voltage of the original STM32, another D/A port is used to output analog voltage for dual channel output, and the output range is 0-2.4V. The analog voltage signal does not fade through the signal receiving circuit and directly carries out the rough measurement and precision measurement, and the measured voltage is obtained. The experiment simulated and measured the voltage of the 0-2.4V range after the attenuation, and the voltage of the 0-24V range was pushed back. The simulated voltage value was multiplied by 10 and the absolute error of the voltage difference was made with the digital voltmeter. The results of the measurement are shown in Table 1. The analog voltage to be measured is the known analog voltage to be measured by D/A, and the voltage measured by the digital voltmeter is the voltage measured by the digital voltmeter designed in this paper.

TABLE I
Measured Data

Pending voltage（V）	Digital voltmeter measurement voltage（V）	Absolute error（V）
0.469661	4.697540	0.000930
0.708661	7.086617	0.000007
1.234567	12.345767	0.000097
1.473662	14.736403	0.000217
1.732236	17.322309	0.000051
1.923226	19.223653	0.008607
2.221292	22.123161	0.089759

According to the measured data of Table 1, the absolute error is 1mV when the simulated voltage is less than 1.732236V, and it does not conform to the index. When the simulated voltage is more than 1.732236, the absolute error increases sharply with the measured voltage, even up to 89.8mV. The specific reasons are not

yet clear.

VI. CONCLUSION

This project has designed a digital voltmeter with two singlechips of STM32 and C8051F350. The STM32 is responsible for the rough measurement and the file position judgment, and the C8051F350 is responsible for the precision measurement, the calculation of the actual voltage value and the control of the final voltage value of the liquid crystal output. System theory range 0~24V, precision 0.1mV. The simulation experiment results the precision of the voltage value is 89.8mV, which needs to be further improved.

References

[1] Li Jie, Wang Ji Feng. A high precision digital voltmeter design [J]. computer and network, 2015,41 (18): 69-71.

[2] Yang Zengwang, CHEN Si, Dai Xinyu. A design for automatic conversion of high precision digital voltmeter, [J]. automation and instrument, 2011,26 (11): 12-15.

[3] Qi Fufeng, Shao Hong. Design of high precision digital DC voltmeter, [J]. technology information, 2010 (31): 490-491.

[4] Wang Qian, Wu and ray. C8051F350 based DC voltage and ripple measurement system [J]. chemical automation and instrument, 2010,37 (08): 72-74.

[5] Yang Zhaojun, Wang Zhangrui, Wang Qijun.C8051F350 in the application of industrial instruments and instruments [J]. instrument and instrument users, 2009,16 (04): 60-62.

[6] Chen Xiao. Design of high precision digital voltmeter for speech [J]. microcomputer information, 2009,25 (11): 122-123.

[7] Li Le Li Le, Cheng Gang.C8051F350 in the application of high precision digital weighing module, [J]. instrument technology and sensor, 2009 (03): 115-117.

[8] Wang Wei, Liu Xiaoping. High precision digital voltmeter scheme design [J]. instrument technology, 2007 (04): 36-38.

[9] Fu Shiji, Yang Hong. Development of high precision DC digital voltmeter [J]. Hubei electric power, 2000 (02): 7-8.

[10] Current situation of digital voltmeter and its test methods two, two kinds of high-precision digital voltmeter [J]. electrical measurement and instrument, 1971 (12): 11-19.

Design of Traffic Light Identification System Based on MATLAB

ZOU Si-Yu; ZHOU Chun-Hao; WANG Yu; ZHENG Fan
(School of Instrtument Science and electrical engineering, Jilin University

***Abstract*-In assisted driving systems, traffic light recognition can be achieved in many ways. Combining with navigation information, visual traffic light recognition can inform the driver of traffic light status in the driving environment. Compared with the driver's own naked eye recognition, the traffic light recognition device based on vision processing algorithm has no fatigue and is not easily affected by complex background and other factors. The characteristics of the impact, traffic light identification capability is also an important aspect of the driverless car. This paper presents a design of traffic light recognition system based on MATLAB, using Haarlike feature extractor to extract features, and then use the Adaboost classifier to classify the extracted features and determine the color of traffic lights based on the RGB three-channel pixel values. The test results show that the recognition results are very accurate and the consumption time is almost the same as expected.**

***Key Words*-Traffic light detection Character recognition Image recognition Feature extraction**

0 THE PREFACE

IN the assistant driving system, traffic light recognition can be realized by many algorithms. Combined with navigation information, vision-based traffic light recognition can inform the driver of the traffic light status in the driving environment. compared with the driver's own visual recognition, vision-based traffic light recognition device based on visual processing algorithm has the characteristics of not fatigue, not easily affected by complex background and other factors, traffic light recognition ability is also an important aspect of driverless cars.

1 DESIGN SCHEME

The scheme flow chart is as follows:

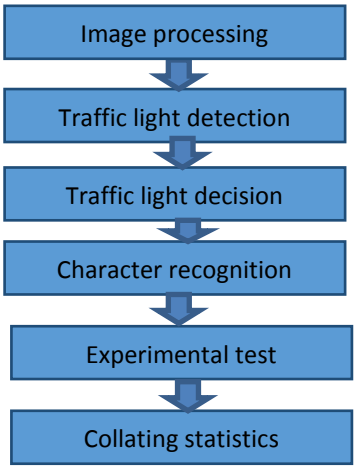

Figure 1.1 Overall flow chart

The first step of image processing needs to convert the color image into gray-scale image, after filtering and denoising, the image is converted into image for easy detection.

The second step of traffic light detection requires the participation of the algorithm, the purpose is to accurately confirm the location of the traffic light in the image, first using Haar like feature extractor to extract features, and then using AdaBoost classifier to classify the extracted features, so as to determine whether the image block is a traffic light. Each image block is then searched for traffic lights by sliding through the entire image[1].

The third step is to confirm the color of the traffic light by judging the pixel value in the area already detected in the previous step.

Finally, the text recognition needs to locate the digital board, after the positioning is completed, cut into two parts, corresponding to the position of the two numbers. The number is then identified.

2 TRAFFIC LIGHT DETECTION

2.1 Haar-like Features

Haar - like features are used for objectsA digital image feature for volume recognition.

The Haar classify algorithm is used as follow:

① using Haar - like features for detection.
② Haar - like feature evaluation was accelerated by integral graph.
③ AdaBoost algorithm is used to train a strong classifier for distinguishing human face from non-human face.
④ filter cascade is used to cascade the strong classifiers together to improve the accuracy.

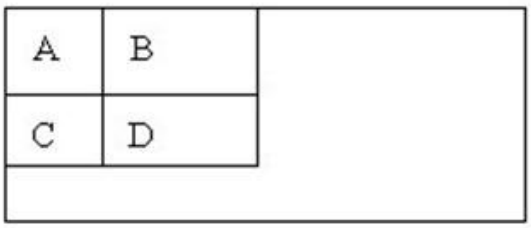

Figure 2.1 Pixel map of the matrix area

The Haar - like feature is calculated quickly by the integral graph. if the four vertices of d are α, β, γ, δ α, β, γ, δ, the sum of pixels of d can be expressed as:

$\sum D=ii(\alpha)+ii(\beta)-(ii(\gamma)+ii(\delta))$ (2-1)

$\sum D=ii(\alpha)+ii(\beta)-(ii(\gamma)+ii(\delta))$ (2-2)

Haar - like eigenvalues are simply the difference between the sum of two matrix pixels, which can also be done in a constant time.

2.2 AdaBoostalgorithm

Adaboost is an iterative algorithm whose core idea is

to train different classifiers (weak classifiers) for the same training set, and then combine these weak classifiers to form a stronger final classifier(strong classifier)[2]. Adaboost classifier can eliminate some unnecessary training data features and put the key on the key data.

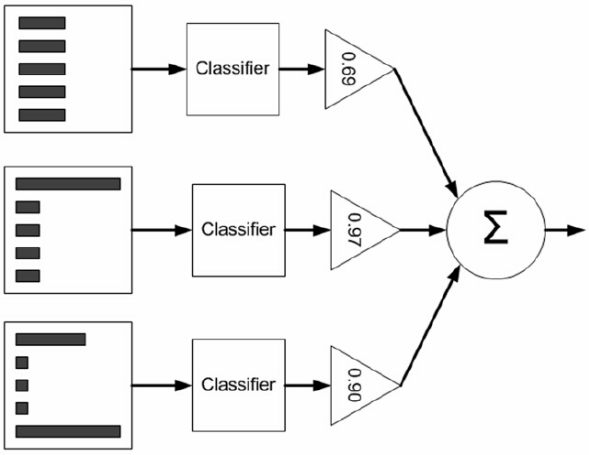

Figure 2.2 Adaboost algorithm diagram

Adaboost algorithm specific steps are as follows:

Let the n training samples input be: { (x_1, y_1), (x_2, y_2), (x_3, y_3) ..... (x_n, y_n) }is the training sample input, and $y_i \in \{0,1\}$ represents the positive sample and the negative sample respectively, wherein the number of positive samples is l, and the number of negative samples is m.. N = l + m, the specific steps are as follows:

(1) initializing the weight of each sample;

(2) for each t = 1, ... t (t is the number of weak classifiers;

1) normalizing the weights to a probability distribution;

2) for each feature f, training a weak classifier h_j to calculate the weighted error rate of the weak classifier corresponding to all the features;

3) select the best weak classifier h_t (has the smallest error rate);

4) adjust the weights according to this best weak classifier.

(3) the last strong classifier is:

$$h(x) = \begin{cases} 1, & \sum_{t=1}^{T} a_t h_t(x) >= \frac{1}{2}\sum_{t=1}^{T} a_t \\ 0, & otherwise \end{cases} \quad (2\text{-}3)$$

$a_t = log\frac{1}{\beta_t}$[3]

3 Traffic Light Decision

When a traffic light is detected, the traffic light can be processed. Cut it into 3 pieces on average, corresponding to the red, green and yellow lights respectively. Then find the center point pixel values for the three blocks. Analyze what color this pixel value is and convert an RGB image into a standard RGB image. To detect a traffic light, a circle filled with one of the colors of the traffic light is detected. Circles detected from edge pictures can be used from a simple circular equation (x-a)2+(y-b)2=r2,substituted into the three-dimensional spatial parameters (a, b and r). The set-up parameter result in a majority of votes present that location and size of the traffic lights.

In order to avoid this deficiency and increase the detection speed, it is assumed that the gray and black pixels in the image are one of the traffic lights in the ankle variable, and for each pixel (x, y), the number of r positions where the black pigment on the image taken into the three-dimensional space enters the ab - line is changed. In the recommended framework, the election is conducted simply because the pigment (a, b) and its four adjacent elements belong to the region to be selected. Voting into a b - line is shown as a result in the image melanin by the recommended method. So that the traffic lights are detected. Identify the specific color of the traffic lights.

4 Character Recognition

Firstly, the digital board needs to be positioned, and after the positioning is finished, the digital board is cut into two parts corresponding to the positions of the two numbers. The number is then identified.

4.1 Positioning of digital boards

Histogram of orientation gradient (hog) feature is a feature descriptor used for object detection in computer vision and image processing[4]. Hog features are constructed by calculating and counting the gradient direction histograms of local regions of the image.

The specific steps are as follows:

Firstly, the image is grayed out and the gamma correction method is used to standardize the color space. at the same time, the effect of noise suppression, illumination change and local shadow of the image can be reduced. The formula is:

$$I(x, y) = I(x, y)^g \quad (4\text{-}1)$$

Where I (x, y) represent that gray value of the image, typically g = 0.5

Calculate the gradient of the pixel point (x, y) [5]:

$$G_x(x, y) = I(x+1, y) - I(x-1, y) \quad (4\text{-}2)$$

$$G_y(x, y) = I(x, y+1) - I(x, y-1) \quad (4\text{-}3)$$

Wherein GX (x, y), gy (x, y), and I (x, y) represent horizontal direction gradients, vertical direction gradients, and pixel values at pixel points (x, y) in the input image, respectively. The gradient magnitude and the gradient direction at the pixel points (x, y) are respectively:

$$G(x, y) = \sqrt{G_x(x, y)^2 + G_y(x, y)^2} \quad (4\text{-}4)$$

$$q(x, y) = \tan^{-1}\frac{G_x(x, y)}{G_y(x, y)} \quad (4\text{-}5)$$

In this paper, the cell size is set to 8 and the gradient direction is divided into 16 intervals. Several cells are combined into a block in which the gradient intensity of all cells is normalized, which makes hog features have better illumination and shadow invariance. If the block

size is set to 2×2 cells, the number of overlapping cells of adjacent blocks is 2. Combining the feature vectors of all blocks to obtain the final hog feature. For 128×64 images, according to the above calculation method, there are 15 scanning windows in the horizontal direction, 7 scanning windows in the vertical direction, the feature vector dimension in each block is 16×4 = 64, and the final hog feature dimension is 15× 7× 64 = 6720.

4.2 Identification of numbers

The method used in this paper is support vector machine (SVM). In the training stage, we use the training samples to learn and train a SVM model, which essentially defines the optimal hyperplane from the most difficult feature vectors[6].

(1) Assuming that the parameterθ, given an x, the feature vector f∈R^{m+1} can be calculated. The SVM assumes that the definition of the function becomes, if $\theta^T f = \theta_0 f_0 + \theta_1 f_1 + \cdots + \theta_m f_m$ >=0 ， h_θ （ x ）=1,otherwise, h_θ（x）=0;

(2) with the kernel function, SVM optimization objectives are as follows:

$$\min\{C\sum_{i=1}^{m} y^{(i)} cost_1 (\theta^T f^{(i)}) + (1-y^{(i)}) cost_0 (\theta^T f^{(i)}) + \frac{1}{2}\sum_{j=1}^{n} \theta_j^2\} \quad (4\text{-}6)$$

Wherein that numb of features in the last term n=m.

(3) parameter c is equivalent to $\frac{1}{\lambda}$ in logical regression[7].

4.3 Traffic lights and a font is implemented with 8 digital tube.

This font is relatively simple, the first position is divided into upper left, upper right, lower left, lower right, upper middle and lower middle, and then determine the situation of each part respectively, through the pixel value to determine which segments are bright, and match with the number, so as to obtain the result.

Fiture 4.1 Single traffic light

5 TEST

Here's a sample from the experiment:

Fiture 5.1 Original traffic light map

Identification result chart:

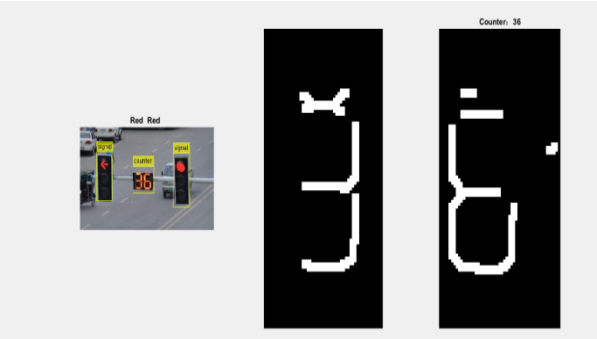

Fiture 5.2 Traffic light recognition chart

Table 1

Recognition schedule

	1	2	3	4	5	6
Time /s	0.201368	0.200616	0.204406	0.223092	0.227989	0.210368

The table data is the result of identifying the same picture six times in succession.

From the results of the image and the data in the table, we can conclude that the traffic lights are judged to be red, the time number is also determined to be 36, is the time because of the use of the algorithm is not mature, to identify the traffic lights took an average of about 0.21 seconds, if some more advanced technology is applied in the algorithm, time is believed to be reduced, the recognition effect will be better.This design can also identify other types of traffic lights, but only some of the more recent traffic lights, if the traffic light version is too old, there are still some difficulties to identify. Of course, even if there are difficulties, the problem is not big.

6 CONCLUSION

Compared with the traditional method, the system also has obvious improvement on the calculation speed, and the time for identifying the traffic lights is controlled at about 0.3s.. Simple design and implementation, suitable for engineering application, has practical application value.In terms of recognition accuracy, we found about 50 pictures of traffic lights, shooting distance, angle is different, through a lot of experiments, finally can identify only 45 pieces, the remaining five digits recognition is correct, but there is

a deviation in color discrimination, these data show that our system in the recognition algorithm has yet to be improved.

References

[1] Zhao cheng. image recognition methods and implementation technology [m]. Xi 'an: xidian university, 2008.

[2] Li Zhiqiang, Li yongbin. license plate recognition technology development and research status [j]. science and technology information, 2012, (05): 110 + 125.

[3] Xu cheng, tan naiqiang, Alex. real - time traffic light recognition algorithm based on lab color space and template matching [j]. computer applications, 2010, (05): 1251 - 1254.

[4] Zhu Jue - ning. intelligent control of traffic lights based on MATLAB image recognition [j]. information communication. 2016 (11).

[5] Song Jianhua, Zhu Yong, Wang erfu, liuyong. research on digital baseband signal and its power spectrum based on MATLAB [j]. information communication. 2016 (11).

[6] Dalal N, Triggs B. Histograms of oriented gradients for human detection [C]. In Computer Vision and Pattern Recognition, 2005. CVPR 2005. IEEE Computer Society Conference on, 2005: 886-893.

[7] Chang C-C, Lin C-J. LIBSVM: a library for support vector machines [J]. ACM Transactions on Intelligent Systems and Technology (TIST), 2011, 2 (3): 27.

Design of automatic polarized window system

WeiShida; WunNa; ZhaoBohao
（*instrument science and engineering institute, jilin university*）

***Abstract*—With the development of electronic technology and the improvement of the people's level, more and more smart windows are being used in modern intelligent buildings. In the next few years, smart window users will continue to increase. Polarized glass is currently the most high-end product, because the glass's superior hardness has created its strong super scratch resistance, can evenly change the incident light and superior light transmittance and other optical properties of other resin lenses can not be compared. Currently shutters, closed fill light, and other traditional equipment to control lighting, there are light transmission is not soft light spots, light transmission adjustment accuracy is too small and other shortcomings. This design is proposed in this paper, with polarized glass as the core of the window, and 51 single-chip microcomputers as the processor cores. Through the data acquisition intelligent technology, a window system is designed. The designed intelligent window system can continuously detect outdoor humidity, temperature, PM2.5 concentration and outdoor light intensity through its data detection and sensing circuit. When the collected value reaches the set value, the processing result will control the rotation of the stepping motor. In order to control the overlapping angle of the polarizing glass, it is equipped with a good anti-theft system[14]. In addition, it can be set to automatically close the window or open the window. When the setting time is reached, the window will be automatically closed or opened, and intelligence will be realized to a greater extent. The design was tested and tested to achieve precise control of the transmitted light brightness, adjusting the light transmission range by 60%-0%, and the light transmission accuracy by 3%.**

***keywords*—Smart home Polarized windows data acquisition Light control stepper motor**

I PREFACE

WITH the development of high technology and information technology, intelligence is a brand-new concept that has been increasingly recognized in recent years. Building intelligence has also become a trend of development. This is the need of people's lives, and it is also a manifestation of the level of civilization[1,2]. Currently, most of the windows implemented in the market are shutters, light-blocking and other traditional equipment for controlling lighting, and there are shortcomings such as poor light transmission and poor transparency of light transmission. Polarized glass has excellent light transmittance, and has optical performance with different transmittance when two pieces of polarized glass coincide at different angles. Nowadays, the control system for realizing the special function of embedded technology has also become a reality. This design proposes a polarization window system based on the STC89C52 microcontroller. The system uses a variety of sensors to the outside environment of the wet temperature, light intensity, PM2.5 concentration, whether there are people outside the window and other factors for signal acquisition and into the microcontroller, after the microcontroller to analyze the data and processing, and issued a command to control the step The motor performs actions to adjust the overlap angle of the polarized glass so that the environmental parameters are well adjusted and a comfortable home environment is ensured[3-5].

II SYSTEM OVERALL DESIGN

This design study is based on the intelligent polarization window system controlled by the STC89C52 microcontroller. The overall system is mainly composed of hardware and software. The hardware part is composed of the external circuit extended by the single-chip microcomputer and various interface circuits that realize the control function of the single-chip microcomputer system; the software part is mainly composed of various programs that the single-chip computer system realizes its specific control function[6].

The whole system collects information through PM2.5 sensor, optical sensor, infrared alarm sensor and temperature and humidity sensor. After being processed by the microprocessor, the data is sent to the upper computer through the STC89C52 serial port, and the real-time data is displayed on the display at the same time. The button or infrared remote control Set the limit range, when the data is in different intervals, the light-controlled stepper motor drives the polarizer to adjust the angle, evenly change the incident light intensity, can adjust the light transmission range 60%-0%, light transmission accuracy 5%.

III SYETEM HARDWARE DESIGN

A. Light-control polarizing window module

The system will automatically send instructions to the stepper motor according to the data of the signal acquisition module to adjust the rotation of the polarization window. The structure of the window is shown in Figure 2.

The sash turning wheel 21 and the inner glass turning wheel 6 can obtain the power output of the motor 5 through gear meshing transmission. For example, both the sash turning wheel 21 and the inner glass turning wheel 6 may be gears, and accordingly, the wheels of the motor 5 are also gears, so that they can be directly connected to each other through tooth meshing or chain transmission, so that the sash turning wheel 21 and the inner glass turning wheel 6 obtain the power output of the motor 5 .

In order to better control the opening or closing of

the window sash 2 and the rotation of the inner glass 12, the diameter of the sash turning wheel 21 and the inner glass rotating wheel 6 may be set to be larger than the diameter of the wheel of the motor 5, making it possible to make appropriate The speed at which the motor 5 is transmitted to the sash turning wheel 21 and the inner glass turning wheel 6 is reduced, thereby reducing the opening or closing speed of the sash 2 and the rotation speed of the inner glass 12.

The polarizing glass includes outer glass 11 and inner glass 12 two polarizing glasses. In order to obtain a better effect of adjusting the light intensity, it is also convenient to rotate the inner glass 12 to adjust the polarization staggered angle between the inner glass 12 and the outer glass 11, and the inner glass 12 is circular.

In a specific embodiment, the inner glass 12 is circular, and the diameter of the inner glass 12 is equal to the side length of the short side of the window sash 2 so that the overlapping area between the inner glass 12 and the outer glass 11 can be more as much as possible. The large, so that the acceptance of the external glass 11 and the inner glass 12 polarized light adjustment more to more accurately adjust the amount of light entering the room, so that the light entering the room as much as possible, uniform, soft; At the same time, it can also not too much light in the outdoor When strong, more light can enter the room than when using a round outer glass 11 . The inner glass 12 and the outer glass 11 are both circular, and the diameters of the inner glass 12 and the outer glass 11 are equal to the sides of the short sides of the window sash 2, so that the inner glass 12 and the outer glass 11 can be completely overlapped, so that all The light can receive the polarization adjustment of the outer glass 11 and the inner glass 12 so that the light entering the room is more uniform and soft.

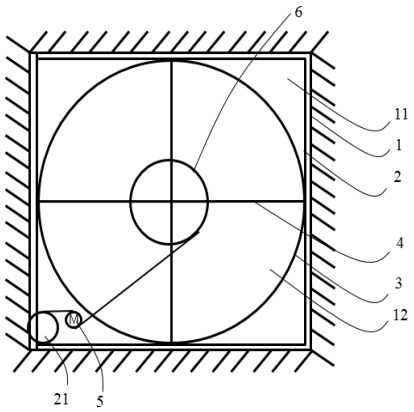

Fig.1 Polarized light control windows

B. Signal Acquisition Device

Based on 51 single-machine signal acquisition device system block diagram shown in Figure 2, including the sensor module, signal acquisition and transfer module and serial communication module, display module 4 parts[11].

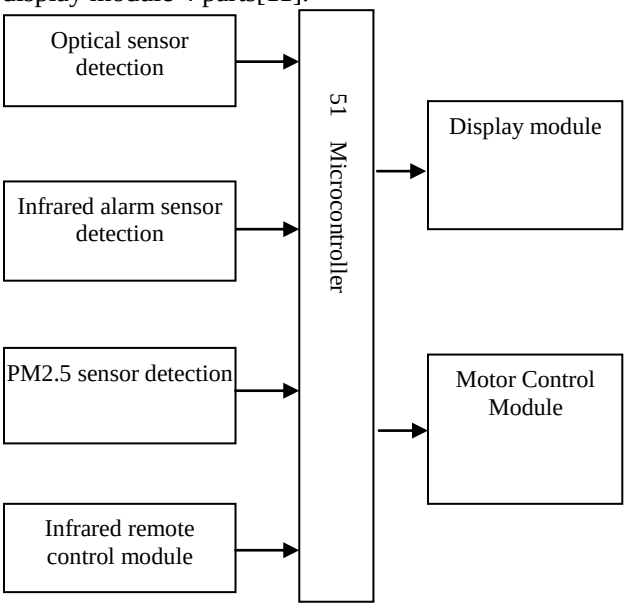

Fig.2 acquisition module structure

(a). Optical Sensors

The system uses photosensitive resistance sensors as the core device of the photoelectric conversion circuit. The module outputs a high level when the ambient light brightness does not reach the set value, and outputs a low level when the ambient light level exceeds the set value. The output is connected to the microcontroller to detect changes in ambient light levels. The circuit diagram is shown in Figure 3, and the light control accuracy is shown in table 1.

Table 1 Optical sensor optical control accuracy

Paramet-er layout	Operati-ng Voltage	Dark curr-ent	Phot-occur-rent	Phot-oelec-tric sensi-tivity	Resp-onse time	Phot-osens-itive area diam-eter
symbol	Umax	Id	Il	Sn	Tr	d
unit	V	uA	uA	A/W	S	min
		U=Umax	U=Umax	U=Umax	U=Umax R=100	
2CU1A	10	<0.2	>80	>0.5	0.0000001	8.4
2CU1B	20	<0.2	>80	>0.5	0.0000001	8.4
2CU1C	30	<0.2	>80	>0.5	0.0000001	8.4
2CU1D	40	<0.2	>80	>0.5	0.0000001	8.4
2CU1E	50	<0.2	>80	>0.5	0.0000001	8.4
2CUI01A	15	<0.0001		>0.6	<0.000005	0.23
2CUI01B	15	<0.0001		>0.6	<0.000005	0.6
2CUI01C	15	<0.0001		>0.6	<0.000005	1
2CUI01D	15	<0.0002		>0.6	<0.000005	2
2CU201A	15	0.005		>0.6	<0.000005	0.5
2CU201B	50	0.001		0.35	<0.001	1
2CU201C	50	0.002		0.35	<0.001	2
2CU201D	50	0.004		0.35	<0.001	4
3DU11	50	<0.3	>500		<0.001	5
3DU22	50	<0.3	>1000		0.001	5
3DU33	50	<0.3	>2000		0.001	5

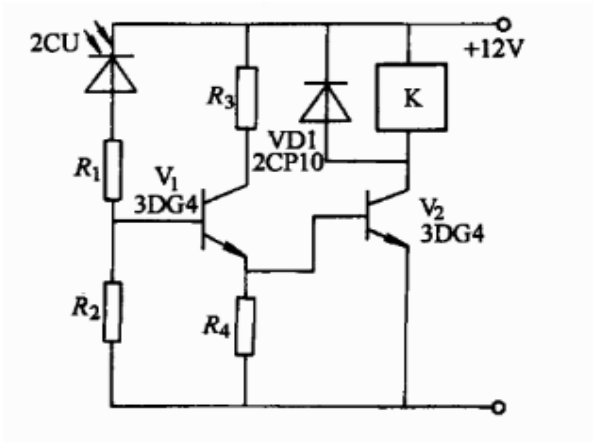

Fig.3 Optical sensor optical control accuracy

(b). Infrared Alarm Sensor

The pyroelectric infrared sensor is a sensor that can detect infrared radiation emitted by humans or animals and output electrical signals. Its goal is being applied to a variety of automatic control devices, such as the corridor automatic switch and burglar alarm that we are familiar with. Infrared sensors consist of ceramic oxide or piezoelectric crystal elements, which are made on the two surfaces of the element. When the temperature within the sensor monitoring range changes by ΔT, the pyroelectric effect will generate a charge ΔQ at the two electrodes. A weak voltage ΔV is generated between the two electrodes and the output is about 3.3V high. Because of its extremely high output impedance, there is a field effect transistor in the sensor for impedance conversion. The charge ΔQ generated by the pyroelectric effect will be disappeared by the ions in the air. That is, when the ambient temperature remains constant, ΔT=0, the sensor has no output, and the low level is 0V. When the human body enters the detection zone, ΔT is produced due to a difference between the human body temperature and the ambient temperature, and then there is ΔT output.

External schematic Typical application

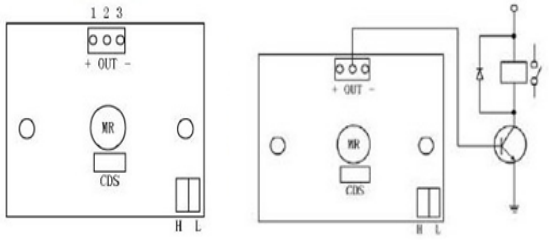

1:Positive power supply 2:High and low output
3:Negative power supply H::Repeatable trigger
L:Cannot be triggered repeatedly CDS:Photosensitive control

Fig.4 Infrared sensor schematic

(c). PM2.5 Sensor

PM2.5 sensors, also known as dust sensors, dust sensors, can be used to detect the concentration of dust in the air around us, that is, the size of PM2.5. Aerodynamics Dust that enters the alveolar region with diameters less than 10 μm is also commonly referred to as respiratory dust. Most dust particles

with a diameter of more than 10 μm are deposited by impact. Most of them are deposited in the nasopharynx when they are inhaled. Dust below 10 μm can enter the deep part of the respiratory tract. The dust deposited in the alveoli is mostly dust less than 5 μm.

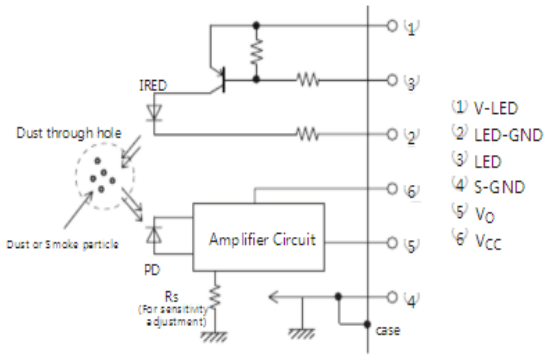

Fig.5 Light sensor circuit diagram

C.Infrared Remote Control Module

Infrared remote control is the use of infrared to transmit control signals to achieve remote control of the control object. The infrared remote control circuit is composed of a transmitting circuit and a receiving circuit, and the transmitting part is composed of a key switch circuit, a control chip and an infrared transmitting circuit. When the remote control button is pressed, the microcontroller generates a corresponding control signal and transmits it through the infrared emitting diode. The receiving part is composed of an infrared receiving head and a control chip. When the infrared receiver receives the control pulse, it is processed by the single-chip microcomputer and the corresponding operation is performed as needed.

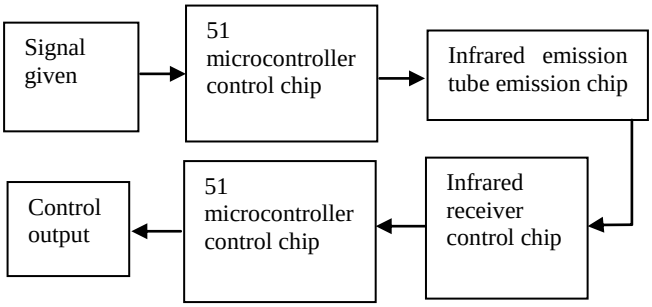

Fig.6 Infrared remote control schematic

D. System Software Design

The entire smart polarized window system collects electrical signals from optical sensors, PM2.5 sensors, and infrared alarm sensors. Each sensor converts the collected signals into electrical signals and transmits STC89C52. The single-chip microcomputer transmits signals to the motor control module according to the programmed program, and the polarization The glass is adjusted to control the amount of incoming light. First of all, it is judged whether there is hot motion outside the window. When someone moves, the MCU sends a control signal and the motor control module closes the window. The concentration of PM2.5 in the air is detected. If the concentration is too high, the microcontroller controls the motor control module to close the window. Finally, according to the sensor's sensitivity to the outdoor light intensity, the microcontroller sends a control signal to the motor control module, adjusts the angle of the polarizer, and then controls the amount of light entering the room. The display shows real-time data on the time and PM2.5 concentration. The user can control the window remotely through the infrared remote control to achieve manual control. You can also open, close, and adjust windows by setting the time. The entire intelligent window control system is realized. System software flow chart shown in Figure 7:

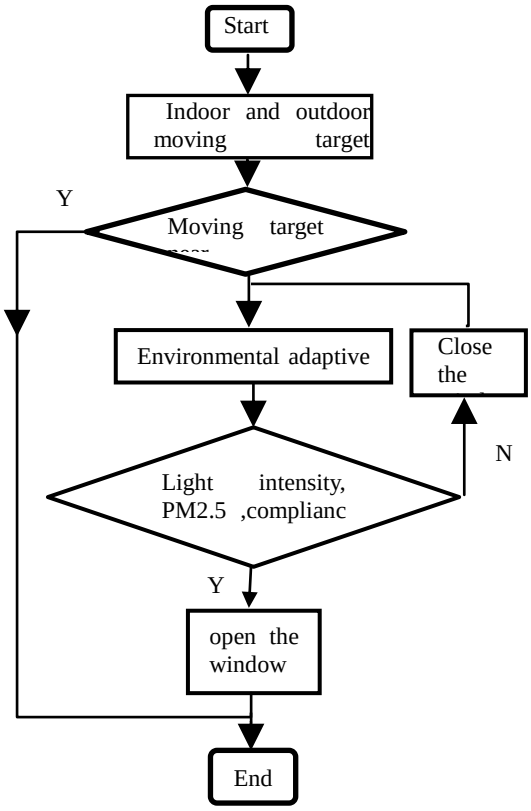

Fig.7 System software flow chart

E.Test and Analysis

Connect the system line, turn on the power, simulate the change of the PM2.5 concentration control signal by lighting the cigarette, test the working conditions and measurement range of the system. As the time increases, the value of PM2.5 on the display continues to increase. When the threshold is increased, the stepper motor closes the window through the hinge device. From the data in the following table, it can be seen that when the smoke value reaches 600, the window automatically closes, and the smoke can be shielded. Effect.

Table 2 PM2.5 test results

measured data	600 +	200-600	150-200	100-150	50-100	0-50
air quality	very poor	differ-ence	gener-al	good	well	very good
automatic control	automatically shut down		do not modify			

By simulating the change of outdoor light intensity through a flashlight, the test system rotates the polarization glass through the light-controlled stepper motor according to the outdoor ambient light, and evenly changes the indoor light intensity. The test results are shown in Table 3. In addition, the data shows that the light transmission range can reach 0-66% to reach the target of 0-60%, and the stepping motor rotation angle can reach 0.9 degrees. The data in the table is not all displayed. The maximum specularity is 3%, close to the expected target of 5%.

Table 3 Light Control Polarization Window Test Data

rotation-angle	0	5	10	15	20	25	30	35	40	45
brightn-ess	66 %	65 %	62 %	59 %	55 %	52 %	47 %	41 %	55 %	40 %
rotation-angle	50	55	60	65	70	75	80	85	90	
brightn-ess	29 %	25 %	18 %	15 %	8 %	5 %	2 %	1 %	0 %	

IV CONCLUSIONS

The design uses STC89C52 to achieve polarization window automation, using infrared remote control technology to achieve remote control, optical sensor light-sensitive characteristics and polarization glass optical principle to achieve automatic control of indoor transmittance, temperature and humidity sensor resistance with temperature characteristics of the detection of outdoor temperature and humidity, And use the LCD screen to display parameters in real time, to achieve a good human-computer interaction[12], and ultimately the entire system reaches a light transmission range of 66-0%, light transmission accuracy of 3%, adapted to some hospitals special drug laboratories, vegetable greenhouses, chemical storage Chambers and other requirements for strict light darkroom, but also to solve the traditional equipment control light accuracy is not high, control light is not soft light spots and other issues[8-10]. Limited by the material of the polarizer, etc. the final light transmittance is a maximum of 66%[7], the light transmission range is not very large, a better polarizer is used, and a stepping motor with a lower step angle is used, I believe there will be more Large light transmission range and light control accuracy. The system design idea provides a reference for the design and development of smart homes and polarized glasses[15].

References

[1] Wu Xue song ,Pan chong Yu,Ni Yi Feng .Based STC89c51 smart window shutters MCU[J].Science and Innovation,2015,01:21-22.

[2] Ni Qingqing, Zhou Yuanyuan. Design of Intelligent Windows Based on AT89S52 Single Chip Computer[J]. Science and Technology Vision, 2015, 18:115-116.

[3] Yang Yuzhu, Zhu Baoli, Pan Guoguang, Takamatsu. Development and application of color polarizer[J]. China Criminal Police University, 1994,01:14.

[4] Xie Shuwei . Polarizer and its use [J]. Light-sensitive Materials , 1997, 02:44-46+63.

[5] Yao Jian , Tao Weidong . Intelligent window and its research progress [J]. Windows , 2009, 06:52-55.

[6] Wang Juan . Intelligent window control system based on single-chip microcomputer [J]. Information Systems Engineering , 2016, 01:100-101.

[7] Liu Ximing . Polarized light film and optical glass bonding [J]. Bonding , 1989,05:44.

[8] Wang Jie , Yang Hao , Cai Jianwen . Design of Intelligent Window Control System Based on Single Chip Microcomputer[J]. Industry & Technology Forum , 2014,12:61-62.

[9] Sun Jian. Design and implementation of intelligent home electric curtains [J]. Mechanical Engineering and Automation, 2012, (2): 133-135.

[10] Jian-Sheng Tan . Analysis of the development of smart homes [J]. Science & Technology Information, 2013,(18):214-214,216.

[11] Zhang Yanhong, Zheng Zhong qiao. Data Acquisition System Based on Microcontroller AT89C52[J]. Control and Instruments In Chemical Industry, 2010,(03):110-112.

[12] Zheng Qinglan . Design of humanized window control system based on AT89S52 [J] .Journal of Shandong University of Technology ,2014,28(06):35-38 .

[13] Zheng Yangping. Research on belt conveyor intelligent control system[J]. Manufacturing Automation, 2014, 36(02):112-113.

[14] Yong Tae Park , Jae-Young Pyun . Smart Digital Door Lock for the Home Automation[C]. 2009 IEEE Region 10 Conference , Singapore , 2009 : 1-6 .

[15] Ping Wang, Huali Jiang. Design and Realizati on of Remote Control in Smart Home System[C]. International Conference on Communicati on Software and Networks, Macau, 2009:13-15.

Based on STM32 wireless bedwetting alarm

Xudong Li; Chengjin Li; Wenyu Jiang.
（instrument science and engineering institute, jilin university）

***Abstract*—As people's living standards improve, caring for babies becomes a top priority for young parents.In order to monitor infantile bedwetting in real time, this paper designs and studies a wireless infant bedwetting alarm based on STM32.When the baby urination, the urine detection circuit to detect urine, immediately produce a signal, after STM32 processing HC05 Bluetooth passed to the phone.Neither affect the baby, but also inform parents to change diapers.**

***keywords*—Bedding monitoring Real-time monitoring Wireless alarm**

1 INTRODUCTION

CHINA is the most populous country in the world, and the total number of infants and young children is also at the forefront. The care of infants has always been an important issue for every parent. For the moment, most babies need their families' guardianship all the time, which creates great inconvenience to their parents in their daily lives.At the same time, taking into account that the baby does not have the ability to work independently, unable to timely inform parents of their own state, can only remind the parents with cries after wet state, causing great trouble to parents and themselves.

Radio frequency identification[1] (RFID) originated very early. P&G's diaper brand Hipogl ós uses Bluetooth and RFID technology to detect baby's diapers and then use mobile phones to remind parents.However, the cost of RFID technology is too high, and involves privacy issues. The use of environmental conditions is too harsh for the family and is not suitable for use as a wet siren.

Tokyo University of Technology developed a curved surface sensor with an organic circuit that can sense humidity, temperature, and pressure changes.The main purpose of this new technology is smart diapers for wireless charging and data transfer.However, due to the lack of improvement in energy consumption and safety issues, it is not yet available.

Our proposed method of detecting humidity based on non-contact capacitance is to observe the change of the capacitance value of a low-cost circuit by charging and discharging an RC, and rely on the hardware anti-interference design and software adaptive filtering algorithm to determine whether the urine is wet[2]. It is not yet available.

In recent years, the geek baby brand introduced a 4.0 Bluetooth and mobile phone connection to detect whether the baby urinate new products.However, this product is attached to the outside of the diaper, the contact area is small, and the urine is required to fully infiltrate the diaper before measuring the diaper, thus alerting the parents.It still cannot remind parents to need to change diapers immediately after the baby urinates.

2 PURPOSIVENESS

Traditional diaper alarms require a humidity sensor to measure the humidity of the diaper, the alarm is not timely, and the cost is high. Most alarms are installed on the diaper or around the baby. When the alarm sounds, it may affect the baby's mood or sleep. This project directly through the urine short circuit is attached to the flexible circuit board inside the diaper. After the circuit is connected, the signal is transmitted to the amplifier circuit on the outside of the diaper. After amplification, the signal is transmitted to the mobile phone app via Bluetooth and no baby will be produced influences.

3 PROCEDURE FOR PAPER SUBMISSION

A. Overall plan

When the baby urination, the urine monitoring circuit to monitor the urine, resulting in a signal, after STM32 processing HC05 Bluetooth passed to the phone.It does not affect the baby, but also inform parents to change diapers.

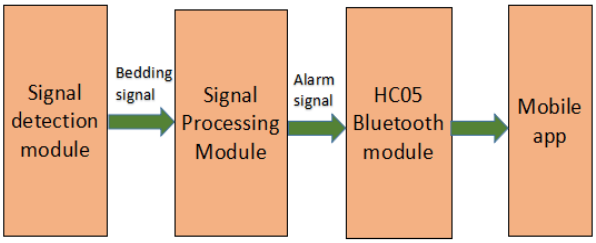

Fig. 1. The overall system structure block diagram

B. Software part

Signal detection module.The system uses the STM32F103C8T6 microcontroller as the core controller, and the STM32F103C8T6 is a single-chip microcomputer based on the ARM32-bit Cortex-M3 core,with a wide voltage range of 2.0 to 3.6V.The CPU operates up to 72MHz, with single-cycle multiply instructions and hardware dividers, as well as programmable priority interrupts.At the same time, it also has 64KB of Flash memory and 20KB of SRAM memory, also integrates a very rich on-chip peripherals such as watchdog, timer, GPIO port, DMA controller, ADC, UART, SPI interface, IIC interface etc.It has the advantages of low cost, high speed, and high cost performance.

The programming software is using Keil MDK.Keil MDK is an integrated development environment provided by Keil Corporation based on Cortex-M, ARM7, ARM9 and other processors.It supports

functions such as editing, compiling, linking, and in-circuit debugging. It can automatically configure startup code.It is easy to learn, superior in performance, and can satisfy most embedded applications[3].

In the STM32, the Universal Synchronous Asynchronous Receiver Transmitter (USART) provides a flexible approach to full-duplex data exchange with external devices using industry-standard NR asynchronous serial data formats.The USART uses a fractional baud rate generator to provide a wide range of baud rate options, supporting synchronous one-way communication and half-duplex single-wire communication.This design mainly uses the USART to complete communication with the Bluetooth module.

(1)The first is to enable the relevant clock.On the one hand is the clock of the device itself, on the other hand, if the device outputs through the IO port, the clock of the IO port needs to be enabled.Finally, if the corresponding IO port is multiplexed IO port, you must also enable AFIO clock.Since the UART's TX and RX and AFIO are both hooked up to the APB2 bridge, the firmware library function RCC_APB2PeriphClockCmd () is used to initialize.UARTx needs sub-situation discussion, if it is UART1, then hung on the APB2 bridge,Therefore, the RCC_APB2PeriphClockCmd (RCC_APB2Periph_USART1 | RCC_APB2Periph_GPIOA, ENABLE) is used for initialization and the rest of the UARTs are hung on the APB1.

(2)The second is to configure GPIO.The GPIO properties are contained in the structure GPIO_InitTypeDef, where for the TX pin.The GPIO_Mode field is set to GPIO_Mode_AF_PP (multiplexed push-pull output).GPIO_Speed switching rate is set to GPIO_Speed_50MHz.For the RX pin, the GPIO_Mode field is set to GPIO_Mode_IN_FLOATING (no floating input) and there is no need to set the switching rate.Finally, IO port is enabled via GPIO_Init().

```
GPIO_InitStructure.GPIO_Pin = GPIO_Pin_9;
GPIO_InitStructure.GPIO_Mode = GPIO_Mode_AF_PP;
GPIO_InitStructure.GPIO_Speed = GPIO_Speed_50MHz;
GPIO_Init(GPIOA, &GPIO_InitStructure);

GPIO_InitStructure.GPIO_Pin = GPIO_Pin_10;
GPIO_InitStructure.GPIO_Mode = GPIO_Mode_IN_FLOATING;
GPIO_Init(GPIOA, &GPIO_InitStructure);
```

Fig. 2. GPIO setting code

(3)Configure UART related attributes.Use the structure USART_InitTypeDef to determine the relevant properties.The fields in UART mode are as follows:

USART_BaudRate:Baud rate

USART_WordLength:Word length

USART_StopBits:Stop bit

USART_Parity:Verification method

USART_HardwareFlowControl:Hardware flow control

USART_Mode:Single / duplex

Finally set USART1 enable.

(4)Send and receive byte data.When sending byte data, set the parameter to unsigned char type and wait for serial port 1 input data: while (USART_ GetFlagStatus(USART1, USART_FLAG_TXE) == RESET).Pay attention to receive byte data to determine whether to receive data.

(5)Interrupted service program design. USART_ IT_RXNE (receive buffer emptying interrupt) to ensure that once the data is received, it enters the interrupt to receive a specific length of data.USART_IT_TXE (sending buffer empty interrupt) said that as soon as the end of a data sent into the interrupt function, in order to ensure continuous transmission of a piece of data.Since the program contains both receive and transmit interrupts, it needs to be determined using the USART_GetITStatus () function.After determining which type of interrupt is used, clear the interrupt flag bit.

(6)Direct output of the main function.Note that you need to use the SystemInit () function to configure the system clock before outputting 72M.

Bluetooth module.

If you want to use Arduino's Bluetooth module, you first need to set the basic parameters of the Bluetooth module.Basic parameter settings include: Bluetooth name, mode and matching passwords.

Set the Bluetooth module You can use Arduino to connect the Bluetooth module to set.Enter the AT mode to set the Bluetooth connection as follows:Arduino 5V-VCC,Arduino GND-GND,Arduino Pin10-RXD, Arduino Pin11-TXD.

Then program the Bluetooth module using the Arduino AT mode to program the Bluetooth module via the serial monitor provided by the Arduino IDE.

Use the Arduino IDE serial monitor for debugging, select the correct port, and set the output format to Both:NL & CR,baud rate is set to 9600.

TABLE1

Commonly used AT command

1	AT+ORGL	Restore factory mode
2	AT+NAME=<NAME>	Set Bluetooth name
3	AT+ROLE=0	Set Bluetooth as slave mode
4	AT+CMODE=1	Set Bluetooth to any device connection mode
5	AT+PSWD=<Pwd>	Set Bluetooth match password

Each service and service attribute is uniquely verified by a UUID (Universally Unique Identifier).Each service and service attribute is uniquely verified by a UUID (Universally Unique Identifier).Bluetooth mobile data transmission similar to Socket.Socket and ServerSocket are used in the network to control the reading and writing of data on the client and server.The Bluetooth communication is also completed by the client and the server Socket.The Bluetooth client Socket is a Bluetooth Socket, and the server Socket is a Bluetooth Server Socket.Both of these classes are in the android.bluetooth package.

Whether it is BluetoothSocket or

BluetoothServerSocket requires a UUID.

The UUID is equivalent to the Socket port, and the Bluetooth address is equivalent to the Socket IP.With ports and IP addresses, data can be received and sent.

The UUID of the client and server must be the same for the Bluetooth adapter and the Android Bluetooth module.The following is the UUID read through the Bluetooth Serial Assistant:

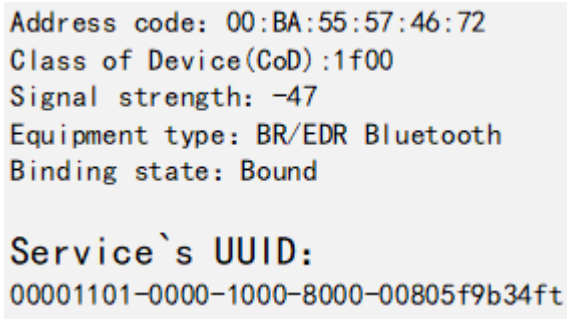

Fig. 3. Bluetooth serial assistant to read information

Mobile APP.

Android is an operating system for Linux kernel-based software platforms, including operating systems, user interfaces, and applications.Its user interface is mainly implemented by the control, and the code can also be directly implemented in the xml script file. The application program is mainly written in Java[4].There are two most commonly used Android APP development environments::Eclipse and Android Studio.Android Studio is the official development environment recommended by Google. Compared with traditional Eclipse, it does not require tedious configuration before the development of the Android APP. It also supports multi-screen browsing and has excellent intelligent prompting function. It is ideal for junior developers[5].

- Feature design.

The software is developed based on the Android platform. There are three main parts:

(1) Start interface: A clear and simple start interface facilitates observation and detection.

(2) Prompt module: When Bluetooth signals, a message is displayed.

(3) Music module: It is convenient for people to prompt when the mobile phone is not around.

- Interface design.

There are five layout methods in Android.They are: LinearLayout, RelativeLayout, FrameLayout, AbsoluteLayout, TableLayout.

The interface is divided into two rows and the left display shows the connected devices.The first row in the right row shows that no device is connected. The second line shows the associated device, corresponding to the EditText control in Android, and the button corresponding to the Button control. The third line shows the alarm status.The interface layout is suitable for LinearLayout, which is the most common layout method in Android development.It is laid out either vertically or horizontally, and the orientation of the linear layout can be set via the "android:orientation" property.The property values are vertical and horizontal.When laid out vertically, there is only one element per line, and multiple elements go vertically down.In the horizontal layout, there is only one row, and each element is arranged to the right.Commonly used attributes are:

(1)android:orientation:set the direction of the layout

(2)android:gravity:used to control the alignment of components

(3)layout_weight:control the relative size of each component in the layout

First, find the automatically generated layout file activity_main.xml in the res/layout folder.In this file, declare that the layout direction of the parent layout LinearLayout is vertical, and set the attribute value of android:orientation to vertical.Second, set the width and height of the text input box EditText to be adaptive and set the prompt language through the android:hint attribute. The prompt language is defined in the res/values/strings.xml file.Finally, complete the calculation button section.The button has two properties that need to be set. One is to set the horizontal centered property of the button android:layout_gravity to center_horizontal and the other is to register the button event listener property[6].

C．Hardware part

Signal detection module.Many similar product testing modules are used for a variety of humidity sensors, however, the temperature can also affect the sensitivity of the humidity sensor, and long-term use can cause severe drifts.

Most capacitive humidity sensors do not have the ability to operate at temperatures above 40℃ and are often failing and damaged.Their corrosion resistance is also lacking. They have a high requirement for the cleanliness of the environment, and some products also suffer from light failure, electrostatic failure and so on.

Therefore, the alarm signal detection module using the structure shown in Figure 2, copper sheet.Copper flakes create resistance when urine contacts. When the resistance reaches a certain value, the signal processing module starts to work.Although the temperature will also affect the metal resistance, the urine temperature is generally 36℃-37℃. It has minimal impact on metal resistance and can be ignored.

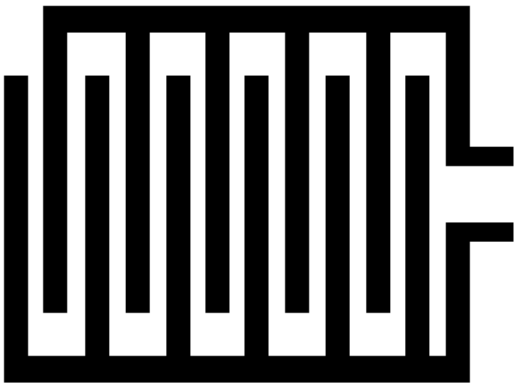

Fig. 4. Detection module

Signal Processing Module.In the detection of no urine, the output of U1 by Schmidt reverse output low 0V.When there is urine, U1's input terminal is connected with a resistance of 10k~500k to ground, together with a

4.7M pull-up resistor, making U1's input voltage change from 0.3V to 1.5V.This input voltage is below the negative threshold voltage of the Schmitt trigger, causing the output signal of U1 to trip to a high level of 5V.At this time,send high level to pin of STM32 one-chip computer.

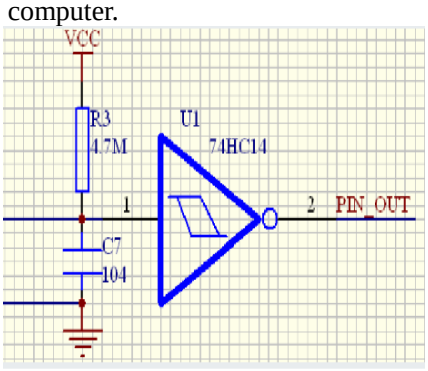

Fig. 5. Hardware schematic

Bluetooth module.Bluetooth wireless transmission in recent years the development of very rapid, ATK-HC05 Bluetooth module using frequency hopping spread spectrum technology.The maximum transmit power of the ATK-HC05 Bluetooth device can be classified into three levels: 100mw (20dB/m), 2smw (4dB/m), and 1mw (0dB/m).

ATK-HC05 Bluetooth module device has its own pairing information when it is in production.After power on, the two devices can be automatically connected.HC05 Bluetooth adopts transparent serial transmission and does not require interference from peripheral circuits.Bluetooth system work is frequency hopping, you can point-to-point, point-to-multipoint connection transfer.

TABLE 2
ATK-HC05 module pin description

Serial number	name	Description
1	LED	pairing status output:if paired successfully output high voltage,output low if not paired
2	KEY	used to enter AT state:high effective,(Floating defaults to low level)
3	RXD	module serial port receive pin(TLL level,cannot directly connect RS232 level),can take SCM TXD
4	TXD	module serial port send pin(TLL level,cannot directly connect RS232 level),can take SCM RXD
5	GND	ground
6	VCC	power supply(3.3V~5.0V)

ATK-HC05 comes with a status indicator: STA. There are 3 kinds of lights in this state, they are:

(1)When the ATK-HC05 module is powered on, the KEY is high (connected to VCC) and the STA is flashing slowly (the bright frequency is about 1 time / second, indicating that the module has entered AT state.

(2)When the ATK-HC05 module is powered on, the KEY will be connected to GND or left floating. At this moment, the STA will flash fast (the frequency of the light is about 2 times/sec), indicating that the ATK-HC05 module has entered a state that can be paired.

(3)At this moment, it is proved that the module already belongs to the pairing success state, and the STA will perform double blinking (the bright frequency is about 2 blinks once, 0.5 times / second).

When the CPU's parallel data characters are converted to continuous serial data to send out, then the serial data into parallel data characters provided to the CPU device.The serial port sends and receives bytes in bits. The serial interface is characterized by the ability to convert CPU parallel data characters and serial data streams[7].

The module needs at least 4 wires to connect with STM32. VCC, GND, TXD, RXD, VCC and GND are used to supply the module. The modules TXD and RXD are connected to RXD and TXD of STM32.

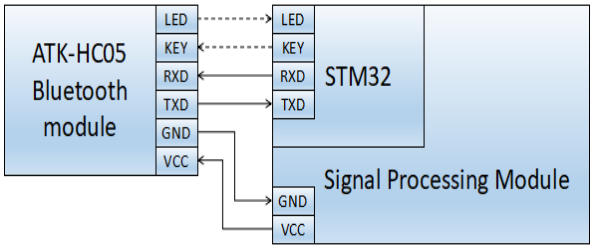

Fig. 6. ATK-HC05 module and processing module connection diagram

4 TEST RESULTS

After the program is checked, it is programmed into the STM32. After the hardware circuit is connected, the test is started.First open the phone app and show the current Bluetooth connection status.Then put a wet cloth instead of a baby diaper on the test piece.The indicator light of the processing module flashes, and the app displays “Please change diapers”. At the same time, the mobile phone rings and prompts parents to prove that the test was successful.

5 SUMMARY

This paper introduced the principle and implementation process of the "STM32-based wireless bed-wetting monitoring alarm".At the time of completing this project, it also encountered many problems, such as: the choice of Bluetooth model, the setting of GPIO_Mode field and the connection between Bluetooth and STM32.But after each problem is solved, many new knowledge will be learned.

The design of the new bedwetting alarm has other shortcomings. For example, it is impossible to distinguish urine from other conductive fluids, and there is room for hardware to reduce space.

The alarm is just the beginning of a baby's remote care.Based on this, some other improvements can be made, such as: distinguishing babies from urine and collecting data to analyze the health of babies.Different

functions can be developed according to different family needs.

References

[1] J. J. Wu, “Radio Frequency Identification Technology and Its Application in Tobacco,” Science and wealth, vol.12, 2013, pp. 85–85.

[2] K. Li, Y. Q. Du, Q. Z. Wang, “*Design of a New Non-contact Urine Wetness Detector”,* Microcomputer and application, vol. 33, 2014, pp. 87–90.

[3] W. Yang, Y. P. Xiao, “Design of LCD Display System Based on STM32F103C8T6 Microcontroller”, Microcomputer and application, vol. 33, 2014, pp. 29–31.

[4] W. Fang, “Research on Chinese Coding and Realization of Lattice Display in Bluetooth Communication”, Computer fan, vol. 18, 2017, pp. 92–92.

[5] S.Y. Sun, “Design and Implementation of Health Management System APP Based on Android Platform”, B.Eng. thesis, Beijing industry university, Beijing, China, 2016.

[6] M. H. Dong, H. W. Li, “Android Starter Development - BMI Calculator”, Computer Knowledge and Technology, vol. 13, 2017, pp. 136–138.

[7] M. Hou, Y. W. Hu, Q. Jiang, “Design of Remote Acquisition System for Electrical Parameters Based on PA and Bluetooth Wireless Transmission”, Electronic world, vol. 5, 2016, pp. 164–166.

The self-excitation circuit of cascaded coupling RTD fluxgate

JinMeng; Bangyan Wang; Zizheng Yang

（instrument science and engineering institute, Jilin university）

***Abstract*-As usual, a damping unforced dynamic system will not oscillates, but when the coupling coefficient excel a critical value and on a no identical starting condition, a system with N(odd) single coupling system will foster self-oscillation, and the self-oscillation can be used to measure some tiny singles quantity. When the N coupling coil achieve self-oscillation, the frequency of N times of the frequency of one oscillator, and with the increasing of N, the frequency of one coil will reduce. The output signal of RTD fluxgate in a positive impulse, and the amplitude is low, which is hard to gather. So we need to design a signal disposing circuit to translate the sharp impulse into level signal which is easy for digital circuit to gather. Its T^+ and T^- use the width of high and low electrical level. The output of the RTD fluxgate goes through a integral circuit to translate it into a rectangular wave approximately, and then go through a summing circuit to translate the wave's height in case of DC bias. Then go through a smoothing circuit to wipe off the noisy. In the end, we use reverse amplification to adjust the polarity in order to perfect the amplification. In addition the preposition of addition circuit and V-I transition circuit is used for cascading.**

Key words-Fluxgate; Cascade coupling; Self-excited; Magnetic field

I.INTRODUCTION

IN the field of field weakening measurement, the fluxgate sensor is the best overall performance. Currently, the mainstream fluxgate sensor is the even harmonic fluxgate sensor. Among them, the excellent fluxgate resolution Is 0.1 nT,Therefore, the research has entered a bottleneck[2]. If we want to further improve the performance of fluxgate sensors, we need to find a new method from the structural principle. Residence Time Difference (RTD) fluxgate is widely concerned by domestic and foreign scholars due to its simple structure, high sensitivity and easy digital measurement[4]. The RTD-type fluxgate work requires a specific excitation source to work, which inevitably will affect the accuracy of the sensor[1~3]. Accordingly, this paper designed a RTD-type fluxgate detection circuit, combined with the Hopf bifurcation theory in nonlinear dynamics, the initial realization of the three-system cascade self-excitation, eliminating the incentive source.

II. THEORIES

RTD fluxgate single-core fluxgate, the excitation coil and the induction coil wound on the same core, the structure shown in Figure 1, in which H_x is measured magnetic field, I_e sinusoidal excitation current. Fluxgate core material for the coercive force H_c small cobalt-based amorphous strip, the characteristic curve shown in Figure 2 (a), under ideal circumstances always work in positive and negative saturation, the excitation current is set to a sine Period is saturated duration of T ^ +, negative saturation duration T ^ -. When the measured magnetic field H_x is zero, there is only sinusoidal exciting current in the coil, and the positive and negative saturation times of the magnetic core are the same, ieΔt = T ^ + - T ^ - = 0; when the measured magnetic field H_x is not zero, In addition to the secondary field generated by the excitation current, H_x is also superimposed, which is equivalent to giving a DC bias to the excitation current. In this case, the positive and negative saturation times of the magnetic cores are different, that is, Δt = T ^ + - T ^ - ≠ 0, Size and H_x related.

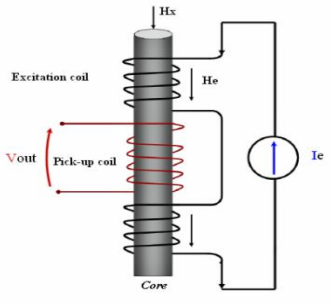

Figure 1 RTD fluxgate structure

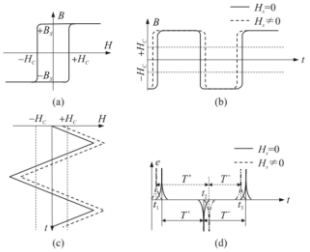

Figure 2 RTD fluxgate working principle

Let the magnetic field where the total magnetic field is $H(t)$, $I_e$excitation magnetic field generated by the cycle T_e,amplitude H_m, then

$$H(t) = H_m \sin\frac{2\pi}{T_g}t + H_x \quad (1)$$

Let $H(t)$ reach the moment of H_c for the first time as t_1, and then reach the time of the first time that arrives $-H_c$ for t_2, then there is

$$\begin{cases} H_m \sin\frac{2\pi}{T_g}t_1 + H_x = H_c \\ H_m \sin\frac{2\pi}{T_g}t_2 + H_x = -H_c \end{cases} \quad (2)$$

Solutions have to

$$\begin{cases} t_1 = \frac{2\pi}{T_g}\sin^{-1}\frac{H_c - H_x}{H_m} \\ t_2 = \frac{2\pi}{T_g}\sin^{-1}\frac{H_c + H_x}{H_m} + \frac{T_g}{2} \end{cases} \quad (3)$$

Thereby

$$\begin{cases} T^+ = t_2 - t_1 = \frac{2\pi}{T_g}\left(\sin^{-1}\frac{H_c + H_x}{H_m} - \sin^{-1}\frac{H_c - H_x}{H_m}\right) + \frac{T_g}{2} \\ T^- = T_g - T^+ = \frac{2\pi}{T_g}\left(\sin^{-1}\frac{H_c - H_x}{H_m} - \sin^{-1}\frac{H_c + H_x}{H_m}\right) + \frac{T_g}{2} \end{cases} \quad (4)$$

RTD fluxgate output time difference

$$\Delta t = T^+ - T^- = \frac{4\pi}{T_g}\left(\sin^{-1}\frac{H_c + H_x}{H_m} - \sin^{-1}\frac{H_c - H_x}{H_m}\right) \quad (5)$$

III. FLUXGATE DIGIT CIRCUIT DESIGN

The signal output by the RTD fluxgate is a positive and negative pulse, and the amplitude is small, it is difficult to meet the acquisition requirements, the need to design a signal processing circuit to spike into digital signals for the level of acquisition, the T ^ + and T ^ - Through the level of high and low level, the signal processing circuit structure shown in Figure 3. Fluxgate output signal amplified by the instrumentation amplifier, and then by the integral circuit into an approximate rectangular wave, the addition circuit to adjust the height of the waveform to prevent DC bias, and then through the filter circuit to remove noise, and finally through the inverting amplifier circuit to adjust the output pole And further improve the magnitude of the signal amplitude, while the magnetic flux gate in front of the addition circuit and voltage and current conversion circuit is to achieve the cascade to prepare.

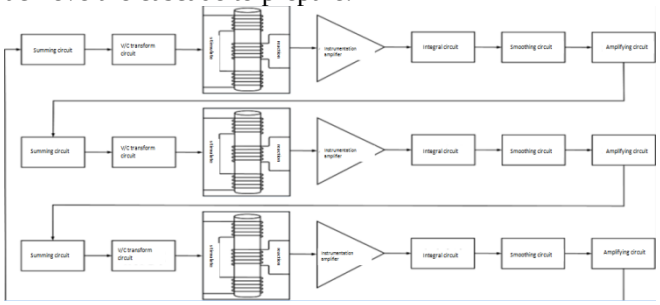

Figure 3 signal processing circuit structure

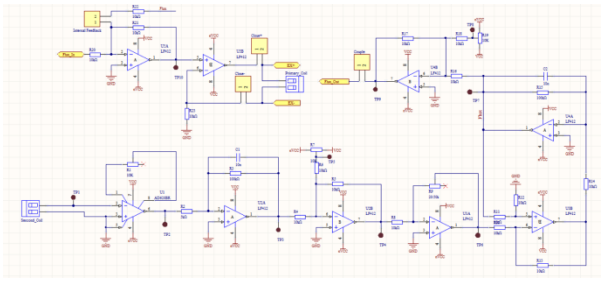

Figure 4 signal processing circuit schematic

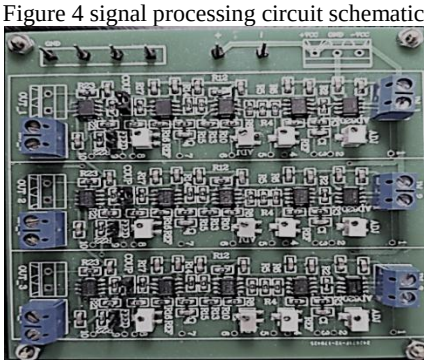

Figure 5 signal processing circuit physical map

Considering various factors, the instrumentation amplifier uses 0.28μV peak-to-peak noise of the low noise, low power integrated instrumentation amplifier AD620, other circuit module op amps are dual op amp integrated chip LF412, the circuit diagram shown in Figure 4, the overall signal Processing circuit using PCB technology to draw, reduce the volume and improve the stability of the circuit, as shown in Figure 5.

Integrating circuit in parallel 100 k Ω resistance provide capacitance discharge circuit and we select 10 nf capacitance is greater than the input signal cycle RC constant, make its approximate integrator for ideal, its diagram is shown in figure 6. The relationship between the output and input of the integral circuit is as follows:

$$v_o \approx -\frac{1}{R_1 C} \times \int v_i\, dt$$

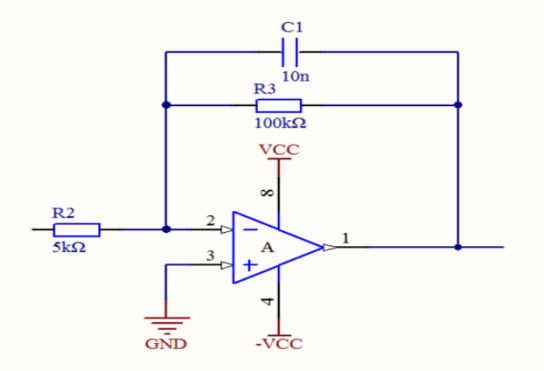

Figure 6 Integral circuit schematic diagram

Noise and interference from outside circuit will also be exaggerated by the integral circuit and amplification circuit, so if you want to get high precision voltage signal, need add filter circuit to filter out the interference, can use type biquadratic filter consisting of low pass filter, as shown in figure 7, after deduction, the open-loop gain is:

$$A_{vf} = \frac{10}{11 + R_{15}SC}$$

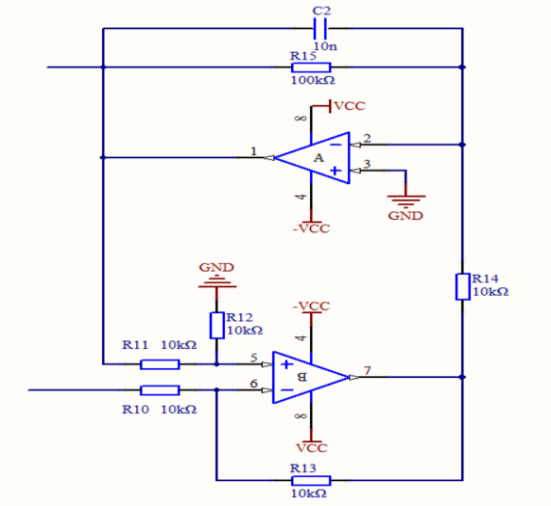

Figure 7 Schematic diagram of filter circuit

The offset circuit shares a LF412 with integral circuit, which structure is shown in figure 8, the role is to adjust the slide rheostat R7 to control the potential of intermediate point, in order to eliminate the integral circuit to produce dc bias signals.

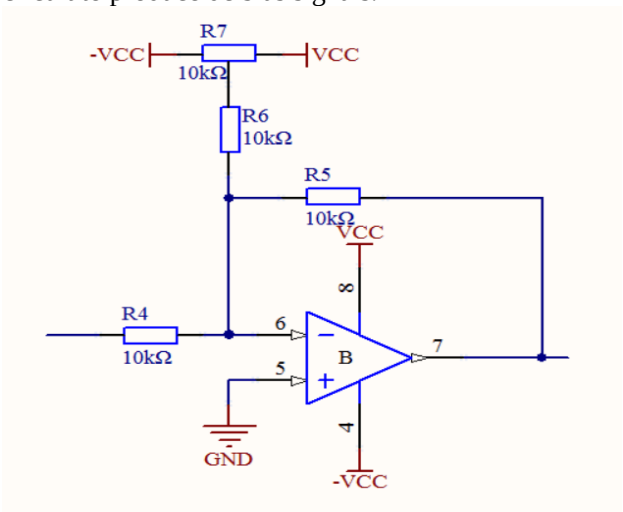

Figure 8 biased addition circuit schematic diagram

The self-excitation can be realized after the debugging of the fluxgate, that is, the input self-excitation is realized by the cascade implementation without external excitation, as shown in fig.9.

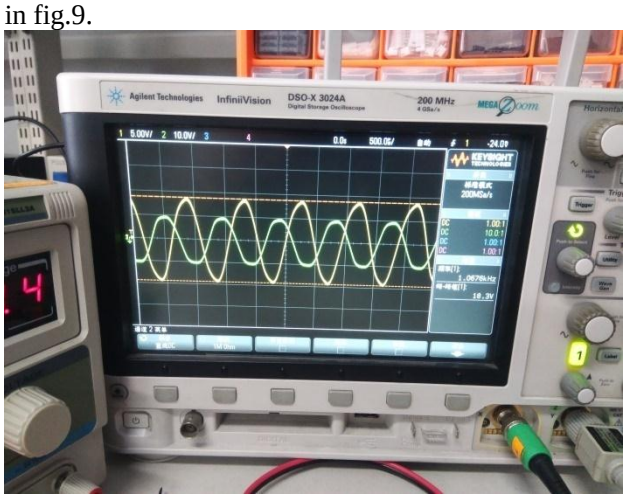

Figure 9 the signal after self –excitation

IV. ANALYSIS

After signal processing circuit and data acquisition and storage circuit, a series of data are successfully stored in SD card. (without the interference of outside magnetic field in the shield room) measurements are shown in figure 10 below. To the left of the data on behalf of the duration of the high level of FPGA clock, data on behalf of the low level on the right side of the duration of the FPGA clock. By the chart shows, in the absence of external magnetic field interference, high and low level clock several basic same, represent in the absence of external magnetic field, after the signal processing circuit, the input signal of FPGA is basically a square wave signals, consistent with theory.

```
00- H0000042463 L0000042671
01- H0000042424 L0000042872
02- H0000042633 L0000042462
03- H0000042377 L0000042823
04- H0000042438 L0000042929
05- H0000042406 L0000042532
06- H0000042470 L0000042388
07- H0000042384 L0000042553
08- H0000042280 L0000042548
09- H0000042005 L0000042802
10- H0000042518 L0000042952
11- H0000042789 L0000042790
12- H0000042284 L0000042278
13- H0000000191 L0000042886
14- H0000042415 L0000042800
15- H0000042640 L0000042618
16- H0000042196 L0000042324
17- H0000042443 L0000042601
```

Figure 10 Part of the data that is measured when there is no external magnetic field

In a normal environment, when the external magnetic field is present, in theory, the time of high and low levels is no longer equal due to the influence of external magnetic field. The measured part of the data is shown in figure 11 below. By the image below shows, when there is external magnetic field, the high level to low level time exists obvious difference, this means that the time field for the quantitative impact on input signal, in theory. After that, the difference in the difference between the magnetic gate and the direction of the magnetic gate is measured,which means that the different components of the external magnetic field are measured after the deflection.

```
00- H0000017512 L0000015218
01- H0000017362 L0000015113
02- H0000017387 L0000015078
03- H0000017155 L0000015260
04- H0000000977 L0000015211
05- H0000017031 L0000015302
06- H0000000830 L0000015281
07- H0000017628 L0000015222
08- H0000017264 L0000015004
09- H0000017567 L0000015188
10- H0000000123 L0000015227
11- H0000017154 L0000015358
12- H0000017214 L0000014946
13- H0000017187 L0000015105
14- H0000017343 L0000014977
15- H0000017153 L0000015152
16- H0000000793 L0000015292
17- H0000017409 L0000015139
18- H0000017208 L0000015137
```

Figure 11 Part of the data that is measured when there exists external magnetic field

The time difference in the measurement of multiple sets of data in different environmentsis shown in figure 12, the FPGA sampling frequency is 50 MHZ, above the blue solid lines represent the presence of external magnetic field in 100 groups of data in high and low level time, below the orange dotted line represents the shielding room when there is no external magnetic field effect under the condition of high and low level 100 groups of data of time lag. Analysis curve, when there is no external magnetic field, under the condition of high and low level lag in 0 fluctuate, and volatility is lesser, can be roughly think at this point, the high and low level almost the same duration. When the presence of external magnetic field, in high and low level time increased obviously, the curve can be quantified by analyzing the outside magnetic field for the influence of high and low level difference, so as to realize the magnetic field of the external world more accurate measurements.

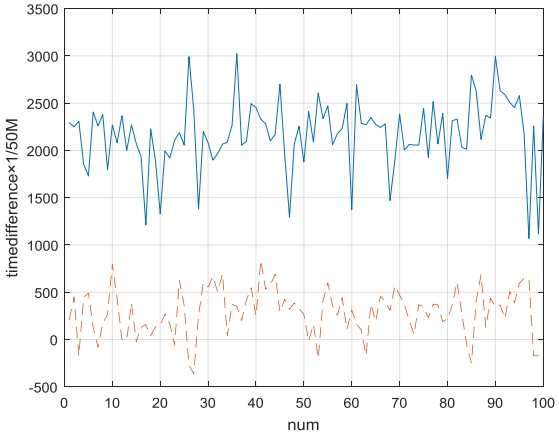

Figure 12The time difference in the measurement of multiple sets of data in different environments.

V. SELF_EXCITED TO ACHIEVE THE PRINCIPLE

In general, over-damped non-forced dynamical systems do not oscillate, but N (odd) individual coupled structures can generate self-oscillating oscillations when the coupling coefficient exceeds a certain critical value and under an unequal initial condition, Oscillator oscillation can be used to measure certain weak signals quantitatively. This feature stems from the Hopf bifurcation and may occur in any system of overdamped bistable cells, but does not produce oscillations if they are separated or removed from each other, so the generation of self-sustained oscillations is closely dependent In the right choice of parameters and system operating conditions. In general, the over-damped bistable dynamic equation can be expressed as $x = -\nabla U_{70}(x)$. In a cascaded coupled RTD fluxgate sensor, $x_{70}(t)$ represents the ferromagnetic material In the magnetic flux density, the dynamic equation can be written as $x^{\cdot} = -x + \tanh_{70}[c(x + \varepsilon)]$, c is a temperature and material related system parameters, ε is the weak signal to be measured, the coupling coefficient The critical value and the oscillation frequency are related to c and ε. After N coupled coils realize self-oscillating oscillation, the oscillation frequency is N times of a certain oscillation frequency alone, and as N increases, the oscillation frequency of a certain coil alone will be reduced. Conventional magnetometers require an extra signal source as an incentive, but since cascade coupling enables self-oscillating and can replace external power sources as an incentive, it is possible to realize a magnetic sensor with low power consumption, low price, and small noise interference .

After the stimulus, the resulting signal is the time difference, signal processing through the FPGA, and then the signal would go through the MSP430 for signal processing, finally through the storage and display circuit to obtain the result.

References

[1] Wang Yanzhang.RTD Fluxgate Sensor Detection System Design.Sensors and Microsystems [J].September 2015

[2] Zhang Ying. Digital Fluxgate Sensor Based on Microcontroller. Northwestern Polytechnical University [J]. 2006-07

[3] Wu Shujun. Digital Quantitative Technology Research of RTD Fluxgate Sensor. Jilin University [J]. 2014

[4] Liu Shibin. Hysteresis time differential fluxgate sensor signal detection method. Northwestern Polytechnical University [J]. 2013

[5] Visarath In. Experimental Observation of Multifrequency Patterns in Arrays of Coupled Nonlinear Oscillstos. 5 February 2003.

The design of active three-dimensional magnetic field offset device

Wang Ruihong; Li Xingtong; Zhang Yumeng
(*College of Instrumentation and Electrical Engineering, Jilin University)*

***Abstract*- This subject derive from the research project:the leader of young and middle-aged scientific and technological talent and team in Jilin Province innovation projects, atomic magnetometer research. Under the circomstance of ultra-low detection, atomic magnetometer needs to work in a weak magnetic field, especially for SERF atomic magnetometer. At the same time, in order to overcome the traditional method of using multi-layer shielding tube to shield the magnetism, which leads to the large volume of the whole device, we proposed to the triaxial Helmholtz coil to offset the magnetic field.**

***Keywords*- Helmholtz coil SCM fluxgate sensor**

Ⅰ.INTRODUCTION

THIS project is mainly composed of three modules: DC constant current source module, Helmholtz coil module, fluxgate sensor module.

Power module according to the compensation coil load characteristics, the controller MCU and DAC as the core, to achieve zero magnetic compensation coil DC drive power supply design, the final real-time amplitude adjustable DC drive signal. Complete welding, debugging, and experimental verification.

According to Biosaveval's law, the coil module is referenced to the MATLAB simulation method of Si Wen Jian of Xuchang University to determine the size and number of turns of the coil by calculation. Through the PCB to complete the coil production.

The fluxgate uses Bartington's three-terminal fluxgate mag-03 and designs an op amp circuit that allows its voltage output to match the voltage range of the on-chip ADC on the MCU.

After the three modules are designed, the three are connected, the fluxgate sensor detects the size of the magnetic field and transmits the analog signal to the microcontroller. SCM received through a certain algorithm to achieve a dynamic offset magnetic field.

The design content of this subject has certain practical significance for the development of SERF atomic magnetometer. In addition, the subject can train students to design the system according to the actual needs of the project, select the appropriate programs and devices according to the needs of the project, and carry out the welding debugging of the unit hardware circuit and the connection between software and hardware. The difficulty lies in the simulation of three-axis Helmholtz coil, the design of AC-DC power supply, the selection of the number of turns of the coil[1], and the solution of the orthogonal problem of the three-axis coil.

Ⅱ. HELMHOLTZ COIL CANCELS THE MAGNETIC PRINCIPLE

A. Helmholtz coil magnetic field generated by the principle

The magnetism of the earth is one of the physical properties of the Earth's interior. The Earth is a large magnet that forms a magnetic field around it, a space that shows the effect of magnetic forces, termed a geomagnetic field. The intensity of geomagnetic field is very weak

A characteristic of the magnetic field is that its intensity at the strongest bipolar is less than 10^{-4}T, and its average intensity is about 0.6×10^{-4} T, which is less variable with location or time. Another characteristic of the geomagnetic field is that the intensity of the geomagnetic field is a vector, and the direction of the geomagnetic field is different in different regions of the earth. The large magnet of Earth, which is also polar, has a geodetic South pole that is the north pole of the magnet and the geographically North pole is a magnetically S pole. Therefore, the magnetic induction line of the geomagnetic field is from the south pole of the earth to the north pole[2]. In the vicinity of the equator, the direction of the earth's magnetic field is parallel to the surface of the earth. In the northern and southern hemispheres, the geomagnetic field lines have vertical components perpendicular to the earth's surface. The geomagnetic field is characterized by a weak intensity, which varies with the latitude on the earth's surface.

From the above can be drawn: the magnetic field is a space magnetic field, local magnetic field measurement in the measurement of magnetic field strength, but also to measure the direction of the magnetic field. In the past, the magnetic field measurement methods known to the magnetic field direction are no longer applicable. The method of measuring the magnetic field in the space can be used to measure the local magnetic field, measure the local magnetic field strength, and measure the direction of the local magnetic field. The following part of the magnetic field from the local offset method to proceed with the discussion. The method of realizing the geomagnetic field offsetting system is to use the three-dimensional Helmholtz coil to generate the canceling magnetic field. The resultant magnetic field of the magnetic field vector is zero within the error range, thus completing the offset of the local geomagnetic field.

B. Helmholtz coil magnetic field generated by the

principl

A straight metal lead passes a current that creates a circular magnetic field in the space around the lead. The larger the current flowing in the wire, the stronger the magnetic field. The magnetic field is circular around the wire. The strength and distribution of the magnetic field are described using the vector of magnetic induction. The basic law of the magnetic field generated by the current carrying wire is Biot-Savart's law, as shown in Figure 1.

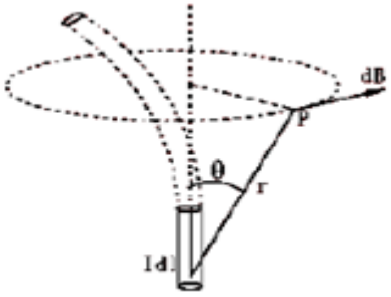

Fig.1 Biot-Savart's law

If, however, a pair of identical current carrying coils are parallel and coaxial with each other and are supplied with the same direction current, the total magnetic field of the two current carrying coils is within a relatively large range around the midpoint of the shaft when the coil spacing is equal to the coil radius average. Therefore, in the production and research have greater practical value, but also commonly used in weak magnetic field measurement standards. This pair of coils is called a Helmholtz coil.

III . SYSTEM WEAK MAGNETIC MEASUREMENT SENSOR SELECTION

A. Inductive coil sensor

Inductive coil sensor for measuring alternating magnetic field, its sensitivity increases with the alternating magnetic field frequency increases, its measurement range is wider, the resolution can reach 10^{-12}-10^{-13}T, as shown in Figure 2.

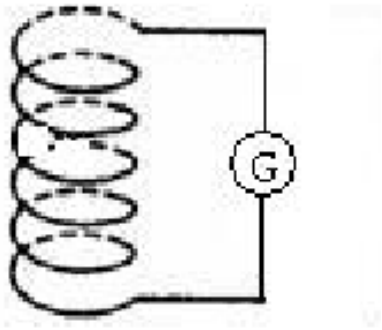

Fig.2 Magnetic measuring coil

A vibrating sample magnetometer is a magnetic measuring instrument that uses an inductive coil sensor that uses an induction coil to measure the magnetic moment of a magnetic sample and the intensity of the external magnetic field where it is located. In the case of known sample quality and demagnetization factor, the material can be easily obtained by magnetization, saturation magnetization, magnetic susceptibility, coercivity, remanence and magnetization curve, hysteresis loop, etc., it is widely used .

Induction coil sensors have high sensitivity to alternating magnetic fields, however, they are not suitable for steady-state weak magnetic field measurements.

B. Design of signal processing module

Proton precession sensor is the use of nuclear magnetic resonance reaction principle, the measured magnetic field in the vertical direction plus the planned magnetic field, when the polarized magnetic field suddenly disappear, the probe's nuclear sample magnetic moment will be measured around the pull rate ω Magnetic field free precession, and the following equations to determine the relationship: $\omega = \gamma\beta$ is the gyromagnetic ratio of the nucleus, the relationship can be used to measure the absolute weak magnetic field, the measurement range is generally 10^{-3}-10^{-5}T, the resolution can reach10^{-10}T. Although the proton precession sensor has a high resolution, but the measurement conditions are demanding, not suitable for field measurements.

C. Fluxgate sensor

Fluxgate sensor is a vector measurement sensor. It is the use of high permeability materials in the coil system of magnetic saturation characteristics to measure the magnetic field. Fluxgate sensor for measuring a constant magnetic field or slow changes in the weak magnetic field, the resolution can reach 10^{-12}T, the measurement range is 10^{-3}-10^{-4}T, it has low power consumption, small size, simple structure, measurement A wide range of features. Fluxgate phenomenon is a common phenomenon of electromagnetic induction, fluxgate sensor is a slightly modified transformer device, which consists of iron core around the excitation coil, induction coil. In order to improve the measurement precision, the fluxgate sensor adopts the differential signal output mode, adopts the double iron core, and generally adopts the runway structure. As shown in FIG. 3, the excitation coils wound on the two iron cores are reversely connected in series and the exciting directions of the two iron cores On the contrary, in the case of complete symmetry of the shape and electromagnetic parameters, the induced electric potentials of the exciting magnetic field in the common induction coil cancel each other to play the role of modulating the magnetic permeability of the magnetic core, and the induced electromotive force of the ambient magnetic field in the induction coil mutually Overlay. This induced electromotive force is the fluxgate sensor output model. Fluxgate sensors, measurement circuits, data acquisition and processing unit composed of three parts fluxgate[3].

Magnetometer using fluxgate technology is the fluxgate magnetometer. For the unknown magnetic field measurement requires the use of three-dimensional measurement magnetometer, from

the magnetic field strength and direction to measure the magnetic field.

In this paper, the magnetic flux to achieve the magnetic field measurem

Ⅳ. POWER MODULE DESIGN

A. DC voltage source

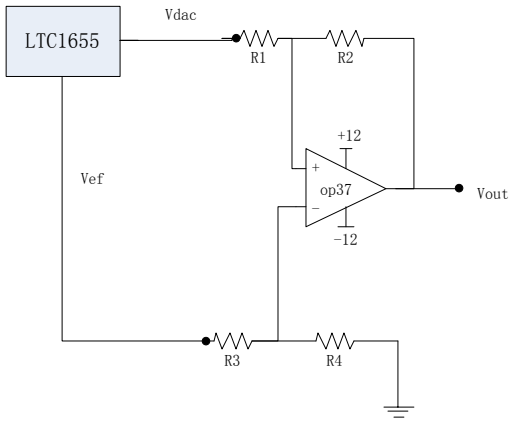

Fig.3 DAC output circuit diagram

The module uses a 16-bit DAC chip LTC1655 output forward voltage generated 0V-4.10V adjustable voltage. Then output to the back by the OP37 build difference circuit, the purpose is to achieve the current bidirectional output. In order to reduce the interference of the operational amplifier noise, the output voltage should be as large as possible, between -10V and + 10V. The voltage at the other end of the difference circuit is provided by the DAC's own reference voltage. In order to avoid the op amp current higher reference voltage, op amp select a larger resistor resistance, we have chosen here is 1MΩ resistor, so that the reference voltage can be maintained at work. If the formula shows $R_1/R_2 = R_3/R_4$

$Vout = \frac{R_2}{R_1} \bullet (Vdac - Vef)$ .When R_1/R_2 =1:5 Voltage output can reach -10V ~ + 10V.

B. Voltage controlled constant current source

Since the current through the coil directly determines the size of the magnetic field generated by the coil, the constant current through the coil must be guaranteed. When the coil or cable changes due to external causes tissue. It must be able to adjust automatically to ensure that the current output does not change[4].

The scheme adopted by us adopts the voltage-controlled constant current source, the voltage-controlled constant current source module adopts the deep negative feedback structure to form a closed-loop control system so that the input signal can ensure a constant current output regardless of the DC voltage or the AC voltage, The current level is adjusted by the input voltage amplitude. The current-sense resistor samples the load current, converts the current signal into a voltage signal as a feedback signal, regulates the gate-to-source voltage Vgs of the MOSFET, allowing the MOSFET to operate in an active linear region and make the output current continuous between 0 and 0.07A

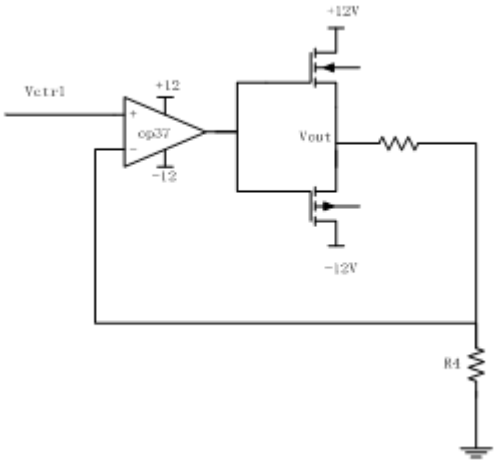

Fig.4 Voltage controlled constant current source circuit

C. Coil winding

By MATLAB Helmholtz coil magnetic field simulation, we can calculate the coil generated magnetic field size and current, the number of turns, the relationship between the diameter of the coil.

After the cost, as well as the current size of the current can be achieved, the comprehensive assessment of magnetic interference, we design the coil diameter of 13cm, the number of turns 40.

D. Design of Fluxgate and STM32 Interface

Thanks to its mag-03 fluxgate, it offers excellent noise performance and temperature stability. It is a small 3-axis fluxgate sensor that accurately measures static or alternating magnetic fields. The sensor's output voltage is -10V to + 10V and can not be compatible with our on-chip ADC, so we also needed an op amp circuit to scale its range from 0V to 3.3V for the STM32 on-chip ADC. The solution we used was to first attenuate the fluxgate input through a resistor and then add the -1.65V through the op amp to get the final ADC input. As part of the attenuation of partial pressure to select a larger value, the op amp current can not be ignored, the need to consider the current into the attenuation module.The final circuit shown in Figure

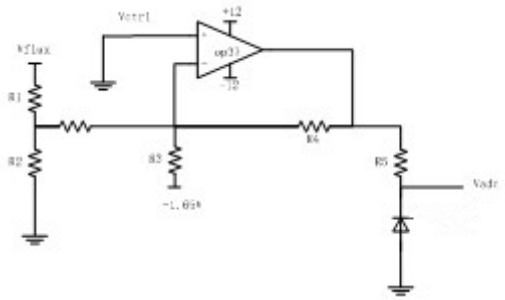

Fig.5 Fluxgate and STM32 interface circuit diagram

E. Offset algorithm selection

In order to be able to offset the earth magnetic field dynamically and quickly, we feed back the signals collected by the fluxgate to the microcontroller. Microcontroller through the size of the voltage collected to determine how to adjust the DAC output in order to achieve the purpose of controlling the current.

In order to be more accurate and fast to reach the balance point, we will change the value of each DAC voltage and the signal collected by the microcontroller is a positive correlation.

F. experiment method

We use data acquisition card Fluxgate data acquisition, the purpose is to be able to detect real-time magnetic field size on a PC. First, we test the static performance, observing the magnitude of remanence and the ripple after offsetting the device. And then test the dynamic performance, the direction of the mobile device, after each movement of a certain angle to observe changes in the size of the capture card magnetic field and speed.

Table 1 Dynamic performance test data of x axis

Time/s	0.05	0.10	0.15	0.20	0.25	0.30	0.35
Magnetic Field(nT)	100.5	50.4	27.9	15.4	7.7	7.7	7.7

Table 2 Dynamic performance test data of y axis

Time/s	0.05	0.10	0.15	0.20	0.25	0.30	0.35
Magnetic field(nT)	57.1	24.3	12.3	6.4	6.4	6.3	6.4

Table 3 Dynamic performance test data of z axis

Time/s	0.05	0.10	0.15	0.20	0.25	0.30	0.35
Magnetic field(nT)	100.5	50.4	27.9	15.4	10.7	3.4	3.4

This is a dynamic performance test after moving the whole device in a certain angle. The static performance tests that the triaxial magnetic field vectors' sum iswithin 10nT.

V. CONCLUSION

The remaining geomagnetic field offset by our unit is within 10 nT. It proves that our device can completely replace the shielding barrel in practical application and has better effect on the remanent magnetism. In the dynamic performance, we can achieve real-time fast dynamic offsetting the earth's magnetic field. When the entire device is moved, the device is able to self-regulate the size of the coil current, eventually reaching steady state.

References

[1] Zhang Yubao, Cao Huiyun, Zhang Bin.Design of NC Constant Current Source Based on Single Chip Microcomputer [J]. Electric Instruments & Measurement, 2011,48 (6): 75-78.

[2] Si Wenjian, Zhou Nan, Cao Yusong. MATLAB based Helmholtz axis magnetic field uniform distribution of dynamic simulation [A]. Xuchang Journal. 2010,29 (5): 72-74.

[3] Tao Linwei, Wang Yingmin, Lei Kaizhuo.Precision NC Constant Current Source Based on Microprocessor [J] .journal of Electronics Technique, 2012 (7): 138-140.

[4] Du table macro. Three-terminal fluxgate sensor interface ASIC design [D]. Harbin Institute of Technology, 2011.

Design of temperature, sound and distance detection device

Xia Changyu; Chen Qian; Zhang Kai
(College of Instrumentation & Electrical Engineering , Jilin University)

***Abstract*-The design of the device is mainly through infrared sensors, ultrasonic sensors, sound detection module to detect the environment temperature, obstacle distance, sound and other information, the information obtained through STM32 microprocessor processing into digital signals, and then through the wireless transmission module to the computer, through the GUI interface for intuitive display. This device can be used for the initial detection of human beings.**

***Key words*-sensors, STM32 microprocessor, wireless transmission.**

I. INTRODUCTION

INFRARED sensors, ultrasonic sensor and sound detection module has small size, high sensitivity, STM32 microprocessor has the advantages of high-performance, Low-cost, Low-power and so on, the wireless transmission module can be to a certain extent, the impact of filtering terrain, sensors and microprocessors composed of temperature, sound, distance detection device is easy to carry, Low cost and good performance. And with the future development of technology, sensor performance is bound to be more and more good, its precision, detection distance will have a greater improvement, processor information processing capacity will be greatly improved, wireless transmission module information transmission distance, stability can be enhanced. So the device in the future will have a lot of room for improvement, design ideas worthy of reference.

II. TEST METHODS AND EXPERIMENTAL SCHEMES

By using the STM32F series microprocessor as the main controller to deal with the detection information collected by infrared temperature sensor, ultrasonic sensor and sound detection module, then transmit to the host computer through the ZigBee module wirelessly, and display the data in real time through the GUI interface written by C #. Provide intuitive information to the tester for easy analysis. Scheme block diagram as follows:

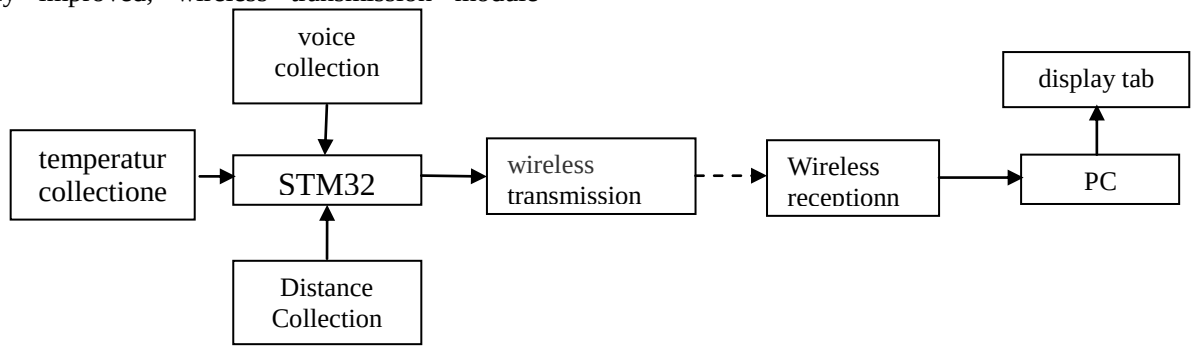

III. MODEL SELECTION AND PRINCIPLE

A. Ultrasonic distance measurement principle and module selection

Ultrasonic ranging is realized by ultrasonic pulse echo transit time method. Set ultrasonic pulse from the sensor sent to receive the time experienced by T, ultrasonic in the air propagation speed of C, then from the sensor to the target object distance D can be used to find: D = ct/2.

This part of the sensor we choose Hc-sr04 Ultrasonic ranging module, hc-sr04 ultrasonic ranging module can provide 2cm-400cm distance sensing function, ranging precision up to 3mm, module includes ultrasonic transmitter, receiver and control circuit.

HC-SR04 Ultrasonic ranging module Basic operating principle: Using IO port trig trigger ranging, to the minimum 10us of high electrical mail, the module automatically sent 8 40khz square wave, automatic detection of signal return; High-level duration is the time from which the ultrasound is sent from launch to return. Test distance = (340m/s)/2[1-3].

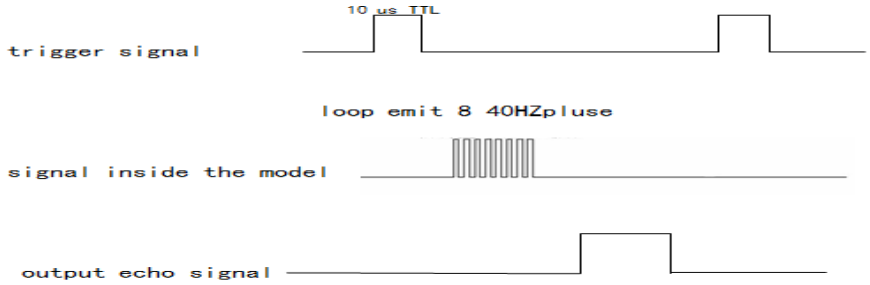

Fig.1 Ultrasonic sequence Diagram

The above sequence diagram shows that you only need to provide a pulse trigger signal above 10uS, which will emit 8 40kHz cycle levels and detect echoes. Once the echo signal is detected, the echo signal is output. The pulse width of the echo signal is proportional to the distance measured. Thus the distance can be computed by transmitting the signal to the time interval of the echo signal received. Formula: us/58= cm or us/148= inches, or: Distance = high electricity peacetime * sound velocity (340m/s)/2; It is recommended that the measurement period be above 60ms to prevent the effect of transmitting signal on the echo signal.

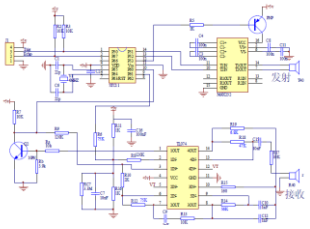

Fig.2 HC-SR04 Ultrasonic distance measurement module schematic diagram

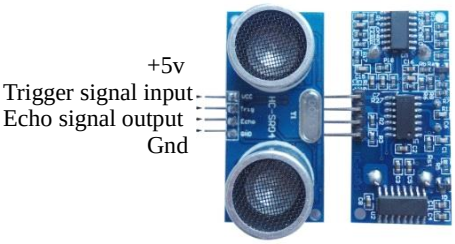

Fig. 3 Physical map

Table.1 HC-SR04 Ultrasonic distance Measurement Module electrical parameters.

working voltage	DC5V
working current	15mA
working frequency	40KHz
as far as the range	4m
The recent range	2cm
measuring angle	15 °
the input trigger signal	10us TTL impulse
the output back to the signal	output TTL level signal, proportional to range
specification and dimension	45*20*15mm

Note：1.This module is not suitable for live connection, to live connection, the first module to the GND end of the connection, otherwise it will affect the normal work of the module.2.Ranging, the object is measured in the area of not less than 0.5 square meters and the plane as far as possible to require leveling or otherwise affect the results of measurement.

B.Principle and module selection of infrared temperature measurement

The size and wavelength distribution of infrared radiation energy is closely related to the surface temperature of the object. Therefore, by measuring the infrared radiation of the object, it can accurately determine its surface temperature, and the infrared temperature measurement is to use this principle to measure the temperature. The infrared thermometer is composed of optical system, photoelectric detector, signal amplifier and signal processing and output. The optical system gathers the infrared radiation energy of the target in its field of view, and the size of the field is determined by the optical part of the thermometer and its position. The infrared energy is focused on the photodetector and converted to the corresponding electrical signal. The signal is converted to the temperature value of the target by the amplifier and signal processing circuit, and the algorithm in the instrument and the target emissivity are corrected.

In this part we choose GY-906 Infrared temperature measurement module to MLX90614 non-contact temperature sensor as the core. Melexis Company production of MLX90614 series of temperature measurement module is a very convenient infrared temperature measurement device, all of its modules are manufactured before the checkout, and can directly output linear or quasi linear signal, has a good interchangeability, eliminating the complex calibration process. The module takes 81101 thermoelectric elements as infrared sensing part. The output is the result of the temperature (to) of the object being measured and the temperature (Ta) of the sensor, ideally the output voltage of the thermoelectric element is: Vir=A（To4 –Tα4）. The temperature unit is kelvin,a as the sensitivity constant of the element. The target temperature and ambient temperature are measured by 81101 built-in

thermocouple measurements, and the two-channel temperature signals output from 81101 are amplified by a high-performance, Low-noise chopper steady state amplifier on the internal MLX90302 device, and then via a 17-bit analog-to-digital converter (ADC) and powerful digital signal processing (DSP) unit after output[4-5].

MLX90614 is controlled by the internal state machine to control the temperature of the object and the ambient temperature measurement and calculation, the temperature after processing, and the results through the PWM or SMBus mode output. ASSP supports two IR sensors (MLX90614XAX only one IR sensor). The output of the IR sensor is amplified by the gain programmable low noise low offset voltage amplifier, converted to a single bit stream via Sigma Delta modulator and fed back to DSP for subsequent processing. The signal is programmable (with EEPROM) Fir and IIR low-pass filter to further reduce the bandwidth of the input signal to achieve the required noise characteristics and refresh rate. The output of IIR filters is measured in the internal RAM, where three units can be used: one is an in-chip temperature sensor (on-chip Ptat or PTC), and the remaining two are IR sensors. Based on the above measurement results, calculate the corresponding temperature Ta and object temperature to, two temperature resolution is 0.01℃. Ta and to can be read in two ways: the RAM unit is read through the two-line interface (0.02℃ resolution, fixed range) or output through the PWM digital mode(10-bit resolution, range configurable).

The final step of the measurement cycle is: Measurement of the received TA and to be adjusted to the output resolution of PWM, and the data exists in the PWM state machine registers, the state machine can produce a fixed frequency and a certain duty cycle to represent the measured data.

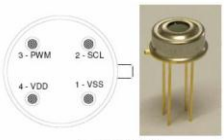

Fig.4 The distribution and physical map of MLX90614

Table 2 The functional foot table of the MLX90614

Designation	functional description
VSS	The metal casing is connected to the foot of the power supply
SCL/Vz	SMBus interface of the clock signal, or 8-16v power supply when the transisto r base
PWM/SDA	PWM or SMBus data signal of the interface, usually the output temperature of the object from the pin through the PWM
VDD	power

MLX9061's PWM/SDA pins can be output as a PWM mode, depending on the EEPROM settings. If set to PWM enable, after the cardioversion bit (POR), the PWM/SDA pin is directly configured as the PWM output. Under the condition of PWM as output mode, the calculated ambient temperature and object temperature exist in RAM, and its resolution is 0.01℃ (bit). The PWM output format is a 10-bit value, so the temperature to be transferred needs to be adjusted to fit the desired range. To this end, 2 units in the EEPROM are used to access the to scope (Tomin and Tomax), one unit for Ta (Ta_{range}:8MSB storage Tamax, 8LSB for Tamin). Therefore, the change accuracy of the to output range is 0.01℃, and the corresponding Ta output range is 0.64℃. Measurement, computation and linearization are controlled by the kernel, which executes the program in ROM. After Por, the chip is initialized with a calibrated value stored in the EEPROM, at which point the chip chooses the IR sensor number to determine the use of that sensor, measurement, compensation, and Linearization program to run in the closed loop process.

C.2.3 Sound detection principle and module selection

Sound sensor built in a sound-sensitive capacitive electret microphone, sound waves in the microphone in the Electret film vibration, resulting in the change in capacitance, and the corresponding changes, according to the voltage can detect the sound of the presence and the size of the voltage. This part of our selection of YL-56 sound detection module, the module works as follows: can detect the ambient sound intensity, use Note: This sensor can only recognize the sound of the noise (according to the vibration principle) can not recognize the size of the sound or the specific frequency of sound; sensitivity adjustable; working voltage 3.3v-5v; Output Form digital switch output (0 and 1 high-low level)[6].

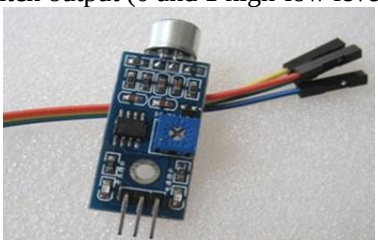

Fig.5 Sound Detection Module Physical drawing of YL-56

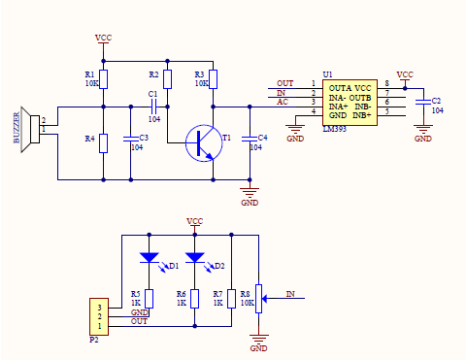

Fig.6 principle diagram of the YL-56 sensor

D. Wireless Transmitter Module Selection

In this part we use ZigBee technology as the core

communication module. ZigBee is a low power domain network protocol based on the IEEE802.15.4 standard. The technology under this Protocol is a short-range, low-power wireless communication technology. This name comes from the Bee's bee, because the bees are flying and "humming" (zig) to shake the wings of the "Dance" with the companion to pass pollen location information, that is, bees rely on such a way to form a group of communication network. It is characterized by close range, low complexity, self-organization, low power consumption, low data rate and low cost. It is mainly suitable for the field of automatic control and remote controlling, and can embed various equipments. In short, ZigBee is a cheap, low-power, short-range wireless networking technology[7].

IV. HARDWARE SYSTEM CONSTRUCTION

Because of the small size of single-chip and PC than the lack of powerful functions, we chose to deal with a good STM32 SCM, compared to 51 SCM, the Single-chip processing capacity is stronger because it is 32-bit. The project is to collect data from multiple sensors and transmit it wirelessly to the computer for display. Because each module has the complete function, therefore each part and the STM32 monolithic integrated system docking, then to the monolithic integrated computer and the wireless transmission part carries on the data to send. Correspondingly, the PC end is supplemented with the wireless receiving part, receiving the information from the microcontroller to collect the processed temperature sound distance. The wireless transmission part uses the ZigBee, and the monolithic computer, the PC interface all is the USB, is very convenient. The temperature acquisition module, the Sound acquisition module, the distance acquisition module, the STM32 MCU, the wireless transmission part and the PC end form the hardware composition of the project[8].

V. SOFTWARE SYSTEM WRITE

In this respect we do the MCU and PC-side programs written. Single-chip computer is mainly used in C language. Because the single chip computer reads the multiple sensor signal by the scanning method, reads the data of each sensor sequentially and circularly. To read the signal has a single chip computer set up in each corresponding circuit for independent operation, the final result is also the use of scanning methods, in sequence and circulation to each output point. SCM of the various input/output points can be independent of each other. So we took the former. The PC-side program is written on a human-computer interface, with C # written on Visual Studio.

VI. DEVICE TEST AND DATA ANALYSIS

After the completion of the programming and module assembly, we have in different environments in the field measurement experiment, will be the data compared to the real data, found the following problems, data error exists but under the control of 5%, the data transmission is sometimes unstable phenomenon. The cause of the problem is studied because of the accuracy of the sensor and the performance of the transmission module.

Table 3 experimental data

group	1	2	3	Actual control group
temperature （。C）	21．3	20.9	21.2	21.5
voice （yes/no）	yes	yes	no	yes
distance（cm）	98	96	98	100

VII. INCLUSION

The experimental results show that it can detect information in the environment, obstacle distance and voice, and it can be used for preliminary exploration before entering the strange area directly. It has practical significance.

References

[1] Yuan Guanghui, Yuan Guangzhan, Li Kai. Design of Ultrasonic Distance Measuring System Based on Single-chip Microcomputer[J].Yunnan Hydraulic Engineering,2017,33(02):115-117.

[2] Yuan Jie. Design of high-precision ultrasonic distance measurement system based on STM32 single-chip microcomputer[D]. North China Electric Power University, 2012.

[3] Zou Y. Design of close-range high precision ultrasonic ranging system [D]. Dalian University of Technology, 2009.

[4] Luo Jiayu, Chen Chao, Ni Zhi, Yang Dingkun, LiSong, Tan Jun. Design of Infrared Temperature Detector for Outdoor High Voltage Circuit Breaker[J]. Electrical Engineering Technology, 2016(02):50-53.

[5] Xue Fei. Development of fieldbus thermocouple temperature detection device [D]. Wuhan University, 2004.

[6] Li Chengzhi. Research on Temperature Field Measurement System Based on Sound Sensor [D]. Northeastern University, 2012.

[7] Youqing, Wu Guangmin, Zhao Jianjun, Yao Yunlong. Design of Intelligent Building Lighting Control System Based on ZigBee Technology[J]. Value Engineering, 2015, 34(04): 230-232.

[8] Yu Huilan, Liang Yuliang, Pang Zhennan, Xue Yu, Zhu Yifeng. Design of three-dimensional monitoring system for rare trees based on multi-sensor fusion[J]. Journal of Northeast Forestry University, 2016, 44(12): 91-93.

Compensation analysis of biological infrared non-contact body temperature measurement

CAI Peng-fei; XI Yu-nuo; CHEN Yu; WEI Qing-li; CAI Jing
(College of Instrument Science and Electrical Engineering, Jilin University)

***Abstract*—Infrared temperature measurement technology is of great significance for biological body temperature measurement.In this paper, the method of temperature compensation is proposed to ensure the accuracy of infrared temperature measurement.According to the blackbody radiation law and the curve fitting method in the least square, a new compensation model of infrared temperature measurement distance coefficient is proposed. The infrared measurement temperature which is adopted at different distances to establish the model which through the infrared temperature measurement distance coefficient compensation. The temperature model is established by solving the undetermined coefficients, and the corresponding temperature is compensated by the actual temperature. And the method is verified experimentally.**

***Key words*—Infrared temperature measurement; distance coefficient; compensation; curve fitting**

Ⅰ.INTRODUCTION

BODY temperature is of great importance to organisms. Generally speaking, the body temperature of a living body reflects the state of health of the organism itself. In general, when there are various conditions in the living organism, it will be accompanied by changes in body temperature, especially when the organism is ill, so accurate measurement of body temperature has very important significance.

Infrared non-contact temperature measurement technology is currently the most commonly used measure of biological surface temperature [1][4]. Compared to contact temperature measurement, infrared non-contact temperature measurement [3][4] has the advantages of fast response time, high precision, non-contact, safe use, easy operation and long service life. In the past 20 years, non-contact infrared temperature measurement has been widely used. With the development of science and technology, the technology has been rapidly developed, performance has been continuously improved, functions have been continuously enhanced, varieties have been increasing, and the scope of application has been continuously expanded. However, infrared temperature measurement also has many factors such as distance and environment. Based on the above problems, the infrared temperature compensation model is constructed and the method of compensating body temperature by the distance coefficient is proposed to ensure the accuracy of infrared temperature measurement and provide the measurement accuracy.

Ⅱ .PRINCIPLE OF INFRARED TEMPERATURE MEASUREMENT

The basic principle of infrared temperature measurement is the black body radiation law [2][3]. In nature, there is thermal motion inside the object. When the temperature of the object is higher than absolute zero, the object will continuously radiate electromagnetic waves to the surroundings, including infrared rays (wavelength between 0.75μm and 100μm).

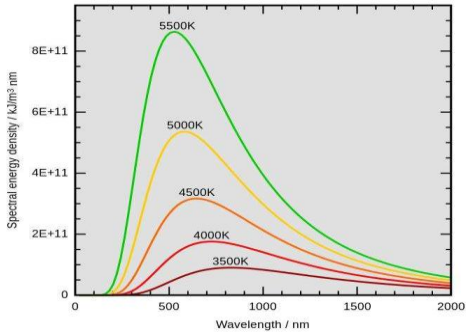

Fig.1 blackbody radiation curves

Its greatest feature is that at a given temperature and wavelength, the radiant energy emitted by the object has a maximum value. This substance is called a black body. It is set to have a reflection coefficient of 1, and the reflection coefficient of other substances is less than 1. Call it gray body. Can be obtained by Planck's theorem that

$$R_b(\lambda T) = c_1\lambda - 5/[\exp c_2/\lambda T - 1] \quad (1)$$

Based on this, it can be seen that as the temperature increases, the radiant energy of the object becomes stronger, and the wavelength at which the peak of the Wien's displacement theorem T0λm=2897.8（μm·K）is satisfied is inversely proportional to the absolute temperature T, and the dotted line is the peak at λm. Infrared temperature measurement must be based on wavelength division temperature measurement range, high temperature in the short wave, low temperature in the long wave, radiation energy changes with temperature changes, short wave temperature is higher than the long wave, and its high sensitivity (curve), anti-jamming Strong.

According to the Stefan-Boltzmann theorem [3][4]: Radiated degree of black body (total radiant power of various wavelengths emitted per unit area of blackbody surface) Pb(T) and the fourth power of temperature T Positive ratio。

$$R_b(T) = \sigma T^4 \quad (2)$$

$$\varepsilon(\lambda) = P(T)/R_b(T) \quad (3)$$

The temperature of the measured object is given by (2)(3)

$$T = [P(T)/\varepsilon\sigma]¼ \quad (4)$$

Formula (4) is the theoretical basis for measuring the temperature of the thermal radiation of an object in the infrared wavelength range.

Ⅲ.INFRARED TEMPERATURE DISTANCE COEFFICIENT COMPENSATION MODEL

Infrared temperature detection at room temperature, only need to compensate for the distance coefficient. The distance coefficient refers to the ratio of the distance S from the temperature measuring probe to the measured object and the diameter D of the measured object. The higher the resolution, the greater the distance coefficient.

Because the model is a nonlinear model, set up parameters, use different measurement distances to test the temperature, curve fitting it, get the equation of the curve after fitting, and make the weighted sum of squares of the model and the actual observation worth residual minimum, ie, minimum The curve is fitted to the data in the sense of squareness, and the relationship between the infrared temperature measurement and the temperature measurement distance is obtained.

Set the fitting curve to $y = Ae^{Bx} + Ce^{Dx}$ 。

If there are n points actually calibrated, the residual between the i-th calibration data and the response value on the fitted curve is $\Delta l = y - y_i$， The principle of fitting is to make the sum of squared residuals the minimum, is that

$$\sum_{l=1}^{n} \Delta l^2 = \min \quad (5)$$

That is, the first-order partial derivative of Δl2 to the undetermined coefficient is equal to zero, that is,

$$\frac{\partial}{\partial N_i} \Delta l^2 = 0 \quad (6)$$

Thus, the expression of the undetermined coefficient Ni is found.

Ⅳ.INFRARED TEMPERATURE MEASUREMENT SYSTEM

The block diagram of the system is shown in Figure 2.

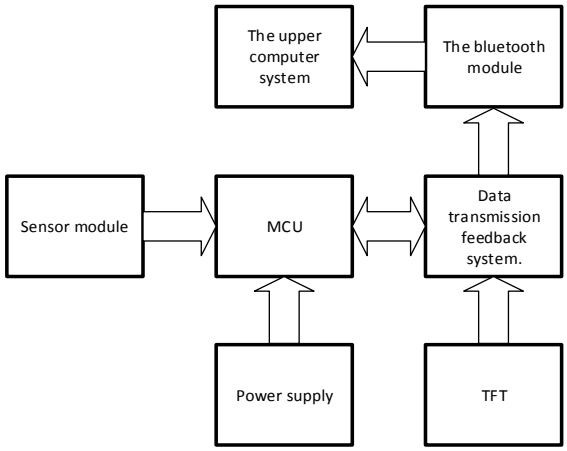

Fig.2 Infrared temperature measurement system

The system is mainly composed of a sensor acquisition module, a microcontroller control module, a data transmission feedback module, a display module, a Bluetooth module and an upper computer system.

Ⅴ.EXPERIMENTAL ANALYSIS

Experimental test, taking the forehead of the human body as the object of temperature measurement, testing the temperature at different distances, and fitting it to the curve, the fitting formula is

$$y = Ae^{Bx} + Ce^{Dx} \quad (7)$$

Fit the curve as shown in Figure 3

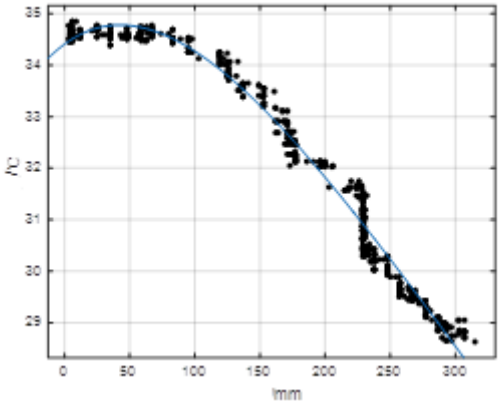

Fig.3 The curves of temperature with distance

By calculation, A=35.4550, B=-0.1353, C=-2.5850, D=-0.8173. After the distance is compensated, the temperature of 0cm to 20cm is measured again. The temperature data is shown in Table 1 below.

Table1 experiments datas

Temperature /Project	Temperature	Error
0cm	35.326	0.214
2cm	35.315	0.225
4cm	35.337	0.203
6cm	35.309	0.231
8cm	35.295	0.245
10cm	35.288	0.252
12cm	35.279	0.261
14cm	35.286	0.254
16cm	35.312	0.228
18cm	35.299	0.241
20cm	35.287	0.253

Based on the 35.540℃ measured forehead of the human body and after compensation, the average error in the range of 0 to 20cm is 0.237℃ in comparison with the experimental data, which greatly improves the accuracy of temperature measurement before the compensation and meets the experimental requirements. Figure 4 is the distance temperature curve after compensation.

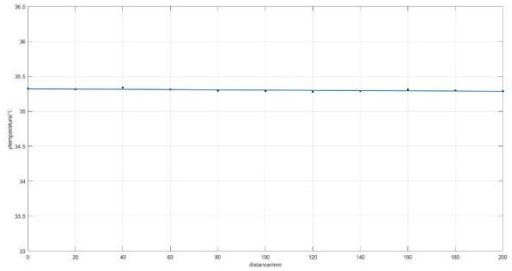

Fig.4 The curves of temperature with distance after compensation

Ⅵ Conclusion

This paper proposes a new distance compensation model for infrared temperature measurement. This new model is validated and compared with uncompensated temperature measurement data. This new method has accurate temperature measurement, sensitive response and fast response. And the direct advantages of the reaction. At the same time, the new model has practical reference and has the advantages of accuracy, realism, and convenient testing in practical applications, and has practical application value.

Reference

[1] Zuo Shouwei, Liu Hao, Jiang Xiangdong, Fan Daihe. A simple temperature measuring instrument based on blackbody radiation theory[J]. Physical Experiments, 2015, (09): 42-45.

[2] iao Panpan, Zhang Jiamin. Research on Influencing Factors of Infrared Temperature Measurement Accuracy and Compensation Methods[J]. Infrared Technology, 2017, (02): 173-177.

[3] J. Manara,M. Zipf,T. Stark,M. Arduini,H.-P. Ebert,A. Tutschke,A. Hallam,J. Hanspal,M. Langley,D. Hodge,J. Hartmann. Long Wavelength Infrared Radiation Thermometry for Non-Contact Temperature Measurements in Gas Turbines[J]. Infrared Physics and Technology,2016: 120-127

[4] J. Manara,M. Zipf,T. Stark,M. Arduini,H.-P. Ebert,A. Tutschke,A. Hallam,J. Hanspal,M. Langley,D. Hodge,J. Hartmann. Long Wavelength Infrared Radiation Thermometry for Non-Contact Temperature Measurements in Gas Turbines[J]. Infrared Physics and Technology,2016,:120-130

[5] Cao Mingchao. Realization and modification of infrared temperature measurement system[D]. Inner Mongolia University, 2015.

[6] Li Cheng. Design of Infrared Temperature Measurement System Based on Distance Compensation[J]. Computer Affaires, 2016, (12): 29.

[7] Wei Tanxun, Guo Liancheng, Zhang Wei. Principle and design of non-contact infrared temperature measurement system based on distance compensation[J]. Industrial Control and Computer, 2012.(11):106-107.

[8] Establishment of animal body temperature model based on the Internet of Things monitoring data [A]. Information Technology Branch of China Animal Husbandry and Veterinary Society. Proceedings of the Tenth Academic Symposium of the Information Technology Branch of the Chinese Academy of Animal Husbandry and Veterinary Medicine [C]. Information Technology Branch of the Chinese Academy of Animal Husbandry and Veterinary Medicine, Hu Yinong.2015:6.:90-95.

[9] GAO Hui. The construction of the optimal model and the intelligent realization of SAS in several types of commonly used nonlinear regression analysis[D]. Chinese Academy of Military Medical Sciences, 2012.

[10] Zhang Guilian. Soft Sensing Method Based on Least Square Regression in Air Permeability of Cork Paper[D]. Kunming University of Science and Technology, 2016.

[11] Lu Jingbo,Wu Yineng. Linear Transformation and Orthogonal Polynomial Regression of Nonlinear Regression Models[J].Statistics & Decision,2009,(23):13-14.

[12] Yi Zhang,Chun Ru Fu,You Yi Zhu,Qun Zhang,Jie Wu. Nonlinear Regression Analysis of Binary Flooding Recovery Influence Factors[J]. Advanced Materials Research,2014,2951:881-883

[13] M. Roozbeh. Robust ridge estimator in restricted semiparametric regression models[J]. Journal of Multivariate Analysis,2015:127-144.

[14] Sun Zhiyuan, Wang Jing, Qiao Yanfeng. Influence of environment on temperature measurement accuracy of medium wave infrared detectors[J]. China Optics and Applied Optics, 2010,(06):659-664.

[15] Hu Jiajun. Design and implementation of infrared non-contact temperature measurement system[D].Heilongjiang University,2016.

[16] Chen Yuanlin. Research on dynamic system simulation model and algorithm based on artificial neural network[D]. Daqing Petroleum Institute, 2006.

[17] Non-contact infrared temperature measurement principle and error analysis[J]. Min Min, Yan Yonghong, Zeng Yun, Zeng Jianping. Metrology Technology. 2005(01):23-25.

[18] Lu Zifeng, Pan Yulong, Wang Xuejin, Sun Qiang, Gu Lishan, Lu Zhenwu, Liu Yichun. Influence of target-to-test system distance on the precision of infrared temperature measurement[J]. Infrared Technology, 2008, (05): 271-274+278.

A small car collision avoidance system based on 51 microcomputer

Liu Lijun; Wang Ran; He Dongze
(*College of Instrumentation and Electrical Engineering, Jilin University)*

***Abstract*-The anti-collision system is applied to the moving vehicle, and the main function is to monitor the change of the speed of the front car, and to detect the objects in front of the vehicle (such as the intruding pedestrians, roadblocks and so on). Based on the practical considerations, this big project set the basis of the principle of vehicle speed, use of signals and systems, analog electronic circuit, single chip microcomputer principle and subject knowledge to feedback signal digital processing, vehicle collision.**

***Keywords*- 51 microcontroller , ultrasonic sensor , infrared sensor**

Ⅰ.INTRODUCTION

THIS project studies the anti-collision system of automatic traveling car, including hardware and software:

Hardware part of the building based on 51 single-chip signal acquisition device, the speed, obstacles and sensor data collection. 51 SCM control three analog signal sampling filter amplification, AD conversion, the converted digital signal through the serial port to the host computer to PC for data analysis and processing.

The software part of the PC software system, to achieve the evaluation algorithm, which can make a qualitative and quantitative judgments of the car and obstacles. The project's software system includes operation control system and feedback system, which consists of two modules: detection and analysis. Operation control system to complete the operation of the control work, and to achieve PC and SCM serial communication, the feedback system to complete the data analysis[1], processing and display, and to achieve the evaluation algorithm.

The project mainly studies the speed monitoring of model vehicles, the change of vehicle trajectory and the sensing of obstacles in front. The key issue is the precise acquisition of signals, changes in vehicle trajectories, the difficulty is how to intelligently determine the trajectory changes and the preparation of the software. The reliability and safety of the model car's automatic deceleration and brakes are the focus of this project.

Ⅱ.PRINCIPLE OF SENSORS

A. Ultrasonic sensor ranging method

Ultrasonic sensor works is a control of the hair over a high level of 1 OUS, you can receive a high output port waiting for an output can open the timer, when the mouth becomes low when you can read the timing When the circuit work, the transmitter circuit to the ultrasonic receiver circuit to receive ultrasonic waves returned through the P32 port to send data to the microcontroller, the microcontroller will be This data is converted into a distance, then this distance and set the distance contrast, if less than this value, the microcontroller feedback the corresponding signal[2].

B. Processing of sensor signals

The photoelectric sensor is a sensor which USES the photoelectric element as the detecting element. It first converts the measured change into a light signal, and then converts the light signal to an electrical signal with the help of a photoelectric element. The photoelectric sensor is generally composed of three parts: light source, optical path and photoelectric element.The processing of sensor signals is shown in figure 1.

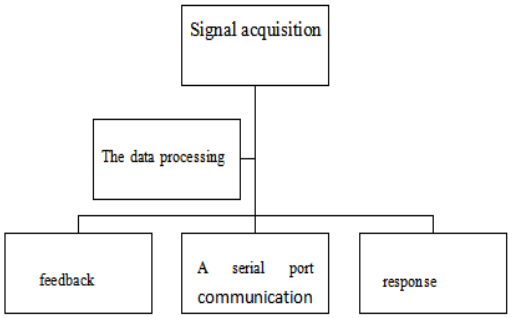

Fig.1 Schematic diagram of signal processing module.

Ⅲ. SENSOR RANGING METHOD

A.Ultrasonic Sensor Ranging Principle

Ultrasonic wave generator sends out the ultrasonic signal at a certain moment, meets the measured object to reflect back, is received by the ultrasonic wave receiver. As long as the ultrasonic signal is calculated from the time of transmitting to receiving the echo signal, knowing the propagation velocity in the medium, the distance from the measured object can be calculated as d = s / 2 = (vt) / 2, where d Is the distance between the measured object and the range finder, s is the distance that the ultrasonic wave passes back and forth, v is the propagation speed of the ultrasonic wave in the medium, and t is the time taken for the ultrasonic wave to transmit and receive. In order to improve the accuracy, it is necessary to consider the relationship between the propagation velocity of ultrasound in air and temperature under different temperatures. If the temperature changes and the ranging accuracy requirements are high, it should be corrected by temperature compensation method. After determining the speed of sound, as long as the measured ultrasonic return time, you can find the distance. This is the mechanism of ultrasonic ranging. The distance S from the ultrasonic launch point to the reception point is: S =

v * t0; where v is the speed of sound and t0 is the transit time. Time-of-flight refers to the time interval that an ultrasonic wave travels from the transmitter to the receiver to receive the sound wave. V = 331.45 (1 + T / 273.16) (1/2) (m / s) of the sound velocity V with respect to the ambient temperature; its Taylor series expansion (only once retained) is: V = 331.4 + 0.607; Each change of 10C, the speed of sound waves change 0.6 (mm / ms). If the transit time to 9ms bounce about 3m), it will produce 5 ~ error. A temperature change of 2 °C produces an error of about 1 cm.

C. Design of signal processing module

Amplifying and filtering, because after the sensor acquisition, the obstacles of information such as weak signal, the signal to noise ratio is low, vulnerable to interference, so need to signal amplification and filtering, in order to obtain higher detection sensitivity; Software system, the programming of upper computer software is written in Visual C++ language, including operating control system and feedback control system. The operation control system completes the operation control, and realizes the serial communication between the upper computer and the single chip microcomputer. The feedback adjustment system completes the analysis and processing of the data and responds to it. The software has a beautiful and friendly interactive interface with signal display and other functions.

Ⅳ. System Operation Design

The design of the circuit is divided into the following major components: microcontroller module, ultrasonic ranging module, infrared ranging module, display module, power module, feedback module, brake module. The relationship between the modules shown in figure 2.

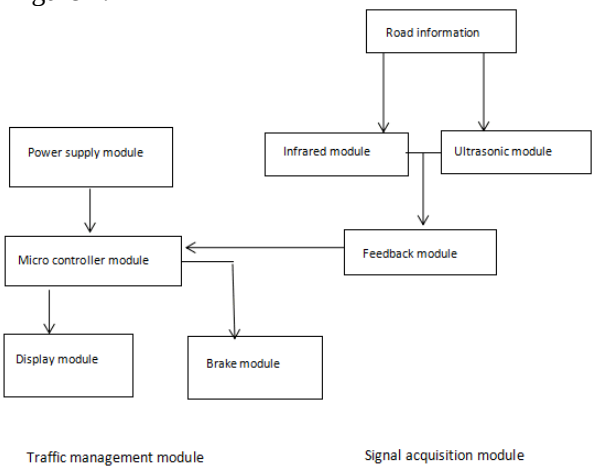

Fig.2 16 module work diagram

When the system is working, made by launch unit, a laser beam to diffuse back after the target under test, after receiving unit receiving, amplifying plastic to distance calculation unit after the calculation shows that the target distance.

The working mode of ultrasonic module (1) USES IO TRIG to trigger ranging, and to at least l0us high level signal; (2) the module automatically sends 8 40khz square waves, and automatically detects whether the signal is returned; (3) a signal is returned, and a high level is output through the IO ECHO. The duration of the high level is the time of the ultrasonic wave from launch to return[3]. Test distance =(high level time * sound speed (340M/S))/2;Its ultrasonic timing diagram is shown in figure 3.

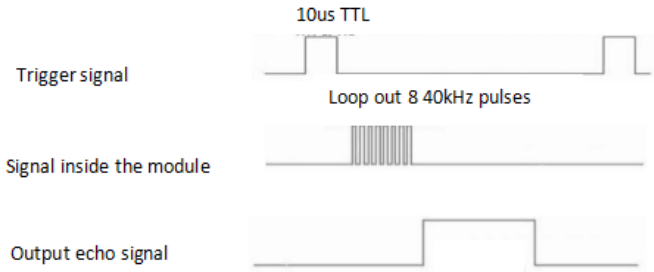

Fig.3 ultrasonic module module work diagram

This module is easy to use, a control port of a high above 1 OUS, you can wait for a high level in the receiving port output an output timer can open a timer, when the port goes low can read Timer value, this time for the distance measurement time, can only be calculated from the distance. So continuous measurement of the cycle, that is, you can reach the value of the mobile measurement.

The speed measurement module runs as shown in figure 4.

chip	74HC14D
Working voltage	3.3V-5V
The output mode	A digital signa
Testing way	Infrared ray interrupt
Signal detection	The detection of obstacles is high level, no obstacle is or beyond the detection range is low level
LED	The two status indicator light, the X-ray stop indicator light, the ray guide light.

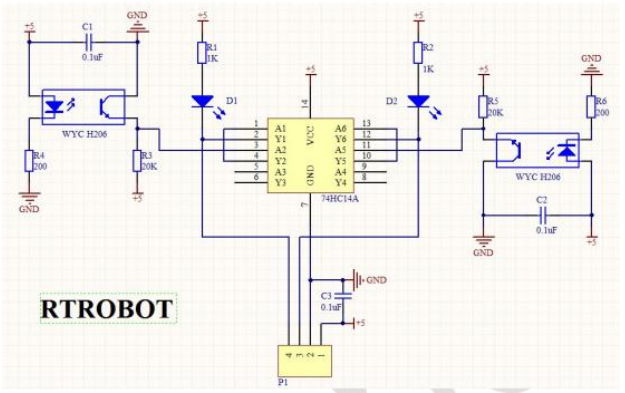

Fig.4 Speed measuring module module working schematic diagram

Traffic management module work process, the feedback module measured the current distance, the microprocessor module to deal with to determine whether the safety distance, if the safety continue to travel, if unsafe to the drive system to send commands to slow down or stop.

Drive module, microcontroller module for the traffic management system to provide judgment data,

controlled by the system drive system deceleration, stop.

The driver module, the micro-controller module provides the judgment data for the traffic management system, and the system controls the driving system to slow down and stop.

Scheme 1: adopts relays to control the on or off of the motor, through the switch to adjust the speed of the car. The scheme has the advantage of the circuit is relatively simple defect is relay response time is slow, easy damage, short service life, reliability is not high.

Scheme 2: using power triode as output control dc motor of power amplifier. The linear driven circuit structure and principle are simple, the acceleration capability is strong, and the h-type bridge circuit composed of darlington tube is adopted (figure 2.1). The control of the darlington tube with a single chip can adjust the speed of the motor precisely[4]. This circuit due to work in the pipe of saturated by the mode, the efficiency is very high, H bridge circuit ensures the simple implementation speed and direction of control, valve switch speed, stability is strong, is a kind of widely used PWM control technology. There are many such chips on the market, I chose L298N.

This way has good speed regulation characteristics of speed and adjust the smooth, wide speed range, large overload capacity, can withstand the frequent load impact, can also realize frequent stepless quick start, brake and reverse, etc[5].

The working diagram of L298N is shown in figure 5.

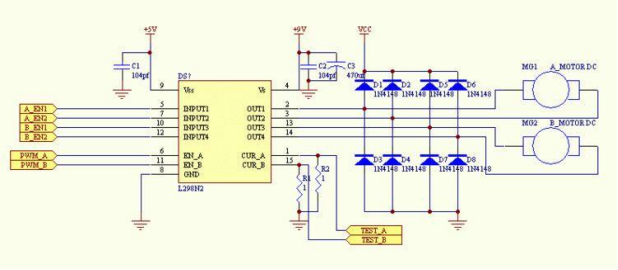

Fig.5 Driver module module working schematic diagram

Power module, the power system USES 12v lithium battery power supply, the battery can charge and discharge many times, the performance is stable, the capacity is large, the volume is small, satisfies each part electricity demand, guarantees the job stability.

Ⅴ. The Methord Of Experiment

Two trolleys were used to simulate the experiment, and the two cars were driven back and forth.

1. in the rear car, the front car decelerates or brakes, and the rear car responds to the situation by collecting signals and signal processing. The rear car shows the distance, the front car shows the speed.

2. In the rear car, the front car will slow down or brake, and the car will brake automatically when the car is too close.

3. During the driving of the car, it suddenly breaks into the small object car to brake automatically.

The safety distance is 50 centimeters, and the experiment has been stopped at 47.0cm many times, proving that this system can be used.

Ⅵ.Conclusion

This research from the perspective of the model car to avoid static obstacles and dynamic car function, the system can not only qualitative analysis to collect signal within the scope of the traffic condition and feedback to system for warning and make the corresponding adjustment, can also be quantitatively according to driving speed and safe distance.

References

[1] Wang Bin, Wang Renguang, He Wei, Wu lijun, Liu zhaodu.Fuzzy control algorithm for variable output of ACC system[J].Computer application research. 2010,(2): 465-467,471.DOI:10.3969/j.issn.1001-3695.2010.02.016.

[2] Zhang dezhao, wang jianqiang, liu jixi, et al. Adaptive cruise control mode switching strategy for continuous acceleration of acceleration [J]. Journal of tsinghua university (natural science edition),2010,(8):1277-1281.

[3] Zhan Jun.Dynamic surface controller algorithm of vehicle ACC J .Journal of Jilin UniverSity(Engineering and Tecnology Edition),2005,35(4):363-367

[4] Tong Baofeng,Liu Weigo,Zhang Junyuan,et al.Research on throttle control strategy of automotive ACC system based on target speed [J]. Traffic information and security,2012,(4):39-43.DOI:10.3963/jisssn.1674-4861.2012.04.009.

[5] Yoshinori Yamamura, Yoji Seto, Hikaru NiShira.An ACC design method for achieving both string stability and ride comfort [C]//Proceeding of International Sym-Posium on Advanced Vehicle Control,2002.

Study on the design of electromagnetic signal source and the method of three dimensional combination control

Liu Naijia; WangHui; Ding Jianchun
(College of materials Science and electrical Engineering, Jilin University)

***Abstract*-The principle of the frequency domain electromagnetic signal source is analyzed through the research on the basic detection principle and the transmitter structure of the ground space frequency domain electromagnetic detection system. The feasibility of using the chopper circuit and the inverter bridge method to transmit three dimensional combined signals is demonstrated. The MATLAB is used to simulate the inverter bridge, and the key problems of the transmitter design are analyzed. The driving circuit and inverter topology of the signal source are designed. The FPGA control method is applied to realize the function of output frequency and phase controllable by manual control. The voltage regulating circuit is designed by switching down voltage DC-DC mode, and the output voltage is adjustable. Through experimental tests, the system can achieve the output frequency 9-999Hz, any integer adjustment, the output phase difference of the three dimensional signal can be adjusted arbitrarily, and the output voltage 1.25-12V can be adjusted. Finally, the signal of the laboratory analog coil is supplied, and the waveform is received and analyzed. The three-dimensional physical simulation of electromagnetic field in indoor field is realized, providing the research foundation for the analysis and suppression of moving noise in the electromagnetic detection of ground air frequency domain.**

***keywords*—Frequency domain electromagnetic detection Inverter circuit Step-down chopper Three dimensional combination**

I. INTRODUCTION

THE frequency domain ground air electromagnetic detection method is a new electromagnetic detection method. Combined with the advantages of the airborne and frequency domain electromagnetic method, this method puts forward the working mode of the ground launch air reception, which has a high speed. The advantages of low cost, wide range of detection and so on. One of the main factors restricting the development of current methods is to ground motion noise, frequency domain electromagnetic method, influence of 3D electromagnetic field and the magnetic field of environmental magnetic field emission source generated in the measurement, the measurement results of the data included in the movement noise caused by data quality is poor, is not conducive to accurate inversion and interpretation[1].

The project is based on the present situation of indoor 3 d electromagnetic field simulation is put forward, by combining the control of 3 d electromagnetic coil signal source, combined with spatial 3 d magnetic coil three-dimensional physical simulation of electromagnetic field in the space. The physical simulation of electromagnetic field is mostly confined to the two level [2], based on the working principle of the helmholtz coil USES a pair of the same circle number, length, height of coaxial parallel to a square coils, with constant current source and single-chip microcomputer control technology, design of electromagnetic field [3-5], the physical simulation system in the laboratory to solve the problems at the aspect of theoretical research on magnetic field provides the necessary technical support, in the field of basic research and half navigation, aerospace, military, medical and other fields has become more widely used.

II. INVETER CIRCUIT DESIGN

A. Inverter circuit principle

Fig. 1 Principle bridge inverter circuit, Uin input voltage signal to the U0, the output voltage signal, when VT1 and VT4 is in a conducting state, while VT2 and VT3 in the truncated state, U0=Uin, while VT2 and VT3 is in a conducting state, while VT1 and VT4 in the truncated state. U0= -Uin. So when the arm bridge switch state conversion to f with a frequency of U0, Uin as the amplitude of the square wave, and its amplitude is expressed as the Jiboke rectangular wave Uo Uin expanded into Fu Liye series: U0=4Uin/ PI (sinwt+1/3 sin3wt+1/5 sin5wt+...), therefore, by controlling the frequency of F to achieve the DC into AC wave to wave[6].

B. Design and analysis of inverter circuit

According to the above principles, the topology structure of the inverter circuit, such as Figure 2, is determined.

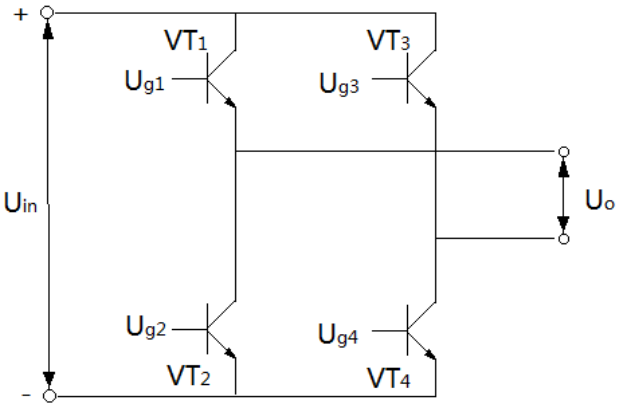

Fig.1 Schematic of inverter circuit

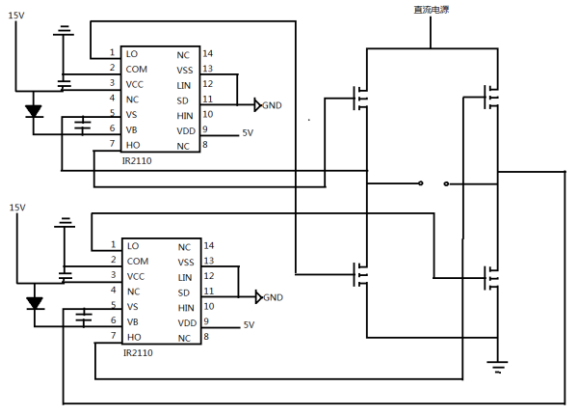

Fig.2 Topology structure of inverter circuit

It includes the driving circuit and the H Bridge Road, and the bridge road part is simulated by SIMULINK, and the simulation results of Figure 3 are obtained.

The correctness of the circuit structure is verified and the square wave signal with fixed frequency can be sent out. In order to meet the output power required by the experimental design, the IRF540 of the bridge's triode and the IR2110 chip with driving and optocoupler isolation function are used to complete the main circuit design.

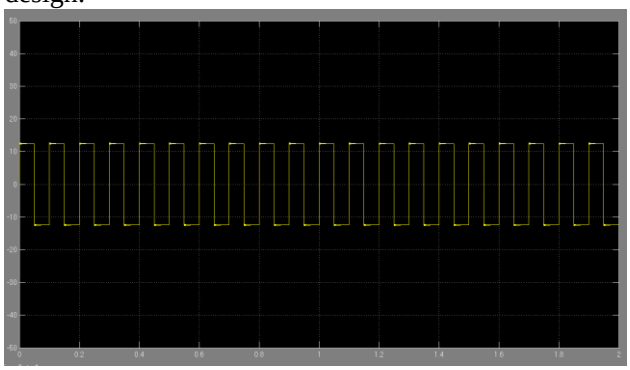

Fig.3 Bridge road simulation diagram

C. Design of control module

The control part is composed of field programmable gate array (FPGA) provides a control signal, the selected FPGA is 50MHz internal oscillator, the oscillator frequency divided into every second rising frequency the number of copies required for experimental way to achieve numerical keyboard output frequency can send out corresponding arbitrary frequency square wave control signal. The output of the controlled square wave signal, as shown in Figure 4, is in accordance with the requirements of the experiment.

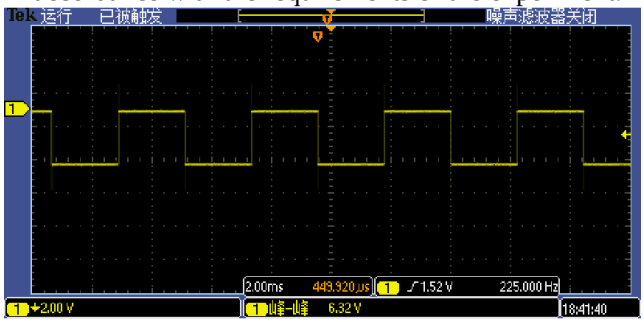

Fig.4 Control signal waveform diagram

III Design of voltage regulating power supply module

A. Main circuit design

In order to meet the design requirements of the 1.25-12V 12V input voltage, output voltage, the switch buck DC-DC converter chip XL4015, the fixed switching frequency 180KHz, with excellent line regulation and load regulation rate, output voltage adjustable between 1.25-32V and support, chip integrated over-current protection, over temperature protection, short circuit protection and reliability module[7-8]. The topology structure of voltage regulation circuit is built with XL4015, as shown in Figure 5.

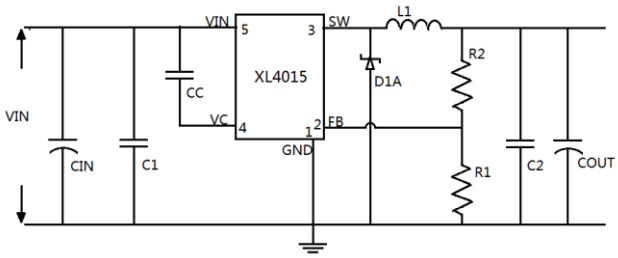

Fig.5 Topology diagram of voltage regulating circuit

B. Selection of device model

Input capacitance selection: in a continuous mode, the input current of the converter is a set of square waves with a space duty ratio of about VOUT/VIN. In order to prevent large transient voltage, a low ESR (equivalent series resistance) input capacitor is selected for the maximum RMS current requirement. The maximum RMS capacitor current is given in the following form:

IRMS≈IMAX*√(VOUT (VIN-VOUT))/VIN,Among them, the maximum average output current of IMAX is equal to the peak current and peak ripple current 1/2 difference, IMAX=ILIM- IL/2. A ceramic capacitor is added to the input capacitance for high frequency decoupling.

The selection of output capacitance: at the output, the low ESR capacitance should be selected to reduce the output ripple voltage. A ceramic capacitor is combined with a low ESR electrolytic capacitor as an output capacitor. The output capacitance ripple is determined by the next type.

ΔVOUT≈ΔIL*（ESR+1/(8*F*COUT)），Inductor selection: inductor does not affect the work frequency, but has a direct effect on the current ripple, inductor current ripple of IL decreases with the increase of the inductance value, and increase with the increase of VIN and VOUT. For a reasonable starting point for setting the ripple current of delta IL =0.3*ILIM, where ILIM is the peak switch current limit. In order to ensure that the ripple current is under a specified maximum value, the inductor value should be selected by the press formula:

L=VOUT/(F*ΔIL)*（1-VOUT/(VIN（MAX）)）

Continuous current diode: a Schottky diode is recommended for a continuous current diode.

IV Test analysis

The whole device can realize the 9-9999Hz output frequency is adjustable, the error is less than 0.2%, phase

0-360 degree adjustable, adjustable amplitude 1.25-12V, error less than 3%, with output power up to 10W.

A. Frequency test

The keyboard inputs the frequency parameters 1000Hz and 3000Hz of the three groups of the same phase, and the output waveform of the system is shown in Figure 6

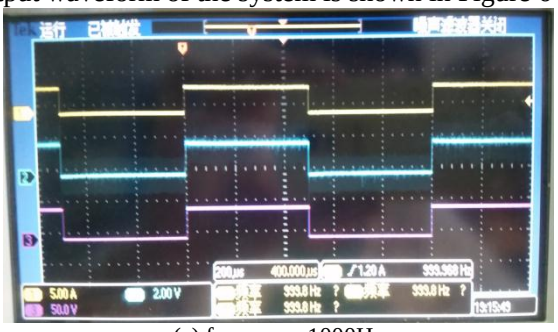

(a) frequency 1000Hz

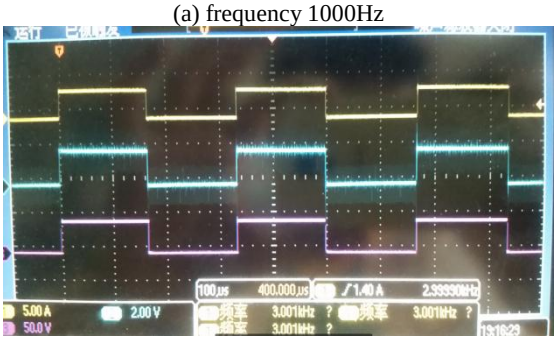

(b) frequency 3000Hz

Fig.6 Output waveform diagram with different frequency

B. Phase test

The phase of the keyboard input is 60 degrees and 90 degrees in turn. The test results are shown in Figure 7.

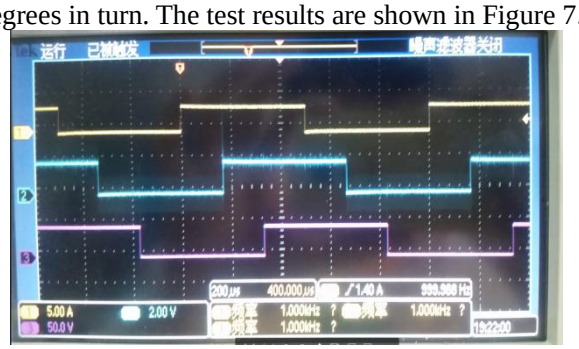

(a) phase difference 60 degrees

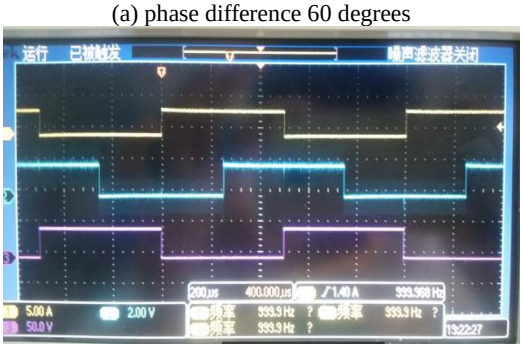

(b) phase difference 90 degrees

Fig.7 Output of different phase difference waveforms

C. Supply coil signal test

The experiment of supplying square wave signals to the simulation coil of the laboratory is carried out after the requirements of the device are reached. The 64Hz square wave signals of different currents are communicated to the three dimensional coils. The corresponding magnetic field is produced by the coil, and the data are collected and processed to get the waveform of the time frequency signal, as shown in Figure 8.

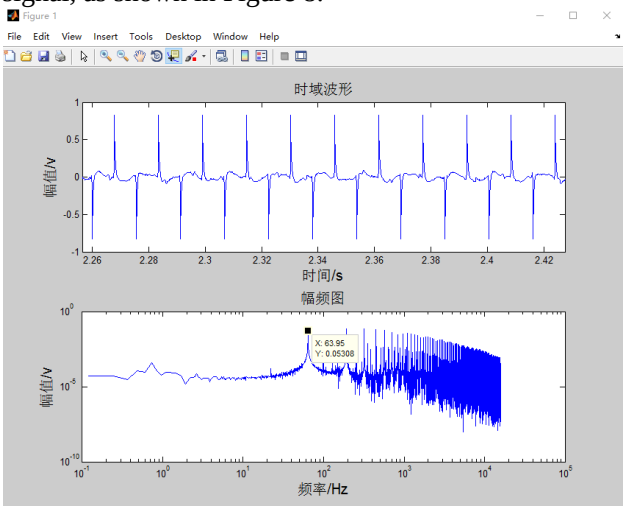

Fig.8 Acquisition of data waveform

When a single coil is supplied, the magnetic field at the center point has a larger value in theory, and the other two components should be 0. Due to environmental factors, at least a few NAT's magnetic fields will be available at any point.

the electromagnetic response table of the three coils

From table 1, we can see from the above table that when the power is supplied to a single coil, the three components of the magnetic field at the center point are more than 10 times the vertical part of the coil surface than the other two components, and the magnetic field values of the other two components are indeed only a few NAT.

At the same time, it can be seen that the magnitude of the corresponding magnetic field is magnified in a corresponding proportion when the current is amplified. Therefore, the current size of each coil should be calculated based on this table.

V CONCLUSION

The combination of experimental design system of voltage power supply and inverter circuit by adjusting the control by the control circuit, the system can achieve the 9-9999Hz output frequency is adjustable, the error is less than 0.2%, phase 0-360 degree adjustable, adjustable amplitude 1.25-12V, error less than 3%, with output power up to 10W. It can be used to simulate the field electromagnetic field in the laboratory, and provide the basis for the analysis and suppression of the motion noise in the electromagnetic detection of the ground and air frequency domain.

TABLE I
THE ELECTROMAGNETIC RESPONSE TABLE OF THE THREE COILS

Symbol	Quantity	Electrified coil and Direction of magnetic field
I	50mA	
B	419nT	X/X
	16.9nT	X/Y
	8.06nT	X/Z
I	50mA	
B	11.3nT	
	269.3nT	Y/X
	8.06nT	Y/Y
I		Y/Z
B	15.3nT	Z/X
	18.5nT	Z/Y
	445.8nT	Z/Z
I	25mA	
B	21.7nT	X/X
	7.2nT	X/Y
	70.96Nt	X/Z
I	25mA	
B	5.64nT	Y/X
	146nT	Y/Y
	7.5nT	Y/Z
I	25mA	
B	9.67nT	Z/X
	200.88nT	Z/Y
	3.22nT	Z/Z
I	10mA	
B	70.96nT	X/X
	3.22nT	X/Y
	2.42Nt	X/Z
I	10mA	
B	4.06nT	Y/X
	52.42nT	Y/Y
	4.06nT	Y/Z
I	10mA	
B	3.22nT	Z/X
	4.03nT	Z/Y
	87.9nT	Z/Z

References

[1] the method of removing the moving noise of coil in the time domain ground air electromagnetic signal. [C]., China International Geophysics instrument and Application Symposium and the fifth session of the geophysical technology committee of the Chinese Geophysical Society,.2012..

[2] Liu Zhixin, Xue Guoqiang, Zhang Linbo. Comparative analysis of regional simulation of effective observation of tensor CSAMT [J]. geophysics, 2017, 60 (8): 3278-3287.

[3] Huang Songtao, Zhang Wei, Zhang Pengfei, et al. Simulation of large and uniform electromagnetic field based on Helmholtz coil [J]. Journal of Beihang University, 2015 (2): 203-208

[4] Cai Xinhua, Zhang Jinsheng, Fan Yutao, et al. Magnetic field simulation generating device based on Helmholtz coil theory [J]. computer simulation, 2014 (7): 54-58, 72.

[5] Wang Zhikui, Fan Qingwen, et al. Design analysis and application of uniform magnetic field generator based on Helmholtz coil and application of [J]. medical equipment, 2014 (10): 1-3,10.

[6] Zhou Junwei, Chen Huiming, Qian. The inverter control strategy of the load series resonant inverter [J]. power technology application.2004,7 (5): 299-303

[7] Liang Shian. Theory and design practice of switching power supply [M]. Beijing: Electronic Industry Press, 2013.

[8] Yang Gang, Wu Wenjie, Ren Feng. Design of a current source for X ray generator [J]. modern electronic technology, 2017,40 (22): 159-162.

Multi frequency electromagnetic signal acquisition system based on second pulse and phase-locked amplification

Guo Ling; Zhang Chunfeng; Hou Yukuo; Liu Changsheng; Wang Shilong
(instrument Science and engineering Institute, Jilin University)

***Abstract*-In view of the measured signal, wide band, the noise signal amplitude and phase extraction difficult, receiver synchronous clock is not stable, the characteristics of the digital phase locked loop (DPLL) and simulation method of combining the phase-locked amplifier, using orthogonal phase lock amplifying technology and pulse synchronization technology, combined with the required characteristics of high precision, long continuous acquisition system, this paper proposes a new air electromagnetic signal acquisition system, realize the air electromagnetic frequency domain signal amplitude and phase information of the real-time acquisition and storage. The experiment shows that the system is stable and reliable, accurate and can meet the demand of distributed electromagnetic detection data acquisition.**

***Key words*-Second pulse synchronization Orthogonal lock amplification Ground air electromagnetic signal**I.

INTRODUCTION

THE frequency domain ground space electromagnetic method is a frequency domain electromagnetic geophysical method for resource exploration. The method is a known frequency alternating electromagnetic field excitation on the ground, if the underground orebody containing electromagnetic sensitivity (such as metal ore), will have two times of induction field, obtaining the system composed of a receiving coil induction voltage, voltage attenuation curve analysis can obtain the underground orebody location, morphology and structure information of [1]. Because of its high precision and efficiency, it has a wide application prospect.

When the frequency domain ground space electromagnetic method is working in the field, [2] is used in the form of ground emission and air reception. In order to evaluate the time domain data collected by the. receiver, mainly using the following scheme: using MCU and FPGA as the main controller of the receiver, in the control of the main controller, to ensure strict synchronous data acquisition through the algorithm, and the time domain data collected through wireless upload to the upper computer monitor or [3] through the SD card storage, back to the ground for analysis. However, there are some shortcomings in the two schemes. Due to the large amount of data in the time domain, during the process of uploading to the upper monitor computer, the wireless transmission and communication pressure is high, and the bit error rate is [3]. The storage of the SD card also greatly increases the power and complexity of the system [2] because of the large amount of data. The two methods require high sampling speed. In traditional design, FPGA and OCXO are usually used to synchronize GPS signals. Due to the drift of the crystal itself, the accuracy of synchronous time service in long time observation will be greatly reduced. Moreover, the computational complexity of the algorithm is large and the process is complex [7]. In the traditional design, the data obtained need to be transformed by FFT on the ground to get the information of the measured signal, so the traditional acquisition system is not real-time.

Since the advent of phase-locked amplification technology, it has been widely applied to the detection of weak signal in [4] because of its no need for multiplication operation, high real-time performance, low hardware requirements, and restraining the influence of high pass characteristic earth medium. However, the normal method can not get the phase difference between the signal to be measured and the GPS reference signal in real time.

AD9548 clock chip built-in a digital phase-locked loop (DPLL), can be arbitrary frequency reference signal output, and can be locked to a standard 1 PPS GPS clock signal, has been widely used in remote optical network and wireless network node, wired infrastructure and data communications equipment [5].

To sum up, a multi frequency electromagnetic signal acquisition system based on orthogonal phase-locked amplification and clock synchronization is proposed in this paper. The system acquires the signal of the in-phase and quadrature components and reference signals in-phase and quadrature components through analog lock-in amplifier, and then through the control chip simple mathematical operation, obtain the amplitude of the signal to be measured and compared to the phase information of the reference signal. The system does not need to carry out the later FFT operation, so it can get the information of the signal to be measured in real time. Because the in-phase components and quadrature components of the acquisition are all approximate to the direct flow, so the requirement of the sampling rate is reduced, the data quantity is reduced, and the reliability of data storage is improved. The reference signal is provided by the clock synchronization chip, which can get the phase difference between the measured signal and the GPS second pulse signal in real time, and reduces the complexity of the main control chip program. The stability of the system is improved.

I. PRINCIPLE OF ACQUISITION SYSTEM

A. The principle of orthogonal phase-locked amplification

Through the orthogonal phase-locked amplification technology, this system detectable the signal to be measured from the noise and obtained its orthogonal component and phase component. At the same time, through the orthogonal phase locked amplification technology, the orthogonal component and the phase component of the reference signal are obtained. The principle of orthogonal phase-locked amplification is shown in Figure 1, and the signal to be measured is set $S(t) = A\sin(\omega_1 t + \varphi) + N(t)$, Reference signal is $R_1(t) = B\sin(\omega_2 t)$, $N(t)$ is noise and is not related to the signal to be measured. A and B are the amplitudes of the signals to be measured and the reference signals, respectively. The two signals are multiplied by the lock

$$U(t) = S(t) * R(t) = \frac{AB}{2}\cos[(\omega_1 - \omega_2)t + \varphi]$$

$$+ \frac{AB}{2}\cos[(\omega_1 + \omega_2)t + \varphi] + N(t)B\sin(\omega_2 t)$$

.

As the frequency of the signal to be measured, the frequency of the reference signal is adjusted to the same as that of the signal to be measured, that is $\omega_1 = \omega_2$, the frequency of the signal to be measured. After the low pass filter, the second item in $U(t)$ is a high frequency signal and is filtered out. $N(t)$ is also filtered because it has nothing to do with the signal to be measured.

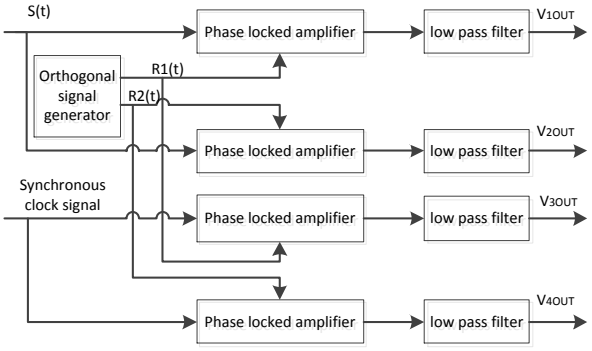

Fig.1. Orthogonal lock phase amplifier module.

Therefore, the output of the low pass filter is $V_{1out} = \frac{AB}{2}\cos\varphi$; when the other reference signal is $R_2(t) = B\sin(\omega_2 t + 90°)$, $V_{2out} = \frac{AB}{2}\sin\varphi$ can be obtained; thus the amplitude and phase of the signal to be measured can be obtained by formula $A = \frac{2\sqrt{V_{1out}^2 + V_{2out}^2}}{B}$; $\varphi = \tan^{-1}\frac{V_{2out}}{V_{1out}}$. The function of the bandpass filter is accomplished by using the phase locked amplifier and the low pass filter.

II. MULTI FREQUENCY ELECTROMAGNETIC SIGNAL ACQUISITION SYSTEM

The adaptive acquisition system of multi frequency electromagnetic signals based on second pulse and phase-locked amplification is composed of control module, GPS synchronization module, phase-locked amplifier module and storage module. Because the receiving system needs to be carried on the aircraft, the system has a higher requirement. It needs to be portable, miniaturized, low power and so on. Through the design of dual phase locked loop, the hardware circuit and program design are simplified, and the power consumption is reduced.

A. Design of GPS synchronization module

Because the acquisition module has no physical connection with the transmitter, it belongs to the distributed acquisition system. Therefore, one of the most important problems is to ensure the strict synchronization of the collected data. In traditional design, the performance of clock synchronization is usually limited by the performance of MCU. It usually requires CPLD or FPGA to cooperate with the GPS receiving device to complete the internal program. The accuracy of the obtained reference signal is not high, and the power consumption and complexity of the system will be greatly increased.

In this system, the synchronization clock signal is generated by using the clock synchronization chip AD9548. The GPS second pulse is received through the GPS receiving device, and it is used as the reference signal of AD9548, and the phase reference signal is output by using the AD9548's digital phase locked loop.

B. Overall design

The overall design of the system is shown in Figure 2; in the control of the main control chip, respectively with the lock multiplication test signal and the synchronous clock signal, using the orthogonal component and phase component 24 ΔΣ structure ADC acquired, and control of the control chip, for data storage. Because the orthogonal component and the in-phase component are approximate to the straight flow, the sampling rate is not very high, and the data volume is not large, so the hardware and software requirements are not high. The power consumption of the system is also reduced.

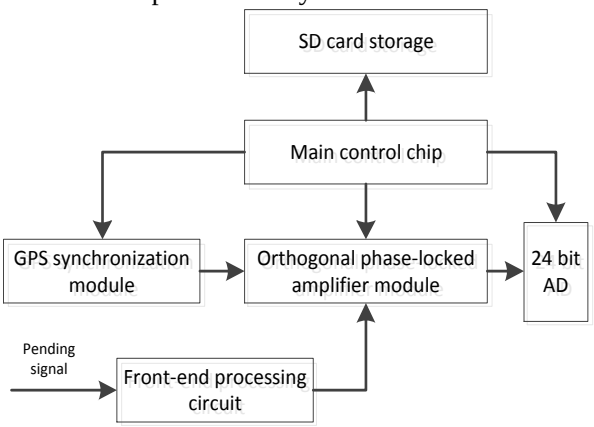

Fig.2 The system design

III. EXPERIMENTAL RESULTS AND ANALYSIS

A. Experimental results of synchronization module

In the actual circuit, the AD9548 is used to synchronize the GPS second pulse. And output the reference signal of the same frequency as the signal to be measured. The input second pulse is shown as shown in Figure 3 (a); by configuring the register of the AD9548, it outputs the synchronous signal of the 1kHz, as shown in Figure 3 (b);

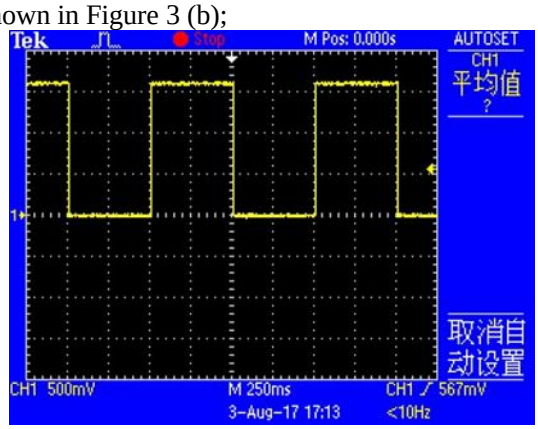

（a）second pulse

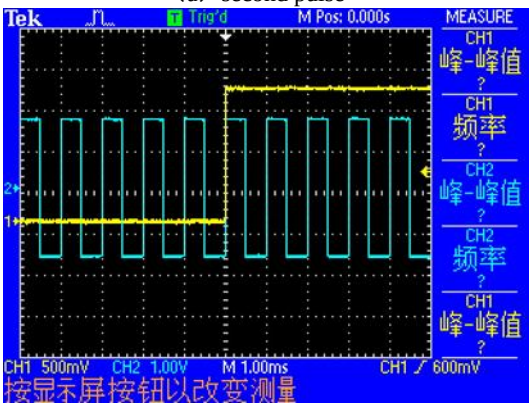

（b） output

Fig.3 Experimental results of synchronization module

B. Experimental results of orthogonal phase-locked amplifier module

In the actual acquisition process, it is now the process of signal to be amplified, filtering and so on, and then access to the phase locked amplifier module. According to the principle of phase-locked amplification, AD630 is used as a phase-locked amplifier, and the orthogonal phase-locked amplifier module is designed, as shown in Figure 1. The 2 - order Butterworth filter is used in the low pass filter, and the orthogonal signal generator is produced by DDS chip AD9854. The physical map is shown in Figure 4.

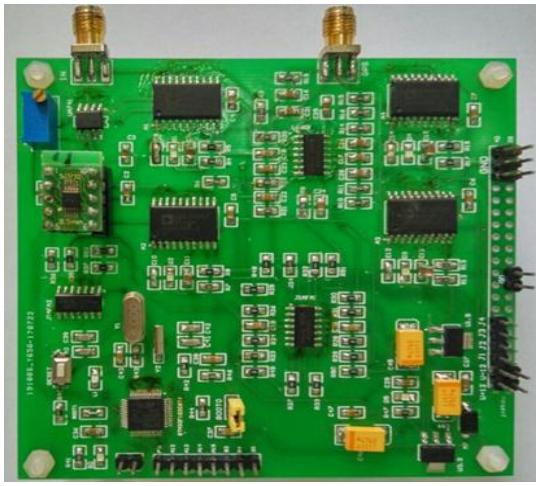

Fig.4 The real picture of the orthogonal lock amplification module

The frequency of the signal to be measured is 1kHz and a sinusoidal signal with a amplitude of 1V, as shown in Figure 5 (a). The amplitude of the measured signal is extracted by the designed phase-locked amplifier module, as shown in Figure 5 (b), and the amplitude is about 2V, which is in agreement with the expected result.

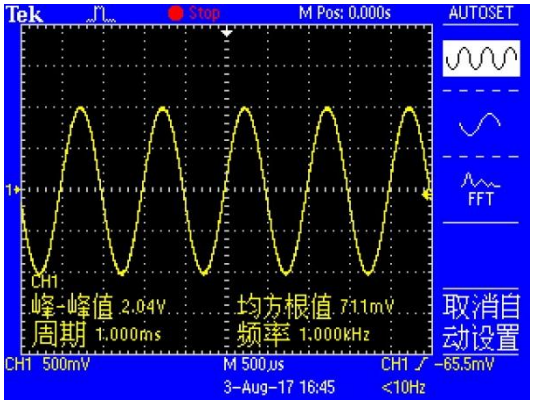

(a) input signal

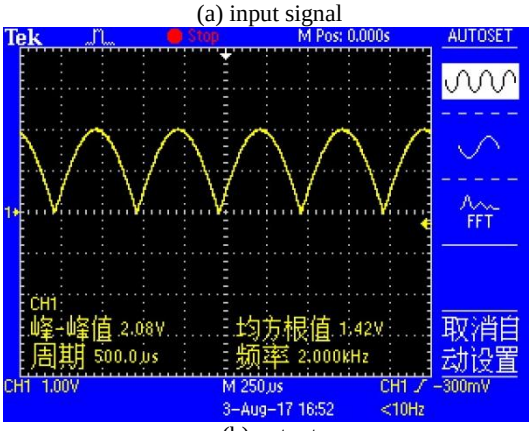

(b) output

Fig.5 Experimental results of the orthogonal phase lock amplification module

C. Comprehensive test results

The system has a continuous sampling of the sinusoidal signal with a frequency range of 20Hz~20kHz and a amplitude of 5mV~1.5V generated by the Agilent 3500B generator. From the amplitude and phase of the waveform data, the realization of the multi frequency electromagnetic signal adaptive acquisition system based on the second pulse and the phase-locked amplification is proved.

When the signal is 20Hz、50Hz、100Hz、200Hz、500Hz、1kHz、2kHz、5kHz、10kHz、20kHz, the amplitude of 5mV、500mV、1000mV、1500mV sine signal, the amplitude of the measured results are shown in Figure 6 (a) is shown; when the signal to be measured is 20Hz、50Hz、100Hz、200Hz、500Hz、1kHz、2kHz、5kHz、10kHz、20kHz, phase $0°$、$45°$、$90°$、$135°$、$180°$、$225°$、$270°$、$315°$ sine signal amplitude error and frequency as shown in Figure 6 (a) is shown; relationship between phase error and frequency Figure 6 (b) shows the physical map;

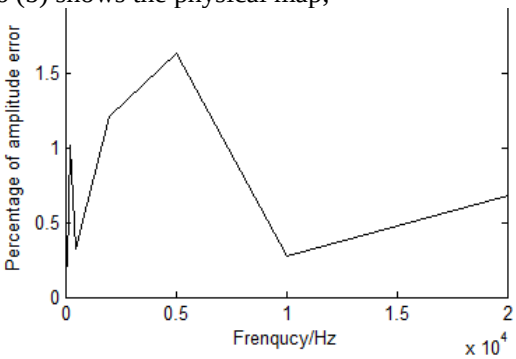

(a) Amplitude error - frequency

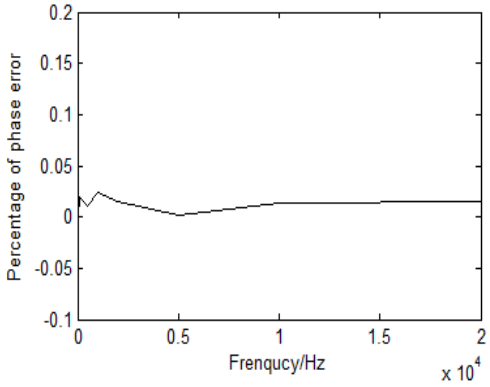

(b) Phase error - frequency

Fig.6 Comprehensive test results

IV. CONCLUSION

Adopt digital phase-locked loop (DPLL) method and analog lock-in amplifier combination, using orthogonal lock-in amplifier technique and pulse frequency domain electromagnetic signal acquisition system designed for synchronization technology, the instrument provides a new collection of ideas in the deep exploration, the system can be used as the airborne electromagnetic data denoising leveling and inversion method can provide practice platform, provide reference for development of UAV and semi air electromagnetic equipment acquisition.

References

[1] Aaron D C.Quantitative characterization of airborne electromagnetic systems [D].Melbourne Institute of Technology University,2007

[2] Ji Yan Ju, Wang Yuan, Lin Jun etc., unmanned airship long wire source to time domain electromagnetic exploration system and its application. Journal of Geophysics ,56.2013.

[3] Zhou Fengdao, Wang Shuang, etc., the improved orthogonal detection algorithm for the controllable source electromagnetic detection. Journal of Jilin University (Engineering Edition).46.2016.11.

[4] Medina-Rodriguez S,Torre-Vega A dela,Fernandez J F,et al.An open and low-cost optical detection of oxygen using a multifrequency phase-resolved method [J].Sensors and Actuators B:Chemical,2013,176:1110-1120.

[5] Analog Devices ， Inc. AD9548 data sheet [EB/OL]. (2010-10)[2011-01-18].http://www.analog.com/static/imported -files/data_sheets/AD9548.pdf

[6] Gentile K. The AD9548 as a GPS disciplined stratum 2clock[EB/OL].(2009-06)[2011-01-18].http://www.analog.com/static/imported-files/application_notes/AN-1002.pdf.

[7] YanHong Kou, Yu Morton,Oscillator Frequency Offset Impact on Software GPS Receivers and Correction Algorithms[J]. IEEE TRANSACTIONS ON AEROSPACE AND ELECTRONIC SYSTEMS VOL. 49, NO. 4 OCTOBER 2013

[8] Mario Luis Ruiz Barrios, Fidel Ernesto Hernández Montero,Application of Lock-In Amplifier on gear diagnosis[J]. M.L.R. Barrios et al./Measurement 107 (2017) 120–127

Design of intelligent air purification system based on 51 MCU

Yun Long; Wenming Zhu; Heshan Yang; Weichen zhang
(instrument science and engineering institute, jilin university)

***Abstract*-Based on MCU AT89C51, we completed the design of an intelligent air purification system, it can real-time monitoring the concentration of PM2.5 in the air, and when the concentration of PM2.5 exceeds the alarm limit, this system can send alarm signal and start up automatically to remove PM2.5 and purify the air. This paper concludes the overall design requirements of the system, the main modules of the system, the sensors in the system, the control circuit and the main components of the dust removal module. Experiments on the dust removal efficiency of the system show that the system has a good effect on removing PM2.5 and purifying air.**

***Keywords*-AT89C51; Air purification; PM2.5; Control System; Sensors**

I. INTRODUCTION

IN recent years, with the development of China's economy and the improvement of people's living standards, the emission of fossil fuel combustion in factories and automobile exhaust makes the air quality unoptimistic[7] [8]. It's especailly obvious in the winter of the north of China, where dense population and economy make enormous emission of PM2.5, as the winter wind speed is low, it is easy to form a stable surface layer of the atmosphere, under the action of multiple factors, it is easy to produce the fog haze. Serious smog can directly affect the indoor air condition, combined with lampblack, cigarettes, decorative materials volatiles and other pollution in daily life, which makes it rather important for purification of indoor air[1] [10].

Negative ion dust removal is a relatively mature technology, ionizing air so the anion can be combined with the dust particles in the air, thus makes natural sedimentation, not only can purify air, but also disinfect it. And HEPA filter as a representative of the new filter material is becoming more and more popular[4], the HEPA filter for multi-layer fold structure, if it fully expanded, its area increases more than a dozen times and even more, because the performance of the filter is proportional with its surface area, the performance of the HEPA filter is very outstanding, is internationally recognized as the most efficient filter material, is applicable to PM2.5 particles of dust filtration purification. At present, a lot of indoor air purification field using a single dust removal technology[2] [5], and the automation is not good, this design aims to combine two different kinds of dust removal purification technology together, using the embedded chip and the related circuit to improve the automation and intelligent level of air purification system, makes the system achieve better purification effect[3]. It can also work independently according to different air condition, so the user will think it is convenient to them.

II. REQUIREMENTS AND MAIN MODULES OF CONTROL SYSTEM

This system is suitable for air purifier, which is mainly used to filter and purify PM2.5, and also has a certain purification effect on other harmful substances in the air. It also includes other functions like high concentration alarm, human-computer interaction, filter condition monitoring and so on. The overall design requirement of this system is that it can effectively detect and purify the indoor low and moderate PM2.5 pollution in real time, and reduce indoor PM2.5 from 100~200 to below 50 in 10min. At the same time, when the indoor high PM2.5 pollution (300 or more) is detected, the alarm will be started ,and pollution can be lowered to the normal range within 20 minutes. The dust removal device is divided into three files, and the user can set the alarm value freely to adjust the working range of different stalls. Considering the HEPA filter needs to be replaced after a period of time, we design HEPA filter monitoring function, when the filter is overused, the warning lights will be turned on to remind the user to replace filter.

The main modules of this system is shown in figure 1, with the single chip processor and accessory control circuit as the core, divided into PM2.5 sensor module, gray scale sensor module, high concentration of warning lamp, warning lamp to change filter net, fan control device, anion device, the user interaction module consists of interface and LCD, the machinery structure module composed of HEPA filter and fan, as well as the single-chip microcomputer control module as the core of the system.

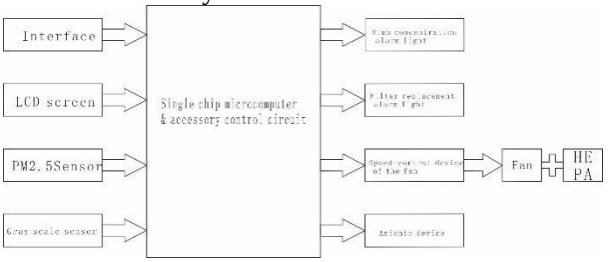

Fig.1 Schematic diagram of main modules of the system

III .THE HARDWARE OF CONTROL SYSTEM

According to the overall design of the system[6], zph-01 dust sensor is selected as PM2.5 sensor. Using particle counting principle, this sensor is sensitive to detect more than one microns in diameter dust particles,

also has high sensitivity, excellent long-term stability, its calibration is calibrated before delivery, built-in heater can realize automatic air suction, it has compact appearance, light weight, easy installation, what's more, its maintenance is also simple, making it is very applicable to air purification system. The principle of this sensor is shown in figure 2. The heating device at the bottom of this sensor can automatically inhale air through the gas convection. The LED module emits light, which is reflected by the dust particles and is received by the PT through the lens to realize the count of dust particles. Actual measurement shows that the type of sensor work well in quiet place when air flow is not too severe, but shaking and strong air flow will cause abnormal output rise, therefore, the sensor was firmly fixed on the shell of air purification system, in the position of the far away from the fan.

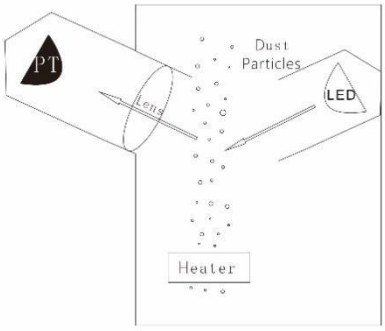

Fig.2 Working principle diagram of dust sensor

The sensor has two output modes: UART digital serial output mode and PWM signal output mode. In this design, the sensor is in serial output mode, and is connected to the serial port of the single chip. When serial output is used, the output format of the sensor is shown in figure 3, and the low pulse rate is the effective data for the output of the sensor. There is a fixed function relationship between the low pulse rate and the concentration of dust particles.

0	1	2	3	4	5	6	7	8
Starting position	Detection type name coding	Company (Low pulse rate)	Low pulse integer part	Low pulse decimal part	Reserve	Reserve	VOC level	Check value
0XFF	0X18	0X00	0X00-0XFF	0X00-0XFF	0X00	0X00	0X00-0X03	0X00-0XFF

Fig.3 The data format used in serial output

The grayscale sensor is used to monitor the working condition of the HEPA filter. When HEPA filter works after a long time, the adsorption of dust particles sticking on the surface, once those particles is accumulated to a certain extent, it will affect the absorption effect of dust, it will also adsorb more bacteria on the filter at the same time. The HEPA filter must be replaced at this time, otherwise it will influence dedusting effect and even be harmful to health. Because the dust particles in the air always adsorb many impurities, most of the particles become colored particles, sticking on the surface mesh, they make the mesh rendering gray, dark gray, brown, tan, and other darker color. At this time, by monitoring the grayscale of the screen, the working condition of the filter can be monitored in real time, so the user can replace the filter in time. The principle of grayscale detection module is shown in FIG. 4. The white protrusion is an infrared generator, and the black protrusion is an infrared receiver, which is separated by the baffle shown by the twill line. At work, the infrared ray is emitted from the white protrusion, reflected by the detection surface ,finally received by the black protrusion. The more gray the surface is, according to the optical knowledge, its ad5bsorption capacity of the light is more strong, so after reflection, the receiver will receive less light. The gray value of the measured object can be obtained by the value of the light received

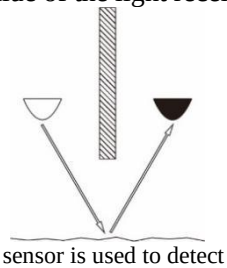

Fig.4 The grayscale sensor is used to detect the principle of the filter

The output for gray level sensor is analog output, range from 0 v to 5 v, when the measured object is absolutely white, and has prefect ideal reflecting surface, the output is 5 v, and when the the measured object is an ideal blackbody that absorbs all the light, the output is 0 v. The higher the gray level is, the lower the output voltage is. As the input module that connected to the single chip microcomputer, it needs to pass through a voltage comparator, by comparing the gray level sensor output voltage with the preset voltage , to make the output of the voltage comparator as an input tocontrol circuit. In figure 5, for example, the core is a LM339 comparator, the reverse input is a voltage that can be set. The positive phase input is the output voltage of the above sensor. Assuming that the voltage of the reverse input is set to 4.18V, when the voltage of positive phase input is less than 4.18V, the output voltage of the comparator is only 0.19v. For a single chip, this voltage is considered low level. When the voltage of positive phase input is greater than or equal to 4.18v, the output terminal voltage of LM339 is 5V, which is regarded as high level for single chip microcomputer.

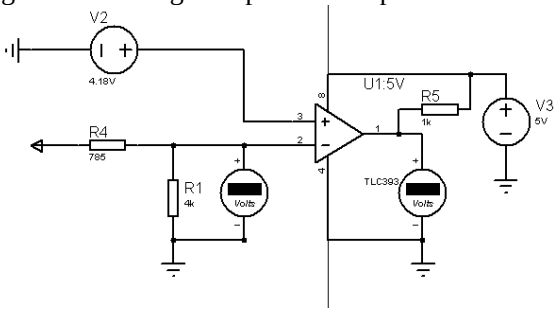

Fig.5 Gray sensor comparison circuit as needed

The fan this design select is a fan for ac 220 v, which is hard to adopt the method of series resistance speed control for it has little effect and brings slow work efficiency, luckily, the application of power electronic technology gives a solution. So the PWM control is a better choice, by adjusting a variable resistor to control the space ratio of the square wave, the speed control can be achieved.As this design only requires 3 stage speed

control, in order to simplify the circuit , we directly select three stepless speed regulation switch, thus single chip microcomputer is only responsible for the output control signal to select which switch to conduct to achieve speed control. In order to realize the electrical isolation between the loop of the control and the high voltage loop of the fan, it is necessary to apply the optical coupler, together with the stepless speed regulating switch, to form the circuit to drive the fan.

Driving the negative ion generator is much more simple, the output of the single chip can control the generator's loop via the optical coupler.

IV.THE SOFTWARE OF CONTROL SYSTEM

Once the system is powered on ,the only thing we need is to turn on the total switch and wait , after the initialization , the sensor begin to test the dust concentration in air, the system read the output of the sensor, after data conversion, the numerical of the concentration of dust display on the LCD screen. Because the serial port output format of PM2.5 sensor is shown in figure 3, it is necessary to deal with it in the program to get the final concentration value.

```
pm_rateH=UART_Upload[3];
pm_rateL=UART_Upload[4];
pm_density=(UART_Upload[3]*100+UART_Upload[4])*1.014705;
```

As shown in the above program, UART serial data of [3] is the integer part of the low pulse rate, UART serial data of [4] is the decimal part of low pulse rate, such as in the case of a 345 mu g/m3, zph01 low pulse rate is(output) 34%. We believe that at low pulse rate like 0-34%, the corresponding concentration is 0-345 u g/m3. So there is a linear relationship between low pulse rate and concentration.

The resulting pm_density is 10 times than the actual value, and it moves the last decimal to the ones place, which is convenient for LCD to display.

```
LCD_Write_String(0,0,"PM2.5:");
LCD_Write_Char(6,0,table[pm_density/1000]);
LCD_Write_Char(7,0,table[pm_density%1000/100]);
LCD_Write_Char(8,0,table[pm_density%100/10]);
LCD_Write_String(9,0,".");
LCD_Write_Char(10,0,table[pm_density%10]);
LCD_Write_String(11,0,"μg/m3");
```

The program of LCD display is shown in the above, pm-density is assumed to be 3452. After this program is run, it can display the words of PM2.5 345.2μg/m3 on the LCD screen, which means again we reduce pm-density to a tenth, so it finally shows the actual value of the concentration.

The design demands that when the oncentration is higher than that of high concentration alarms, the alarm starts up automatically. Also it demands that the value of the warning alarm can be change. It is clear that the value should be displayed in the LCD screen and comply with the corresponding button to achieve these functions. Set the alarm value for pm-URV in the program, using "if" statements to judge which one is bigger between pm-density and pm-URV , once pm-density is greater than the pm-URV that we set, the alarm will be trigged , automatically turn on the high speed switch.

```
else if(pm_URV<pm_density)
{
  led1=1;     // Led1 represents the power indicator light, which represents normal work and will be extinguished when the alarm state is in.
        led3=1; // Led3 represents the replacement of the filter alarm indicator light, which will light up when the filter screen is too gray.     out1=0;     // Out1 represents low speed .
  out2=0;// Out2 represents middle speed
  out3=1;// Out3 represents high speed
 if(beep==1) // Led2 represents a high concentration alarm lights, flashing at this time, and the buzzer (alarm_buzz) beeps. Beep is produced by a timer interrupt, whose value fluctuates between 0 and 1 every 10ms.
    {led2=0;alarm_buzz=0;}
    if(beep==0)
    {led2=1;alarm_buzz=1;}
}
```

In order to make the pm_URV adjustable, set key_add key_minus two key state variables, and detect whether button state changes, when the button state changes, the button state changes by the add = key_add or minus = key_minus and was read into the add and minus, two variable that control the increase or decrease of pm_URV.(0 signals are produced when you press the button so reading starts, then 1 signals produced by loosing the button will be send to add or minus).

```
if(add==1)  //When signal add is 1
{
pm_URV++;   // Pm_URV keeps increasing, which is suitable for pressing and holding, which can rapidly increase pm_URV.
if(pm_URV>=10000)//When pm_URV is too large, it can automatically return 0, so the user can recover as soon as possible.
{pm_URV=0;}
   SectorErase(0x2000);
byte_write(0x2000,pm_URV/256);
   byte_write(0x2001,pm_URV%256);//The value of pm_URV is written to the eeprom, so that the value of pm_URV can be saved after shutdown, so when you restart it don,t have to be reset
}
```

V.MECHANICAL MODULE AND OVERALL PACKAGE

The mechanical module of this design is centered on two fans. The air intake fan is a 10-inch ac 220AC fan with a rated speed of 2800r/min, which can produce strong wind and absorb air into the dust removal device. The speed regulating function of the software and

hardware is designed to control the speed of the air intake fan, so that it can work in three different kinds of wind. And the outlet fan uses the dc fan with a small power, which keeps it working at the rated power. The intake fan (via the HEPA filter) is connected to the outlet fan by a L-type pipe to enhance the convection of air.

HEPA filter has a certain thickness and hardness, puts HEPA filter after the air intake fan card slot , so the air that can go through a HEPA filter at a higher speed, dust will be attached on the filter. Fixed grayscale sensor at 1cm in the L pipe behind the filter (a strong plastic bracket is needed, because the wind is strong when the fan is opened). Anion generator is placed near the outlet fan L-type pipeline internal, pay attention to the anion generator should be firmly fixed, it may produce electrostatic at work, pay attention to make it not come into contact with the pipe wall.

The PM2.5 sensor is placed in panel of the device, but must keep a certain distance with the air intake fan to prevent air disturbance. The sensor can seal within the dust cover when power off, to prevent the fugitive dust pollute the lens inside PM2.5 sensor. The interface and the LCD screen is placed below the sensor, a reserved hole is needed on the acrylic shell to let the lines of the sensor ,the operation interface and the LCD screen to connect with the internal control module inside the device.

The processing module and relay are placed on a piece of circuit board, fixed inside the device, and maintained a certain distance from the L-type pipe. A triangular hole is reserved at the bottom of the rear panel of the device, so the ac power supply to the device can be connected to the external 220V power supply. At the same time, the variable voltage rectifier is placed inside the device, so the external 220V alternating current is supplied to the control module and the sensor by the voltage and rectifier. Wrap around a ring of sound insulation around the L-type pipe and fill the gap between the L-type pipe and the device to reduce the noise of the device running.

The packaging of the entire device is shown in figure 6 and figure 7.

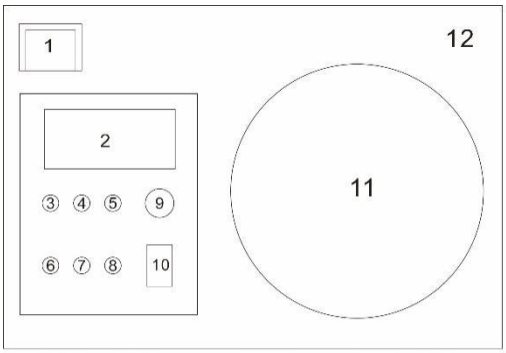

1PM2.5 Sensor&Dust cover 2LCD screen 3Power indicator 4Alarm light 5Filter replacement light 6Add button 7Minus button 8Reset button 9Buzzer 10Main switch 11Air intake fan 12Acrylic panel

Fig.6 Device front panel diagram

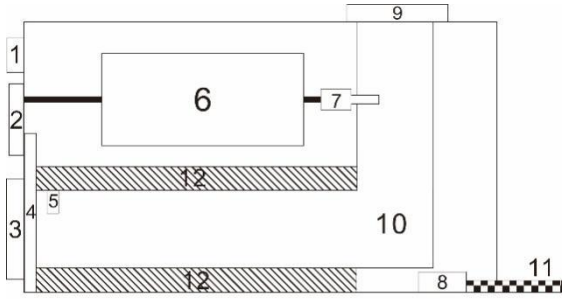

1 PM2.5 Sensor&Dust cover 2Interface 3Air intake fan 4HEPA filter 5Gray scale sensor 6Control module 7Anionic device 8Transformer&Rectifier 9Air inlet fan 10L-pipe 11Wires&Cable 12Sound insulation cotton&Foaming agent

Fig.7 Profile view of the device

VI. Analysis of Dust Removal Effect in Experiment

The experiment of PM2.5 dust removal in the enclosed room can be approximated that the temperature and humidity in the room will not change during the test period.

At the time of the experiment, the most powerful stage was opened to verify the best dust removal efficiency of the device. The PM2.5 sensor attached to the device was used to monitor the concentration of PM2.5 and draw a curve. This experiments using cigarette combustion to simulate release of PM2.5. When the concentration of PM2.5 is relatively stable (mixed well), open the fan, so concentration of PM2.5 will change over time, which reflects the dust removal effect of the device. Also we set up another group that the fan is closed to determine the natural attenuation of the concentration of PM2.5, we record data every 30 s, the result is shown in figure 8 and figure 9 (The zero point of the timeline shown in the figure is the point that the concentration of PM2.5 gradually rise until relatively stable).

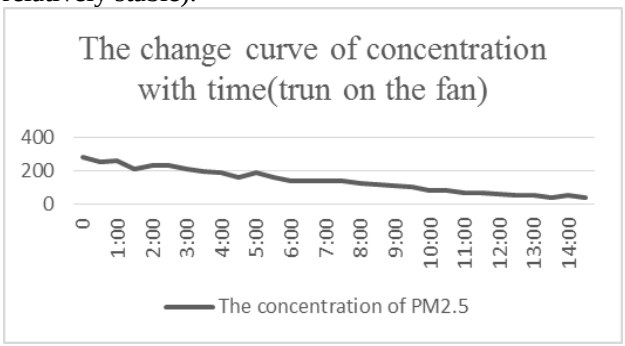

Fig.8 The concentration of PM2.5 when opening the fan.

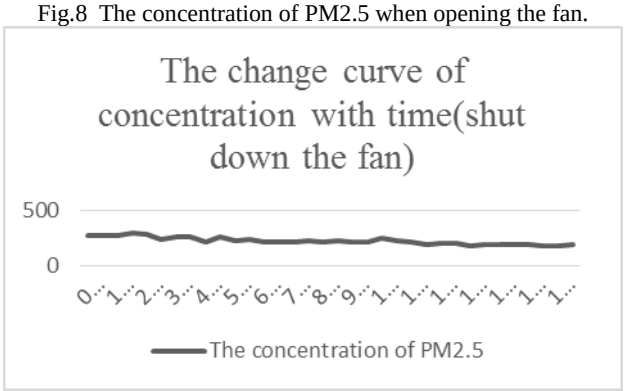

Fig.9 The concentration of PM2.5 when the fan is not turned on.

Obviously, filters with fan and HEPA have good dust removal effect, within 10 min has concentration of PM2.5 can be dropped from 280+ to below 100, at 14 min30s, the concentration even dropped to 43.4, this number is even smaller the initial concentration before the test, which is 87.7. (because the test room has bad ventilation, poor air). (note: due to the sensor we use has a little hysteresis, and the smoke flaps randomly, it's normal that the data fluctuates during a short period of time) Although the concentration of PM2.5 is still in fall after a period of time even you don't start the fan, it decreased slowly, At 17 min it remains at close to 180, so the room is still full of stimulating gas. (note: the zero point of PM2.5 concentration is slightly different because it is hard to get the same in the two experiments of the initial concentration of PM2.5, the two curves is the average of many experiments , so that the error can be minimize)

Four compared experiments with four different conditions were carried out after the device was basically formed, the result is shown in figure 10.

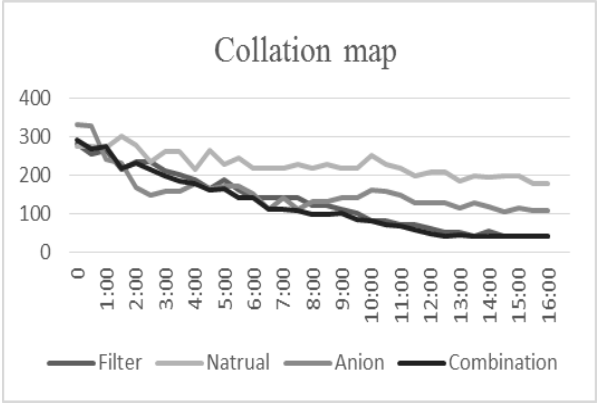

Fig.10 A comparison of the four conditions

Obviously, no matter whether the filter with HEPA and fan or the negative ion generator , the dust removal effect is apparent compared with the no-dust removal device. Negative ion dust removal effect is excellent in the first place even better than that of the filter, but when concentration of PM2.5 is down to about 150, negative ion dust removal effect becomes unideal, eventually the concentration of PM2.5 has failed to fall to below 100. It can be explained by the principle of negative ion dusting. The oxygen molecules near the negative ion generator are gradually converted into oxygen ions[9], which combine with the particles in the air to settle. But after a period of work, the concentration of oxygen ion near the anion generator has reached a critical value, it's hard to continue to convert oxygen molecules to oxygen ions, so the working effect becomes unideal. To solve this problem, we must spread out oxygen ion that we convert in time, so this device choice to place the anion generator near the outlet fan to make the dust removal effect better.

The experimental results show the effect of dust removal can be improved when the negative ion generator and HEPA filter are combined[4], ,this device has reached the design requirements of the dust removal effect.

VII. CONCLUSION

This design basically realizes the design requirement, but still has a lot of improvement space,noise problems for example, although the use of foaming agent and sound insulation sponge can absorb most of the noise, but careful study can found that the rotation surface is not level when the fan in rotation, and the axis of rotation is not always stay in the central vertical line, this may be an important cause of the noise.

It can be seen that this phenomenon is normal in domestic fans, and it is difficult to improve it. With better fans, it is believed that the end result will be better. Another place to improve is ZPH01 dust sensor now we use, the sensor is slightly hysteresis, and its inlet hole is small, the air we sampling is limited in the nearby area, which often cause the measured concentration fluctuation. As to which sensor can achieve the best results, a great deal of comparative work is needed, which needs further study.

References

[1] Zhang Bei , Xiang Haien, Hao Pan-pan, Xiao Jun.Study on Purification Impact of Various Air Purifiers on Indoor Particulate Matter[J].China Environmental Protection Industry,2017(09):56-58.

[2] Wang Lei, Bao Lei,Yuan Jingguang. Design of an intelligent combined PM2.5 air purifier [J]. Sensor World,2016,22(11):35-39.

[3] Lu Li,He Junhui,Tian Hua,He Bo, Yang Qiaowen.Novel aircleaners and their evaluation methods [J]. Science & Technology Review,2015,33(12):101-109.

[4] Yang Qian,Dong Yude,Chen Guangchao. Design of the control system of multi-functional air cleaners based on ATmega128[J]. Journal of Xi'an Polytechnic Universit,2015,29(03):375-380.

[5] Shen Ai-lian,Auto Air Cleaning System Design Based on 51 Series of Single Chip [J]. J Chongqing Technol Business Univ. (Nat Sci Ed),2012,29(02):62-65.

[6] Sung Hwa Lee. Development of Photocatalyst Plasma Air Cleaning Filter Used in Air Conditioner[J]. Journal of Advanced Oxidation Technologies,2003,6(1).

[7] Hua Qian,Yuguo Li,Hequan Sun,Peter V. Nielsen,Xinghua Huang,Xiaohong Zheng. Particle removal efficiency of the portable HEPA air cleaner in a simulated hospital ward[J]. Building Simulation,2010,3(3).

[8] Sung Hwa Lee. Development of Photocatalyst Plasma Air Cleaning Filter Used in Air Conditioner[J]. Journal of Advanced Oxidation Technologies,2003,6(1).

[9] Daniel W T Chan,K C Law,Chris H S Kwan,W Y Chiu. Application of an Air Purification System to Control Air-borne Bacterial Contamination in a University Clinic[J]. HKIE Transactions,2005,12(1).

An automatic currency Exchange Machine based on Internet payment Technology

ZHOU Zhijian; YANG Guizhong; LIU Hongjie; WANG Yinpan
(College of Instrumentation & Electrical Engineering, Jilin University)

***Abstract*-In this paper, a kind of equipment for automatic coin exchange using WeChat Pay technology is studied.It is used to solve the problem of changing small denomination currency in daily life and realize "zero cash" travel. The device has small denomination notes for coins and WeChat Pay for coins. According to the hardware and software module, the overall layout, the stability of the equipment and the accuracy of exchange, the related design and research are carried out. The experimental results show that the equipment is safe and stable and can meet the exchange demand in daily life.**

***Keywords*-Internet WeChat payment currency exchange accuracy**

I. INTRODUCTION

WITH the rapid spread of network payment, people are more and more used to use mobile devices to pay, this fast and safe payment method makes "zero cash" travel become the general trend.Following the coins of 15 cents and 50 cents, some cities in Shandong Province have started to implement the project of "1 yuan coupons and coins". At present, many countries in the world have adopted coins on the small amount of basic currency, and the elimination of 1 yuan paper currency is also in line with the development trend. In addition, the introduction of 1 yuan and 5 dimes is conducive to the promotion and application of vending machines, parking lot automatic toll collection machines, subway and bus ticket vending machines, and is convenient for people to live in. However, due to the inconvenience of carrying coins, it is urgent to be able to pay for coins quickly through the Internet.At present, there is no equipment on the market to exchange coins through the Internet, and there are self-help coin changers and vending machines that can partially realize currency exchange. But its function is single, the use limitation is big, therefore in the existing equipment foundation carries on the function adjustment and the software innovation, realizes through the Internet payment direct exchange small currency has the more realistic significance.

On the basis of the functions of self-help coin changer and vending machine, this paper studies an exchange machine with STM32 as the main processor. The function is innovated and integrated, which greatly reduces the volume of the equipment. WeChat Pay has been added to exchange coins so that it can exchange coins in cash and pay for coins on the Internet. The use of QR codes in WeChat Pay improves the security of payment by transmitting information between the converters and mobile devices.

II. HARDWARE SYSTEM ARCHITECTURE

As shown in figure 1, the STM32 is used as the main board to drive and control the banknote machine, the cash dispenser, the display screen and the keys. The power box supplies power to the motherboard, the banknote machine and the coin dispenser. Here is a brief introduction to the various hardware modules:

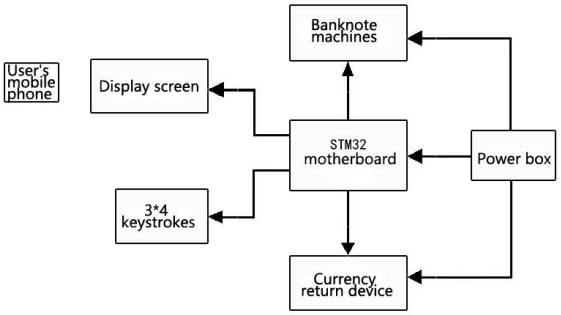

Fig.1 Hardware system structure

A. Power box

MD-9916A-24V power box can convert 220V daily AC voltage to 24V, 12V and 5V DC power supply voltage, the output power is only 130W, working efficiency is high, output ripple noise is low, it is very suitable for power supply for each working module.

B. STM32 motherboard.

The STM32 series belongs to the 32-bit ARM microcontroller at the middle and low end. The chip series is produced by Italy Semiconductor STS, the core of which is Cortex-M3. The chip integrated timer can be used for ADCI I2CU UART and other functions.

C. Currency return device.

The machine is widely used in all kinds of game machines and coin exchange machines. The 8-hole motor of this equipment has the advantages of quick response and accurate coin delivery. The working voltage is 24 V / 0. 4 A and the maximum storage capacity is 2, 000 coins in the hopper[1].

D. Banknote machines.

According to the different denominations of banknotes, the paper currency recognizer has different characteristics, such as paper, magnetism, size and so on. It uses fluorescence detection technology and magnetic detection technology to distinguish the true and false denominations of banknotes.

E. display screen.

A flat ultra-thin display device consisting of a certain number of color or black and white pixels placed in front of a light source or reflection. Its main principle is to stimulate the liquid crystal molecule to produce the

point, the line, the surface with the back light tube to constitute the picture. The resolution of the 3.2-inch TFT LCD screen in this device is 240*320, and the power consumption is 5.5V 6.3W.

*F.3*4 keystrokes.*

Matrix keystroke, which is a keyboard group similar to a matrix used in the peripheral equipment of a single chip microcomputer, and is used to input signals from the outside. When the button is not pressed, all inputs are high, representing a key-free press. When a key is pressed, a low level is input, and by reading the state of the input line, you can see if a key has been pressed.

III.SOFTWARE SYSTEM ARCHITECTURE

A.Control flow of banknote exchange coin module

Turning on the power supply of the equipment, entering the normal operation state after initializing the system, waiting for the signal of the banknote machine; when the banknote machine receives the banknote, the system judges the received banknote denomination through the data sent by the banknote machine, and calculates the corresponding return number. Then the system starts the interrupt controller and timer and drives the coin return device to start the coin return; after the return currency is finished, the interrupt, timing and return device are closed, and return to the state of the uncollected banknote, waiting to be exchanged again[2]. The module workflow is shown in figure 2.

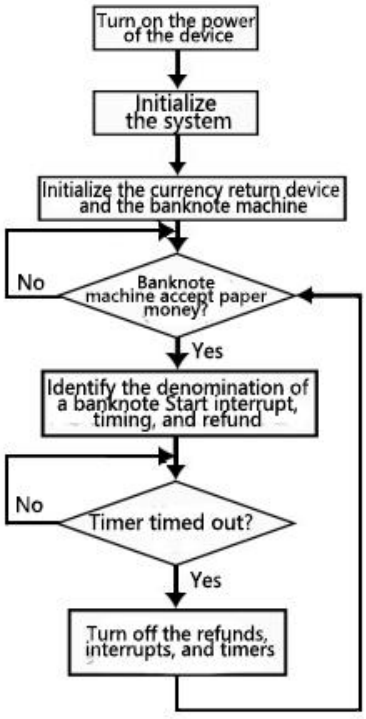

Fig.2 Control flow of "banknote exchange to cions"module

B.Control process of WeChat Pay coin exchange module

After power supply, the system initializes operation, then enters normal working state, circulates and waits for the serial port signal of the keystroke. The user selects the amount of money exchanged through the button, analyzes and processes it according to the determination of the processor, and generates the random six-digit verification code. After that, the QR code with the verification code is transmitted to the display. The essence of the QR code is a link. The user scans the QR code through WeChat and links to the background server to complete the communication between the server and the mobile phone[3]. When the server receives the payment information from the user, it sends 6 bits of CAPTC-code to the user. The user inputs the CAPTC-code into the exchange machine, and the processor checks the received CAPTC-code with the previously randomly generated CAPTC-code. Send a signal to output the coin if it is correct and prompt the error if it is an error[4]. The module workflow is shown in figure 3.

C.WeChat Pay

WeChat, a free messaging app for smart terminals, was launched by Tencent in January 21st 2011. WeChat supports cross-communication operators, cross-operating system platforms to quickly send voice messages, video, pictures and text over the network. WeChat public platform is a functional module of WeChat. In this article, the WeChat public platform is the platform that we offer the currency exchange service to the user through WeChat. Public platform development interface is the basis for providing services, we create Official account in the public platform website, access to interface rights, can be developed with the help of WeChat public platform development text, not detailed here.

We transform a link into a QR code, users scan the QR code using WeChat, WeChat automatically links to Official account backstage to realize the interaction between users and WeChat backstage. After the payment was completed, Official account returned the verification code back to the user's mobile phone, and the user entered the verification code to the currency exchange machine, and after the input was completed, the currency exchange machine began to proofread and verify, the correct start of interruption, the puff out of the corresponding coin, and the error of sending out the prompt[5]. The payment and transfer function of WeChat, as well as the powerful development and application of WeChat public platform, can realize the exchange of currency on the Internet of this machine.

D. Generation Technology of Two-Dimensional codes

Because the device needs to link the phone to the server, the. The convenient way is to generate the QR code with the verification code and the link, the user can scan the code to realize the communication with the server[6]. Two-dimensional code records the symbolic information of the data with a certain geometry distribution in the plane (two-dimensional direction) of black and white graphics. Two-dimensional code storage data large, can contain numbers, characters, and Chinese text and other mixed content, there is a certain fault tolerance after partial damage can be read after

normal, space utilization rate is high. Because of the huge code and complex algorithm, the STM32 with small memory can not put down the huge data of the code[7]. Open source QR code can be used online, because the open source code is running on the LINUX platform, in order to adapt to STM32, do some transplanting work[8].

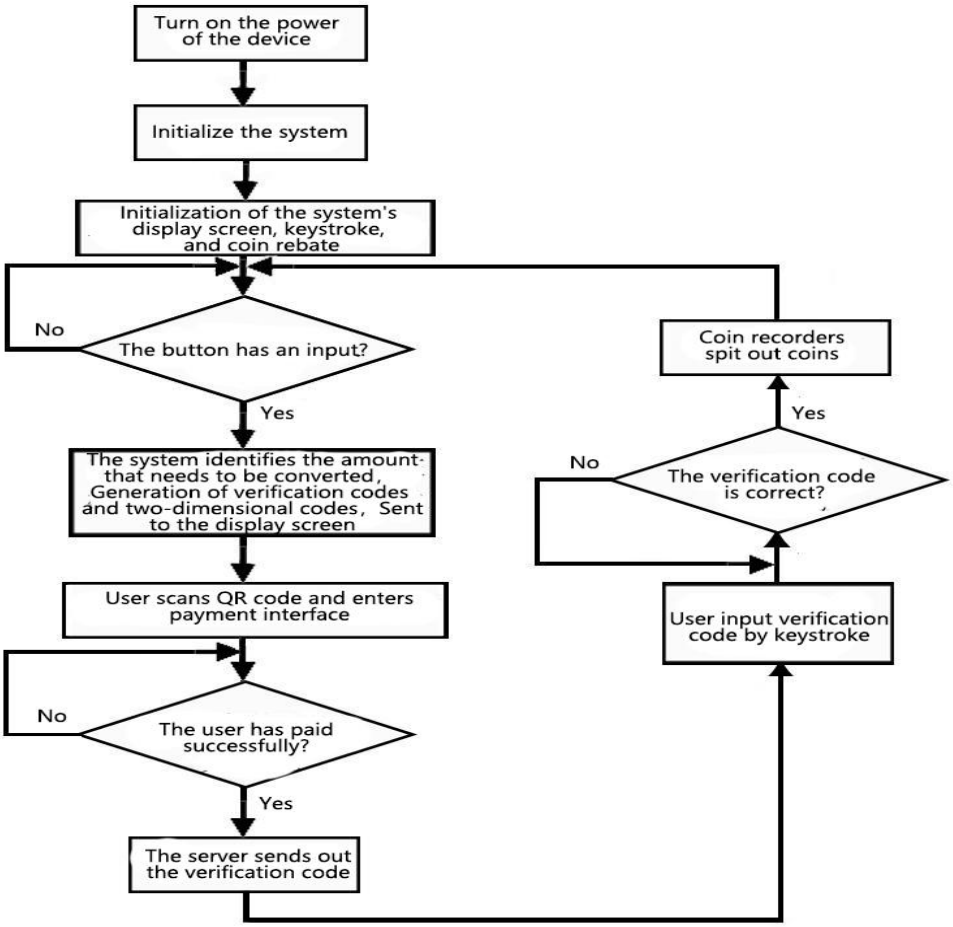

Fig.3 Control flow of "WeChat electronic money exchange to coins"module

Ⅳ.EXPERIMENTAL RESULTS AND ANALYSIS

A.physical drawings of converters

Fig.4 The picture of the machine

Size （mm）：500*250*500

The first picture on the left shows a paper machine on the left, a keystroke on the middle and a display on the right. The second picture on the right is the puff. The third picture on the left shows the banknote machine. The bottom right 4th pictures are power lines.

B.randomness testing and results of captcationcode.

In order to obtain feedback signal and ensure payment security, the device uses STM32 as the main board and generates a six-digit verification code at random. In order to verify the randomness of the verification code and ensure the uniqueness of each QR code, we have carried out many experiments on the same amount of money and different amount of money. A large number of test results are presented in the following table:

Table 1 The QR code generation results

banknotes to be exchanged	Verification codes generated through 20 tests
1yuan	493583 157349 613482 244371 943367 543168 746281 015746 487351 164872 339441 149732 448256 648771 124060 346715 641578 312435 973465 315479
5yuan	349751 164825 347751 433543 846791 216487 102556 794152 731684 439715 394137 081883 429932 526518 773170 327488 856914 801001 069545 867640
10yuan	965481 309041 414876 314054 087764 013645 369742 469746 764158 564821 564408 310405 492113 336879 794885 412649 895425 994794 422615 223579

It can be seen from the table that the verification code is generated randomly and irregularly, and it is almost impossible to generate fully repeated verification code in the short term. Because the verification code is a part of the information of the QR code, it ensures the uniqueness of the QR code each time, and then shows that the coin is safe enough to fully meet the requirements of the equipment.

C.Stability Test and results of equipment Coin

In order to ensure the stability and fluency of the coin, we tested 20 groups of time from the input paper currency to the end of the coin. The results are as follows. In the table, we can see that the time of each time is about 3.95 s, the average absolute deviation is 0.17, which indicates that the speed of the equipment is fast, and it is very stable.

Table 2 The time of the machine needed to exchange

Time needed to issue coins(s)				Average time	Mean absolute deviation
4.21	3.96	3.76	3.80	3.9495	0.17255
3.48	4.19	3.82	3.84		
4.04	4.19	4.10	4.13		
3.50	3.97	3.76	4.11		
3.92	4.18	3.94	4.09		

D. accuracy test and results of currency exchange

This equipment is a currency exchange machine, its most important performance index is to exchange currency. For this reason, we tested the dollar, five and ten dollar notes and the online currency of one, five and ten yuan WeChat Pay to get the number of coins out. From the results of the test samples, we can see that the different denominations of the same currency, the same denomination of different currencies, the number of currency out and the exchange amount are the same. The result shows that the equipment can be exchanged accurately.

Table 3 The accuracy test results

Payment method		Be paid in cash			WeChat Pay		
Denominations paid		1元	5元	10元	1元	5元	10元
Number of coins issued	First test	1	5	10	1	5	10
	Second test	1	5	10	1	5	10
	Third test	1	5	10	1	5	10
	4th test	1	5	10	1	5	10
	5th test	1	5	10	1	5	10
	6th test	1	5	10	1	5	10
	7th test	1	5	10	1	5	10
	8th test	1	5	10	1	5	10
	9th test	1	5	10	1	5	10
	10th test	1	5	10	1	5	10
	11th test	1	5	10	1	5	10
	12th test	1	5	10	1	5	10
	13th test	1	5	10	1	5	10
	14th test	1	5	10	1	5	10
	15th test	1	5	10	1	5	10
	16th test	1	5	10	1	5	10
	17th test	1	5	10	1	5	10
	18th test	1	5	10	1	5	10
	19th test	1	5	10	1	5	10
	20th test	1	5	10	1	5	10

Ⅴ.CONCLUSION

In this paper, a currency exchange equipment based on Internet payment technology is studied. The function of each hardware module, the whole system structure, the principle of Internet payment and the generation technology of QR code are introduced in detail. The randomness of the generation of the verification code, the fluency of the equipment and the accuracy of the currency exchange are tested. The experimental results show that the currency changer can monitor the input signals of banknote recognizer and key code in real time, and can react rapidly according to the received signal, and the uniqueness of the QR code can be ensured by using the randomly generated verification code. Thus, the security of payment is guaranteed, and the money out is fast, stable and accurate. The equipment has the characteristics of safety and stability and fully meets the expected requirements.

References

[1] Design and implementation of vending Machine Control system [J] .Microcomputer Information system 201127 8: 36-38.

[2] Zheng Ying-ying. Embedded Anti-cracking automatic

currency transfer Machine system based on STM32 [N] .Journal of Guangdong Radio and Television University: 2014 / 23 / 6: 105-110.

[3] Xu Guohui, Chen Jexian. Principle and Application of Mobile QR Code Technology [J] .Information and computer: 01: 18-19.

[4] Zhang Mei. Realization of Electric vehicle charging platform based on WeChat [J].

[5] Huang Jian, Shi Xiu Lu, Huang Qi he. Design of passenger order Service system for High-speed Railway based on WeChat Public platform [J].

[6] Liu Qiang, Wang Chuanbei, Yu Zusong.Study on the Two-Dimensional Code Generation and display system based on STM32 [J] .Information Technology and Informatization: 201510: 174-176.

[7] Fan Jingcheng. Method and device of Two-Dimensional Code Generation [P] .China Patent 106156820 / 2016-11-23.

[8] procedures. Methods for generating and verifying QR codes [P]. Chinese Patent: 104881698 / 2015-09-02.

Measurement of subcutaneous fat thickness based on near-infrared light

Sun Tianyun; Wang Yushu; Chen Xue
(College of Instrumentation&Electrical Engineering , Jilin University)

***Abstract*— In modern society, obesity has become a pandemic, it seriously affects the modern people's health. Fat content is a very important health indicators for the human body , it has to do with high blood pressure, coronary heart disease, diabetes and many other diseases. Therefore, measuring the thickness of subcutaneous fat, not only meet the demand of testing the health of the fat content, but also satisfy the fitness needs of fitness crowd. According to the biological characteristics of human subcutaneous tissue and the principle of using near-infrared light to measure the thickness of subcutaneous fat, identified the sensitive wavelengths of fat thickness change. The design adopts the four groups of light-emitting diodes,through the processing of measurement data, fat thickness linear model is established, and the collected data will be transmitted through bluetooth transmission to PC for further analyze, the fat thickness parameter of subcutaneous was obtained.Experiments show that the method has good repeatability, stability, low power consumption.**

***keywords*— Near-infrared light Subcutaneous fat thickness Linear model**

I. PREFACE

IN recent years, with the improvement of people's living standard, people's diet structure has also made great changes. The proportion of overweight people is rising. THE LANCET, a leading British medical journal, conducted a 40-year health survey of 19.2 million adults worldwide, showing that THE world's obese population is now over 641 million.

In 2017, the American association of clinical endocrinologists (AACE) and the American academy of endocrinology (ACE) jointly issued a statement, pointing out that obesity is the underlying chronic disease[1-3].In recent years, the world health organization has warned that overweight and obesity are the fifth leading cause of death worldwide, with at least 2.8 million people dying each year.

Body mass index is a commonly used measure of body weight in the international standard, besides, it can also distinguish the degree of obesity according to the thickness of fat.Different fat thickness distribution has different risk, and the most important one is the relationship between visceral fat and subcutaneous fat thickness.

From the above, it can be seen that the real-time monitoring of subcutaneous fat thickness in real life is of great significance to the obesity problem worldwide

II. THE PRINCIPLE OF SUBCUTANEOUS FAT THICKNESS MEASUREMENT BY NEAR INFRARED LIGHT.

A.The absorption and scattering of light under the skin.

Near infrared light is an electromagnetic wave between visible light (VIS) and medium infrared light (MIR), according to ASTM (the American association of experiment and materials testing definition)refers to in 780nm ~ 2526nm wavelength range of electromagnetic waves.Traditionally, the near infrared region is divided into two regions: near-infrared short-wave (780 ~ 1100nm) and near-infrared long wave (1100nm ~ 226nm).

Light has two effects in biological tissue: absorption and scattering.When the skin is irradiated by near-infrared light, the skin has a good permeability to the near-infrared light.After the light enters the adipose tissue, the backscatter mainly occurs, and most of the light occurs backscattering and then passes through the skin and leaves the body, while the light entering the muscle tissue is mainly absorbed. Therefore, the signal received by the detector consists mainly of subcutaneous fat information[4-6]. FIG. 1 is a schematic diagram of the principle of near infrared light measurement.

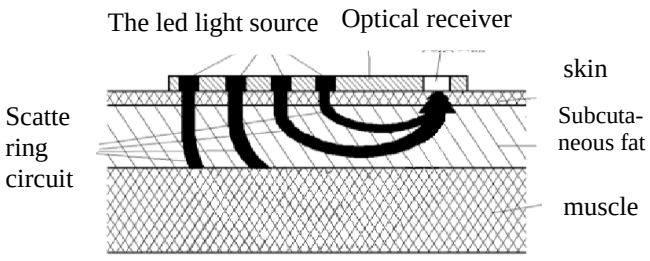

Figure 1 the measurement of the subcutaneous adipose with near infrared light

B.Lambert's laws

Lambert - beer's law is the classical theory of quantitative analysis of spectra.Lambert - bill's law mathematical expression A=lg(1/T)=Kbc.

A for absorbance, T for transmittance, project the light intensity is better than the incident light intensity, K as the molar absorption coefficient, c is the concentration of the material suction light, b for the absorption layer thickness, The physical meaning is when a beam of parallel monochromatic light passes vertically through a uniformly non-scattered absorbent material, the absorbance A is directly proportional to the concentration c and the absorption layer thickness to b.As shown in FIG. 2, the light intensity is I_0, the monochromatic parallel beam of light is passed along the horizontal direction through the homogeneous material. After a distance of x, the light intensity has been reduced to I, and after dx, it becomes I-dI.

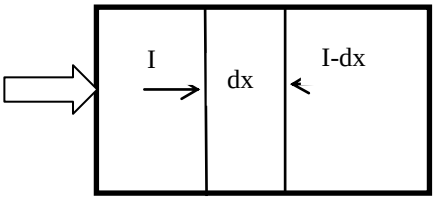

Figure2 Chang of light intensity and path through media

In an extremely wide range of light intensity, it is equivalent to the exact proportion of I and dx, namely dI= alpha Ldx[8-9]. If the wavelength of the incident light is constant, the degree of light absorption is only related to the concentration of the material and the length of the light. When the wavelength of incident light, the concentration of matter and temperature are certain, the absorbance of the material is directly proportional to the optical path length, which is called the lambert's law[7].

III . NEAR INFRARED LIGHT SUBCUTANEOUS FAT THICKNESS MEASUREMENT SYSTEM.

A. Probe composition

Light scattering effect in the fat is the principle of using near-infrared light to measure human body subcutaneous fat thickness, so the distance between the light source and photoelectric diode determines the distance of return light and the diffuse light which contains information of biological tissues.In order to include more comprehensive information about the subcutaneous tissue of the human body, a light-emitting diode with different distance from the photodiode is designed, and its appearance structure is shown in figure 3 .

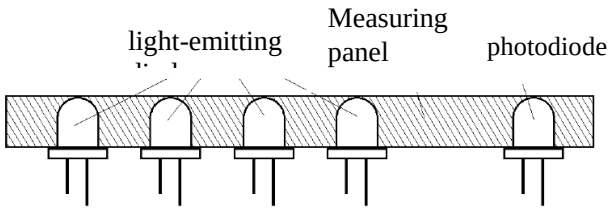

Figure 3 Structure of measurement panel

B. Led drive circuit

The driving circuits of each led are the same. In order to eliminate ambient light interference on the measurement, the measurement of fat selects the duty ratio of 0.5 for 30 Hz frequency square wave as drive signal, the interference of ambient light is eliminated by the difference between the high and low levels of the received signal, namely the difference between luminescence and closed light. In fact, the single chip I/O port can directly drive the LED luminescence tube, but considering that the LED light intensity and stability need to meet certain requirements, the driver circuit shown in figure 4 .

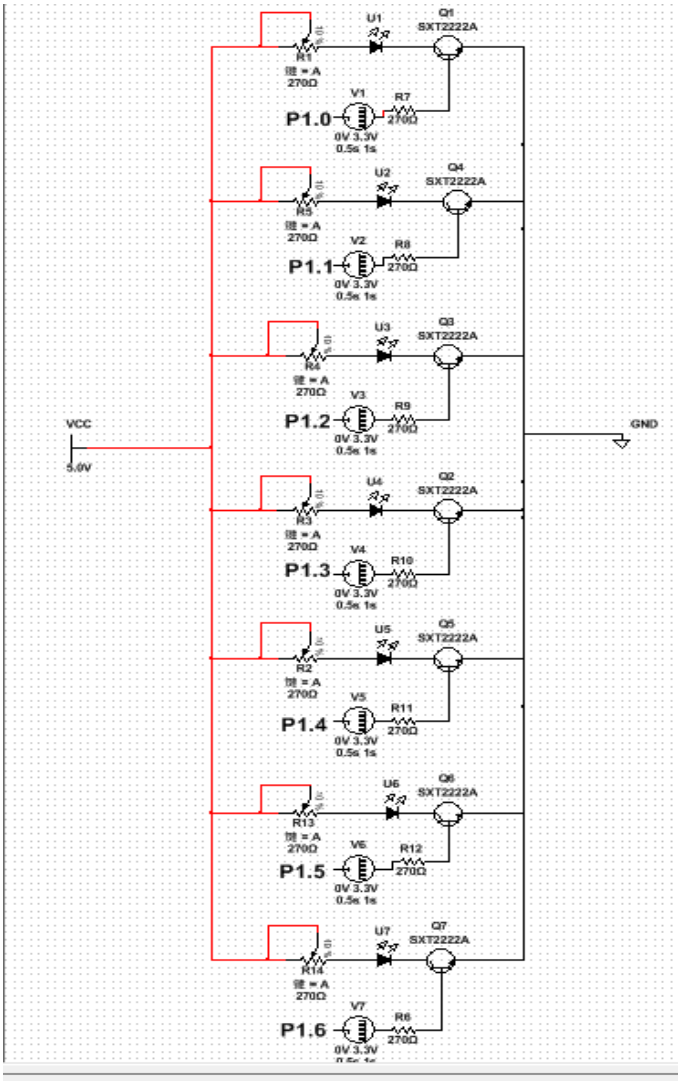

Figure 4 Light emitting diode drive circuit

C. The signal processing

For the subsequent amplification circuit, we adopt OP37 module, which belongs to the amplifier with low noise, precision and high-speed operation. By using the offset current to eliminate the circuit, OP37 can realize low input bias current of plus or minus 10nA and the disturbance current of 7nA.

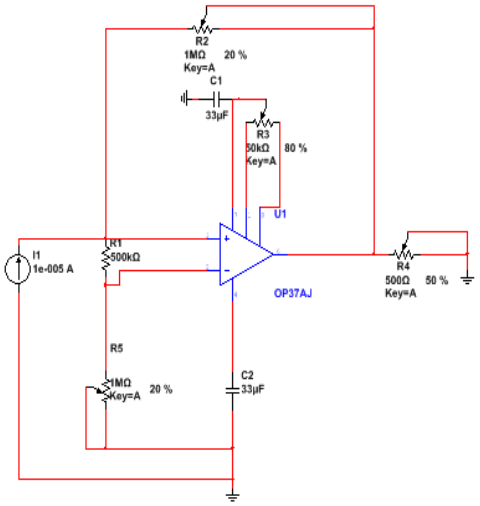

Figure 5 Amplifying circuit

Ⅳ. SOFTWARE PROCESS

A. Upper computer part

The design interface of a software based on labview platform is designed, and the initial communication debugging of the upper computer interface and bluetooth is successful.The interface includes the configuration of various serial port resources; Four waveform window displays the data collected from four groups of leds. The frequency of the sampling and the final data to be collected. This interface is shown in FIG. 6 below.

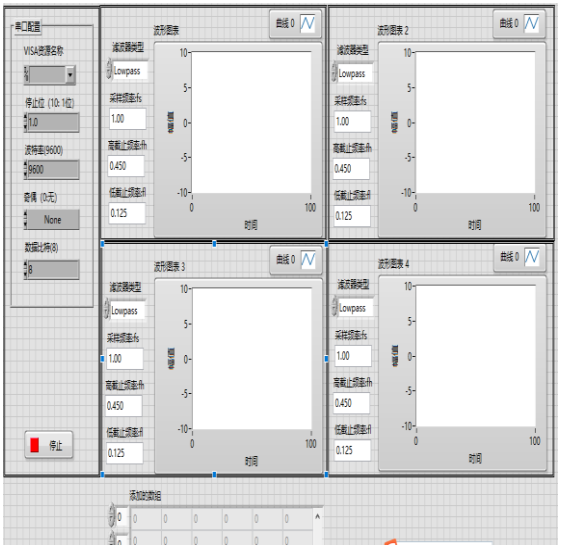

Figure 6 Upper computer processing interface

B. Software architecture

The following is the software flow chart of the subcutaneous fat thickness measurement system near infrared light.

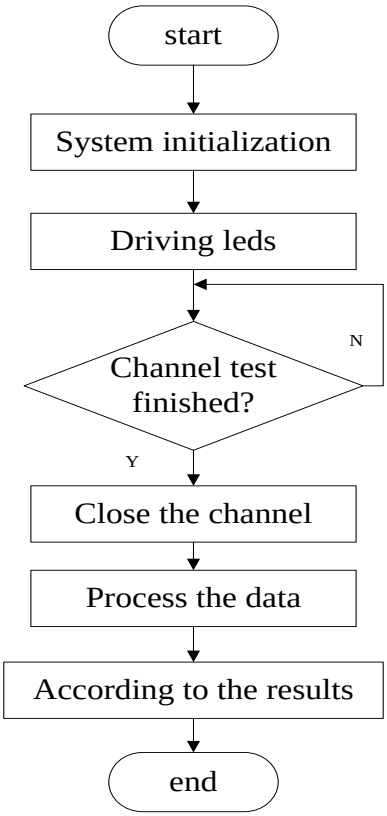

Figure 7 Flow chart of microcontroller program

Building four LED channels with a wavelength of 850nm near infrared light. After a series of processing such as amplifying circuit and filtering, the analog signals are converted into electrical signals by the AD conversion, and the detected data is sent to the upper computer to collect data. The program of upper computer was based on labview. The linear stepwise regression model was established by matlab. Calculate, output and display through the upper computer. The communication between the upper computer and the lower computer is realized through the bluetooth set.

Ⅴ. THE TEST RESULTS

The test results include using waveform diagrams and data tables to display the measured voltage data, and save them in a file for viewing. The following figure is part of the test results for the data.

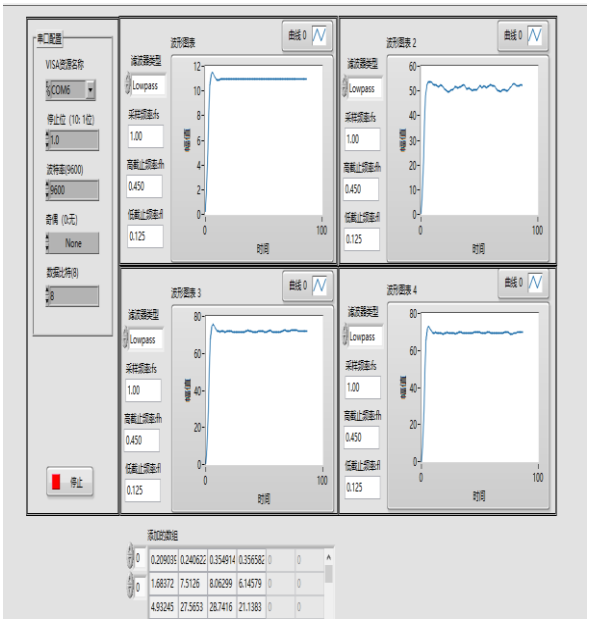

Figure 8 The test results

0. 209039	0. 240622	0. 354914	0. 356582	2018/3/27	8:53:02
1. 683717	7. 512603	8. 062988	6. 145786	2018/3/27	8:53:04
4. 932448	27. 565334	28. 741551	21. 138264	2018/3/27	8:53:06
8. 363337	50. 550095	52. 179212	37. 717306	2018/3/27	8:53:08
10. 515100	65. 688641	67. 566654	48. 106607	2018/3/27	8:53:11
11. 400172	72. 269302	74. 475088	52. 497426	2018/3/27	8:53:13
11. 517372	73. 335897	75. 920294	53. 601164	2018/3/27	8:53:15
11. 332845	72. 239469	74. 980036	53. 666329	2018/3/27	8:53:17
11. 119804	70. 789195	73. 581308	53. 756479	2018/3/27	8:53:19
10. 980457	69. 817849	72. 575993	53. 514656	2018/3/27	8:53:21
10. 920092	69. 538029	72. 063906	52. 768457	2018/3/27	8:53:23
10. 909629	69. 628503	71. 794172	52. 420129	2018/3/27	8:53:26
10. 919886	69. 685038	71. 710560	52. 554023	2018/3/27	8:53:28
10. 933044	69. 494614	71. 965719	52. 369233	2018/3/27	8:53:30
10. 942030	69. 296235	72. 203646	51. 875792	2018/3/27	8:53:32
10. 946117	69. 325224	71. 976796	51. 777266	2018/3/27	8:53:34
10. 946974	69. 327154	71. 622592	52. 153952	2018/3/27	8:53:36
10. 946420	69. 166761	71. 608339	52. 389388	2018/3/27	8:53:38
10. 945612	69. 045407	71. 804499	52. 150191	2018/3/27	8:53:41
10. 945035	69. 045478	71. 963681	51. 571607	2018/3/27	8:53:43
10. 944760	69. 269054	72. 109392	50. 861768	2018/3/27	8:53:45
10. 944694	69. 601859	72. 193710	50. 446406	2018/3/27	8:53:47
10. 944722	69. 688556	71. 980557	50. 108354	2018/3/27	8:53:49
10. 944772	69. 567831	71. 659959	49. 684011	2018/3/27	8:53:51
10. 944809	69. 425112	71. 672825	49. 823758	2018/3/27	8:53:53
10. 944827	69. 300286	71. 761312	50. 249508	2018/3/27	8:53:56
10. 944832	69. 382721	71. 565862	50. 329739	2018/3/27	8:53:58
10. 944831	69. 532560	71. 413114	50. 385504	2018/3/27	8:54:00

Figure 9 The stores the results

Points in the test results have four channels, each channel is different from the light emitting diode of the data as a result, then sampling, take out the relatively stable value of each channel averaging, reduced the accidental error, and reduced the system error.

Ⅵ. CONCLUSION

Firstly, the design of the subcutaneous fat thickness

measurement system based on near-infrared light is described from the hardware and software.Four sets of light-emitting diodes with different distances from the optical receiver are set as the light source, which improves the driving circuit and amplifying circuit of the light-emitting diode, improves the intensity of the light source, and reduces the error.

References

[1] Ma lifang, Guo hongwei. Analysis of the hazards and influencing factors of adult overweight and obesity [J]. Environmental and occupational medicine,2007 24(4):375-378.

[2] Dingdong. Near infrared spectroscopy and its application in biomedicine [D]. Jilin university,2004.

[3] Li wei. Study on the measurement system of subcutaneous fat thickness by ultrasonic method [D]. Hebei university of technology,2015.

[4] Wang yu. Improvement and experimental study of subcutaneous fat thickness measuring instrument [D]. Beijing university of technology,2014.

[5] Lu yanhui. Study on the measurement of subcutaneous fat thickness in the infrared method [D]. Tianjin university,2004.

[6] Zhang yongyu, miao xiaojin, cong tao,et al. Comparison of two measurement methods of subcutaneous fat in abdominal wall [J]. Journal of applied plastic surgery,2002(06):302-303.

[7] Yang zhen gang, yao xingjia, fu qiufan. Trial system of subscale fat thickness measurement [J]. Journal of China medical university,1982(02):32.

[8] HOFFMAN DJ ,WANG Z GALLAGHERD,HEYMSFIELD S B .Comparison of visceral a dipose tissue mass in adult African Americans and whites[J].Obes Res,2005,13(1): 66-74.

[9] LIU J ,CAROLINE S,FOX,et al. Impact of Abdominal Visceral and Subcutaneous Adipose Tissue on Cardiometabolic Risk Factors:The Jackson Heart Study[J]. J Clin Endocrinol Metab，2015,95(12): 5419-5426.

Research on Multi - sensor Data Fusion Bionic

QIAN Chenghui; HU Mengyuan; LI Bingyang; LI Ruilin
(College of Instrument Science and Electrical Engineering, Jilin University)

***Abstract*-Bionic manipulator based on the multi-sensor information fusion technology, use PVDF piezoelectric thin-film sensor to collect the charge signal of four fingers,through the charge-voltage conversion, signal conditioning, and signal acquisition circuit to extract the useful signal sent to the controller. The controller collapses the touch, slip, thermal sensation and the object space state information obtained by 3D modeling, and obtains further action instruction to control the manipulator to adjust the grasping mode. This bionic robot to solve the current majority of robots can only repeat the implementation of fixed action, can not self-adjustment and soft grab and other shortcomings. After testing and analysis, the design of the manipulator can grab irregular shape and fragile objects such as raw eggs in 1.0s, and according to the fusion information reflects the general shape of the object, robot bionic function can be achieved**

***Key words*-integrated information; piezoelectric film sensor; bionic manipulator; 3D modeling**

I.PREFACE

ROBOTS will replace people's heavy labor to achieve the mechanization and automation of production, reduce the risk of accident[1-3], has been used in variety of fields.Currently, the robots on the market mostly just repeat the implementation of a single two-dimensional or three- dimensional fixed action. Based on the multi-sensor data fusion, the bionic manipulator takes four PVDF sensors[4-7] to obtain the piezoelectric signal values collected on the four fingers, and then determine the corresponding finger touch [8] and thermal sensation.And the three-dimensional modeling of the real-time location of the mechanical information for multi-sensor information fusion[9] , all the data analysis, integration and processing, can be roughly grasp the actual shape of the object, and then control the robot to take the appropriate way to grab objects, to achieve the purpose of self-adjusting soft grab.

II. FUNDAMENTAL

2.1. Multi - sensor information fusion principle

The basic principle of multi-sensor information fusion technology[12] is to make full use of multiple sensor resources, through the multi-sensor and its observation information reasonable control and use of multi-sensor space or time redundant or complementary information based on a certain criteria, to obtain a consistent interpretation or description of the measured object. Specifically, the multi-sensor information fusion is:

(1) Using four PVDF sensors to obtain the capture of the target piezoelectric signal;

(2) Transforming the characteristic extraction of the discrete time function data of the sensor, extracting the feature vector representing the observed data;

(3) The pattern vector processing is performed on the feature vector, and complete the target description of the sensor. According to the extracted signal characteristics, the tactile, sliding and thermal sensation signals sensed by the manipulator are judged;

(4) The description data for each sensor on the target are grouped by the same number, which is association. Specific performance for the four fingers of the touch, sliding and thermal sensory signals are divided into three groups;

(5) Each sensor data is synthesized using a fusion algorithm.

2.2. Principle judgment of Touch, sliding and thermal signal

PVDF sensor in the pressure or tensile will produce the corresponding charge in both surfaces, through the charge changes can distinguish between touch or sliding.The tactile signal is a pulse signal, the signal generated by the sliding signal is a series of signals, the tactile signal peak is larger than the maximum value of the wave of the sliding series signal, the thermal signal is a step signal, and then the regression is slow. Which can distinguish between touch, sliding and thermal feel.

III. OVERALL DESIGN

3.1 System design block diagram

The system consists of signal acquisition unit, signal conditioning, sample and hold circuit and A / D conversion unit, central processing unit, servo drive unit, manipulator structure, as shown in Figure1.

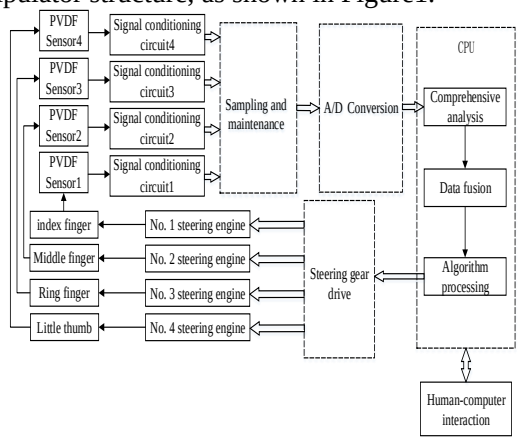

Figure 1 system block diagram

3.2 Signal conditioning circuit design

Since the PVDF sensor[10-11]releases the charge signal, the charge amplifier is first passed through which as a preamplifier circuit during signal conditioning. PVDF has the characteristics of high output impedance, according to the principle of impedance matching, in the charge amplifier circuit

select 10 megohm large resistance to improve the accuracy of the signal. Due to crawl the object when the sliding frequency is not too high, usually below 30Hz. Taking into account the use of power supply frequency 50Hz mains, Because the signal is susceptible to frequency signal interference, so using a low-pass Butterworth active filter in the second step, to cut-off frequency of 40Hz, remove the power frequency interference and high frequency noise. Finally, adding a phase in-phase amplifier circuit, the signal amplification processing, both to improve the signal sensitivity, but also allows the central processor to collect the signal relative error decreases, improve the accuracy of the entire system. Signal conditioning circuit schematic diagram shown in Figure 2.

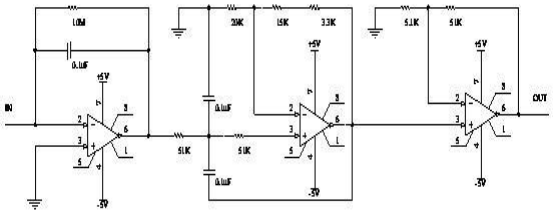

Figure 2 signal conditioning circuit schematic

3.3 A / D sampling analysis

A / D converter is the core of the data acquisition circuit, the A / D converter bits not only determine the analog voltage dynamic range of the acquisition circuit, but also greatly affect the conversion accuracy of the acquisition circuit. Therefore, the A / D converter bits should be selected according to the conversion range and the conversion accuracy of the acquisition circuit. The signal collected by the manipulator is converted into voltage signal by charge-voltage, and then the voltage signal through signal conditioning circuit is 100mV ~ 3200mV. The A / D bit number is calculated as follows:

$$m \geq (20\lg\frac{V_{i,\max}}{V_{i,\min}})/6 = (20\lg\frac{3200}{100})/6 = 6$$

.

Considering the accuracy of the data acquisition system is 1%, then the number of bits m required for A / D is estimated as follows:

$$\frac{10}{2^{m+1}} \leq 1\%$$, then $m \geq 9$.

In summary, the number bit of A / D converter should be greater than 9. As the use of controller is stm32, its internal comes with 12 bit A / D, enough resources, no need to add A / D converter anymore.

IV. DATA FUSION

The multi-sensor data fusion is to synthesize information from multiple sensors or multiple sources, resulting in more accurate and reliable conclusions [12]. The host computer shows the piezoelectric signal of each finger and establishes the three-dimensional model of the object. The working state of the system is obtained by optimizing the combination of touch, slip, thermal sensation and spatial state information of the manipulator, and then the grasping method of the manipulator is adjusted and analyzed and adjusted until the object is grasped without slippery. The fusion process is shown in Figure 3.

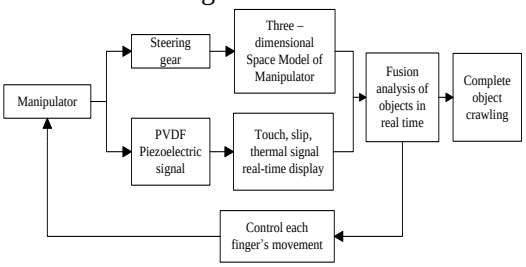

Figure 3 Fusion process block diagram

Establish three-dimensional model of the object on the host computer. Take the left hand of the mechanical wrist as the origin and build the three- dimensional coordinate system, the angle value θ of the manipulator 's steering gear is fitted with the spatial coordinates x, y and z,when θ<108°:

$$x=-0.1048*\theta+17.4$$

$$y=1-0.008*\theta2+0.921*\theta+2.8095$$

When θ<108 °,The finger of the manipulator reaches the maximum degree of bending.

(1) The host computer display finger piezoelectric signal promptly. 1, 2, 3 and 4 mean the index finger to the little finger respectively, which also shows the voltage signal.

(2) First, the controller synthesizes the object space signal and the finger touch signal to analyze the approximate shape of the object, and then analyzes the sliding trend with the different finger's sliding signal to obtain the next step of the manipulator instruction.

(3) The robot adjusts the grab mode according to the job instruction when the object is not completed.

The robot synthesizes the object spatial signal and the finger tactile signal, analyzes the approximate shape of the obtained object, and analysis the next step of the manipulator instruction, then send it to the controller. According to the signal characteristics received by the controller, the thermal threshold is compared first. If the thermal threshold is higher than the set thermal threshold, it is proved that the object temperature is too high to be discarded. If not, the crawling operation is performed. The robot jaws close to the crawled object slowly, if the touch is detected shows that the two contact, so the controller judge the relative position of the current object in the manipulator by collected multi - channel tactile signal data fusion, and then adjust the manipulator so that the finger on the tactile signal is relatively uniform, making the robot in the optimal grasping state.

After receiving the control signal from the central processor, the steering gear in different positions drives the manipulator assembled from the hard aluminum alloy mechanical parts to bend or stretch, the robot attempts to grab the object. The four sensor signals obtained by separating sensor signals are judged by fusion, and the sliding state of the current object is obtained. By adjusting the driving force of each mechanical finger, making the whole object gradually tending to static, at this time, each robot finger on the object of the intensity is relatively uniform. When the

robot does not complete crawling, it adjust the crawl way according to the work instruction, and finally be able to crawl objects successfully, to achieve the purpose of optimal soft crawl.

V. TEST RESULTS

5.1 Thermal signal analysis

At room temperature, the robot is close to the test tube with 72 ℃ water, and the thermal sensation signal perceived by the robot is shown in Figure 4. When the robot feels more than the preset value of 60 ℃, all the mechanical fingers bounce and discard the object.

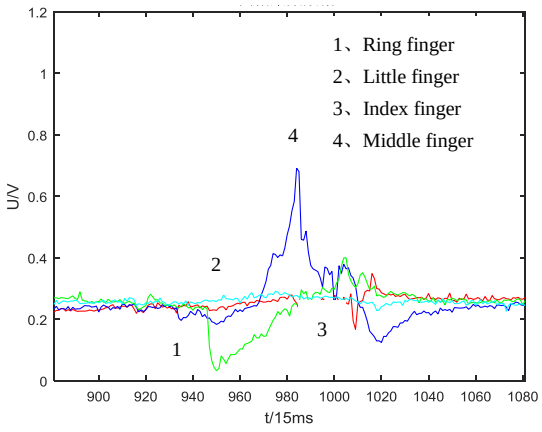

Figure 4 Thermal signal analysis

5.2 The robot grips irregular objects

At room temperature, the robot scratches the irregular objects printed through the 3D printer, the object is shown in Figure 5.

Figure 5 robot grabs irregular objects

Manipulator moved, tried to make four fingers contact with the object completely, the process of collecting the tactile signal shown in Figure 6.

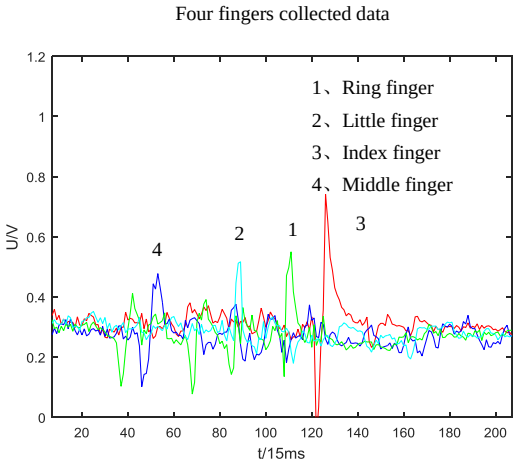

Figure 6 irregular object tactile fusion signal

Tried to grab the object until it did not slide. The slip signal collected during the process is shown in Figure 7.

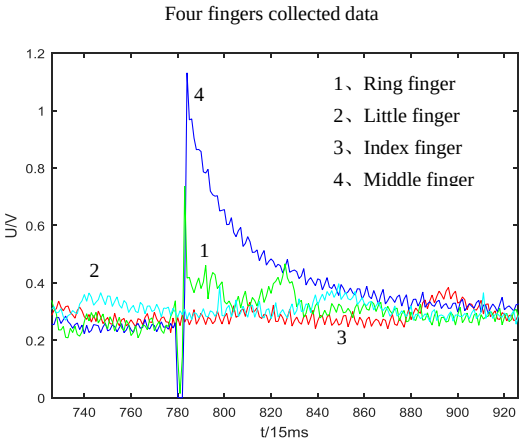

Figure 7 irregular object sliding fusion signal.

The physical space state analysis is shown in Figure 8.

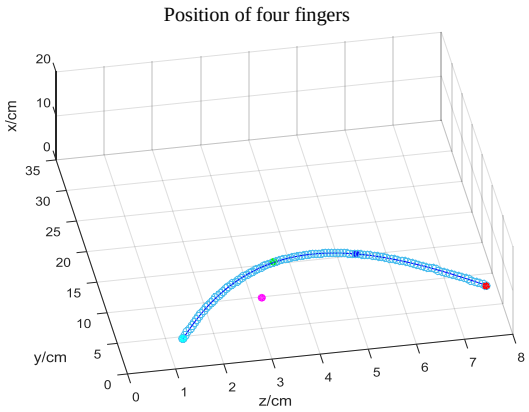

Figure 8 Analysis of irregular object position

The real-time state analysis of the manipulator's object is compared with the actual shape of the object, and it can be seen that the two are basically matched.

5.3 Robot to grab fragile items

As shown in Figure 9, the robot scattered the fragile items of raw egg, and it could be seen that the manipulator grabbed the egg without slippery while ensuring that the egg are not broken.

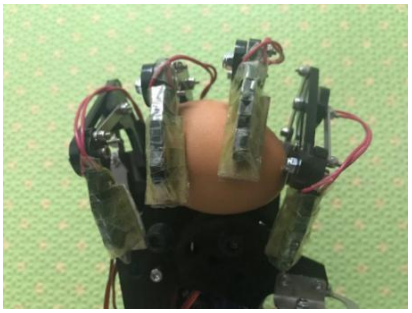

Figure 9 Robot grab fragile items

The tactile signal collected in the process of capturing raw eggs by the robot is shown in Figure 10.

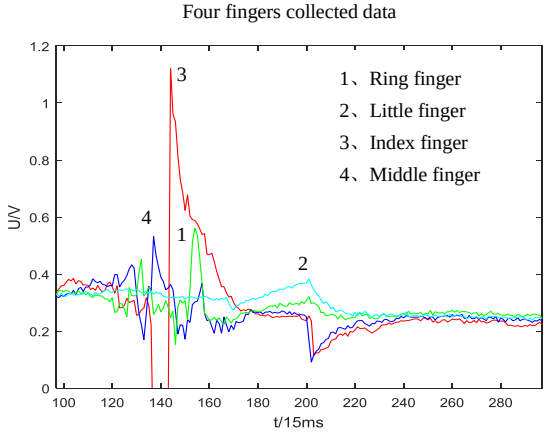

Figure 10 Touch signal analysis of fragile item

Tried to grab the object until it did not slide and then to catch the object. The slip signal collected during the process is shown in Figure 11.

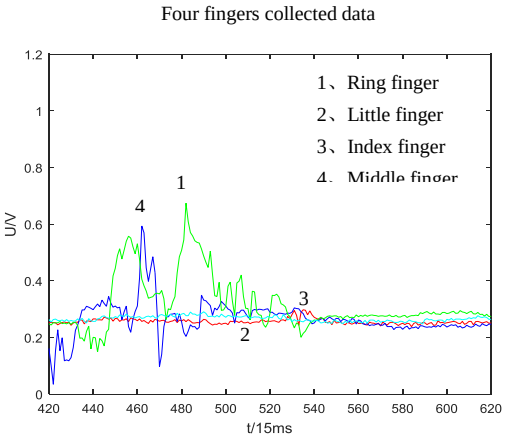

Figure 11 Signal fusion analysis of fragile items

The physical space state analysis is shown in Figure 12.

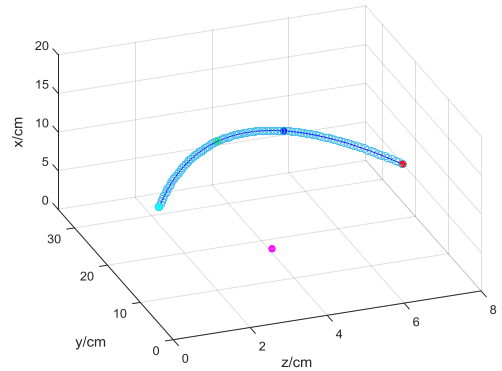

Figure 12 Spatial analysis of fragile objects

The manipulator fetched egg without sliding and without crushing. Analyzed the real-time spatial state of the host computer. Compared with the actual shape of the egg, the two are basically matched.

VI. Concluding Remarks

Bionic robot based on multi-sensor data fusion has some of the human perception function, it can sense the touch, sliding and thermal signal; the host computer establish a three-dimensional model of the robot, the controller analyze the state of the caught object in real-time, quickly adjust the robot's grasping posture and intensity. Bionic manipulator can grab any irregular objects within 1.0s, can safely grasp the brittle objects without breaking them, when close to more than 60 ℃ objects the robot will abandon the crawl and bounce to achieve a bionic function. Bionic manipulator can be widely used in medicine, information, and scientific research, has a good market prospects.

References

[1] BIAN Hongye, HE Shulong, HE Yuanyi, et al. Talking about lightweight robots prospects[J]. Science and Technology Innovation Herald, 2015, (35): 112-114.

[2] HU Ruizhi.Design of five-DOF mechanical arm and the control system[J]. Shengyang: Journal of Northeastern University, 2011

[3] GUO Hongwu.Analysis on the Application and Developmet Trend of Manipulator [J]. China West Technology, 2012, (10): 3+12.

[4] QIAN Chenghui, LIU Hongli, JIANG Yao, et al. A soft fetching manipulator research based on the piezoelectric thin film sensor[J]. Piezoelectrics & Acoustooptics, 2016, (04): 523-526.

[5] LIU Xu, WU Peng, LYU Yanjun. Preparation solution soft flexible PVDF piezoelectric film sensor[J]. Instrument Techniq ue and sensor, 2016, (01): 4-6.

[6] XIN Yi, TIAN Hongying, Jiang Qi, et al. Tactile-slip sense recognition system made of PVDF film based on LabVIEW[J]. Piezoelectrics & Acoustooptics, 2015, 37(05): 793-795+801

[7] XIN Yi, YANG Qingyu, ZHENG Haotian. Study of tactile & slip sensor on structure and signal conditioning circuit design based on PVDF piezoelectric film[J]. Piezoelectrics & Acoustooptics, 2014, 36(01): 76-78+84.

[8] JIANG Mingwen, WANG Rencheng, LUO Zhizeng, et al. Myoelectric prosthetic hand with tactile and slip feedback functions[J]. Journal of Tsinghua University(Sci & Tech), 2004, 44(08): 1051-1053.

[9] HUANG Manguo, FAN Shangchun, ZHENG Dezhi,et al. Research progress of muti-sensor data fusion technology[J]. Transducer and Microsystem Technologies, 2010, (03): 5-8+12.

[10] XIANG Ting, CHEN Jinjun. Soft grabbing manipulator research based on a new piezo- resistive sensor[J]. Manufacturing Automation, 2013, 35(06): 69-71.

[11] SHEN Guowei. Principle and design of the capacitive touch

sensor array[J]. Technology & Application , 2007,(03): 13-15.

[12] YAN Huaicheng, HUANG Xinhan, WANG Min. Multi-sensor data fusion technique and its application[J]. Journal of Transducer Technology, 2005, (10): 6-9.

Design of high voltage reactor inspection equipment

Zhao Zixu; Cai Xinshan; Zhao Zhiwen
(instrument science and electrical engineering institute, Jilin university)

***Abstract*-High-voltage reactor due to corrosion, contamination and other factors lead to reactor partia l burn affect the normal work,aiming at the inspection inside the coil, a device based on single Chip microcomputer was designed; this device consists of the main part of the image collection module and the moving guide rail；in the stepper motor driven, the main part on the rail back and forth movement，at the same time taking pictures or video, and real-time back to the host computer；the article provides two kinds of exercise guide rail options.This device can effectively observe the internal high-voltage reactor and found damaged parts burned. .**

***keywords*-High-voltage reactor; Microcontroller;Image collection; Stepper motor;slideway**

I NTRODUCTION

SUBSTATION high voltage reactor has a number of important role, including weaken the idling time lineman frequency voltage rise, the improvement of line reactive power distribution and reduce the line loss, reduce the power flow, accelerate the latent power of arc extinguishing, improve line automatic reclosing success rate and so on.Series reactor can limit short circuit current and maintain high residual pressure[1] .Corrosion and pollution factors can easily cause local burning of reactor, which can affect the normal operation of electric power system and bring serious economic damage to people's life, industrial production and country.Therefore, once the coil of the reactor is found to be partially burned, it is necessary to locate the burning site immediately, take timely measures to repair the damage, and minimize the loss. Check the internal coil of the reactor regularly, find hidden trouble and defect, and fix it in time[2].

At present, the domestic company has designed a kind of aerodynamic force cars crawling reactor inspection machine, basic consistent condition using reactor coil spacing, the head camera installed in the car, the car has the rubber mass crawl feet, make the car can be just the card between the coil car bottom connection air flushing tube, put the car into the coil spacing, people on the ground with cheer cheer device to power cars, rubber mass crawl feet bobbing up and down, the car moving up, between the camera and back to the coil.This device realizes the internal inspection, image or video data transmission of the reactor, but the disadvantages are also obvious, mainly as follows:1. Use people to provide power, without realizing automation; 2. The wear of rubber skin is too serious and needs to be replaced; 3. There are differences between the coil spacing of the reactor, resulting in real-time adjustment of the length of the crawling foot, which takes time and effort.

In addition, there are some research and design of inspection robots for high voltage lines in China [3-4], but there are few researches on the inspection of high voltage reactor in substation.Compared with the domestic research time of the inspection machine, the research and use of the substation inspection robot in Japan and Canada are also ahead of the domestic market, but the research on the inspection of transformer substation high voltage reactor is relatively rare.

II. APPLICATION OF INSPECTION EQUIPMENT.

A.Demand analysis

The electric reactor used in the substation with high general voltage grade is very large, and the coil spacing is narrow (about 100mm*50mm), and the routine maintenance means can't work. Therefore, a kind of automatic inspection device that can penetrate into the reactor and freely travel through the coil is needed, and the internal image of the reactor coil can be transmitted by the camera in real time, and video display and capture display can be realized through the upper computer[5-6].

Therefore, this design must ensure that the maximum thickness of the whole device is less than the width of the coil spacing (about 50mm), so that the device can be put into the gap to achieve the purpose.

B.Overall structure

This design is a kind of inspection device, especially involving a high voltage reactor inspection device. The design is mainly composed of motor control part, motion sliding block device with camera and guide rail. The sliding block device is placed on the guide rail, and the motor is driven by the movement, and the video data is collected through the camera, and real-time observation is made through the upper computer.

III.MOTOR CONTROL

Under the control of the motor controller, the motor turns and provides the power of the round-trip motion for the device through the power transmission system. The overall block diagram of the motor control system is shown in figure 1:

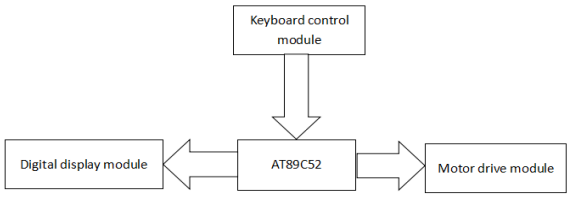

Fig.1 Motor control system overall block diagram

$$\text{Dc motor speed } n = \frac{U - IR}{k \cdot \Phi} \quad (1)$$

Which U as the armature terminal voltage, I as the armature current, total resistance R of the armature circuit, Φ per pole flux, k to the motor structure parameters.

The basic principle of PWM speed regulation control is according to a fixed frequency to connect and disconnect the power supply, and according to the need to change a cycle on and off time ratio (duty cycle) to change the dc motor armature voltage "duty cycle", which changes the average voltage, control the turning speed of the motor.When the motor is connected to the power supply, the motor speed is the maximum v_{max}, and the duty ratio is D=t/T, and the average speed of the motor is $v_d=v_{max}*D$. It can be seen from the formula that the average speed v_d of the motor can be obtained by changing the duty ratio D, which can achieve the purpose of speed regulation.

In the dc motor drive control circuit, the PWM signal is provided by the external control circuit, and after the high-speed photoelectric isolation circuit, the motor drive logic and the amplifying circuit, the switch of the lower arm MOSFET is driven to change the average voltage on the armature of the dc motor, so as to control the speed of the motor and realize the PWM speed regulation of the dc motor.

Ⅳ.DESIGN OF UPPER COMPUTER.

The image collection part of the software is divided into three parts, including video data collection, image display, and to the continuous acquisition of image taking pictures and save at any time, and then respectively using labview graphical programming design, and integrate them together, so as to achieve the expected design video display and capture save target function.

The complete labview main program diagram is shown in figure 2:

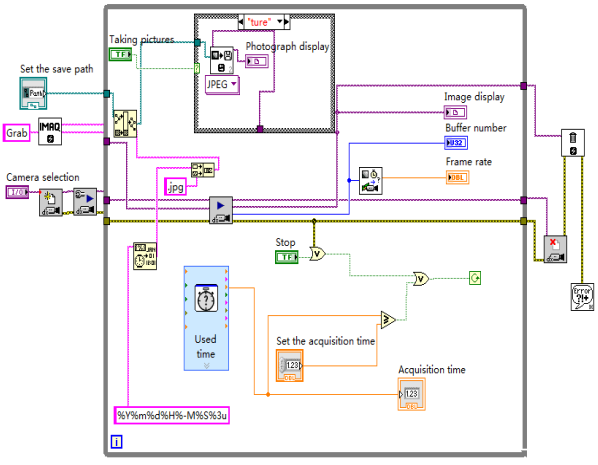

Fig.2 Complete labview main program map

Ⅴ.THE MECHANICAL STRUCTURE

The design of guide rail is the focus of this design, and two designs are given in this paper, which is combined with the motor control system and the upper computer to achieve the desired purpose.

A. Screw guide structure.

This design chooses the screw rod as the guide rail, and the power transmission system also includes the screw and the screw nut, and the upper and lower ends of the screw are connected with the upper and lower ends of the guide rail, and the lower end of the screw is connected with the motor through the coupling through the coupling. The sliding block is provided with a through-hole, and the screw nut is located in the through-hole and is set on the screw.There's a data transfer module on the slide, the data transfer module is connected to the camera, and the camera is connected to the top machine through the data transfer module, which can be a laptop with a monitor, and a cell phone and other terminal devices.Its upper and low end are provided with limit switch, that limit switch is connected with the motor controller, the motor driver is set between the motor and the motor control, the motor drive is set on the base, and the motor controller is provided with a display screen and a control key.The overall structure diagram of the lead rail design scheme is shown in figure 3.

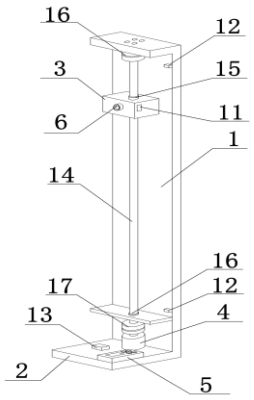

Fig.3 The overall structure of the use of lead screw rail design scheme

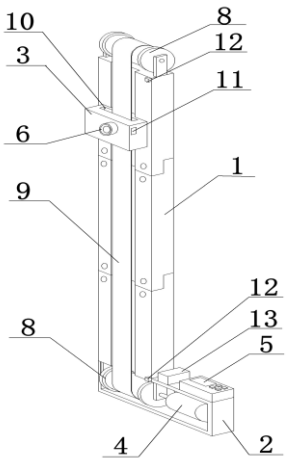

Fig.4 The overall structure of the use of 3D print rail design scheme

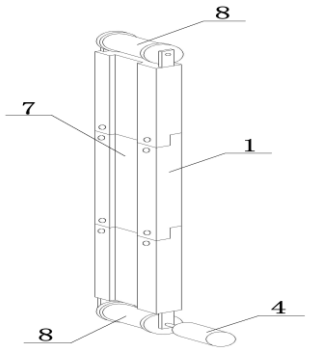

Fig.5 Schematic diagram of rail structure using 3D print rail design

(1、Guide 2、pedestal 3、sliding block 4、electrical machinery 5、machine controller 6、camera 7、chute 8、Transmission belt 9、Transmission belt 10、pass hole 11、data transmission module 12、limit switch 13、motor driver 14、screw 15、screw nut 16、bearing 17、coupling。)

B. 3D printing splicing guide structure.

This is a modular can be spliced type guide rail guideway. The model map of the guide rail unit is first plotted, the track unit is printed out with 3D printer, and the guide rail is spliced according to the actual requirement, the first and the end of each length of guide rail is provided with intermeshing interfaces.It has a chute on the surface of the track, and the slide of the data transfer module and the camera is embedded in the chute, and the motor is driven by the power drive to slide the slide up and down the slide of the guide rail.The power transmission system including driving wheel and belt, the driving wheel is located in the guide rail ends up and down, the bottom are connected to the motor driving wheel; There's a hole in the slide, and the belt goes through the hole in the slide, and it's wrapped around the wheel of the guide rail.

The overall structure diagram of the 3D printing guide design scheme is shown in figure 4. The guide structure diagram is shown in figure 5.

Ⅵ.TEST RESULTS

By comparing the above schemes, the final selection of the screw as the guide rail of the motion carrier has the advantages of: 1. Stable operation and stable image transmission; 2. The mechanical structure is simple, so as to facilitate the connection and assembly; 3. The guide rail will not be affected by external environment; Disadvantages: 1. Because the bottom is not fixed, the noise is loud during the movement; 2. High cost;

Assemble the modules and run the test.

1. The motor can be divided into speed regulation, the maximum speed is about 300r/min, the minimum speed is about 60r/min, and the speed of the moving module under each speed is measured at the speed of the guide rail and the motor speed under each gear. In this way, that motion speed of the motion module in the guide rail can be calculate by measuring the time of the motion module move from one segment to the other at the same motor speed. For every 10 revolutions of the motor, the motion module moves 1cm on the track, calculating the RPM's RPM. The motor speed and motor speed data are shown in table 1 below.

Table 1 comparison of movement speed and rotation speed.

gear	0	1	2	3	4	5
movement speed （cm/s）	1.2	2.4	3.3	4.2	5.3	6.0
rotational speed （r/min）	60	120	165	210	265	300

2. The main program achieves the function.

After testing, the main program can achieve the following functions:

(1) the image information acquired by the selected camera can be displayed in real time at the front panel visual interface specifying area, and the image display is stable;

(2) the image can be captured in the image display, display the position in the visual interface, and save to the specified location, and the saved format name is "snapshot time."

(3) it can read the buffer number and frame rate of the camera in real time and display it;

(4) stop the program when it reaches the set time.

3. Visual interface function and display information.

(1) support the selection of the camera that collects the image information, and then click the corresponding pull-down arrow for selection;

(2) the captured images can be installed at the front panel of the save path, click on the folder to storage location choice;

(3) the acquisition time can be set; in the corresponding box, the acquisition time value is keyed into the corresponding box so as to reach the stop after the setting time is reached;

(4) the large window displays and collected video image in real time; the small window is displayed as the picture of the last capture;

(5) real-time display of collection time, current frame rate and buffer number;

(6) "run", "stop" and "photo" control buttons to manipulate the program;

Ⅶ.CONCLUSION

It is a kind of technical mean for patrol inspection of that substation reactor to use the inspection device to patrol the high voltage reactor of the substation in the high voltage substation.This design has the following advantages:

1. Inspection automation: in this utility model, the microprocessors are used for control, so that the inspection process is automated. The staff only needs to observe and analyze the images received in real time to confirm the internal damage;

2. Flexible and lightweight, easy to operate: the utility model fully takes into account the structure and space limitation of the inspection object, can penetrate into the coil, close inspection coil to burn the area, and send back pictures or video data in real time, and select the suitable guide rails according to the height of the coil in the reactor, and the splicing guide can be freely spliced into a highly suitable inspection device, which is more flexible.

3. Fast and accurate: the patrol device can transmit the internal information to the staff in real time to assess it, so that the staff can quickly and accurately locate the damaged areas of the coils, to repair the damage to the reactor, or to actually assess the potential damage.

References

[1] Zeng zhaohua, li hanxiang. The function and choice of 500kV high voltage reactor [J]. China power, 1993(01):15-18+24.

[2] Li zheng. Research on autonomous patrol robot of high-voltage transmission line [D]. Shanghai university, 2013.

[3] Fu yuan, lu ning, tian yue. On the key technology and development trend of substation inspection robot [J]. Electronic technology and software engineering, 2014,(03):145.

[4] Shou-yin lu Zhang Ying jian-xiang li, MuShiYou. Mobile robot application in high voltage substations [J]. High voltage technology, 2017 lancet (01) : 276-284.

[5] Zhang tingyu. Research on high-voltage line inspection robot [D]. Shanghai university,2009.

Intelligent wearable devices for patients with Alzheimer's disease monitoring

Qiu Shilin; Lv Yuemeng; Qin Zichang
（instrument science and engineering institute, jilin university）

***Abstract*-Alzheimer's disease is a very common disease and is very harmful to the elderly. At present, there is no effective cure for Alzheimer's disease. It can only reduce the harm of Alzheimer's disease to the patient, family and society through nursing. Alzheimer's disease is a chronic disease and the nursing cycle is long, so it often causes great physical and mental stress to the nursing staff. In order to reduce the patient's pain and relieve the burden of the caregivers, an intelligent wearable device based on signal acquisition and wireless communication is developed. On the one hand, it can monitor the patient's behavior in real time. The PVDF sensor is closely attached to the sole of the patient, and the foot pressure changes are acquired through collection, charge / voltage conversion and conditioning circuit to determine the behavior, inform the nursing staff and ensure the safety of patients. On the other hand, we can locate the patient's position information by GPS and notify the caretakers in real time by SMS, and the device has the function of emergency notification. This smart wearable device adapting to Alzheimer's patients can help the caregivers take care of the patients and ensure the safety of the elderly.**

***Keywords*-Intelligence Care Wearable PVDF GPS GSM**

Ⅰ. INTRODUCTION

ALZHEIMER'S disease patients generally have different degrees of cognitive impairment and memory loss. At present [1], there is no effective treatment for Alzheimer's disease, so after the patient's disease, most of them will choose the family care model. The main reason is that after the onset of Alzheimer's disease, the development of the disease is slow, the time of hospitalization is long, and the cost of medical treatment is huge, so we choose to take home care. The method of family care is most simple, such as putting the paper on the way of family contact, hiding the dangerous items and other physical methods. However, most of the patients are accompanied by abnormal behaviors, which often cause stress to the nursing staff, even lead to the decline of the health level of the family members of the nurses, the weakening of the immune system function, and the increase of cardiovascular events such as hypertension [2]. In order to ensure the safety of Alzheimer's patients and relieve family caregivers, a smart wearable device [3] was developed to help care for patients.

For the protection of Alzheimer's patient safety, and reduce the pressure of family care, we have developed a set of intelligent wearable device to help care for the patients[3].

Ⅱ. OVERALL DESIGN

Wearable devices are mainly divided into two parts, smart socks and portable positioning devices. As shown in Figure 1.

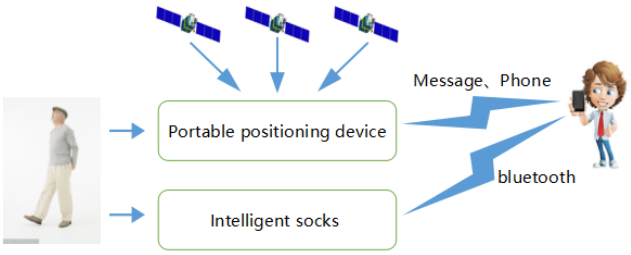

Fig.1. Wearable device schematic

Smart socks[4-6] consist of a signal acquisition unit, signal conditioning, A/D conversion unit, and a central processing unit and a Bluetooth module, which can sense patient behavior and notify family members by sensing changes in the plantar pressure of the patient. It can effectively relieve physical and mental stress caused by 24-hour care and prevent dangerous behaviors such as midnight and sleepwalking.

The portable positioning device[7-9] consists of a GPS module, a GSM module and a processor. The main function is to obtain patient location information through satellite positioning, and can be sent to the family's mobile phone via SMS, or you can press the emergency button to call the stored number.

Ⅲ. WORK PROCESS DESIGN

According to different functional requirements, two STM32F103C8T6 are used to control separately, and according to the following work flow and hardware platform, the corresponding program is written to achieve the required functions.

A. Smart Socks Work Process

Detection of plantar pressure in patients with Alzheimer's disease uses a PVDF sensor. Since the output signal is weak, the charge integral amplification circuit and the low-pass filter circuit ensure that the signal is accurate and stable while obtaining the best amplification effect. After A/D conversion, the processor converts the analog signal to a digital signal and determines whether the value exceeds the rated value. When the patient is lying down, the pressures on

the sensor is small and close to zero; when the patient sits on the ground, the pressure changes significantly and exceeds the rated value, and the patient's caretaker is notified via Bluetooth.

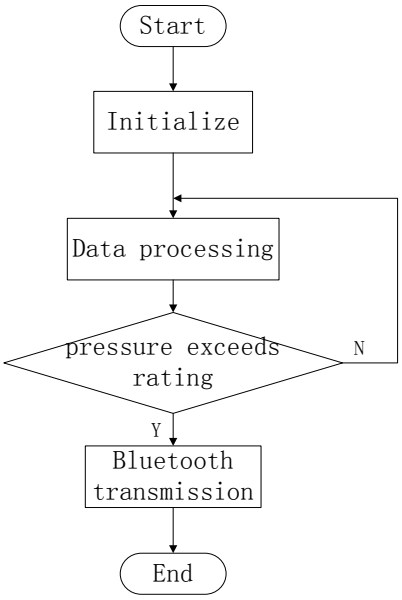

Fig.2. Work flow chart of intelligent socks

B. Portable Positioning Device Work process

After the portable positioning device is powered on, module communication test and GPS positioning will be performed first. When ready, enter normal working condition. When the patient is lost, the family member can send a short message with a content of "GPS" to the device. When the device receives the short message, it will send a short message containing the patient's location information to the stored mobile phone number, so that the patient's family can quickly find the patient and ensure the safety of the patient.

Similarly, when the patient realizes that he is lost or in danger, he can press the emergency button on the device. When it is detected that there is a button press, the device will call the stored mobile phone number and send it a short message containing patient location information to remind the patient's family.

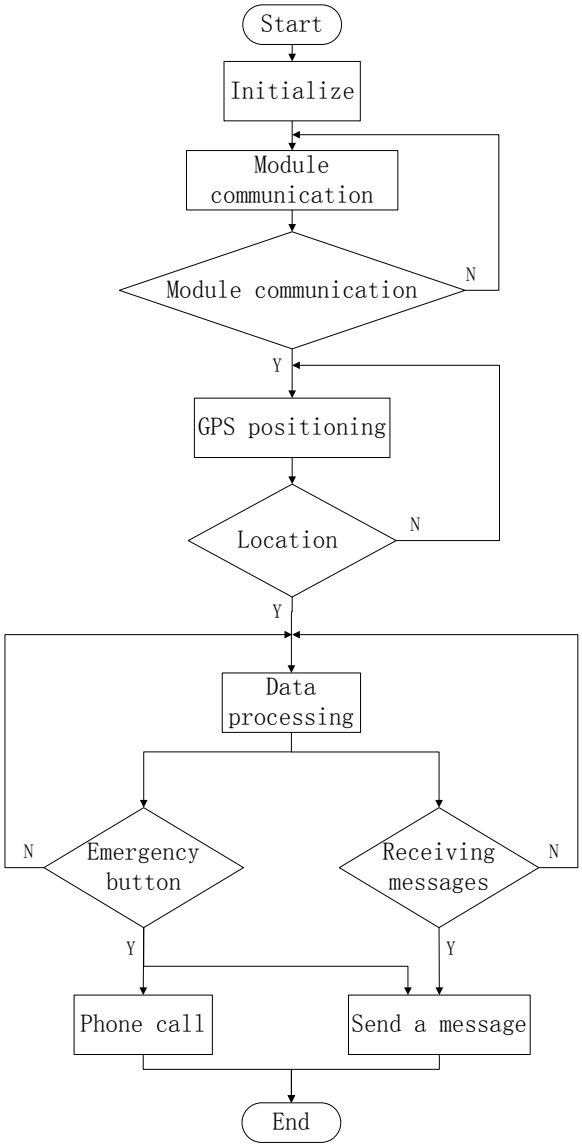

Fig.3. Portable positioning device work flowchart

Ⅳ. HARDWARE DESIGN

A. Smart Socks

(1). Design of signal conditioning circuit

PVDF piezoelectric thin film sensor is used as sensing material to make the sensing core of the plantar pressure sensor. When it deforms, it will release the charge signal. So when the signal is processed the charge amplifier should be selected for the preamplifier circuit.

Because one of the characteristics of PVDF is higher output impedance， and the impedance matching principle, a 10 MΩ large resistance resistor is selected at the first stage of charge amplifier circuit, so as to improve the accuracy of the signal.

Human walking step frequency is generally not more than 10Hz, in order to eliminate the high frequency interference, so it is necessary to level second to two order Butterworth low-pass filter, cut-off frequency is 20Hz.

$$\omega_c = \frac{1}{R_3 \times C_3} \tag{1}$$

$$f_c = \frac{1}{2\pi\omega_c} \quad (2)$$

In the formula, the ωc is the characteristic angular frequency and the fc is the cut-off frequency.

At the last stage, the same direction amplifying circuit is added to amplify the filtered signal. It not only improves the signal sensitivity, but also reduces the relative error of the signal collected by the central processor, and improves the accuracy of the whole system. The schematic diagram of the signal conditioning circuit is shown in Figure 4.

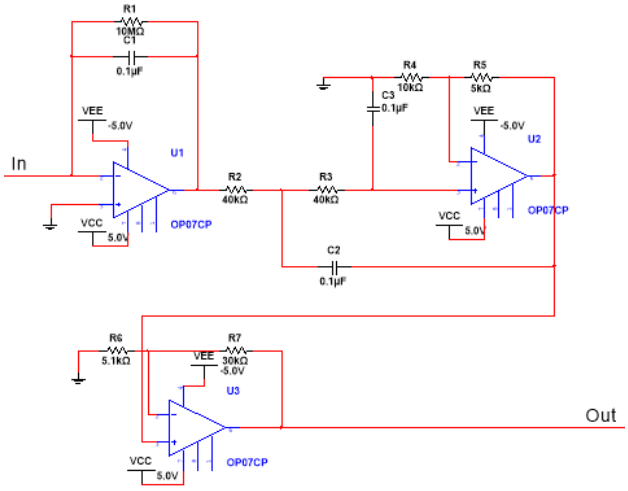

Fig.4. Schematic diagram of signal conditioning

(2). A/D conversion and Data processing

STM32F103C8T6 internal analog digital converter (ADC), using T to represent the clock cycle of the analog to digital converter after 6 frequency division of the clock cycle of the controller. That is, ADCCLK=12MHz. The conversion time can be calculated by the next type.

$$Tcovn = t_0 + t_c \quad (3)$$

$$t_c = 12.5T$$

In the type: Tcovn is the total conversion time, and t0 is the sampling time.In this program, the software is set up and the conversion time is the sampling period.

Because the frequency of the input signal is smaller and it only uses 1 channels of 1 ADC, it is easy to draw the conclusion that the sampling rate is far greater than the required frequency, and satisfies the sampling requirement.

The analog signal output from the signal conditioning circuit is converted to digital signal through ADC. The processor processes it, judges the pressure of the sensor and the patient's behavior, and transmits the result to the Bluetooth module.

Bluetooth sends the signal to the upper computer. The upper computer software recognize the Bluetooth serial port and judge whether the patient's family should be reminding to the signal.

B. Portable Positioning Device

The GPS receiver of the terminal receives the location data from the satellite every second, calculates the coordinates from its geographical location based on the data from more than three different satellites.The coordinate data is sent to the guardian cell phone in the form of latitude and longitude by short message, so that we can locate patients on the mobile phone map according to the coordinate information.

Meanwhile, when the patient is in an emergency, it can manually press the emergency button through this device. The GSM module calls the pre stored cell phone number and sends the location short message to remind the guardian.

Ⅴ. Experimental Results

When the patient walks on both feet, the pressure changes acquired by the PVDF piezoelectric film sensor are obvious, as shown in Figure 5.

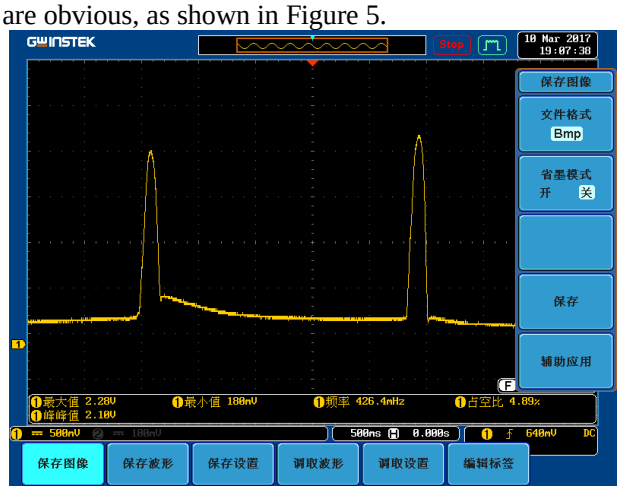

Fig.5. Patient walking signal changes

When sending a short message to GPS, it will receive a short message containing location information; when the button is pressed, it will receive a phone and a short message with location information.

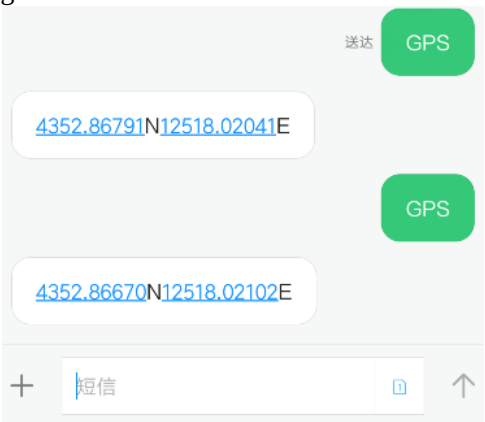

Fig.6. About receiving short messages

Ⅵ. Concluding Remarks

This suite is applicable to Alzheimer's patient's smart wearable devices, combining Alzheimer's patient care with smart devices.

It can monitor in real-time whether the patient will perform dangerous behavior such as getting out of bed or sleepwalking at night, or it can locate the patient

position in real time to prevent the occurrence of lost patients. This will help caregivers take care of patients, reduce the difficulty and burden of care, and ensure the safety of patients.

References

[1] Sun wei,Liu Xiaoting. Status of nursing research on Alzheimer's disease [J]. Overview.2015 (01).

[2] Xiong Lina, Jin Yanfei, Jin Changde.Research on the psychological intervention of family members of patients with Alzheimer's disease [J]. Review.2015(02).

[3] Liang Lijun, Hu Yao, Liu Hao, Li Xiaojiu, Li Jin. The status and prospect of wearable devices [J]. International textile journal,2016, (10) :62-64.

[4] Shu Fangfa, Jiang Shoushan, Zhang Xin, Ma Li. Application of PVDF piezoelectric film in the measurement of foot pressure [J]. Piezoelectric and acoustic light.

[5] Duan Jianrui, Li Bin, Li Shuzhen. Advances in the research of new flexible sensors [J]. Review and review.2015 (11).

[6] Jin Man. The development of measurement insoles of foot pressure distribution [D]. Donghua university 2010.

[7] Zhao Guoqiang, Ren Li. Construction of GPS data processing platform based on GAMIT/GLOBK [J]. Mapping geographic information,2016, (01) :37-42.

[8] Chen Jiqing. Design and implementation of handheld positioning device [D]. Dalian maritime university 2009.

[9] B.Hofmann-Wellenhof,H.Lichtenegger,J.Collins.Global Positioning Systems: Theory and Practice. 2001.

Electronic metal coin sorting device based on eddy current testing method

FAN Yao-long; MA Tian-lu; LIU Kai
(College of Instrumentation and Electrical Engineering, Jilin University)

***Abstract*-The eddy current testing method has been widely used in coin identification detection due to its characteristics of no contact, relatively low cost, and high detection speed. Based on the eddy current testing method, a metal coin identification and sorting system was designed. The system uses STM32F407 as the core of data processing and control. The L298 module is used to drive the motor. Through the control of the software part, the hardware structure passes through the horizontal direction. A conveyor belt is used to send a number of input coins to the detection section one by one, and the detected coins are then sorted by vertical conveyor belts. The detection method is based on the principle of electromagnetic induction. Using self-made simple inductors, each type of coin results in different magnetic permeability μ due to different materials, and has different influence on the induced magnetic field. The signal is digitized through AD conversion and compared with the initial sensing signal to determine the coin value or sheet metal material of the coin. Through trial and error, the coin sorting accuracy meets the design requirements and has a high degree of practicality.**

***Key words*-Coin sorting; eddy current testing; AD conversion; STM32; signal processing**

I. INTRODUCTION

COINS are widely used in transportation, commerce, communications, entertainment, and various vending systems due to their advantages such as low wear, durability, and ease of use.

Multiple countries study coin counting equipment. Japan's GLORY Co., Ltd. produced the WR-400c Coin Counting and Packaging Machine, Switzerland's SCANCOIN Co., Ltd. produced small coin sorting equipment such as the SC22, and LAuREL produced Lac-16, Laurel LPS-25, etc. including coin sorting and packaging. Large-scale integrated processing equipment [1]. The main feature of these structures is the large number and speed of coin sorting, but the structure is complex and expensive.

In recent years, China's research in this area has also made some achievements. However, due to technical problems that cannot be produced in batches and the occasions when large-scale processors are adapted are limited, generally small banks such as banks do not purchase them and cannot be widely used. Although small-scale coin processors are sold on the Internet at home, most sorting performances are unstable, and missed picking or wrong picking often occurs. Therefore, it is significant to study a small, highly reliable coin separation device [2-3].

This subject compares commonly used coin detection methods, weight detection method, eddy current testing method, and image analysis method, and finds that using the eddy current method, one of the two inductors is used as the transmitting end, and the other is used as the receiving end. The transmitting end and the receiving end face each other. When there is metal When the coin passes through, the induced electromotive force changes significantly, and the change of each coin is different, which can effectively measure the types of coins, and the cost is very low. Combined with the innovative design of the hardware structure of the device, rapid coin sorting can be realized.

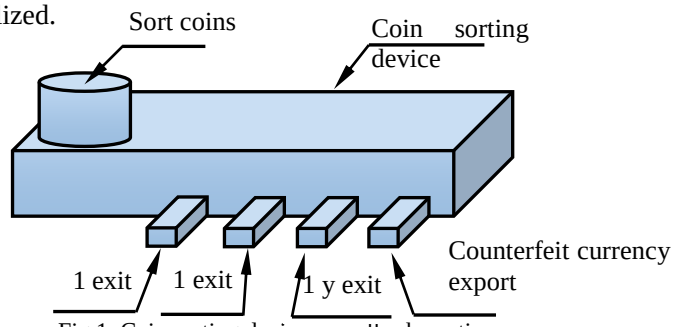

Fig.1 Coin sorting device overall schematic

II. DESIGN

A.Overall mechanical structure

Coin separation device consists of 4 parts, the overall structure:

(1) Picking station: stacking coins vertically and feeding them into the pusher;

(2) Pusher: Each time a coin is introduced into the sorter;

(3) Detector: push the coin over the coil to complete the measurement;

(4) Sorting belts: Different kinds of coins are sent to different exits.

The top of the picking table is designed as a bowl, ensuring that a large number of coins can be placed at the same time. The bottom is designed as a cylindrical body with a diameter of 27 mm. As the coins fall freely, they can be automatically arranged in a vertical row. There is a gap of 2mm between the cylindrical pipe and the inspection platform, ensuring that only one coin is pushed out by the pusher at a time. The characteristics of the coins are shown in Table 1. The pusher is driven by the motor through a belt and pushes a coin through the detection device to the sorting belt. After sorting according to eddy current testing, the sorting belt stops at the corresponding coin outlet and sorts the coins. The overall structure of the device is shown in Fig. 2 [12]

Table 1 The fifth set of RMB coins standard parameters

Value	Category	Diameter（mm）	Thickness（mm）	Material	Weight（g）
1y	coin	25	1.85	Nickel plated steel core	6.1
5j	coin	20.5	1.65	Steel core copper plating	3.8
1j	coin	19	1.67	stainless steel	3.2

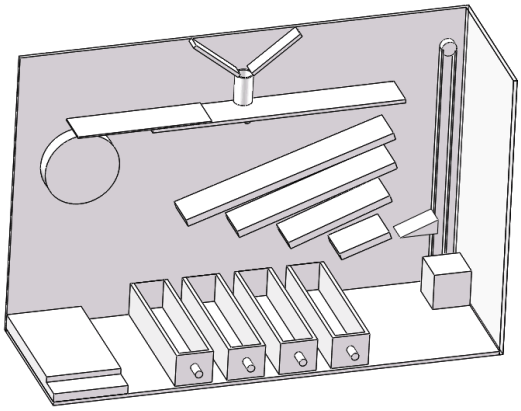

Fig.2 Coin sorting device structure diagram

B.Eddy Current Detector Design

According to Faraday's law of electromagnetic induction, when an AC signal is passed through an exciting inductor, an AC magnetic flux is generated so that the secondary coil induces an AC signal of equal frequency. When the metal passes between the two inductors, the magnetic flux changes and the sensing signal then occurs. Change, by observing the induction coil induced changes in the electromotive force, find the minimum [7]. Because of the difference in surface area and the metal material of the coin, the minimum value of the voltage is also different, so that different kinds of metal coins can be judged. The excitation inductance and inductance are shown in Figure 3 below.

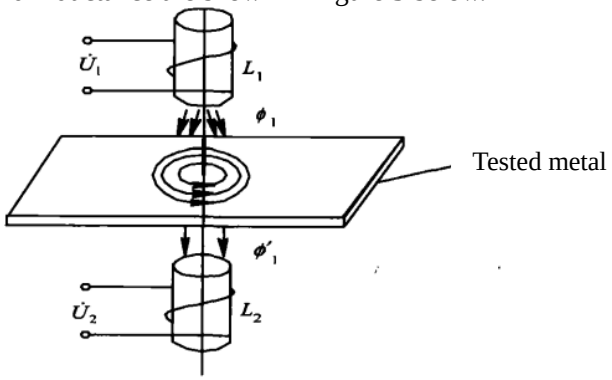

Fig.3 Induction coil eddy current testing principle

C．Drive motor options

Option one: DC motor. DC motor is a rotary motor that can convert DC energy into mechanical energy, and can convert DC energy and mechanical energy into each other. The advantages are good start and speed control performance, wide speed range, strong overload capacity, and low electromagnetic interference. However, the structure of the DC motor is complex, and it is inconvenient to use and maintain, and DC power is required.

Option Two: Digital servos. The digital steering gear is divided into a 180-degree servo and a 360-degree servo according to the steering angle of the servo. The advantage of the digital servo is that the power to excite the motor can be adjusted according to the microprocessor's program calculation to adapt to different functional requirements and optimize the performance of the servo. Digital servos provide higher accuracy and better fixing force. In addition, there is the advantage of anti-shake and fast response.

Option Three: Stepper motor. Stepper motors are open-loop control elements that convert electrical pulse signals to angular or linear displacements. In the case of non-overloading, the speed of the motor, the position of the stop depends only on the frequency and number of pulses of the pulse signal, and it is not affected by load changes. Its rotation is performed step by step at a fixed angle. By controlling the number of pulses to control the amount of angular displacement, so as to achieve the purpose of accurate positioning; at the same time can control the pulse frequency to control the speed and acceleration of the motor rotation, so as to achieve the purpose of speed control.

In view of the above three options, since the gear is connected to the belt for transmission and the stepper motor is more accurate in the transmission control, the third option is selected.

D．Control system options

OptionOne: 51 series microcontrollers. Using AT89C52's minimum system version, although it can realize the control of stepping motor, but taking into account the high-speed acquisition of the signal and a large number of data processing, 51 microcontroller capacity is limited, so give up this program.

OptionTwo: FPGA solution. FPGAs are field-programmable gate arrays with a large number of internal flip-flops and I/O pins. FPGA is a complex programmable logic device. It has flexible programming, high integration, short design and development cycles, and FPGA has great advantages in high-speed signal generation and processing. FPGAs have great flexibility in programming and are suitable for completing sequential logic.

OptionThree: STM32 series microcontrollers. The STM32F407 microcontroller with ARM Cortex-M4 core from ST company is used as the control core, including external crystal oscillator module, AD, 3.3V regulator module, basic I/O port and a series of rich peripherals, which can meet the requirements of the system. A large number of data analysis and processing capabilities, and can improve the accuracy of the timing, with high cost performance, low power consumption, comprehensive consideration of the use of the program

three [6].

Ⅲ. EDDY CURRENT TESTING CIRCUIT DESIGN

A. Signal generation circuit design

Using an RC bridge oscillator circuit, the feedback coefficient of the feedback network is

$$F_v(s)=\frac{V_f(s)}{V_o(s)}=\frac{sCR}{1+3sCR+(sCR)^2}.$$

Available $s=jw$, $w_0=\frac{1}{RC}$ then the formula becomes when $w=w_0=\frac{1}{RC}$ or $f=f_0=\frac{1}{2\pi RC}$, the magnitude of the amplitude-frequency response is the largest, that is, the phase-frequency response phase angle is zero, that is to take R = 8200Ω, C = 1nF, then $f_0=\frac{1}{2\pi RC}=19.4$ [15]. Circuit simulation schematic shown in Figure 4.

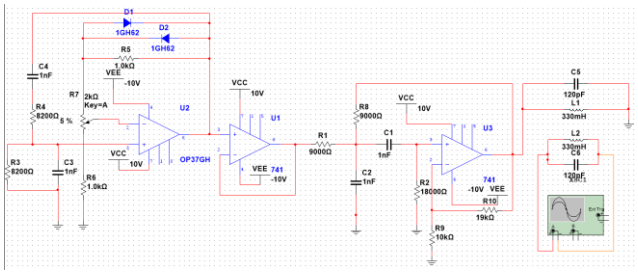

Fig.4 Signal generation circuit schematic

B. Center frequency calculation

When making the inductance of the detection part, it is necessary to ensure that the frequencies of the two parts remain the same. According to the formula $f=\frac{1}{2\pi\sqrt{LC}}$, when the inductance is a fixed value of 330mH, after the actual measurement f is within the range of 10kHz-20kHz, the voltage value changes most obviously, so the capacitor selects 120pF.

C. Filter circuit design

$$A(s)=\frac{A_{sf}sCR}{1+(3-A_{sf})sCR+(sCR)^2}$$ In the formula, the voltage gain of the same amplifier circuit is the same, and the circuit can work stably.

$$A(jw)=\frac{A_0\frac{1}{Q}\frac{jw}{w_0}}{1-(\frac{w}{w_0})^2+j\frac{w}{w_0Q}}=\frac{A_0}{1+jQ(\frac{w}{w_0}-\frac{w_0}{w})}$$

At that time, the circuit had a maximum voltage gain of R=9000Ω, C=1nF, and =17.7K (Hz). The circuit simulation principle is shown in Figure 5 [17].

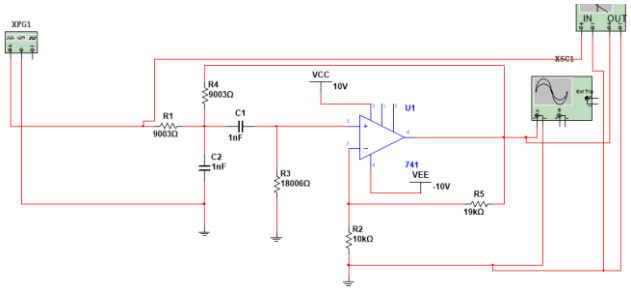

Fig.5 Filter circuit schematic

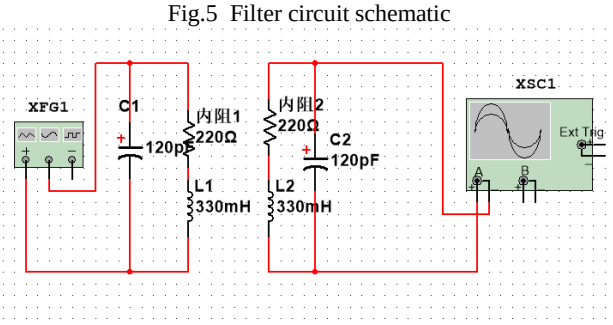

Fig.6 Detector circuit schematic

Ⅳ. COIN SORTING DEVICE DESIGN

The system is mainly composed of a transmission module, a detection module, a control module, a power supply module, and a display module. The transmission part is selected by controlling a stepping motor, and a self-made eddy current detector is used for detection, and the detection information is collected into the STM32 controller for processing. , Control the realization of the sorting process, and finally display the information statistics of the coins detected on the TFT touch screen. The system design block diagram is shown in the figure.

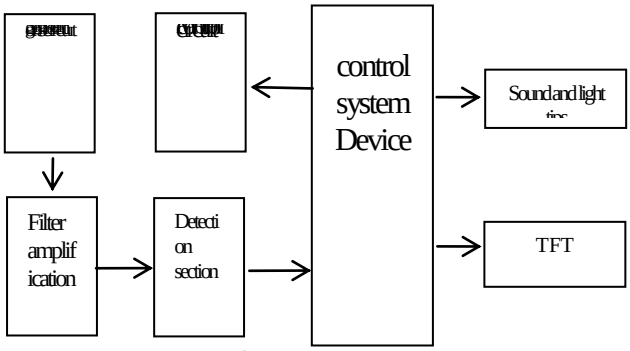

Fig.7 System Design Diagram

Ⅴ. EXPERIMENTAL RESULTS AND ANALYSIS

A. Detector measurement

In order to verify the performance of the eddy current detector, the voltage value of the inductive coil when the different kinds of coins pass the detector is measured before the experiment as the standard value of the next detection, and the feasibility of the eddy current detection scheme is further verified. After the measurement, the test data of the induced voltage are shown in the following table, and the direct difference of each coin can obviously be classified.

Test conditions: Check multiple times, the simulation

circuit and the hardware circuit must be exactly the same as the system schematic, and the check is correct. The hardware circuit guarantees no welding.

Test Instruments: High-precision digital millivoltmeters, analog oscilloscopes, digital oscilloscopes, digital multimeters, analog multimeters.

Table2 Test data for induced voltage of each coin

inductance	capacitance	fre	Vpp	1yuan	5jiao	1jiao	false
330 mH	68nF	3.5 kHz	14.6v	664 mv	544 mv	776 mv	888 mv
330 mH	120pF	18.5k Hz	20.4v	472 mv	544 mv	624 mv	720 mv

B. Actual measurement

In order to better illustrate the performance of the coin sorting system and its correctness, Table 3 lists the correctness of coin sorting performed by the device under different experimental conditions, and it is possible to achieve a single type of coin at the sorting speed. Ten picks are sorted in minutes, and 15 coins of mixed types are sorted for two minutes. In the sorting process, the display can display the coin types and quantities in real time. The physical map is shown below.

Table3 Experiment data under different conditions

species	total	Correct number	Correct rate
1 y coin	10	9	90%
2 j coin	10	10	100%
1 j coin	10	9	90%
False coin	5	5	100%
mixing	15	14	93%

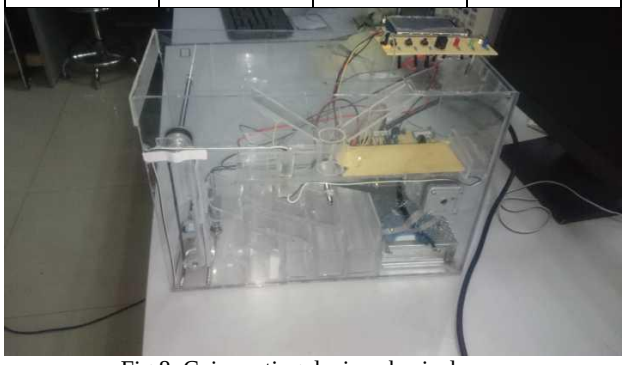

Fig.8 Coin sorting device physical map

VI. CONCLUSION

Through the above findings, this article starts from practical problems and uses Faraday's Law of Electromagnetic Induction to find that the coin, due to the difference in material and shape, will affect the magnitude of the induced voltage generated by the induction coil when it passes through the transmission coil and the induction coil. The induced voltage is amplified by a fixed factor, and the induced voltage generated by different types of coins is used as a reference value. By contrast, automatic classification and collection of coins can be achieved. In addition, through the use of stepping motors and the use of the potential energy from top to bottom of the coins in the structure design, this article speeds up the sorting speed of the entire device, thereby improving the efficiency of coin sorting. In summary, the entire device took full advantage of the eddy current testing method, using self-made eddy current sensors, to achieve a great degree of cost reduction, coupled with the device's high rate of sorting accuracy, so it has a certain universal in practical life applications Sex and reliability.

References

[1] SHEN Xiaojun, TANG Shanshan, ZHAO Dong, LI Shuai, JIA Jun. Design and research of coin separation device based on vibrating screen [J/OL]. Science and Technology Economic Market, 2018(01):8-9[2018-03-20].http://kns.cnki.net/kcms/detail/36.1122.N.20180313.1352.010.html.

[2] Zhu Junda. Sorting and counting of coin sorters [J]. Technology and Market, 2018, 25 (02): 168.

[3] Zhang Changyu,Ning Lijia,Hou Jun,Wang Wei,Chen Zhe.Design of hard sorter based on eddy current sensing[J].Heilongjiang Science,2018(02):34-36.

[4] Gong Linan. Design of Automatic Coin Sorter Control System Based on STM32[J]. Electronic Manufacturing, 2017(23):66-67.

[5] Kang Zhiqiang, Cheng Ruifeng, He Qiuming. Innovative Design of Coin Sorting Machine with Overlapping Track Fusion Belt[J]. Mechanical Design and Research, 2017, 33(05): 68-72+92.

[6] Yang Zhonghan. Design of Metal Coin Sorting Device[J]. Agricultural Development & Equipment, 2017(06):72-74.

[7] Qian Hongzhi, Hu Tianli, Chen Zhi, Xi Jiajun. Design of a smart coin sorter based on STC80C51 single chip microcomputer[J]. Wireless Network Technology, 2017(09):58-59.

[8] Yang Zhangfan. Automatic coin sorting device based on photoelectric sensor [J]. Equipment Manufacturing Technology, 2017(03): 259-261.

[9] Li Huiqin, Ding Li, Wang Peiyun, Wu Yawen, Liu Yonggan. Development Status and System Design of Coin Sorter[J]. Henan Agriculture, 2017(04):55-56.

[10] Xia Kaihu, Wu Wenjin, Xia Hui. Design and research of a new coin sorting mechanism[J]. Heilongjiang Science and Technology Information, 2017(04): 101-102.

[11] Lin Jun, Zhao Xinyue. Design of Simple Electronic Coin Sorting Device [J]. Shandong Industry Technology, 2016(23):141.

[12] Hao Zhiwei, Liu Sicong, Cheng Yaya, Tian Shiyong, Shang Shangli, Ma Zhihao. Design of a New Coin Sorting and Packaging Machine[J]. Science and Technology Innovation Herald, 2016, 13(22):68-70.

[13] Ding Fengjuan, Hong Tengbiao, Chen Kangdi, Gao Shuaishuai, Meng Fansheng, Chen Feng. Design and

manufacture of the fifth RMB coin sorter[J]. Journal of Anhui Science and Technology University, 2016, 30(05): 71-74.

[14] Lin Xianxin. Coin automatic sorting count display device [J]. Guangxi Education, 2016 (27): 188-189.

[15] Lei Yonggang, Wei Peidong, Hou Wenlong, Han Shikang. Design and implementation of a simple coin sorter[J]. Henan Science and Technology, 2016(07):61-62.

[16] Huang Hongxia. Discussion on Double Eddy Current Testing Method in Coin Identification and Sorting[J]. Science & Technology Information, 2012, 36(36):67+69.

[17] Dong Xianglong. Design and Research of Coin Sorting and Packaging Machine with Automatic Sorting and Automatic Discrimination [D]. Donghua University, 2010.

[18] Coin Sorting Counting and Packaging Machine [N]. China Packaging News, 2004-01-21(003).

Design of mobile intelligent microwave heating control system based on microcontrollers

Liu Yezhao; Yu Fengjun; Guo Qixuan
（College of Instrument Science and Electrical Engineering, Jilin University）

***Abstract*-In the process of microwave heating of food, the main influencing factors are: the types of food, the initial temperature of the food, the quality of the food. Because of the different types of food, although the initial temperature and the same quality, but the heating time is not the same for the same kind of food, because the quality of different heating time is not the same. And. The heating temperature requirements of different cooking different foods. And now use microwave oven on the market when we can only through their own experience to determine the heating time and heating temperature. But it is very difficult for some people who are not good at cooking. So, we hope that through these problems This study can solve the above problems, give people convenience and increase the practicability of microwave heating**.

***Keywords*-Microwave heating Microcontrollers Control system**

I. INTRODUCTION

As an emerging energy, microwave has been widely used in heating, drying, food processing, insecticidal sterilization and biomedicine. Microwave heating is essentially a medium heating, and its energy is generated inside the heating material. [1]Compared with ordinary heating, microwave heating has the advantages of fast heating rate, high thermal efficiency, uniform heating and easy to realize automatic control.[2] As one of the household electrical appliances, microwave ovens have been widely entered people's lives, its type also develops from the initial mechanical control to the current computer control. Usually the user according to the experience, takes the form of key presses, heating time, because everyone's experience is different, so the set of control time also exist certain differences. Under the traditional control method, microwave heating time in the process of cooking.

II. SYSTEM HARDWARE DESIGN

A.System Block Diagram

The overall block diagram of the system is shown in figure 1.Mainly by microwave heating module, main control unit module, pressure sensors, temperature sensors, data collection and processing module, buzzer hint module, electromagnetic relay control module and so on several parts.By pressure sensors measure the weight of food, by temperature sensor measuring the temperature of the food, data module to collect feedback back to the main control unit, main control unit with a buzzer hint, electromagnetic relay control the action of all simulation component.The temperature and pressure signal is processed by the PID signal through the single chip I/O output, which is the trigger pulse of the thyristor.It can control the duty ratio of the magnetron and realize the power adjustment of the microwave heater to achieve the purpose of heating food time and temperature.

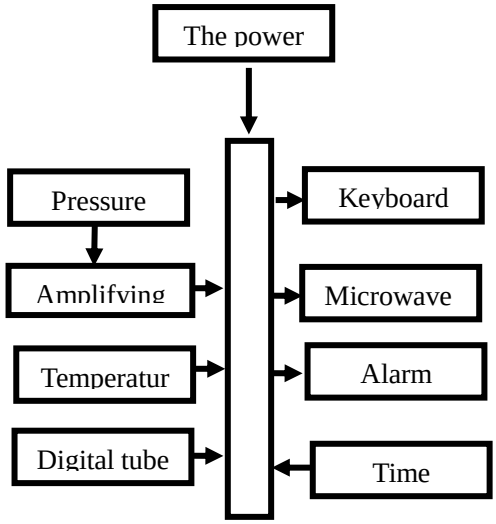

FIG. 1 overall block diagram of the system

.B.SCM core control module.

The main control chip USES STM32f103zet6, which has the features of simple interface, fast working speed and low power consumption.[3]

STM32 development board by pin PB0, PB1 and pin PG11 receives respectively from the value of pressure and temperature module, the quality of the measured object is obtained by formula conversion and the measured temperature, and the two Numbers by pin PB10, PB11 and PB12, PB13, transmitting numerical PB15 display module.

C.Pressure test module

Resistance pressure variable type pressure sensor, circuit of voltage changes, the signal transmission to HX711 amplification and A/D transformation chip to produce A digital signal (duty cycle changes), again through the STM32 board PB0 and PB1 pin to 32 chip, chip will receive digital object is obtained by formula conversion quality.

The principle diagram of the pressure sensor +HX711 module is shown in figure 2.

D.Temperature test module

After feel temperature DS18B20 temperature sensor, circuit voltage changes, the signal through the STM32 board PG11 pin to 32 chip, chip will receive digital by A/D conversion and the measured temperature is obtained by formula conversion.

The principle diagram of DS18B20 temperature module is as follows:

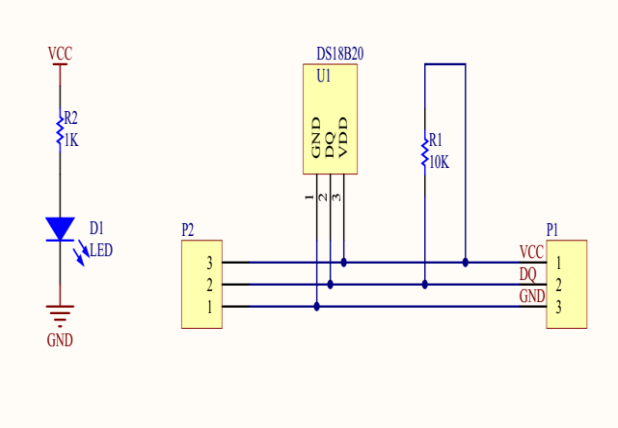

FIG. 2 schematic diagram of DS18B20 module.

E.OLED Display Module

12864 OLED LCD screen by pin PB10, PB11 and PB12, PB13, PB15 receives the STM32 development board after the data sent, through their own program definition glyph, location information, such as the quality and temperature values displayed on the screen.

F.Microwave Heating Module

Magnetron is an electrical vacuum device used to generate microwave energy.It is essentially a diode in a constant magnetic field.Tube electron in perpendicular constant under the control of constant magnetic field and electric field, interacts with the high frequency electromagnetic field, and transform from a constant electric field energy into microwave energy, so as to achieve the aim of producing microwave energy.[4]

The magnetron consists of a tube core and a magnetic steel (or electromagnet).The structure of the core consists of four parts: anode, cathode, energy output device and magnetic circuit system.Maintain a high vacuum inside the tube.[5]

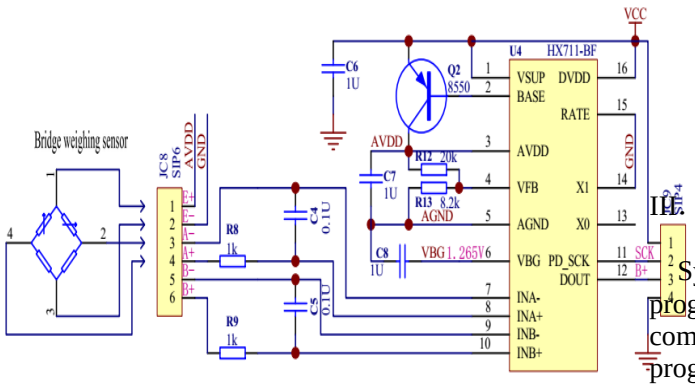

FIG. 3 schematic diagram of HX711 module

a. The anode is one of the main components of the magnetron, which together with the cathode forms the space between the electron and the high frequency electromagnetic field.Under the action of a constant magnetic field and a constant electric field, the electron completes the task of energy conversion in this space.The anode of the magnetron is the same as the anode of the ordinary diode, and it also plays a decisive role in the oscillation frequency of the high-frequency electromagnetic field.

b. The cathode of the magnetron is an electron emitter and an integral part of the interaction space.The performance of the cathode has great influence on the performance and life of the tube, and is regarded as the heart of the whole tube.There are many types of cathodes, with different properties.In continuous wave magnetron, it is commonly used in direct heat type cathode. It is made of tungsten wire or pure tungsten wire in spiral shape, and the electric current can be heated to the specified temperature.

c.The energy output device is a device that transfers the microwave energy produced in the interaction space to the load.The function of the energy output device is no loss, no puncture through the microwave, to ensure the vacuum seal of the pipe, and to make it easy to connect with the external system.The small power continuous wave magnetron is mostly used in the field of the high frequency magnetic field of the anode resonator.A coupling ring is placed, and when the flux varies across the torus, the high frequency induction current will be generated on the ring, which will lead the high frequency power to the outer ring.The larger the coupling ring area, the stronger the coupling.[6-8]

d.When the magnetron is working normally, it requires a strong constant magnetic field, and its magnetic induction intensity is usually thousands of gauss.The higher the working frequency, the stronger the magnetic field.The magnetic circuit of the magnetron is the device that produces a constant magnetic field.

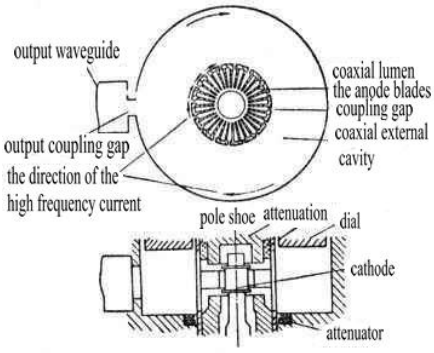

FIG. 4 structure of the magnetron.

III. SYSTEM SOFTWARE DESIGN.

System software design mainly USES C language programming, in KeiluVision4 environment debugging complete.It mainly includes the main control module program, the reload module program, the temperature measurement module program, the display module program, the heating module program, the interrupt service program.

A. Main Control Module Workflow and Program design.

The flow chart of the main control part is as Figure 5.

B.The Program design of Measurement Module

The program consists of three parts: first, initialization;Second, data collection and data processing;The third is the transmission of data, and the processed data is sent to the master chip via serial port.

HX711 is used as A/D conversion device for this module, and the communication between HX711 and MCU consists of A serial communication mode composed of Sck and Dout.When Dout from high level to low level after Sck pulse input 25 at A time, will be 24 bits A/D convert data into single chip microcomputer, and during the next 25 A clock pulse to choose good conversion of input channel and gain.

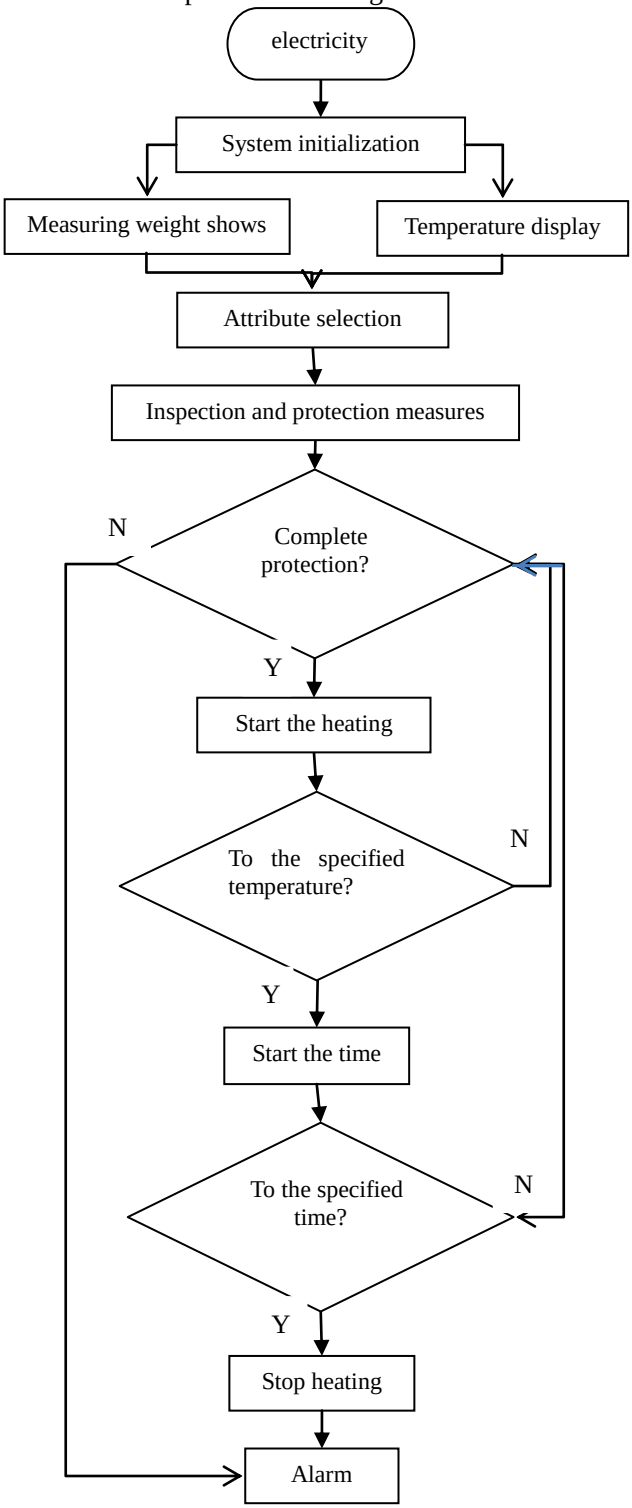

Figure 5. Flow chart of main control part.

C.Design of Temperature Measurement Module.

Typical temperature DS18B20 reading process is: reset, hair SKIP ROM command (0 XCC), hair began to convert command (0 x44), time delay and reset and send the SKIP ROM command (0 XCC), hair read memory (0 xbe), continue to read the two bytes of data (i.e., temperature),end.[9-12]

The temperature of DS18B20 is read by the DS18B20_Get_Temp function. The return value of this function is the short plastic data with symbol, and the range of return value is -550~1250, which is that the temperature value is increased 10 times.

D.Display Module Program Design.

The relevant setup steps required for OLED display are as follows:

a.set STM32 to connect with the OLED module;

In this step, we set the IO port connected with the OLED module to the output, and the specific IO ports are used, which needs to be determined according to the communication mode set by the connection circuit and the OLED module.

b.initialize OLED modules;

In fact, this is the content of the above initialization block diagram, and the display of OLED is started by initializing the OLED related registers.Prepare for subsequent display characters and numbers.

c.displays the characters and Numbers to the OLED module by function.

E.Heating Module Programming.

The heating time/temperature is determined by the following fuzzy rules:

If m ={very light}and c ={small}then time/temperature =0.6625;

If m ={light}and c ={small}then time/temperature = 1.3250;

If m ={light}and c ={small}then time/temperature = 1.9875;

……

If m ={heavy}and c ={large} then time/temperature =4.5.[13]

Table 1 fuzzy rule determination table.

	Mass/ kg
Very light	0～ 0.2
Light	0 .2～ 0.4
Secondary	0 .4～ 0.6
Heavy	0 .6～ 0.8
Very heavy	0 .8～ 1.0

According to the distribution of food specific heat capacity, the fuzzy sets are defined as follows:

Table 2 fuzzy set of specific heat capacity

	Birerong/(kJ/ kg·℃)
Small	0～ 1.5
Secondary	1 .5～ 2.5
Large	2.5～ 3
Very high	Over 3

In order to facilitate the interaction of human-computer information, we temporarily replace the fuzzy types of food with the following: starch (small), vegetable (medium), meat (large), and water (large).

Secondly, through the research, we have all kinds of representative food from room temperature rise to

edible theory of time and the actual time of microwave heater heating, and compared to them, find out their relative error, as follows.[14-15]

Table 3 comparison of theoretical heating time with actual heating time.

type	g	temperature/ ℃	time/ s	time/ s	error
vegetables	300	27	132	135	.2%
	500	27	198	205	.4%
	700	27	263	269	.2%
	900	27	329	337	.4%
meat	300	27	106	110	.6%
	500	27	159	164	.3%
	700	27	212	218	.8%
	900	27	265	274	.3%
Starch	300	27	97	100	.3%
	500	27	145	149	.7%
	700	27	193	201	.9%
	900	27	242	251	.6%
water	300	27	115	119	.4%
	500	27	173	179	.4%
	700	27	230	237	.3%
	900	27	287	295	.7%

Through the above table, we found that the relative error between the actual heating time and the theoretical heating time is still relatively low enough to meet the normal use demand.

IV. CONCLUSIONS

After testing, the device has reached the preset requirement and can automatically determine the heating time according to different food types,different quality and different temperature.

This study focuses on the problems that are difficult for people who are not good at cooking in real life, and designed a simple and easy to operate microwave oven.The weight and temperature of the cooking object are detected to control the heating time and temperature.Solve the problem that microwave oven function is single and easy to operate.

References

[1] programmable microwave controller system design [J]. Wang xiaoli. Laboratory research and exploration. 2009(01)

[2] design specification of small micro-controller system [J]. Christian Siemers. Modern manufacturing. 2005(27)

[3] micro-controller system development and micro-controller development system shallow knowledge [J]. Xing zhongzhu. Electronic technology application. 1998(09)

[4] design of the translation door controller system based on AT89C51 [J]. Xu koming. Electronic production. 2012(10)

[5] design of programmable controller based on single chip microcomputer [J]. Zhang li. Innovation guide for science and technology. 2010(29)

[6] research and design of intelligent microwave controller [J]. Wang xiaoli. Information technology. 2008(09)

[7] design of programmable microwave controller system based on 89C52 [J]. Cao weifang, che linlin, yuan qinghui, cui dong. Science and technology information (academic research). 2007(26)

[8] intelligent control system design of microwave oven [J]. Wei yunmao, xiao huihui, li chuan, zhou taowen, Chen zhonghua. Journal of chongqing institute of technology (natural science). 2007(12)

[9] design of microwave controller system based on FPGA [J]. Gao yiling, zhao weidong, zhang xiujuan, ni qian, zhang jian. Fujian computer. 2005(12)

[10] A current-mode dual-slope CMOS temperature sensor. Hung C,Chu H. IEEE Sensors Journal . 2016

[11] Study On a Novel Optical Fiber Pressure Sensor. Guang Wang,Yiton Fu, et, al. IEEE . 2008

[12] A CMOS Thermistor-Embedded Continuous-Time Delta-Sigma Temperature Sensor with a Resolution FoM of 0.65 pJ℃2. C.Weng,C.Wu,T.Lin. IEEE Journal of Solid State Circuits . 2015

[13] Re-view:semiconductor piezoresistance for microsys-tems. ALVIN B,WOO T P,JOSEPH R M,et al. Proceedings of Tricomm .2009

[14] Direct Al-Al contact using low temperature wafer bonding for integrating MEMS and CMOS devices. LIN H,STEVENSON J T M,GUNDACH A M,et al. Microelectronics Journal . 2008

[15] Sensitivity analysis of packaging effect of silicon-based piezoresistive pressure sensor. TSUNG L C,CHEN H C,CHUN T L,et al. Sensors and Actuators .2009

Design of vehicle wine driving tester based on single chip microcomputer

Lian Ning; Guan Zhe; Zhang Lei
(College of Instrumentation&Electrical Engineering, Jilin University)

***Abstract*-Aiming at the limitation and error of single alcohol sensor information acquisition point in vehicle side alcohol test system, multi-sensor, including alcohol, body temperature and pulse detection, are used to improve the reliability of the results. The system uses STC89C52 as the main controller, sensor selection MQ-3 semiconductor alcohol sensor, ST188 photoelectric sensor, temperature sensor, SMC1062A (thin film transistor liquid crystal display) as the display module, the design of a self testing, when the three vital signs of abnormal automatic alarm and notify the police and family vehicle alcohol detection system. The experimental results show that the design can effectively reduce the cost, prevent the driver from drinking and driving effectively, and it is also very effective to prevent other illegal driving.**

***Keywords*-STC89C52 MQ-3 Vehicle wine driving test system Sensor SMS platform**

I. INTRODUCTION

AT present, the popularity of cars is higher and higher. Meanwhile, traffic accidents are also increasing. More than 50% of accidents are related to drinking and driving. Drunk driving has become the first "killer" of traffic accidents[1]. And many drivers often have a fluke after drinking, and they don't know enough about the serious consequences of drunk driving so that they cause the tragedy of drunk driving[2] Now the traffic police checkpoints on the road, using a portable alcohol detector to make quick judgments of drunk driving, drunk driving behavior but very scattered, causing police work pressure, but the efficiency is not high, prone to leakage phenomenon of drunk driving driver fled. In this paper, a vehicle concentration detection system based on embedded system is designed. The system combines embedded technology and sensor detection technology to monitor alcohol concentration in real time, and effectively control the occurrence of drunk driving[3].

II. PRINCIPLE OF SYSTEM WORK

A. System design structure

The embedded based vehicle alcohol concentration detection system can be divided into two modules from the system design: unit detection module and core control module. The unit detection module is mainly used to collect user information and detect the concentration of alcohol in the car. The core control module is mainly used to handle the schematic diagram of the design structure of the unit detection system, such as the data transmitted from the Module shown in Figure 1 and the corresponding control action. When the driver enters the car, the engine is in a closed state and can not be started. After the alcohol sensor is preheated, the alcohol concentration in the car is detected. After the alcohol sensor detects, the voltage signal is proportional to the alcohol content. Therefore, the alcohol concentration in the car can be judged according to the voltage signal.

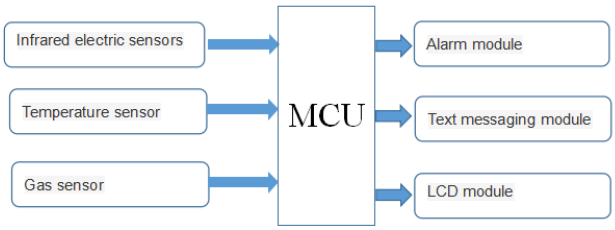

Fig.1 System design schematic diagram

When the alcohol concentration in the car exceeds the set value, the relay contacts are operated, the ignition circuit is disconnected, and the car is unable to start, which produces a sound alarm signal; conversely, the relay does not send out an action by the electric shock. The car is allowed to start [4]. In addition, when the driver enters the vehicle to start, if the alcohol concentration in the vehicle is detected to exceed the standard, the ignition circuit is cut off, The sound alarm. LCD monitor is used to display the alcohol concentration in the vehicle in real time. The basic information is sent to the driver's relatives or the traffic control department through the GPRS module [5].

III. HARDWARE DESIGN

1. Pulse detection circuit

The function of this part of the circuit is to transform the pulse signal into electrical signal by the sensor, which is usually tens of MV. It must be amplified to achieve the voltage required for the shaping circuit, usually a few volts. The amplified signal waveform is irregular pulse signal, so it must be filtered and plastic, the output voltage of the plastic circuit should meet the requirements of the counter. ST188 photoelectric sensor uses infrared photoelectric converter. It acts on the blood flow of human fingers through infrared light and transforms pulse pulse into electrical signal. Its principle circuit is shown in Figure 2.

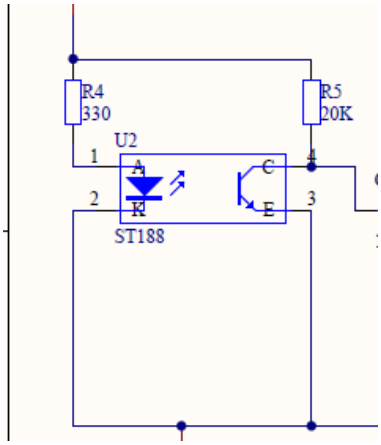

Fig.2 Circuit diagram of the principle of sensor signal adjustment

The infrared tube VD uses ST188. Using a +5V power supply, R1 takes 150 Omega, R2 takes 33K Omega, when people put their fingers between the light emitting diodes and the photodiodes, light

The signal received by the diode varies with the change of the pulse intensity.

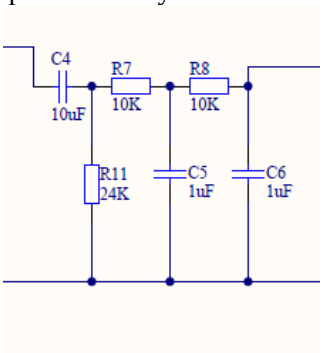

Fig.3 Amplifying filter circuit

2. Amplifying and shaping circuit

After amplification and filtering, the pulse signal is still irregular pulse signal, and has low frequency interference. It still does not meet the requirements of counters. It is necessary to use the shaping circuit. Here we use the hysteresis voltage comparator, as shown in Figure 4, the purpose is to improve the anti -interference ability. The integrated op amp adopts the LM358, in addition to LM358, a LED is also used to indicate the state of pulse pulsation.

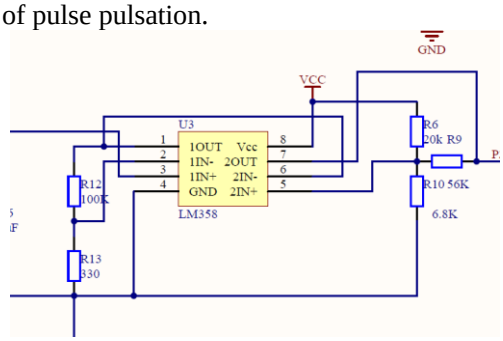

Fig.4 Waveform shaping circuit

3. Detection circuit for alcohol concentration

Two tin oxide using MQ-3 (Sn O2) as a gas sensor, when the sensor in the presence of alcohol vapor environment, the sensor conductivity increases with the increase of alcohol gas concentration in the air, using a simple circuit to change the conductivity conversion and signal for thecorresponding to the gas concentration [6] . The main features are:

But with the signal output instructions.

※ The dual channel signal output (analog output and TTL output).

※ The TTL output signal is low.

※ The analog output voltage of 0~5V, high concentration of high voltage.

※ I have a very high sensitivity and good selectivity to ethanol vapor.

※ It has long service life and reliable stability.

※ The fast response characteristics.

The physical drawings are shown in Figure 5, as shown in Figure 6.

Fig.5 Reverse side diagram of MQ-3

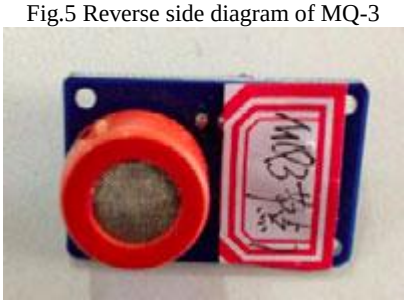

Fig.6 MQ-3 front face diagram

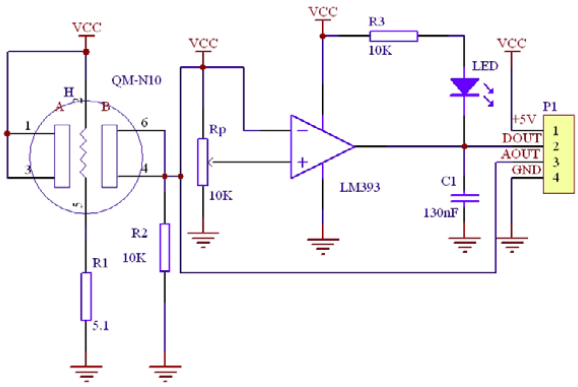

Fig.7 MQ-3 working principle circuit diagram

4. Liquid crystal display module

The liquid crystal display is used in LCD12864, the main consideration is that the LCD12864 is a 4 bit /8, 2 bit parallel wire or 3 wire serial interface mode, the resolution is 128 x 64, 8 x 4 line can display 16 x 16 dot Chinese characters can also complete graphical display, low voltage and low power consumption is also a remarkable characteristic

5. Hardware design of GPRS module

The module uses Goouuu-A6 GSM development board, communication module, support Chinese short message can be used to transmit voice and data signals, Short Message it supports TXT and PDU format, and the use of serial communication module, the RXD and

the TXD pin respectively with the MCU TXD, RXD connected to send commands and data.

IV. SOFTWARE PART DESIGN

1. Software development environment

With the continuous development of communication technology, the function of single chip microcomputer is more and more powerful, and the speed is improved. The compilation environment is also emerging, such as IAR, Keil and so on [8]. The software is designed in assembly language, C language, JAVA language and so on. It provides a convenientfor the development of the vehicle alcohol system software [9] . The vehicle alcohol detection system is based on STC89C52 as the main controller. Under the environment of MDK development, the software is written in C language.

2. The software structure of the syste

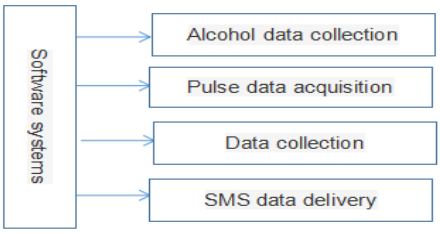

Fig.8 Software structure diagram

The software system structure is shown in Figure 8. The main structure is to integrate and display the alcohol content and pulse data collected by analog circuit, and use the corresponding algorithm to determine whether the driver involved in drunk driving. The use of MQ-3 alcohol detection sensor detects alcohol content, infrared photoelectric sensor fingertip photoelectric signal driver filter amplifier incoming MCU to compute, get the pulse data, and 18B20 as the temperature sensor to provide auxiliary data to ensure data to judge the correct signs. The collected data will be displayed on the LCD screen, alcohol and pulse data acquisition to data processing on whether the driver has drunk driving [10] preliminary judgment, if the alcohol concentration and the pulse beyond the normal range of simple identified involving drunk driving, starting the GSM module to the specified phone to send text messages, take this as the output response.

V. TEST RESULT

Calibration method: control variable method

In order to calibrate the alcohol detection system, to control the volume of the alcohol, the distance between the sample and the tester, the time of alcohol volatilization, and so on, to change the concentration of alcohol. The alcohol concentration, the distance between the sample and the tester, the time of alcohol volatilization and so on were controlled to change the volume of the alcohol. Alcohol detector and hand-held alcohol detector were used to measure.

Calibration process: the designed alcohol detection system is tested in vehicle. When there is no alcohol in the air, the potential resistance of the measuring circuit of the alcohol detection system is changed. Make the alcohol concentration zero. Calibrate the hand-held alcohol detection system and obtain the system-to-alcohol test curve.

Laboratory equipment: a cube-sealed box with a hand-held alcohol detector placed at the top, alcohol dripping into the entrance at the bottom, as shown in Fig. 9. Alcohol detector as shown in Fig. 10.

Figure 9 handheld alcohol detector

Fig. 10 Alcohol detector

Experimental steps:

1) Put the hand-held driving tester and MQ-3 alcohol sensor on the top of the closed box and seal the MQ-3 alcohol sensor and adjust the zero.

2) Turn on the equipment power supply MQ-3 alcohol sensor preheating.

3) From the closed box alcohol injection port, use syringe to drip into the medical alcohol, and immediately close the alcohol injection port. Wait for the alcohol detector to show stability, record the alcohol value of the MQ-3 detector and the hand-held detector respectively.

4) Open the box, let the alcohol volatilize fully, then repeat the above five times, and fill in the experimental data in Table 1.

Table 1 Alcohol Measurement Calibration Table

Alcohol measurement calibration results			
volume	potency	Hand-held alcohol detector	MQ-3 alcohol detector
10ml	75%	0.15g/l	206mg/l
	50%	0.14g/l	161mg/l
	37.50%	0.11g/l	112mg/l
	25%	0.08g/l	72mg/l
	12.50%	0.06g/l	28mg/l
5ml	75%	0.13g/l	183mg/l
	50%	0.12g/l	121mg/l
	37.50%	0.08g/l	86mg/l
	25%	0.05g/l	64mg/l
	12.50%	0.03g/l	28mg/l

In keeping the alcohol volatilization time consistent, the other variables are controlled, the alcohol

concentration is changed to get the test data, the data of the hand-held alcohol detector and the MQ-3 alcohol detector are proportional to each other in a certain range, and the whole system works stably. More in line with the need for drunk driving test.

VI. CONCLUSION

This paper focuses on the design of the alcohol detection system with multi sensor vehicle based on fusion, the main innovation design is the use of multiple sensors and embedded micro controller to detect the vehicle interior alcohol concentration, alcohol degree of the driver, the driver to determine whether the violation of driving on the prevention of accidents, and take corresponding preventive measures. The device is small in size, low in cost, high in intelligence, strong in feasibility and high in accuracy. Therefore, it has a great effect on the safety performance of the car and has a good application value. Although this system compared with the previous simple use of alcohol sensor for alcohol detection system has some progress, but because of the lack of knowledge and technology, there are more research space in the software algorithm, the anti-interference performance of the system is not superior, these are the places where need to be improved.

References

[1] Xue Qinbo, Lang Minghua, Liang Jingyu. Research on the development of alcohol detection and anti driving system based on single chip microcomputer [J]. technology information, 2013 (08): 176.

[2] 2.. Qufu Normal University Qin Yongyi vehicle alcohol detection system design based on STM32 [D]., 2014.

[3] The 3. bears Yepan. [D]. research and development of infrared breath alcohol testing system based on embedded Linux based on the Zhejiang Sci-Tech University, 2010.

[4] Yang Zhigang. Design of automobile anti alcohol driving and anti-theft system based on ARM [D]. North Central University, 2014.

[5] Xu Jinglian, Han Junfeng, Pan Shenghui, Tong Qiwu. Multi sensor fusion vehicle alcohol detection system design based on [J]. instrument technique and sensor, 2010 (07): 105-107.

[6] Ge Yu. Design of vehicle alcohol detection and control circuit based on GPRS/GPS [D]. Nanchang University, 2010.

[7] Sun Dan. Design of a car based drunken driving and prohibition system based on GPS/GSM [D]. Dalian University of Technology, 2013.

[8] Zhang Jie, He Yulong, Xiong bin, Sun Wenliang, Xu Erhong. Application Research of vehicle alcohol detection equipment [J]. (World traffic transportation. Vehicles), 2013 (08): 145-147.

[9] 9.. Meng lucky ocean breath alcohol tester STM32F407ZG content of [D]. based on the Hebei University of Technology, 2015.

[10] 10. Sun Yanbo, Su Feng, Liu Meili. Design of STM32 based vehicle alcohol detection system [J]. electronic technology and software engineering, 2015 (24): 112-113.

[11] 11.Patrick Magnusson, Lisa Jakobsson, Sven Hultman. Alcohol Interlock Systems in Sweden[J]. American Journal of Preventive Medicine 2011 (3).

[12] 12. Peng Ning, Wenliang Du, Maxim Raya, Jean-Pierre Hubaux. Securing vehicular ad hoc networks[J]. Journal of Computer Security 2007 (1).

Research on the Analysis Method of Crosstalk in Automotive Cable Networks and Its Uncertainties

Xingzhao Yu; Xingzhen Liu; Wenbin Cheng
（*instrument science and engineering institute, jilin university*）

***Abstract*—Based on the mirror image method combined with the electromagnetic field theory, the calculation formula for the distribution parameters of the wire without consideration of the insulating layer and the insulating layer is deduced.Calculate the distribution parameters of the wire harness of the vehicle using the derivation formula;After that;Using Chain Parameter Matrix Method to calculate crosstalk of automotivec ables,and study the length of wire, the height of the ground and the mutual distance of the wire to crosstalk;Then for the non-deterministic geometric arrangement of the wires in the automotive wiring harness,using the Monte Carlo method to calculate the relevant statistical parameters of the distribution parameters and crosstalk at this time, to realize the analysis of the cable crosstalk uncertainty problem.Thus, it provides a theoretical basis for the automotive electromagnetic compatibility design and automotive cable layout.**

***keywords*—EMC distribution parametersautomotive wiring harness crosstalk mirror method Monte Carlo method**

I. INTRODUCTION

WITH the continuous development of automotive electronics technology, people's pursuit for vehicle safety, comfort, and ease of operation has increased. The number of on-board electronic devices has increased and the complexity has increased. Automotive electronic devices are found throughout the body, and different electronic devices are tightly connected by wiring harnesses. Electromagnetic interference between devices is becoming increasingly serious.Interference signals are transmitted to the electronic equipment along with the harness of the vehicle, which affects the performance of the equipment.Car wire harness crosstalk is the most important conductive interference, it can increase the noise level of the nearby wires, destroy data, affect the transmission of the system to the launch and radiate emissions, making the overall electromagnetic compatibility of the car decline strongly[1].In the early stages of designing automotive electromagnetic compatibility performance, crosstalk was the primary projected goal.Crosstalk occurs through inductive coupling and capacitive coupling of the wire distribution parameters. Distribution parameters are the root cause of crosstalk.Car wire harness crosstalk can not only cause errors or loss of the data transmitted on the wire, malfunction of the functional equipment, but also may affect the electromagnetic radiation and electromagnetic radiation sensitivity of automotive electrical and electronic equipment. Therefore, cross-talk for automotive wiring harness The study has very important significance.

II. CALCULATION OF DISTRIBUTION PARAMETERS OF HARNESS UNIT LENGTH

This article uses 7 VW automotive cable standard harnesses consisting of #18 gauge wires.The conductor in the wires harness is made of copper, and the material of the insulating layer is polyvinyl chloride (PVC).The relative permittivity is $\varepsilon_r = 2.7$: the radius of the conductor is R = 1mm, in which the radius of the conductor is r = 0.5mm, the thickness of the insulating layer is $\Delta r = 0.5$ mm, The distance from the center of the harness to the ground h = 30mm, and the length of the harness is L = 1.5m.Assume that the harness wires are not weakly coupled.The cross section of the automotive wiring harness used in this example is shown in Figure 1.

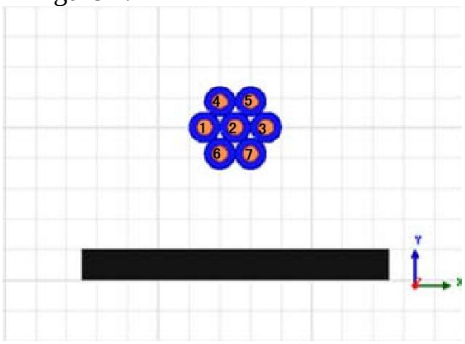

Fig.1. Schematic diagram of wiring harness cross section

A. Neglecting calculation of per-length distribution parameters of insulation layer harness

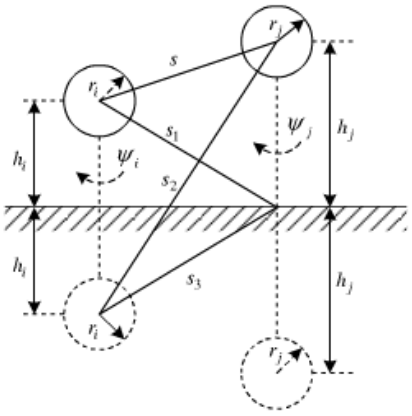

Fig.2. Imaging Method for Solving Inductive Matrix Per Unit

Harness i has a radius of r_i ,harness j has a radius of r_j ,the height from the ground is h_j and the distence between two wires is s .

The unit length inductance matrix can be defined as:

$$\psi = \mathrm{LI} \qquad (1)$$

Formula (1) is expanded:

$$\begin{cases} \varphi_1 = \mathrm{L}_{11}\mathrm{I}_1 + \mathrm{L}_{12}\mathrm{I}_2 + \mathrm{K} + \mathrm{L}_{1n}\mathrm{I}_n \\ \varphi_2 = \mathrm{L}_{21}\mathrm{I}_1 + \mathrm{L}_{22}\mathrm{I}_2 + \mathrm{K} + \mathrm{L}_{2n}\mathrm{I}_n \\ \mathrm{M} \\ \varphi_n = \mathrm{L}_{n1}\mathrm{I}_1 + \mathrm{L}_{n2}\mathrm{I}_2 + \mathrm{K} + \mathrm{L}_{nn}\mathrm{I}_n \end{cases} \quad (2)$$

The magnetic flux can be expressed as:

$$\varphi = \frac{\mu_0 \mathrm{I}}{2\pi} \ln \frac{1}{r} \quad (3)$$

This paper derives the unit length inductance formula using the principle of mirror image[2-3]:

$$\begin{aligned} \mathrm{L}_{ii} &= \left.\frac{\varphi_i}{I_i}\right|_{I_1=\mathrm{K}=I_{i-1}=I_{i+1}=\mathrm{K}=I_n} \\ &= \frac{\mu_0}{2\pi} \ln\left(\frac{2h_i}{r_i}\right) \end{aligned} \quad (4)$$

$$\begin{aligned} \mathrm{L}_{ij} = \mathrm{L}_{ji} &= \left.\frac{\varphi_j}{I_i}\right|_{I_1=\mathrm{K}=I_{i-1}=I_{i+1}=\mathrm{K}=I_n} \\ &= \frac{\mu_0}{2\pi} \ln\left(\frac{s_1}{s}\right) + \frac{\mu_0}{2\pi} \ln\left(\frac{s_2}{s_3}\right) \\ &= \frac{\mu_0}{2\pi} \ln\left(\frac{s_2}{s}\right) \end{aligned} \quad (5)$$

In the formula (5):

$$s = \sqrt{{d_{ij}}^2 + \left(h_i - h_j\right)^2} \quad (6)$$

$$s_1 = s_3 = \sqrt{{d_{ij}}^2 + {h_i}^2} \quad (7)$$

$$s_2 = \sqrt{{d_{ij}}^2 + (2h_j)^2} \quad (8)$$

Therefore,

$$\mathrm{L}_{ij} = \frac{\mu_0}{4\pi} \ln\left(\frac{4h_i h_j}{{d_{ij}}^2} + 1\right) \quad (9)$$

$$\mathrm{LC} = \mathrm{CL} = \varepsilon\mu \quad (10)$$

In the formula (9), d_{ij} is the distence between two wires.

In the case of ignoring the wire harness insulation layer, the capacitance per unit length can be calculated by the important formula (10).However, for the wire harness of the insulating layer, the dielectric around the conductor is inhomogeneous due to the presence of the insulating layer. Therefore, the capacitance C per unit length can no longer be obtained by formula (10), and it needs further derivation.

B. Considering the Calculation of Parameter Distribution Per Unit Length of Insulating Layer Harness

The insulator of the wire harness used in this article is polyvinyl chloride (PVC). Since the magnetic permeability of the insulating medium changes very little compared with the permeability of the air, the presence of the insulating layer has a negligible effect on the inductance per unit length of the wire harness,The equations (4) and (9) can still be used in calculations;The dielectric constant of the dielectric has a large variation compared to that of air, so calculations taking into account the capacitance per unit length of the insulation bundle must be further deduced.

Using the mirror analysis method to derive the capacitance of the automotive wire harness per unit length considering the insulation layer:

$$\mathrm{C}_{ii} = \left[\frac{\rho_i}{2\pi\varepsilon_0}\left(\frac{1}{\varepsilon_r}\ln\frac{1}{r_i} + \frac{\varepsilon_r - 1}{\varepsilon_r}\ln\frac{1}{R_i} - \ln\frac{1}{2h_i}\right)\right]^{-1} \quad (11)$$

$$\mathrm{C}_{ij} = \left[\frac{\rho_i}{2\pi\varepsilon_0}\ln\frac{d_{ij}'}{d_{ij}}\right]^{-1} \quad (12)$$

In the formula (11), R_i is the wire radius.

III .MULTI-CONDUCTOR CROSSTALK AND ITS INFLUENCING FACTORS

A. (2+1) ulti-conductor crosstalk calculation

For the calculation of wire harness crosstalk in the frequency domain, select the two conductors numbered 5 and 3 shown in Figure 1 and the chassis of the car to form a (2+1) uniform multiconductor transmission line system as an example to perform data experiments.Let the wire 3 be the interference wire, and the wire 5 be the victim wire. The coupling voltage generated on the side close to the power supply end (near end) of the interference wire is called the near-end crosstalk voltage, and it is connected to the interference wire load end (far The coupling voltage generated on one side is called the far-end crosstalk voltage[4].

Using formulas (4), (9), (11), and (12), the unit length inductance matrix and unit length capacitance matrix of the (2+1) uniform transmission line system composed of the wire harness and the chassis of the vehicle are calculated as:

$$\mathrm{L} = \begin{bmatrix} \frac{\mu_0}{2\pi}\ln\left(\frac{2h_1}{r_i}\right) & \frac{\mu_0}{4\pi}\ln\left(1+4\frac{h_1h_2}{d^2}\right) \\ \frac{\mu_0}{4\pi}\ln\left(1+4\frac{h_1h_2}{d^2}\right) & \frac{\mu_0}{2\pi}\ln\left(\frac{2h_2}{r_i}\right) \end{bmatrix} \quad (13)$$

$$\mathrm{C} = \begin{bmatrix} \frac{1}{2\pi\varepsilon_0}\left(\frac{1}{\varepsilon_r}\ln\frac{1}{r_1} + \frac{\varepsilon_r-1}{\varepsilon_r}\ln\frac{1}{R_1} - \ln\frac{1}{2h_1}\right) & \frac{1}{4\pi\varepsilon_0}\ln\left(1+\frac{4h_1h_2}{d^2}\right) \\ \frac{1}{4\pi\varepsilon_0}\ln\left(1+\frac{4h_1h_2}{d^2}\right) & \frac{1}{2\pi\varepsilon_0}\left(\frac{1}{\varepsilon_r}\ln\frac{1}{r_2} + \frac{\varepsilon_r-1}{\varepsilon_r}\ln\frac{1}{R_2} - \ln\frac{1}{2h_2}\right) \end{bmatrix} \quad (14)$$

The parameters are brought into equations (13) and (14) to obtain:

$$\mathrm{L} = \begin{bmatrix} 945.18 & 686.19 \\ 686.19 & 954.95 \end{bmatrix} \ (\mathrm{n}H/\mathrm{m}) \quad (15)$$

$$\mathrm{C} = \begin{bmatrix} 42.87 & -35.44 \\ -35.44 & 42.54 \end{bmatrix} \ (\mathrm{pF/m}) \quad (16)$$

The conductor 3 is excited by a single-frequency sinusoidal steady-state voltage with an amplitude of 1V. Its frequency is varied from 3kHz to 3MHz and the

length of the conductor is 1.5m.Using the chain parameter matrix method and programming with MATLAB software, the voltage and current across the victim wire 5 shown in FIGS. 3 and 4 are obtained:

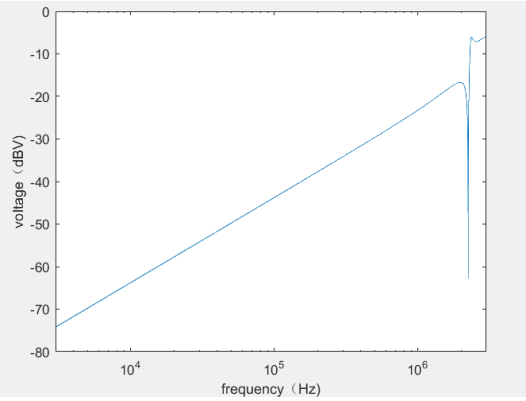

Fig.3 The voltage across wire 5

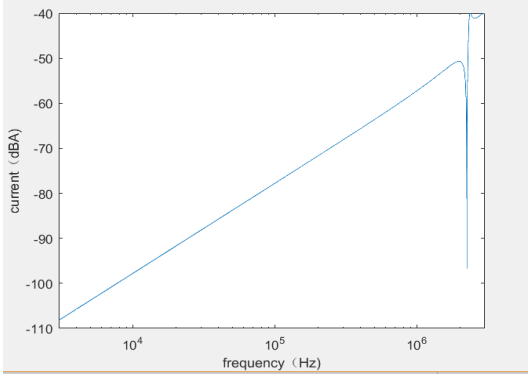

Fig.4 The current across wire 5

From the analysis, it can be seen that the voltage and current across the wire 5 shown in FIGS. 3 and 4 are the crosstalk voltage and the crosstalk current.

B. Influence of Related Factors on Harmonic Wire Crosstalk in Frequency Domain

a.Influence of Length on Harmonic Wire Crosstalk in Frequency Domain

The discussion takes the (2+1) multi-conductor transmission line model in 2.1 as an example, assuming that the other parameters of the two conductors are not changed.The length l of the wire is 0.6m, 1.0m, 1.4m, 1.8m, and 2.2m, respectively.Get the result shown in Figure 5:

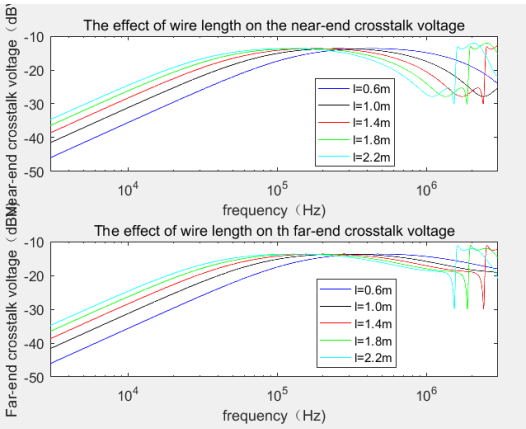

Fig.5 Effect of wire length on crosstalk near-end voltage and far-end voltage

From Figure 5, we can see that for the wire harness wire defined in this article, in a certain frequency range, as the wire length l increases, the crosstalk voltage of the vehicle wire harness wire increases continuously, but the rate of crosstalk voltage change gradually decreases as the wire length increases small.

b Influence of wire-to-ground height on crosstalk of wire harness wires in frequency domain

Assuming that the other parameters of the two conductors remain unchanged, the crosstalk voltages at the heights h = 1mm, 10mm, 20mm, 30mm, and 40mm, respectively, are calculated. The results are shown in Figure 6:

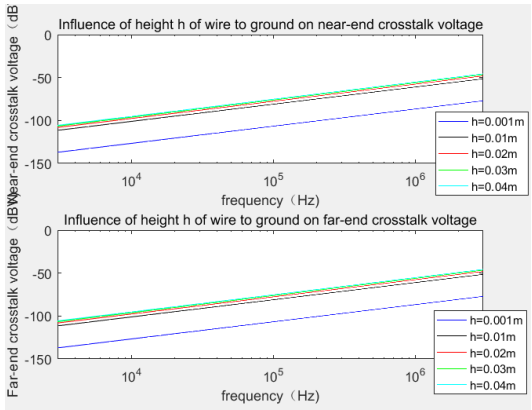

Fig.6 Effect of wire height h on crosstalk near-end voltage and far-end voltage

From Figure 6, we can see that for the wire harness wire defined in this article, in a certain frequency range, the crosstalk value increases as the wire height to the ground h increases, but the rate of crosstalk voltage change gradually increases with the length of the wire decrease.

c. Influence of the relative distance of the wire on the crosstalk of the wire harness in the frequency domain

Same as above, assuming that the other parameters of the two wires are unchanged, the near-end and far-end crosstalk voltages at the relative distances d=2mm, 5mm, 10mm, 15mm, and 20mm are calculated respectively. The result is shown in Figure 7:

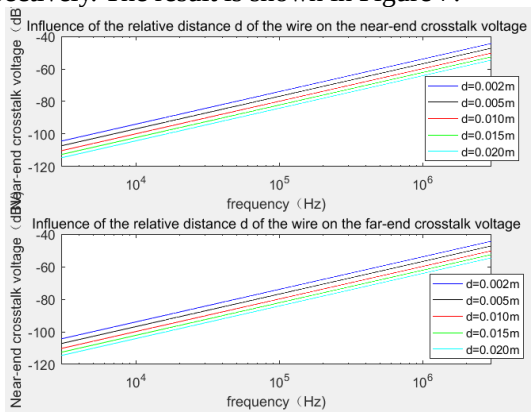

Fig.7 Effect of wire relative distance d on near-end voltage and far-end voltage of crosstalk

From Figure 7, we can see that for the wire harness wire defined in this article, in a certain frequency range, the crosstalk voltage decreases with the increase of d, but the rate of decrease of the crosstalk voltage gradually decreases as the relative distance d of the wire increases. small.

Ⅳ .Analysis of Statistical Characteristics of Vehicle Harness Distribution Parameters and

CROSSTALK VOLTAGE BASED ON MONTE CARLO METHOD

The Monte Carlo method is also called the stochastic simulation method, sometimes called the random sampling technique statistical test method[6].When the number of sampling trials N is large enough, the probability is replaced by the frequency and the mathematical average is used instead of the mathematical expectation to obtain the solution to the problem[7].In the static state, the geometric position of the wire in the vehicle wiring harness is a fixed value, and the distribution parameters and crosstalk values can be uniquely determined;When the car is moving, because the geometric position of the conductor wire in the wire harness is a random amount, the error of the solution method used in the static method at this time will become larger. Therefore, it is necessary to analyze the statistical characteristics of the vehicle wiring harness distribution parameters and crosstalk voltages during exercise in conjunction with the Monte Carlo method.

A. The Inductive Characteristics of the Unit Length Based on the MC Method

When the wire in the automobile wire harness moves in the automobile, its geometric position is random, assuming that the interference wire height to the ground is h_1 ,the height of the victim line to the ground is h_2 ,and the relative distance between the interference line and the victim line is d ,these three parameters are independent random variables that are normally distributed.

Satisfies the normal distribution h_1 $N_1 \sim (25,1.3)$, satisfies the normal distribution $N_2 \sim (25,1.3)$, satisfies the normal distribution $N_1 \sim (4.5,1.1)$ .Using the MC method, when N = 3,000, the unit length inductance matrix statistics between two wires are calculated in combination with equation (13) as shown in Figs. 8 and 9:

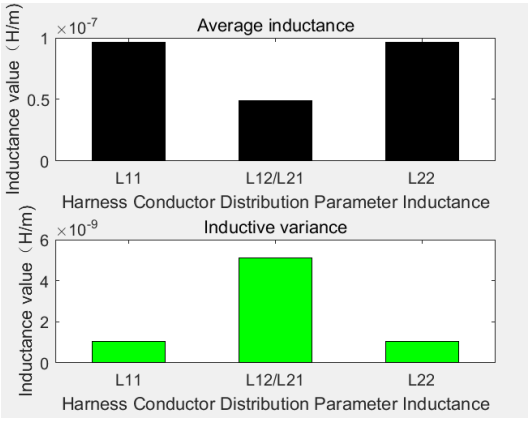

Fig.8 Mean and Variance of Inductance Matrix per Unit Length Based on MC Method.

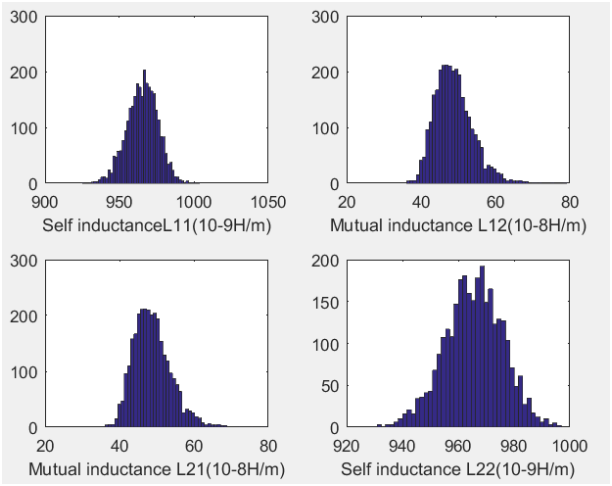

Fig.9 Probability Density Function of Inductive Matrix L Per Unit Length Based on MC Method

From the analysis of Figure 9, we can see that the range of variation of the self-inductance L11 and L22 is $60\times(10\text{-}9H/m)$, mutual inductance $20\times(10\text{-}9H/m)$

B. The statistical properties of capacitance per unit length based on MC method

In the same way as in 3.1, when N=3000, the results shown in Fig. 10 and Fig. 11 are obtained by formula (14):

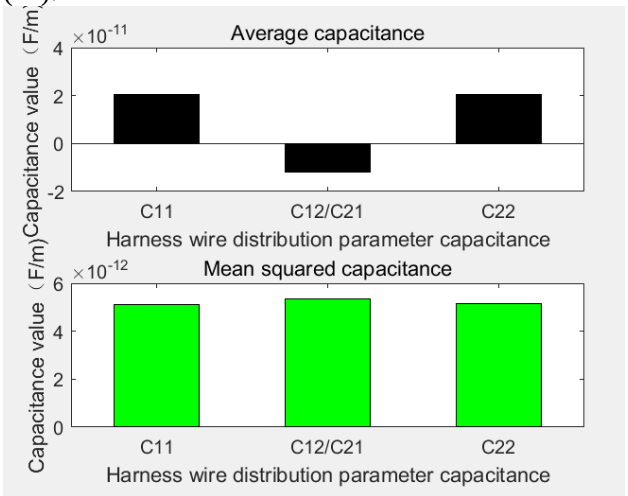

Fig.10 Means and Variances of Capacitance Matrix per Unit Length Based on MC Method

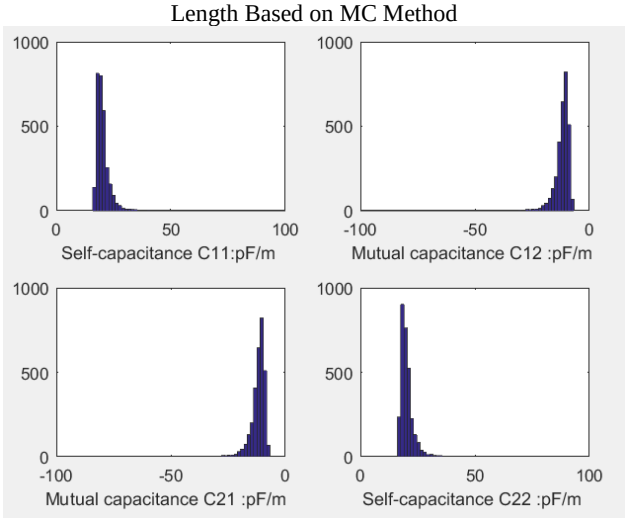

Fig.11 The Probability Density Function of Capacitance Matrix C Based on MC Method

According to the analysis in Fig. 11, the variation range of self-capacitances C11 and C22 can reach 15 pF, and the variation range of mutual capacitances C12 and C21 can reach 20 pF.

C. Analysis of Statistical Characteristics of Crosstalk Voltage Based on MC Method

Take the frequency f = 3MHz, the termination impedance is 50Ω, the number of tests N = 3000, the simulation results in the near-end crosstalk voltage and far-end crosstalk voltage shown in Figure 12 and Figure 13 below:

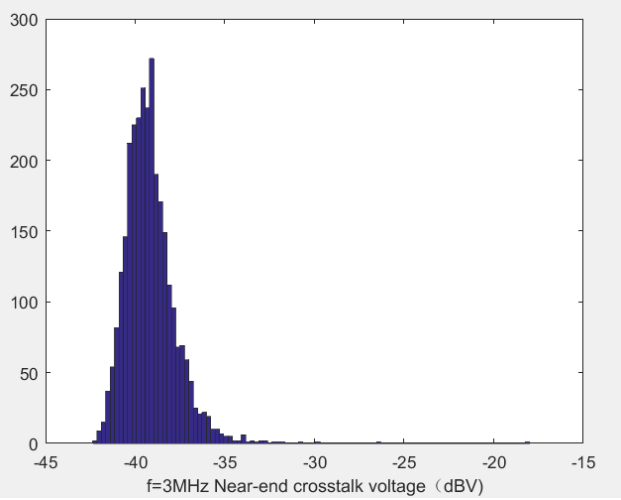

Fig.12 Proximity Crosstalk Voltage Probability Density Function

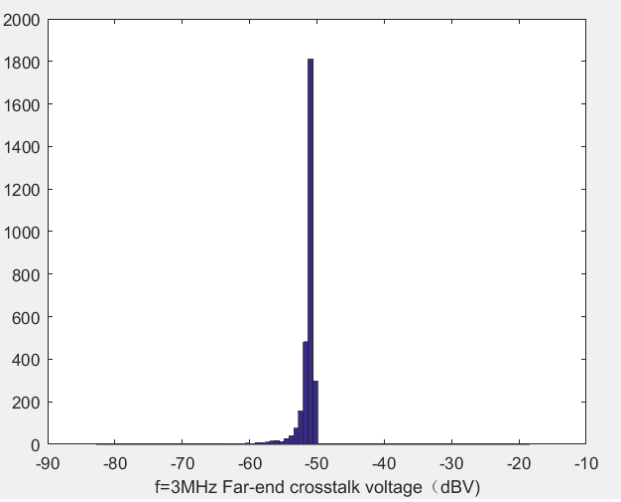

Fig.13 Far-end crosstalk voltage probability density function

From Fig. 12 and Fig. 13, it can be seen that due to the uncertainty of the geometric position of the wire harness of the vehicle, the crosstalk of the vehicle harness crosstalk in the frequency domain can reach about 10dB.

Ⅴ. SUMMARY

From the above analysis of the factors that affect the influence of the wire harness crosstalk on the vehicle wiring harness, it can be seen that there are three points in the connection wires between the devices in the automobile:

(1)Should be installed in the shortest possible path;

(2)Close to car chassis;

(3)Distance between adjacent conductors should be maximized.

Through the use of the MCM study on the random position of the wire harness of the vehicle, it is found that the fluctuation of the distribution parameters and the crosstalk value due to the change of the geometric position can not be ignored. This shows that the research on the uncertainty of the cross-talk of the automotive wire harness has very important significance.

References

[1] Jin Songtao, Ding Liangxu, Liu Qingsong. The importance of vehicle electromagnetic problems and research[J]. Passenger Car Technology and Research, 2011(4):1-5.

[2] Ni Guangzheng. Principles of Engineering Electromagnetic Fields [M]. Beijing, 2007: 81- 138.

[3] Fu Junmei, Feng Enxin. Advanced Electromagnetic Theory [M]. Xi'an: Xi'an Jiaotong University Press, 2004:22.

[4] Clayton R. Paul (USA). Analysis of Multiconductor Transmission Lines [M]. Beijing: China Electric Power Press, 2013:65.

[5] Wang Tianhao. Harmonic crosstalk in automotive electromagnetic compatibility and its statistical characteristics [D]. Changchun: Jilin University, 2016: 89-94.

[6] Xu Shuyan, Application of Monte Carlo Method in Experimental Nuclear Physics [M]. Beijing; Atomic Energy Press, 2006: 1.

[7] Xu Zhongji, Monte Carlo Method [M]. Shanghai: Shanghai Science and Technology Press, 1985: 5.

Time domain three dimensional electromagnetic numerical simulation accelerating algorithm

Nie Dan; Sun Meiyue; Zhao Chang
（*instrument science and engineering institute, jilin university*）

***Abstract*-Applying the theory and algorithm of parallel computation to the study of three-dimensional electromagnetic computation in time domain. Based on the traditional serial computation, a combination of CPU and GPU, serial computation and parallel computation are applied to time domain three-dimensional electromagnetic numerical values.Acceleration calculations are performed, and the experimental results accelerate the calculation without reducing the calculation results and reduce the calculation time.**

***Keywords*-Three-dimensional time domain Serial calculation Parallel computing**

I. INTRODUCTION

TRADITIONAL time-domain three-dimensional electromagnetic finite difference numerical calculations are based on Wang and Hohmann's research and change the calculation time by changing the time step. The time step is strictly limited by many factors, affecting the computational efficiency. Three-dimensional electromagnetic computation in the time domain requires a large amount of calculation, the calculation process is complex, and the time required for the serial calculation is long and cannot meet the requirement of the calculation duration[1-3]. The time domain three-dimensional electromagnetic computation has certain parallelism. Therefore, this paper adopts a combination of parallel computing and serial computing to calculate, in order to reduce the calculation time and improve the calculation efficiency.If your paper is intended for a *conference*, please contact your conference editor concerning acceptable word processor formats for your particular conference.

Ⅱ .PARALLEL COMPUTATION OF ELECTROMAGNETIC NUMERICAL VALUES OF CPU+GPU

The GPU is designed to perform complex digital and geometric calculations. In recent years, GPU technology has developed rapidly. GPUs have attracted a lot of attention from the industry through the development of computing technology. Facts have proved that GPUs can provide tens or even hundreds of times more CPU performance in terms of floating point operations and parallel computing. Therefore, in the calculation of three-dimensional electromagnetic problems in the time domain, the use of CPU + GPU can significantly increase the calculation time and improve the calculation efficiency[4-6]. The CPU section is mainly used to control the logic of the calculation and control the GPU operation. The GPU is mainly used to calculate more complex and more data loops.

A.Parallel Computing of Initial Fields

Electric field step expression:

$$\begin{aligned}Ex=&-\frac{I}{4\pi}\int_{-L}^{L}\hat{z}\int_{0}^{\infty}r_{TE1}e^{-u_1 z}\frac{\lambda}{u_0}J_0(\lambda R)d\lambda\,d\acute{x}\\&+\left(\frac{I}{4\pi}\frac{x}{R_2}\int_{0}^{\infty}\left(\frac{u_1}{\hat{y}_1}r_{TM1}-\frac{\hat{z}}{u_0}r_{TE1}\right)e^{-u_1 z}J_1(\lambda R_2)d\lambda\right.\\&\left.-\frac{I}{4\pi}\frac{x}{R_1}\int_{0}^{\infty}\left(\frac{u_1}{\hat{y}_1}r_{TM1}-\frac{\hat{z}}{u_0}r_{TE1}\right)e^{-u_1 z}J_1(\lambda R_1)d\lambda\right)\end{aligned}\quad\cdots\cdots(1.1)$$

$$\begin{aligned}Ey=&-\frac{I}{4\pi}\left(\frac{y}{R_2}\int_{0}^{\infty}\left(\frac{u_1}{\hat{y}_1}r_{TM1}-\frac{\hat{z}}{u_0}r_{TE1}\right)e^{-u_1 z}J_1(\lambda R_2)d\lambda\right.\\&\left.-\frac{y}{R_1}\int_{0}^{\infty}\left(\frac{u_1}{\hat{y}_1}r_{TM1}-\frac{\hat{z}}{u_0}r_{TE1}\right)e^{-u_1 z}J_1(\lambda R_2)d\lambda\right)\end{aligned}\quad\cdots\cdots(1.2)$$

From the above formula, it can be seen that Gauss integration and Bessel function integrals need to be solved in the calculation. The calculation of the two kinds of integrals is complicated and the calculation is time-consuming. And the size of the initial field is related to physical properties such as emission current, wire length, conductivity, and permeability (these variables are the same for the electric fields at various points in the model), and only the electric field Ex is in the mesh x The positions of y and z are related, and there is no correlation between them. This is suitable for parallel computing.

The initial field calculation consists of internal and external bi-level integration. For this reason, 241 filters are performed by the CPU for loop in the paper, and GPU parallel computing is used in a single filter. Since the earth model is split into three-dimensional grids, coordinates, conductivity, and permeability The rates are all three-dimensional arrays. Three-dimensional arrays are converted to one-bit arrays before parallel calculations. After the calculation is completed, one-bit arrays are converted to three-dimensional arrays. Finally, Hankel on each Gaussian-integral node is added.

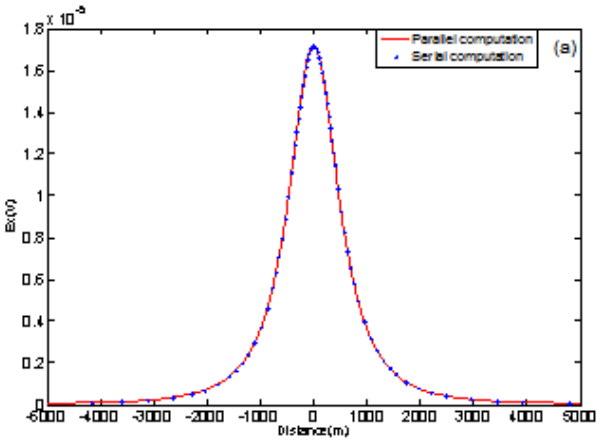

Figure 1 Initial field Ex component serial parallel results comparison

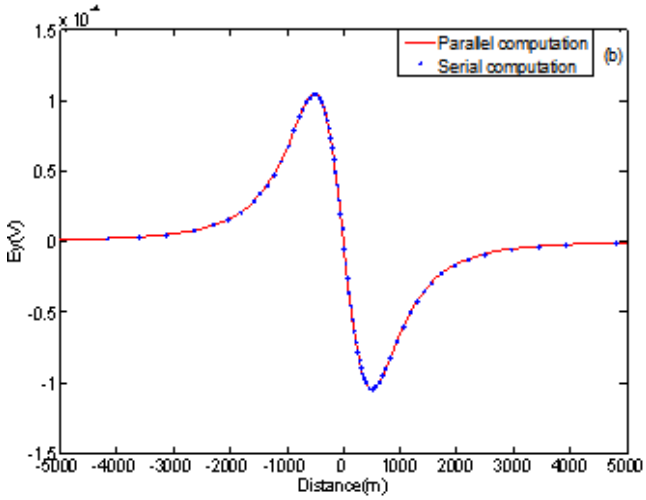

Figure 2 Contrast of initial and field Ey components in series and parallel

The lines in Fig. 1 and Fig. 2 show the parallel calculation results, and the results shown in the points are the serial calculation results.

From Fig. 1 and Fig. 2, it can be seen that the parallel calculation and the serial calculation are completely consistent, and the parallel calculation method is correct and applicable. For the 221×221×75 grid model, the serial calculation and the parallel calculation are respectively used for calculation. The time for the Ex component serial calculation is 3481.08 s, and the time for the parallel calculation is 2096.51s. The acceleration ratio after the parallel calculation method is used. For 1.66, the Ey component serial calculation time is 3860.99s, the parallel calculation time is 2298.06s, and the parallel calculation method has an acceleration ratio of 1.68. Shows that parallel computing effectively increases the speed of calculation of the initial step field

B Iterative Field Parallel Computing

In the iterative calculation process, the value of the electric field Ex is independent of the values of the electric fields Ey and Ez, and is related only to the values of its own front and rear moments. However, the value of the magnetic field Hx is independent of the values of the electric fields Hy and Hz, and is related only to the values of its own front and rear moments. This feature makes iterative fields suitable for parallel computing. In this paper, the CPU+GPU parallel processing method is used in iterative calculations. First, the three components of the electric field Ex, Ey, and Ez are calculated simultaneously, and then the Hx and Hy components of the magnetic field are calculated. Finally, the magnetic field Hz component is calculated by using the Hx and Hy components of the magnetic field. The electric fields Ex, Ey, Ez, and the magnetic fields Hx, Hy are parallel. Calculation method. Before the calculation, we must first convert the three-dimensional array into a one-dimensional array, and then convert the one-dimensional array into a three-dimensional array after the calculation is completed.

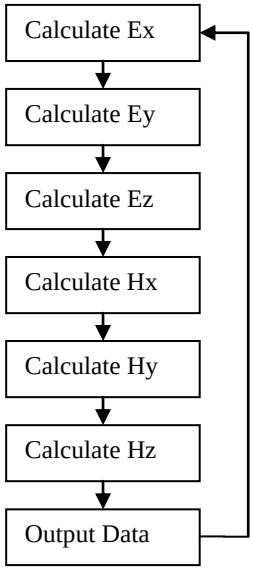

Figure 3 Serial iteration diagram

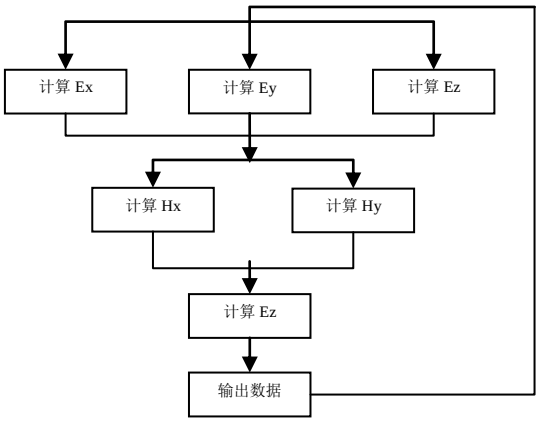

Figure 4 Parallel Iterations

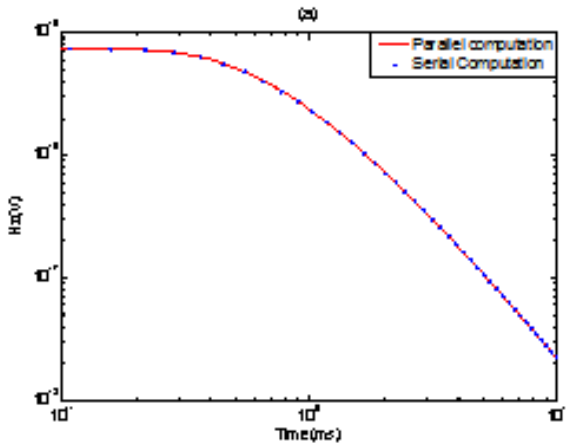

Figure 5 Comparison of serial parallel computing results of an iterative field conductivity 0.1S/m uniform half-space model

The lines in Fig. 5 show the parallel calculation results, and the results shown in the points are the serial calculation results.

For the 221 ×221 ×75 mesh model, the two methods of serial calculation and parallel computation are respectively used for calculation. The serial computing time is 809.03s, the parallel computing time is 321.669s, and the parallel computing method has an acceleration ratio of 2.51.

III. ACCELERATED ALGORITHM FOR TIME ITERATIVE FORMAT

Time-domain finite-difference time progression uses the Du Fort-Frankel method, and the time step size is strictly limited by the minimum conductivity and the minimum grid. Even if the parallel calculation method is adopted, the problem of long calculation time may still be caused when the high-resistance model or the small-mesh model is simulated. In order to more efficiently perform time domain electromagnetic numerical simulation, Commer et al. proposed a time-iteration format acceleration method in 2006 and 2015, respectively, to improve the computational efficiency by reducing the time sampling rate, but since the improved time step has grown at a late stage. Fast, resulting in an increase in late-time electromagnetic simulation errors[7-9]. Based on the characteristics of time-domain electromagnetics, and based on Commer et al.'s research, this paper further reduces the time-domain electromagnetic sampling rate and further reduces computational time.

A Accelerated Iteration Function

After the emission current is turned off, the time domain electromagnetic wave changes strongly in the early stage and decays rapidly. As the measurement time increases, the high frequency part of the time domain electromagnetic wave weakens gradually and the late decay is approximately DC. In this paper, we use time-domain electromagnetic characteristics to further increase the time-domain finite-difference iterative time steps[10,11]. Oristaglio and Hohmann (1984), on the basis of the traditional grid diffusion time, describe the maximum distance that the diffusion field generated by the full-space Green's function radiates after the emitter is turned off. This distance is called the penetration depth. The form is expressed as:

$$\delta(t)=\sqrt{\frac{2t}{\mu\sigma_{\max}}},\delta(t\le 0)=0 \quad \text{.....(2.1)}$$

In equation (3.1), t is time, μ is the permeability, and σmax is the maximum conductivity. The depth of penetration and the minimum grid length of the model are used to construct the acceleration function. The formula for the acceleration function is:

$$F(t,\beta)=\left(\frac{\delta(t)+\Delta_{\min}}{\Delta_{\min}}\right)^{\frac{1}{\beta}} \quad \text{.....(2.2)}$$

β in formula (3.2) is a dimensionless constant and is called acceleration factor.

B Accelerated Iteration Time Format

In order to achieve fast simulation of electromagnetic time domain, the acceleration function is introduced into the time iterations. The improved time iteration format is expressed as:

$$\Delta t=\sqrt{\frac{\mu\sigma_{\min}t}{6}}F(t,\beta)^{\beta}\alpha\Delta_{\min} \quad \text{.....(2.3)}$$

Analytical formula (2.3) shows that the time step can be adjusted and controlled by changing the size of the accelerating factor. Smaller accelerating factors can increase the time step and reduce the time sampling rate of electromagnetic time in the time domain, effectively reducing the numerical simulation. Time-consuming; the greater the acceleration factor, the closer the time step after improvement to the original time step.

In order to verify the calculation results of the acceleration time iterative format, in the uniform half-space model with a resistivity of 0.001S/m, the time domain electromagnetic response of the electric dipole source is calculated using different acceleration factors, and it is compared with the original time iterative format. Comparing the calculation results and analyzing the calculation error.

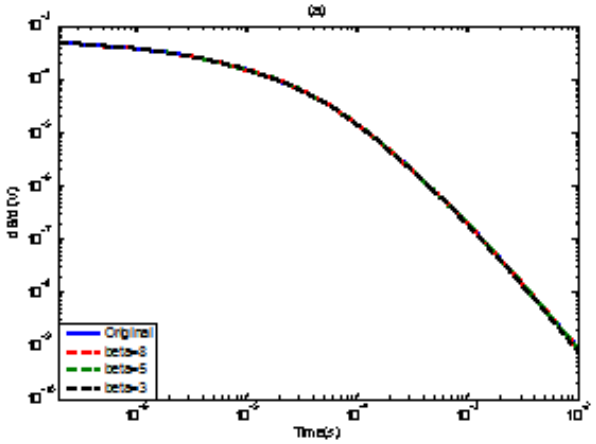

Figure 6 0.001S / m uniform model of different accelerating factor calculation results

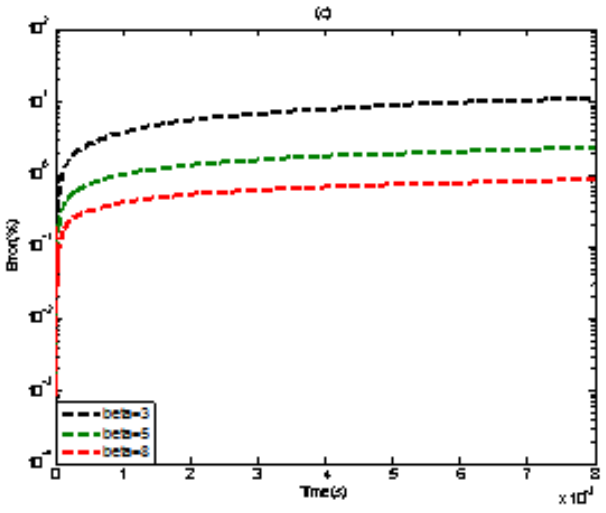

Figure 7 Calculation error of different acceleration factors for 0.001S/m uniform model

In FIG. 6 and FIG. 7, the black line represents the calculation result when β=3, the green line represents the calculation result when β=5, and the red line represents the calculation result when β=8. The result of calculation when the blue color represents the initial β value.

Through analysis, it can be seen that as the acceleration factor increases, the calculation result of the acceleration time iteration is closer to the original time iterative calculation result; as the calculation time increases, the late calculation error also increases, and the reason for the increase in the error lies in the adoption of With the acceleration time iterative format, the time step is further increased, especially in the late stage of calculation, resulting in a large calculation error. In addition, under the same grid conditions, using the same acceleration factor, the smaller the conductivity is, the smaller the calculation error is. This is because the smaller the conductivity is, the smaller the time step is.

Ⅳ. CONCLUSION

Through the study of time-domain three-dimensional electromagnetic numerical simulation acceleration algorithm, it is found that when parallel computing is used to process multiple data calculations, it can indeed achieve less computing time and improve computational efficiency. In this paper, the use of CPU + GPU, parallel computing and serial computing combined, significantly reducing the calculation time and improve computing efficiency.

References

[1] Chen Guoliang, Miao Qiankun, Sun Guangzhong, et al. Hierarchical parallel computing model [J]. Journal of University of Science and Technology of China, 2008(07): 841-847.

[2] Chen Guoliang, Sun Guangzhong, Xu Yun, et al. Parallel Algorithm Research Methodology [J]. Chinese Journal of Computers, 2008(09):1493-1502.

[3] Chen Guoliang, Sun Guangzhong, Xu Yun, et al. The current status and development trend of integrated research in parallel computing [J]. Science Bulletin, 2009(08): 1043-1049.

[4] Huang Yi, Shi Xueming, Fan Jianke, et al. Parallel computing technology and its status and prospects in exploration geophysics [J]. Progress in Geophysics, 2010(02):642-649.

[5] Jin Liang, Qiu Yuntao, Yang Qingxin, et al. Parallel calculation method for electromagnetic problems based on cloud computing [J]. Chinese Journal of Electrotechnics, 2016(22):5-11.

[6] Li Yu, Hu Xiangyun, Wu Guiju, et al. MPI-based two-dimensional magnetotelluric forward parallel computing [J]. Seismology and Geology, 2010(03):392-401.

[7] Luo Tao. Parallel computing model for large data processing and performance optimization [D]. Hefei: University of Science and Technology of China, 2015.

[8] Lu Jie, Zhang Tianxu, Zhang Biyin. MPI parallel computing applications in image processing [J]. Infrared and Laser Engineering, 2004 (05): 496-499.

[9] Pan Yu, Li Zhanhuai. Research progress of parallel computing model in big data environment [J]. Journal of East China Normal University(Natural Science),2014(05):43-54.

[10] Su Huayou. Application-oriented GPU parallel computing key technologies [D]. Changsha: National University of Defense Technology, 2014.

[11] Zhou Yong. Research on Data Stream Processing Method Based on Parallel Computing [D]. Dalian: Dalian University of Technology, 2013.

Fog and haze monitoring and purification system based on STM32 single chip

Kangda; Mengfanjie; Zhengce
（*College of instrumental science and electrical engineering, Jilin University*）

***Abstract*-According to the monitoring range of integrated purifier purification and small haze problem of low efficiency, the design of distributed wireless distributed monitoring of indoor air, three block detection module in the control module to transfer real-time data; in air purification, the closed loop of purification device control; the design of the WeChat small program for remote monitoring of air condition in the mobile phone terminal.**

***Key words*-Distributed Closed-loop control Remote monitoring**

I. INTRODUCTION

IN recent years, the fog and haze weather has appeared frequently in our country. The problem of air quality has attracted the attention of the whole society. The indoor environment is small, PM2.5 is easy to exceed the standard, causing the human body to be affected, and even the usual cooking, burning incense, smoking and other behaviors will dramatically increase the concentration of indoor PM2.5. At present, a variety of air purifiers have been detected on the market, which can detect and purify PM2.5, but most of the effects of these air purifiers are very one-sided. The area of purification is also very small, which has not effectively improved PM2.5. However, the monitoring and purification system designed here can achieve closed-loop control, and monitor the indoor humidity, temperature and PM2.5 concentration[1] at any time. It can purify in time when it exceeds human health. At present, the air purification products on the market can basically be divided into two categories. One is a variety of adsorption materials, such as activated carbon and photocatalyst, which absorb harmful substances. The other is to use plasma discharge technology to produce ozone and to decompose pollutants in the air. Ozone is itself a pollutant, experts say, and the principle of adsorption material is the same as the purifier of drinking water. It must be changed frequently. Otherwise, it will be released as a source of pollution again. Therefore, the system chose to use the first class of adsorbate material for air purification, so as not to produce worse conditions. The haze monitoring and purification system by monitoring and purification separation mode, this point and the market existing products has a very big difference, integrated purifier detection range on the market is very small, often only the air quality around the purifier can be detected, it is difficult to achieve effective purification of the entire room or even the whole house. The monitor module of the purifier can be set at the location of PM2.5, such as kitchen, window, doorway and so on. When haze enters the monitoring space, the purifier will be cleaned immediately[2], so as to prevent the haze from affecting human health.

A.Design scheme of monitoring module

DHT11 is a digital sensor with integrated wet temperature. The sensor consists of a resistive humidity measuring element and a NTC temperature measuring element, which is connected to a high performance 8 bit single chip microcomputer. The local humidity and temperature can be collected in real time by the simple circuit connection of microprocessors and other microprocessors[3]. DHT11 and MCU can use a simple single bus to communicate, only a I/O port is needed. The data of humidity and temperature data of 40Bit are transmitted to MCU at a time. Data is checked by checksum mode, which ensures the accuracy of data transmission. The power consumption of DHT11 is very low, and the average maximum current is 0.5mA under the 5V power supply voltage.

DS18B20 is a temperature sensor of a "line bus" interface launched by DALLAS semiconductor. Compared with traditional thermistors and other thermosensitive elements, it is a new type of digital temperature sensor with small volume, wide application voltage and simple interface with microprocessors. The first bus structure is simple and economical features, users can easily set up sensor networks, and introduce a new concept for the construction of the measurement system, the measurement temperature range of -55~+125 DEG C, precision: - 0.5 DEG C. The field temperature is transmitted directly by the "line bus" digital mode, which greatly improves the anti-interference of the system. It can read the measured temperature directly, and can realize the digital value reading of 9~l2 bit by simple programming according to the actual requirement. It works in the voltage range of 3 to 5.5 V, and adopts various packaging forms, so that the system is designed flexibly and conveniently. The setting resolution and user set alarm temperature are stored in EEPROM, and remain after power failure.

The type of sensor used is pms5003. Pms5003 sends a single frame of data to a single chip computer by serial port, with a total length of 32 bytes for one frame, and a default baud rate of 9600bps. The thirteenth bits are eight high in the PM2.5 value, and the fourteenth for the lower eight of the PM2.5 value. Usually we use the interrupt service program that uses the serial port function of STM32 to use RXNE interrupts[4]. When a single chip receives a byte, a RXNE interrupt will be generated. Pms5003 sends a frame of data, so this interruption cannot be used. IDLE interrupts can be used, and when a frame of data is received, a IDLE interrupt will be generated. Special attention: in the interrupt function, the corresponding bits need to be

cleared, otherwise the next data will be affected. For example, RXNE receives data interrupts, and the interruption will be cleared as long as one of the received bytes is read out. F1 series of singlechip, the cleaning method is "read the SR register first, then read the Dr register."

NRF24L01 wireless module, the use of the chip is NRF24L01, the main features of the chip are as follows:

1) 2.4G global open ISM band, free license use.

2) the maximum working rate is 2Mbps, and the GFSK modulation of the university is strong.

3) 125 optional channels to meet the needs of multipoint communication and FM communication.

4) built-in CRC error detection and point to multipoint communication control.

5) low operating voltage (1.9~3.6V).

6) the automatic response can be set up to ensure the reliable transmission of the data.

B. The design of the purification module and the overall design of the device

Three monitoring boards are used to monitor the real time status of the air in the doorway, window and indoor center respectively, so that we can better monitor the air condition in the room.

Figure 3 installation drawings in the room :

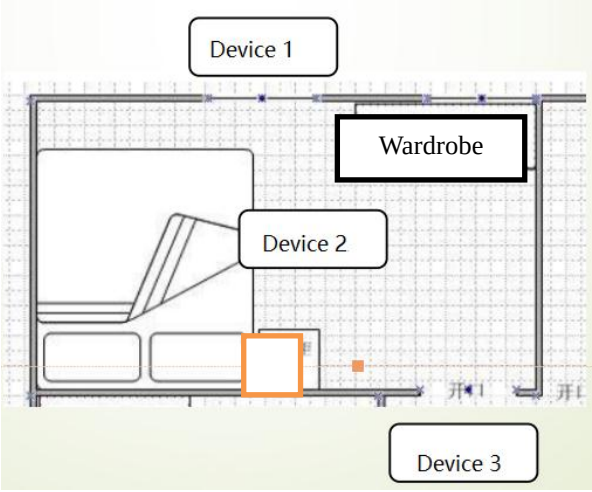

Fig. 1. plane diagram of purification device

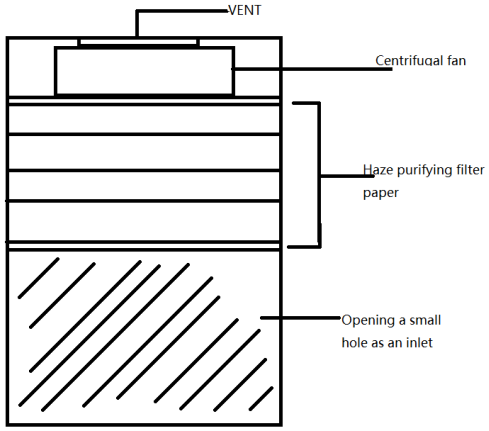

Fig. 2. plane diagram of purification device

Three monitoring boards are used to monitor the real time status of the air in the doorway, window and indoor center respectively, so that we can better monitor the air condition in the room.

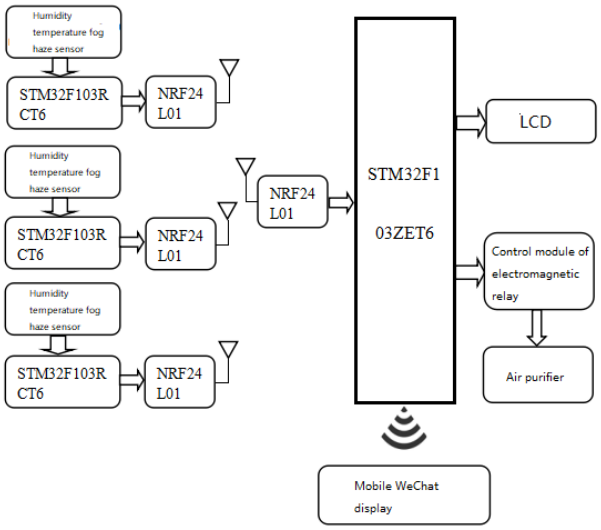

Fig. 3. Overall design block diagram of the device

C. WeChat small program design

WeChat applet, or short program, is an application that can be used without downloading and installation. It realizes the application of "within your grasp" dream. Users scan or search it to open applications.

Light is one of the main advantages of small procedures, many lightweight APP in the past, we still have to download to use in mobile phone installation, which adds unnecessary trouble, process, have a certain share of mobile phone memory, the actual user experience is not good.

WeChat applet, or short program, is an application that can be used without downloading and installation. It realizes the application of "within your grasp" dream. Users scan or search it to open applications.

Light is one of the main advantages of small procedures, many lightweight APP in the past, we still have to download to use in mobile phone installation, which adds unnecessary trouble, process, have a certain share of mobile phone memory, the actual user experience is not good.

WeChat applets are wirelessly connected to the device by Bluetooth and can be opened in the WeChat interface to receive real time data :

Fig. 4. interface for the use of a small program

Bluetooth connection rough flow:

1. Open Bluetooth adaptation

2. get the Bluetooth adapter status to determine whether the device Bluetooth is available.

3. Judge the Bluetooth adapter to open the Bluetooth

device and open the connected Bluetooth device when the Bluetooth adapter is available

4. if the scanning Bluetooth device is unsuccessful after the failure of 5S, the scan is automatically turned on

5. Open the device for scanning the scanned Bluetooth device after it is successful

6. if the new device that has been scanned contains the FeiZhi name (personal product needs), the device begins to connect to the device

7. open and acquire the connected Bluetooth device. After opening and acquiring the device successfully, it is judged that the device name that contains the FeiZhi (personal product need) string will start to connect the device.

8. start getting the Bluetooth device that has been connected without successfully getting the connected Bluetooth device 5S to reopen it automatically.

9. Stop scanning equipment when starting to connect a device, stop the loop and get the connected device.

10. After the connection is successful, the scanning device is stopped and the connected device is obtained by stopping the loop.

II. EFFECT TEST

Through the purification effect of the device and the ordinary haze purifier in the same time to the sealed room, the test results show that the purification effect of the device has obvious advantages, and it can be automatically opened when the haze fog exceeds the standard again, and keeps the indoor air quality continuously.

III. CONCLUSION MODULE

In this paper, the research and design of haze monitoring and purification device, through the use of monitoring module and purification device separate the distributed structure, compared with the traditional integrated haze purifier, the monitoring is more precise and the monitoring range is bigger. By adopting closed loop control, it can make indoor cleaning work automatically, purify efficiency is higher, add the WeChat small program by mobile phone to monitor remotely. It can control the indoor air at any time and anywhere. The existing air purifier has been improved.

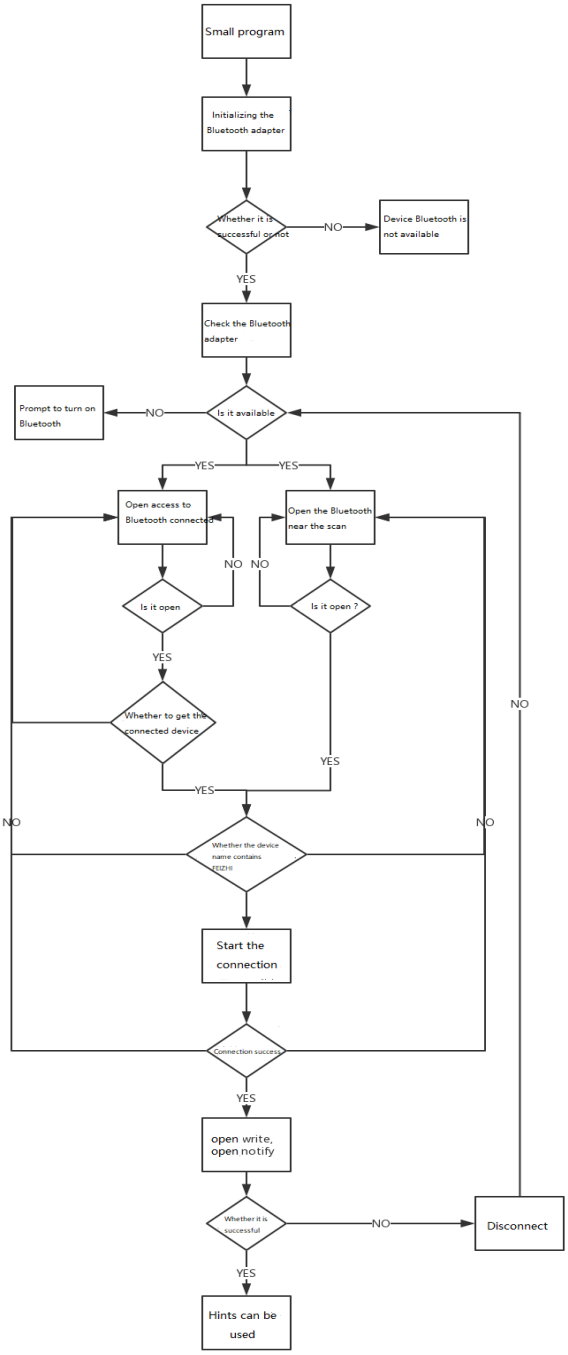

Fig. 5. Program flow chart

References

[1] Cole Brokamp,M.B. Rao,Zhihua (Tina) Fan,Patrick H. Ryan. Does the elemental composition of indoor and outdoor PM2.5 accurately represent the elemental composition of personal PM2.5?[J]. Atmospheric Environment,2015,101.

[2] Giannadaki Despina,Lelieveld Jos,Pozzer Andrea. Implementing the US air quality standard for PM2.5 worldwide can prevent millions of premature deaths per year.[J]. Environmental health : a global access science source,2016,15(1).

[3] Li Qingcai, Zhai dragon, high Yongshan. PM2.5 air purifier single-chip control of the design and research of [J]. based on electronic world, 2016, (22): 55+57.

[4] Liang Yu Chen, Ni Yuanyu, Yu Xi. Air purifier to purify the physical properties of [M]. PM2.5 University, 2015

[5] He Jiajing, Zhou Hui, Liu Tingting, Zhao Jingyi, Xu Zhiyong, Huang Qijun. A consider humidity correction haze detection system [J]. electronic measurement technology, 2015, (10): 96-100.

Design of an automatic search platform for near field interference source based on single probe

Wang Zunxian[1]; Yang Fan[1]; Wang Xueliang[2]; Zeng Guangquan[2]; Wang Shilong[1]
(1.College of Instrument Science and electrical engineering, Jilin University; 2.College of Physics, Jilin University)

***Abstract*-In this paper, the theoretical analysis and production process of an automatic search platform for near field interference source based on single probe are reviewed. The EMC scanning system designed in this paper focuses on combining EMC scanning probe, mechanical arm, analytical instrument and computer to build an automatic scanning platform integrated with scanning, plotting and analysis. The platform collects electromagnetic field information by using the manipulator to control the single probe mobile scanning mode. With the scanning control software and spectrum analyzer, after the computer processing, the electromagnetic field information of the circuit board is obtained, and the subsequent intelligent analysis is carried out automatically.**

***Keywords*-EMC Near field-scanning single probe Mechanical arm**

1 INTRODUCTION

THE electromagnetic compatibility test is used to detect whether all kinds of electronic or electrical products can work normally in the electromagnetic environment, and at the same time, it will not cause any interference to other systems and devices. In recent years, there have been some electromagnetic compatibility scanning devices on the market, which have improved the shortcomings of the time-consuming and low efficiency of manual handheld scanning. For example, EMC-Scanners of foreign Detectus AB company adopts single point scanning mode. EMSCAN's EMSCAN electromagnetic interference scanning system (currently only surface scan scanner) adopts probe array and electromagnetic switch switching scanning technology [1]. At present the domestic only EMC Technology Co. Ltd and the contents of the science and Technology System Co Ltd sales agent automatic scanning near-field scanner. For EMC's automatic scanning platform, Micorosoft, Inpries, Rational, sun, Symantec and other manufacturers have launched various integrated development platforms based on components and Web, including a large number of software structure and component library [2]. NI (National Instrument) and HP (Hewlett-Packard) for the development of the automatic test system developed LabVIEW and VEE automatic test system development platform for large scale, puts forward the concept of virtual instrument, with integrated modular components of hardware and software to realize the automatic test platform, and the hardware board DAQ support for set up automatic test system more convenient[3]. Although most of EMC laboratories have automated test system for EMC test, there are many shortcomings, such as high cost, poor scalability and imperfect functional layer.

The EMC scanning system designed in this paper is based on the current technology, and combined with EMC scanning probe, mechanical arm, correlation analysis instrument and computer, we design a set of PCB electromagnetic radiation interference source automatic search device. The intended target of the device is to automatically obtain the EMI signal of PCB, automatically locate the PCB in the work, and realize the scanning of different positions of PCB. After the scan is completed, the results are fed back to the testers, and the EMI analysis of PCB and the rough diagnosis of the interference source problem are realized. And the platform of the project has no hard requirement for the matching scanning probe and analyzer, which is convenient for the user to further expand in the use.

2 THE COMPOSITION OF THE NEAR FIELD TEST

The near field test system is usually composed of three parts: the spectrum analyzer, the near field test probe and the low noise preamplifier. The frequency spectrum analyzer requires that the frequency range is at least 9K~1.8G, and the matching of interface impedance and the selection of resolution bandwidth should be paid attention to in order to improve the accuracy [4]. The near field test probe is usually divided into a wideband electric field probe, a needle like probe and a circular probe, which can be used to measure the electric field radiation and the magnetic field radiation respectively. The wide-band electric field probe can quickly determine the noise area on the circuit board, and the frequency range can reach more than 1GHz. A needle - like probe can be used to test the electromagnetic interference sources on the printed and IC pins. The frequency range can be up to 700MHz. The annular probe is mainly used to measure the radiation interference of the magnetic field below 100MHz, especially when it is used to measure the sealing performance of the shield machine, especially [5]. The preamplifier requires high gain, high flatness, big obihiro, low noise, fast response and so on. When using the probe, the probe is connected to the input end of the preamplifier through the connection line, and then the output end of the preamplifier is connected to the spectrum analyzer through the connection line. A typical near field test system is shown in Figure 1. After the electronic equipment is tested by conducting and radiating emission, the accurate location of the interference source with electromagnetic interference can be quickly determined through the near field test.

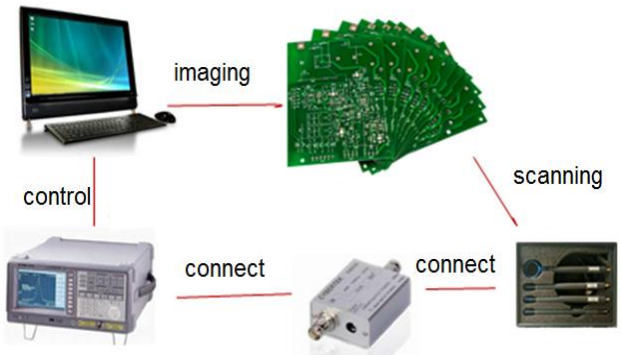

Fig.1 Typical near field test system

3 PLATFORM COMPOSITION

3.1 Hardware platform composition

The hardware part is made up of GPIB (General Purpose for Interface Bus) card, near field probe, low noise preamplifier and U-Arm type mechanical arm, which are computer, spectrum analyzer, spectrum analyzer and computer communication. The hardware connections and relationships of the platform are shown in Figure 2. The actual near field test system is shown in Figure 3.

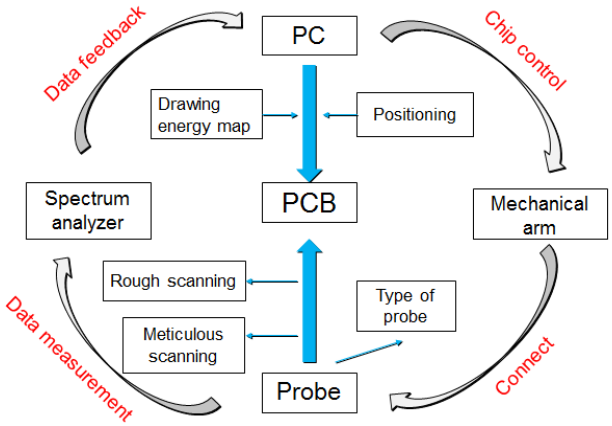

Fig.2 Hardware connection of scanning platform

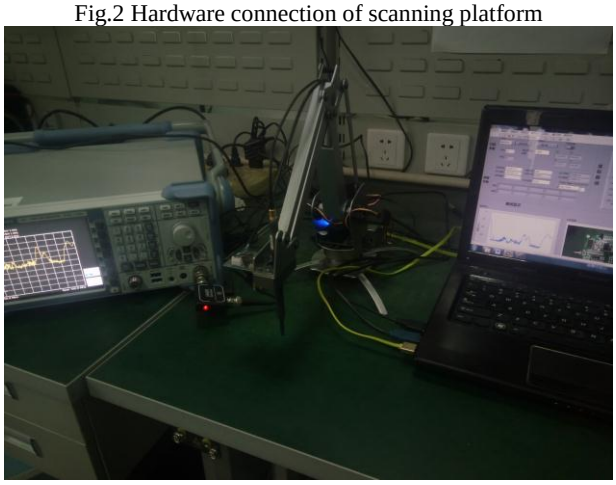

Fig.3 The actual figure of near field test

3.2 Software platform composition

The software of the scanning platform can be divided into three parts: human-machine interaction interface, manipulator scanning module, data processing module, and image rendering module. Finally, the output of PCB electromagnetic radiation energy map is achieved. The relationship block diagram of each part of the software in the work is shown in Figure 4.

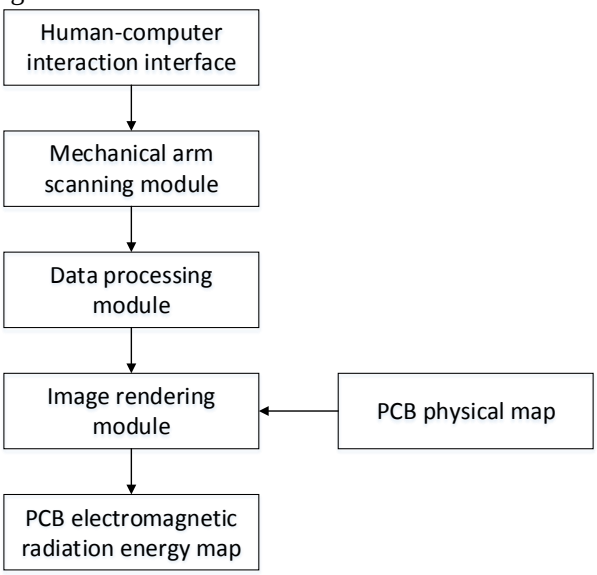

Fig.4 Software connection of scanning platform

4 CONTROL PROGRAM BASED ON LABVIEW

The program based on LabVIEW includes the communication program between the computer and the spectrum analyzer, the control program of the computer to the manipulator, and the user oriented man-machine interface program.

4.1 Communication between computer and spectrum analyzer

The computer program based on LabVIEW includes the communication between the computer and the spectrum analyzer, the processing of test data and the display program of the test results, and the user oriented man-machine interface program. The communication between computer and spectrum analyzer is achieved through GPIB-USB-HS line connection, based on virtual instrument technology. The control program and scanning mode are divided into two data processing modes.

The peak amplitude (Peak Maximum) of each point is marked and recorded in the coarse scan mode, which focuses on the analysis. The amplitude data of each frequency is saved by point scan, and the image is easy to draw. The main program flow chart is shown in Figure 5.

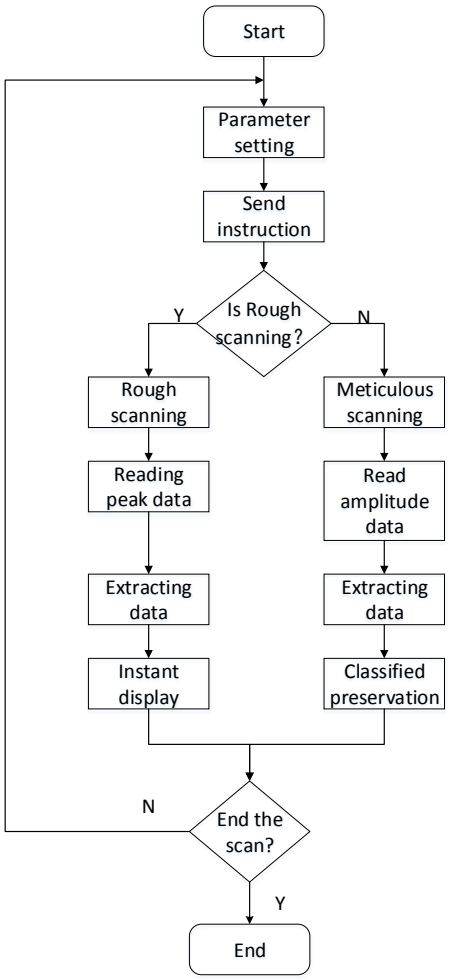

Fig.5 Flow chart of computer controlled spectrum analyzer

4.2 Manipulator control program

The mobile part of the clamping probe is controlled by the manipulator, which is characterized by its convenience in control, large flexibility and easy to meet the requirements. The manipulator is Uarm Metal, and the motherboard is rebuilt based on Arduino UNO. The basic working principle has not changed. The way of interface is serial port RS232. According to the communication protocol, we can control the movement way of the manipulator.

The main content of this module is to control the way of scanning the PCB by controlling the manipulator. By establishing the coordinate system of PCB, the relationship between the location of probe and the point of PCB is one-to-one correspondence. Based on that, an ideal mathematical model can be built between probe and PCB.

In the process of finding the source of PCB interference, the scanning is carried out in two steps. The first step is coarse sampling and scanning. Five points are selected for the picking point, so that the maximum area coverage of PCB can be achieved under a shortest path. The frequency of interference source and the approximate area of the interference source can be analyzed from the data of sampling points. The second step is fine scanning. According to the amplitude of the interference frequency, the scanning path in the jamming area is serpentine scanning. From the start point, the probe moves with a suitable step size as a scanning cycle, and the scanning flow chart is shown in Figure 6. The size of the amplitude of the different points of the frequency is recorded under this path, and the drawing is drawn

In comparison, if the abnormal area is observed in the image, that is, the color is deeper or the area is larger, it may be the region of the interference source.

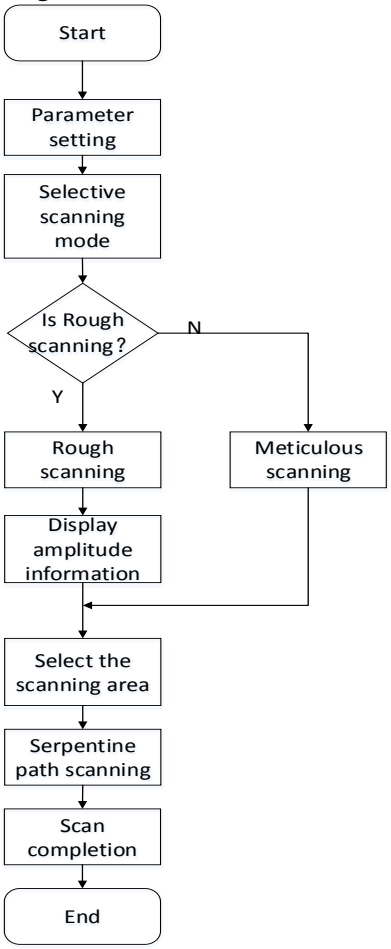

Fig.6 Mechanical arm scanning flowchart

4.3 User oriented human-computer interface

This part of the program uses the controls provided by LabVIEW to achieve human-machine interaction interface similar to the control panel style, which is convenient for the experimenter to modify the relevant test parameters and debug. The human-computer interface includes the selection of the scanning area of the manipulator, the scanning bandwidth and the setting of the sampling rate, the real-time display of the spectrum information, and the drawing of the image. The scanning and spectrum parameter setting interface is like Figure 7.

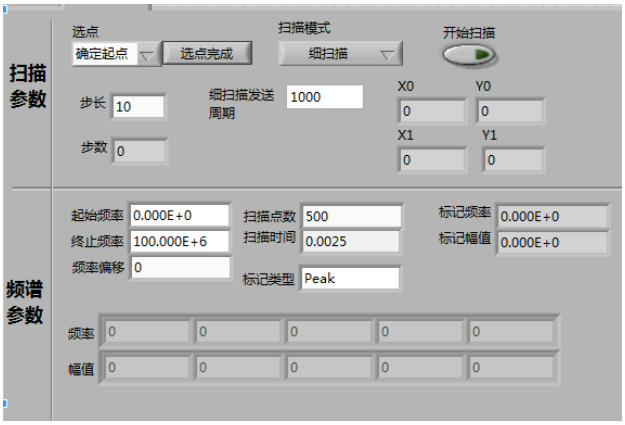

Fig.7 Scanning and spectrum parameter setting interface

5 A HIERARCHICAL DRAWING ALGORITHM BASED ON MATLAB

5.1 An overview of the hierarchical drawing algorithm

After drawing the amplitude circuit board can detect the amplitude distribution of various parts of the circuit board, but the amplitude range of different devices in the normal working hours are not the same, so only by judging the circuit board which point the maximum amplitude or minimum amplitude and cannot find circuit board problems. Therefore, a layered drawing method is designed for the platform to make the amplitude map and physical map combined and display, so that the operator can further analyze the electromagnetic compatibility of the circuit board.

5.2 The principle of hierarchical drawing algorithm

The hierarchical drawing is the selection of a reasonable range of amplitude, and only the point of the range is marked on the circuit board. The user can find it quickly and intuitively when the amplitude of the labeled devices working normally should not fall in the selected range.

After getting the amplitude, the amplitude range of software automatic retrieval of the graph, and convert it to the corresponding value in a range with changes to the standard scale; then the user selected screening range, which depicts the software point falls in the range, and marked in the circuit diagram.

5.3 The realization of stratified drawing

The algorithm flow of the layered drawing is shown in Figure 8, as shown in the drawing of the amplitude diagram and the physical combination diagram, as shown in Figure 9. The implementation steps are as follows:

The first step is to get the amplitude map of the circuit board, and then transform the amplitude map to the corresponding gray scale. The amplitude of each point corresponds to a value between 0 and 255 of the gray value.

The second step, set upper limit m and lower limit n (M and N are 0 to 1 real number, M is greater than or equal to n), then the filter range is [255*n, 255*m];

The third step is to determine whether the gray value of each point falls in the above range. If we fall in the above range, we mark it with color A. If we fall above the above range, we mark it with color B.

The fourth step, put the third step of the layering map and circuit board picture superposition.

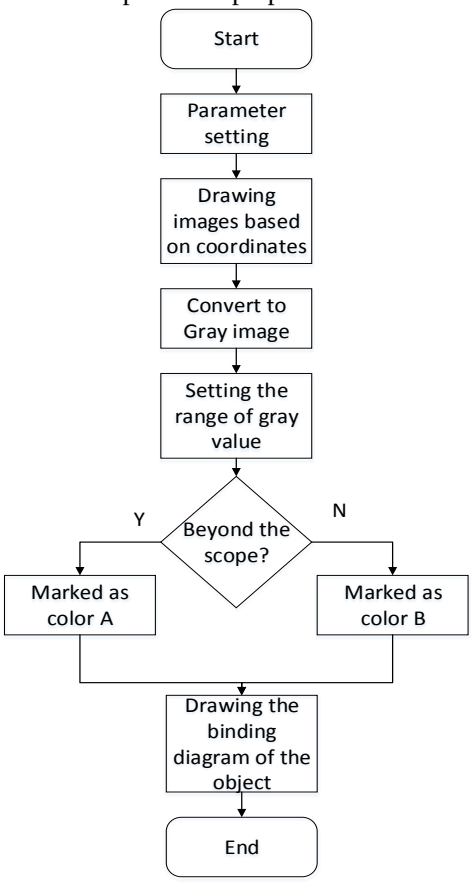

Fig.8 Flowchart of hierarchical drawing algorithm

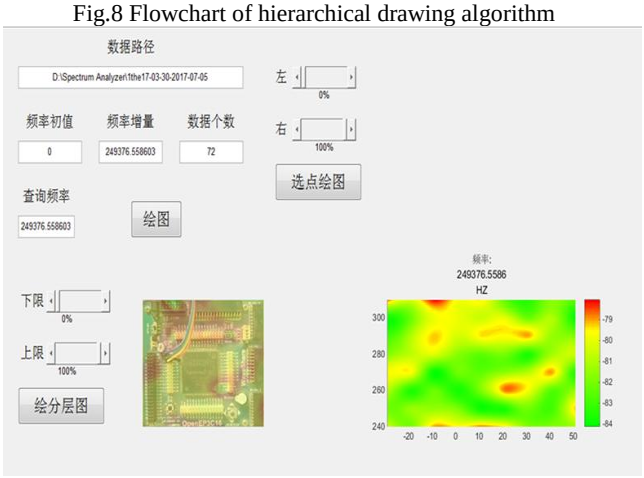

Fig.9 Drawing amplitude diagram and combining with object

5.4 Image result analysis

The color magnitude image MATLAB rendering as Figure 10, draw the real combination of Figure 11.

By combining real figure can be seen in the observation area and power interface chip circuit board power supply interface area to the red area is obvious, which means that the amplitude of the two regions is high, with power in regional power supply when there are high electromagnetic energy, but also can be observed that there exists an obvious red area in the upper left area, for the serial interface, but the interface is not connected to the external device, indicating that this region may be abnormal, and then further analyze whether the existence of regional feedback again or fault analysis personnel to electromagnetic interference.

From this, the electromagnetic energy information of PCB is obtained, and then feedback is given to the analyst to further analyze whether there is a fault in the area or electromagnetic interference.

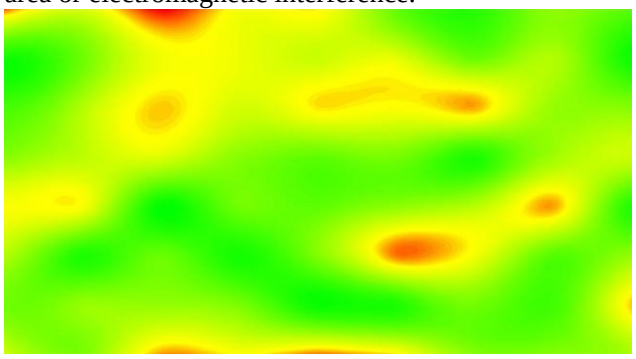

Fig.10 Amplitude diagram

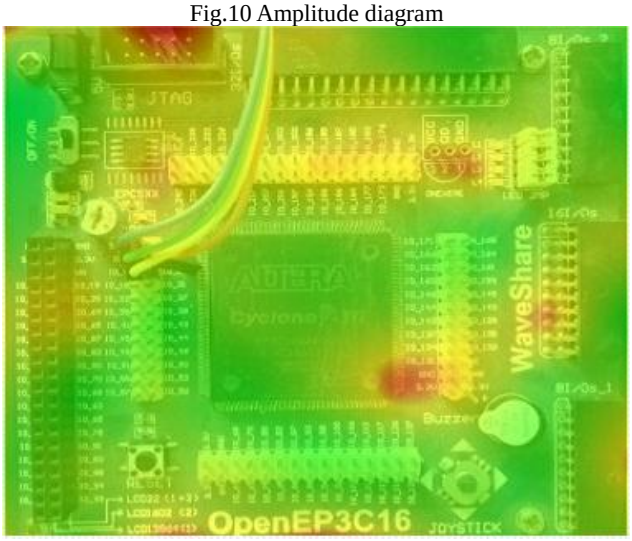

Fig.11 Amplitude diagram and combining with object

6 CONCLUSION

This paper designed a kind of automatic search platform for circuit board single probe near field interference source based on the manipulator control method is the use of single probe scanning mode to collect electromagnetic data, with the scanning control software and spectrum analyzer, after computer processing can get the same circuit board frequency, amplitude and other information, and this project is still on the scan mode is improved and optimized near field test, color distribution map and the physical map image will be drawn out by combining the use of more convenient and fast analysis of interference conditions. It is beneficial for the staff to further analyze and deal with the electromagnetic compatibility of PCB.

References

[1] Wang Kang. Electromagnetic near-field detection technology research [M].: Beijing Institute of Technology 2014.

[2] Zhang Liang. EMC EMC technology and application examples detailed [M]. Beijing: Beijing Industrial Press, 2014.

[3] Gou Jiangchuan, Zhu Feng, Liu Guanghui, Ye Jiaquan, Yang Xiaojia. Design of electromagnetic interference near field test system based on virtual instrument [J]. Computer measurement and control, 2015,23 (01): 16-18+21..

[4] Li Di, Zhu Rui, Tang Hao. Near field test system determination of electromagnetic interference source [J]. space electronic technology, 2000 (03): 52-58.

[5] Wang Zhenyi, Liu Tong, Zhang Yang, Zhou Changlin. A three-dimensional electromagnetic radiation scanning device based on a near field array probe [P]. China: 2014.07.15

The design of remote monitoring system for the control and protection device on the cable of electric vehicle

Sun Legeng; Wang Kaiwen; Guan Bowen
(College of instrumentation Science and electrical Engineering, Jilin University)

***Abstract*-For electric vehicle charging cable when unattended, high real-time requirements, timing dynamic monitoring point acquisition equipment and the operation parameters of the variable problem, designed a GSM wireless network SMS service as a remote monitoring system of each acquisition node and communication medium computer information center. According to the requirements of remote monitoring system, the hardware circuit of the system is designed. The whole machine is composed of 16 bit MSP430F2132 microcontroller with ultra-low power consumption, which is composed of acquisition circuit, GSM module circuit, serial port to USB circuit and so on. Using the computer as the monitoring center, the whole system is verified, and the high efficient and practical data transmission of the electric vehicle charging monitoring system is realized.**

***Key words*-Remote monitoring; micro controller; GSM module**

0 THE PREFACE

WITH the development of mobile communication technology, GSM network has developed into a very mature wireless communication network, which has been gradually applied to the monitoring field. On using GSM network as the electric car line charging information transmission platform of remote monitoring system is an effective method and its principle is simple, high confidentiality, do not need to form a special network and maintenance of the network, and the GSM network coverage is extensive, so compared with traditional monitoring system has its unique advantages in[1] . Therefore, designed a GSM network transmission platform based on electric cars line charging remote monitoring system, the system of computer information center, monitoring terminal and maintenance personnel to communicate, in the form of short message on this model of the electric car line charging remote monitoring system has wide application prospect.

1 THE COMPOSITION OF THE REMOTE MONITORING SYSTEM

It is composed of microcontroller, sensor information acquisition and GSM module of data acquisition subsystem, network information center and GSM module block of monitoring subsystem, wireless communication subsystem and other parts[2] . With MSP430 microcontroller as the core of data acquisition subsystem is mainly to complete the information collection and sensor signal acquisition, storage, display, coding, PC and send data, receive send control information and control system of the operation of the terminal equipment, etc. It collects information through the microcontroller and sends it to the wireless communication subsystem after data encoding and processing to complete the real-time monitoring. Its design block diagram is shown in figure 1.

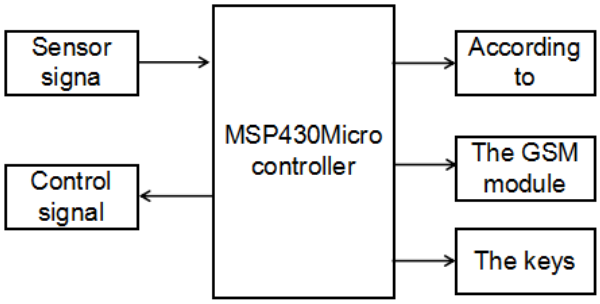

FIG. 1 design block diagram of data acquisition subsystem

The main task of monitoring system is to send remote command, receive data information and conduct data processing. After receiving the data sent by the data acquisition subsystem, the information center is processed by the computer of the network information center for data decoding, analysis and storage[3].When the system determines to receive the alarm information, the network information center sends the message to the maintenance personnel, which is helpful for the system maintenance personnel to grasp the operation state of the equipment in a timely and accurate manner. Its design block diagram is shown in figure2.

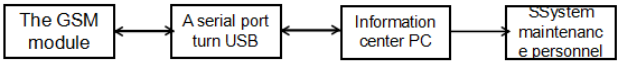

FIG. 2 design block diagram of monitoring subsystem

The wireless communication subsystem in the remote monitoring system is the core of GSM module, and it relies on the GSM network platform to complete the sending and receiving of SMS messages. When the whole system runs, the information center PC communicates with the acquisition node of the data acquisition subsystem. The specific principle is as follows: the data acquisition subsystem, by collecting sensor signals, encodes the system's equipment and operation parameter information into short message strings and returns the monitoring sub-system[4]. The monitoring subsystem receives the short message sent back by the data acquisition subsystem. After the decoding, the data acquisition subsystem's equipment and operation parameter variable information can be

obtained. The monitoring subsystem sends instructions to the data acquisition subsystem through GSM module to control the operation of related equipment.

2 SYSTEM HARDWARE DESIGN

System adopts micro controller of TI company MSP430F2132 constitute the main control circuit, by the acquisition equipment or environment information circuit, display circuit, key circuit, control circuit, GSM module circuit, a serial port turn USB circuit, etc. MSP430F2132 sends the information encoded by the set to the digital tube, and the MSP430F2132 controls the GSM module and sends the encoded information in short message mode. At the same time, another GSM module receives the information via the serial port to the information center PC. After the PC decodes, the information is stored in the database. When the PC determines the alarm information, the information center sends the message to the maintenance personnel, so that the monitoring terminal equipment can be maintained timely[5]. This method can reduce the system expenditure, avoid the huge economic loss caused by the accident, ensure the whole system works and play a role.

2.1 Micro controllerMSP430F2132

Based on the principle of low power consumption, energy saving and environmental protection, MCU adopts the MSP430F2132 of TI company as the micro-controller.[6] It is a 16-bit ultra-low-power microcontroller with built-in hardware resources, including 512 bytes of static RAM, 8KB FLASH, multiple serial input interfaces, real-time clocks, and so on. Under the clock condition of 1MHZ, the chip current is about 200 ~ 400 mu A, and the lowest power consumption in the clock mode is only 0.1 mu A; It has 5 power saving modes and can be aroused by RTC and external interrupts. These functions integration makes MSP430F2132 suited for measurement and control, and qualified for remote monitoring of control function module, its abundant internal resources can not only reduce the area of the circuit board, and can reduce the cost of the whole system.

2.2 Digital tube drive circuit

The digital tube is mainly responsible for displaying the operating state and time of the system. The traditional digital tube occupies MCU pin resources, which can be controlled by the I/O level trigger. With the increase of the digital tube, the number of pins occupied will also increase [7]. In order to solve this contradiction, easyarm company launched a integrated digital tube driver chip ZLG7290B management function and the keyboard scan, it can directly drive 64 were Yin type digital tube or eight independent leds, can manage up to 64 keys at the same time. The chip adopts the I2C bus mode, which is convenient to connect with MCU. At the least, it only needs 2 I2C interface signal lines, so it can greatly save I/O resources. Its biggest advantage is that can choose the number of digital tube according to system requirements, and the expansion of the digital tube need to increase the MCU hardware overhead, there are 10 kinds of 21 kinds of letters and Numbers at the same time provide the decoding display function, and save the workload of MCU, which can be used in signal detection and control of pooling resources. As an industrial-grade chip, the chip has strong anti-interference ability and is widely used in industrial measurement and control. In this design, 8 digital tubes are adopted, and the schematic diagram of digital tube circuit is shown in figure 3.

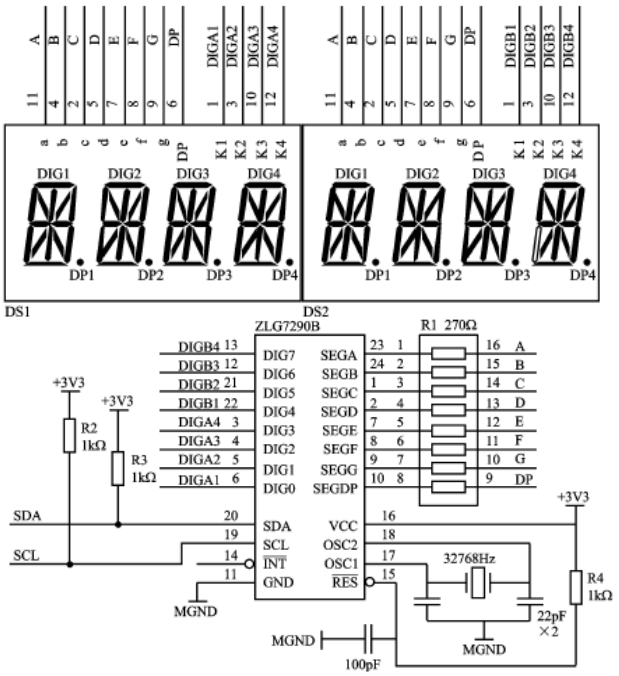

FIG. 3 schematic diagram of digital tube driving circuit

In figure 3, ZLG7290B requires only two CPU's I/O lines, respectively, the I2C bus port data transmission line SDA, the clock transmission line SCL, DS1 and DS2 are the common negative digital tubes. Since both the SDA and SCL pins are the output structures of the drain open circuit, it is necessary to add 1K upper pull resistance. The advantage of the open leakage structure is that when the bus is idle, both of these signal lines are kept high and almost no current is consumed; The electrical compatibility is good, the upper pull resistance is connected with 5V power supply, and the upper pull resistor is connected with 3.3V logic device. Because of the open leakage structure, between SDA and SDA of different devices, SCL and SCL can be directly connected, no additional conversion circuit is required. R1 is a current-limiting resistor with a resistance value of 0.27K. If the brightness of the digital tube is to be increased, the resistance value can be reduced appropriately.

2.3 GSM Module circuit

GSM module selects GC65 module in this system, compact design, greatly reduce the volume of the user product, the integrating radio frequency circuit and baseband module, to provide customers with the standard of the AT command interface, for data, voice, short message and fax to provide fast, reliable and safe transmission, convenient for the user's application development and design. Therefore, this system USES MSP430F2132 (microcontroller) working mode of the

GC65 module for real-time adjustment, setting module is dormant for a long time, when the need for data communication, through the AT command to activate module, data communication over, timely restore a dormant state, in order to reduce the power consumption of the system as a whole. The GSM module circuit is shown in figure 4. The start pin PWRKEY of GC65 is connected to the I/O port of MSP430F2132, serial port TXD and RXD are connected to the serial port of MSP430F2132. SIM-VDD, SIM-DATA, SIM-CLK, SIM-RST for SIM card interface, and connect SIM card through 6 pin slot. The P10 in the figure is the antenna interface, the VBAT is the power supply of GC65, and the working status indicator of GC65 is connected to the collector of the three-level tube. When GC65 is working normally, NETLIGHT is alternating between high and low levels, which drives the triode to guide and cut off, so the LED flashes indicate the state of work.

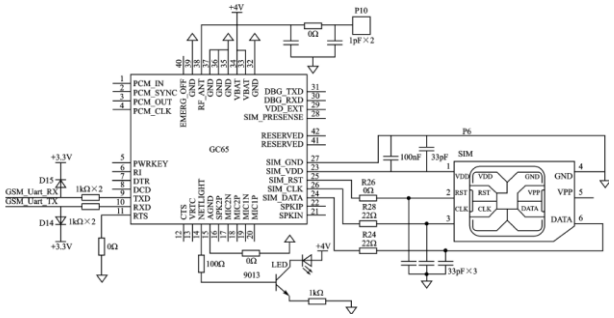

FIG. 4 circuit diagram of GSM module

2.4 Serial port transfer USB module circuit

Due to monitoring subsystem, the GSM module USES RS232 communication, traditional motherboard has the interface, but due to the motherboard market positioning is different now, a lot of new motherboard is not with serial interface, for example, the laptop is rarely again with the old interface. And USB interface is a whole new set of PC system in the industry standard, with its low cost, simple to use, flexible protocol, interface standardization and the advantages of easy to port extension, quickly occupied the dominant position in the field of computer peripherals interface, it has a very wide range of the application of [8]. In order to solve the communication problem between GSM module and PC, we adopted the chip PL2303, which is introduced by the company, to realize the serial port transfer USB interface . The PL2303 built-in USB function controller, USB transceiver, oscillator and UART with full modem control signal can realize the conversion of RS232 signal and USB signal with only a few capacitors. The serial port transfer USB module circuit is shown in figure 5. The TXD and RXD of PL2303 are connected to the RXD pins of GC65 and TXD pins respectively, thus completing the conversion between the serial port of GC65 and the USB port. GC65 data sent out from the serial port is converted to a USB data stream via the PL2303 chip and transmitted to the host device via a USB connector. As you can see, the connection between PL2303 and GC65 is very simple, just two signallines.

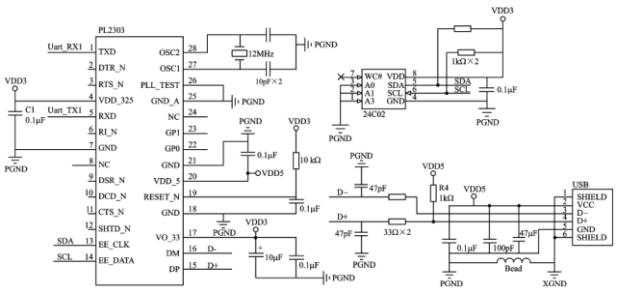

FIG. 5 circuit diagram of USB module in serial port

3 System Software Design

System software design system mainly includes data acquisition subsystem. MPS430F2132 lower computer software and remote monitoring center upper computer software. The software of singlechip processor system is focused on MSP430F2132 programming, the main program including sensor assembly module, digital tube display module, keys module, control module, GSM SMS communication module and so on, finally by these modules to complete the equipment running status monitoring. The main program initializes the system first, including the initialization of the clock, initialization of timer, initialization of asynchronous serial port communication, and initialization of I/O port of MSP430F2132. The communication between the upper computer and the lower machine adopts GSM short message mode for wireless transmission. The implementation of the upper computer USES Labview,as shown in figure 6.

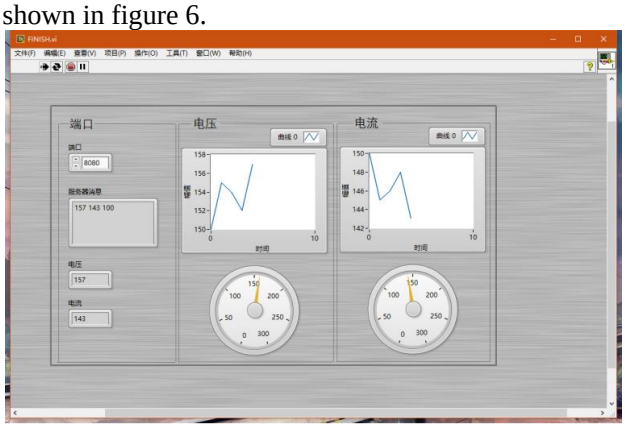

FIG. 6 Labview test results

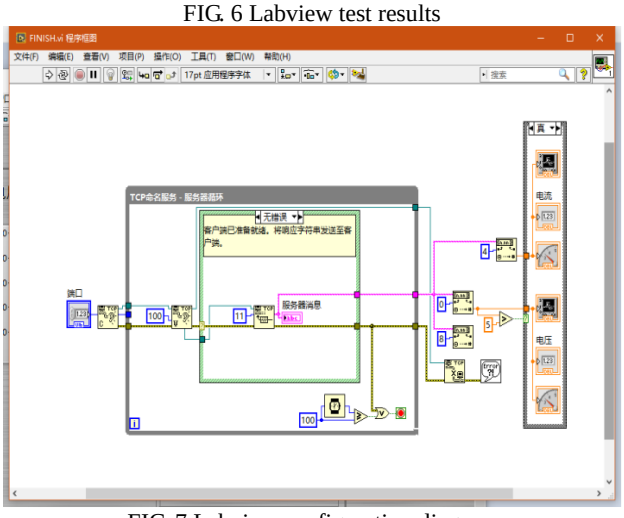

FIG. 7 Labview configuration diagram

4 THE CONCLUSION

Wireless technology has been used increasingly in industry and daily life, the role is becoming more and more prominent, especially some monitoring and data transmission system, achieved through the method of traditional cable is very complex, even could not realize, and wireless technology has made some monitoring and the establishment of the data transmission system implemented and become very simple. Combined with the GSM wireless data transmission and network application technology, single-chip microcomputer technology, sensor technology, automatic control technology and software technology to design a set of electric vehicle based on GSM remote monitoring system of charge on the rope. In mobile, unattended, point to point of low real-time demand and large network coverage, not timing dynamic monitoring data acquisition, compared with traditional monitoring system, the system has the user less small investment, operation cost, wide coverage, high safety, simple operation, strong commonality, etc.

Reference

[1] song chao, li xin, dong jingwei. Wireless data acquisition system based on tc35i and MSP430F149 [J]. Journal of Harbin Institute of Technology, 2007,12 (2) : 103-106.

[2] jiang jin, wang xin, Yang huizhong. Design of wireless environment monitoring system based on MSP430 SCM [J]. Journal of jiangnan university: 2011,10 (1) : 45-48.

[3] li haitao, lei wendong, wang jianmin, etc. Design of man-machine interface module based on ARM7 [J]. New device applications, 2010,12 (3) : 7-10.

[4] Yang kai. USB interface design and its application in control system [D]. Beijing: Beijing university of posts and telecommunications.2010.

[5] IQURE V.Security issuesinscadanetworks [J]. Computers and security, 2006, 25 (7) :498-506.

[6] fan jing, wang jianming. Design of wireless detection system for museum status based on cc2530 [J]. Electronic measurement technology, 2011,34 (6) : 105-108.

[7] Chen Wei. The research and development of GSM network quality detection system using single chip microcomputer technology [J]. Automate the expo. 2009,12:86-88.

[8] wen junfeng, zhang wen-ai, wang cheng, etc. Research and design of multi-interface data communication module [J]. Microcomputer information, 2007,23 (4-2) : 143-145.

Survey of Noninvasive Blood Pressure Measurement Technology

Xiaoyu Li; uyuan Wang; Yuyao Yang
（*Instrument Science and Electrical Engineering College，Jilin University*）

***Abstract*-This paper describes several non-invasive blood pressure measurement methods,including stethoscopy, oscillometric method, volume compensation method, arterial tonometry, pulse wave velocity and pulse wave parameter determination. Focusing on the domestic and foreign non-invasive continuous blood pressure measurement of new and practical techniques for a more detailed introduction, this paper contains ultrasonic method and the application of wavelet analysis and fuzzy recognition in blood pressure measurement etc. Based on the current situation of research, the prospect of non-invasive blood pressure measurement, especially pulse wave velocity measurement, is put forward. It is proposed that continuous measurement of non-invasive blood pressure measurement should be the current development direction.**

***key words*-Noninvasive; Blood pressure; Continuous measurement**

I.FOREWORD

BLOOD pressure is an important parameter in the human blood circulatory system. As one of the important physiological indicators of the human body, blood pressure can reflect many physiological information of the human body and provide an important basis for assessing the health condition. Non-invasive arterial blood pressure measurement is safe, convenient, and low in infection rate compared to invasive arterial blood pressure measurement. It has been widely used in clinical practice. The obvious shortcoming of traditional intermittent blood pressure measurement is that continuous monitoring can not be achieved and enough continuous data can not be provided. Continuous measurement of blood pressure can obtain continuous change of blood pressure data, which is of great significance. Therefore, the study of non-invasive continuous blood pressure measurement will be the focus of future development of blood pressure measurement [1]–[3].

II.TRADITIONAL NONINVASIVE BLOOD PRESSURE MEASUREMENT TECHNOLOGY

The body's noninvasive blood pressure measurement study began in 1875. In 1876, Marey, a French physiologist, put forward the prototype of the measurement technique of constant volume method. In 1896, Recklinghuasen first discovered the most widely used noninvasive blood pressure measurement technology, oscillometric blood pressure measurement technology. In 1905, Soviet scientist Korotkoff discovered Korotkoff sound, which laid the foundation for Korotkoff auscultation blood pressure measurement. Since then, noninvasive blood pressure measurement has been widely accepted and applied clinically, and has also been praised as the "gold standard" for noninvasive blood pressure measurement. Noninvasive blood pressure measurement developed to today, there have been a variety of measurement techniques and products, and because of its easy to carry, simple operation, stable measurement results and other characteristics are widely used, the most representative of which is Korotkoff sound method, Wave method and constant volume method.

A. Auscultation method (Korotkoff sound method)

Auscultation, also known as Korotkoff sound method, is the earliest method used to measure blood pressure. The specific operation is to pressurize the cuff, blocking the blood flow, and then gradually deflated, the use of stethoscope to listen to the pulse of sound, the first pulse of the sound pressure is considered to be high pressure, systolic blood pressure, continue to deflate the pulse slow When the pulse sound stable and normal, then that the blood vessels are not squeezed, that is, as a low pressure, diastolic blood pressure, but its accuracy by human factors, including the subjective perception of the human body and cuff standards.

In 2012, Yuan Yuan and others from the School of Communication and Information Engineering of Shanghai University improved the traditional Korotkoff sound method and proposed an automatic control system based on Korotkoff sound recognition. The system collects Korotkoff signals through the pickups. After passing through the second-order low-pass filter circuit and the amplifier circuit, the system accesses the mobile phone of the Android module through the MIC port. The systolic and diastolic blood pressures are identified by the Korotkoff's power recognition algorithm, Effectively solve the noise reduction and recognition problems of Korotkoff[4].

B. Oscillometric method (Oscillometric method)

Oscillatory method, also known as shock method, the application began in the 1970s, is the most commonly used blood pressure measurement method. The principle is to block the upper arm arterial blood flow by inflating the cuff, and then intermittent deflation to establish the relationship between pulse wave and cuff pressure to assess systolic, diastolic and mean pressure. Oscillometry compared with Korotkoff sound, oscillometric method to measure blood pressure interference is small, easy to operate, good repeatability, measurement error is relatively small, etc. However, the measurement of blood pressure, systolic and diastolic pressure calculation algorithm is not uniform Standard, most of the current equipment to determine blood

pressure are based on empirical algorithms, the accuracy is relatively low, while it still inflated and deflated process, it can not be achieved continuous measurement of blood pressure. In order to further improve the existing oscillometric method and improve its measurement accuracy, many domestic and foreign scholars have made some improvements [5]. Oscillometry method to measure blood pressure is the key to accurate collection of blood pressure and pulse wave signals, and finally calculated by systolic and diastolic blood pressure by appropriate algorithms. Blood pressure and pulse wave signal acquisition accuracy is mainly to improve the pressure sensor, filter circuit and amplifier circuit, which has been very mature, the space for improvement is not large, so most scholars mainly study blood pressure algorithm, through the algorithm Improve its accuracy.

In 2008, Bo Rongqing et al proposed a "condition selection type" electronic sphygmomanometer. The design concept of the sphygmomanometer is to use different characteristic coefficients for different physical conditions of the population, and to use statistics to obtain the characteristics of different body conditions in the research and development process Coefficient, this sphygmomanometer is more accurate than the current electronic sphygmomanometer on the market [6]. In 2011, Majid Mafi et al. of the School of Information Technology and Engineering at the University of Ottawa developed a novel pulse-based method for estimating blood pressure, which was obtained by oscillometric blood pressure measurements. Quantitative measurements are made by using the pulse waveform to obtain the estimated mean arterial pressure, systolic pressure, and diastolic pressure. The quantitative measurement of the oscillometric pulse waveform is different from the parallel cuff pressure curve. The total maximum and minimum values for each quantitative measurement are known. The maximum and minimum values of the pulse are used to calculate the average pressure (MAP) [7].

III.CONTINUOUS NON-INVASIVE BLOOD PRESSURE MEASUREMENT TECHNIQUES

A. Artery tension test

Arterial tensiometry was first proposed by Pressman in 1963, and in 1967 Japan's Colin and CBM developed commercial products. Arterial blood pressure tension measurement method is a continuous measurement of blood pressure method, by placing a pressure transducer placed in the radial artery site, the artery is located near the bones to pressurize, so that the arteries flattened, then the force on the surface And the arterial blood pressure is approximately proportional to the pressure transducer can be detected on the surface of the pressure, so you can get a cardiac cycle pressure waveform, and maximum and minimum arterial pressure signal to obtain the blood pressure value [8] . This method requires a high positioning of the sensor. The artery must be pressured on the arm during the measurement. For continuous measurement, it is difficult to keep the position of the sensor for a long time. Therefore, most of the instruments applying the method are in the experimental stage.

In 2013, Byeungleul Lee and Jinwoo Jeong of the Korea University of Science and Technology and Seoul National University proposed a cantilever-arranged blood pressure sensor that uses a tonometry to measure blood pressure. Developed a blood pressure sensor array consisting of a cantilever array of small sensors, which increases its spatial resolution and improves the accuracy of blood pressure measurements [9].

B. Volumetric compensation method

Volume compensation method, also known as constant volume method. In 1973, the Czech Jan Penaz in-depth studied the constant volume method of blood pressure measurement technology; in 1980, Yamakoshi.K applied photoplethysmography to the blood pressure measurement [10]. Assuming that the volume of the blood vessel does not change and the pressure inside and outside the blood vessel is the same, the blood wall is under no-load action. When the pressure inside the blood vessel changes, the pressure outside the blood vessel changes accordingly to ensure that the volume of the blood vessel does not change. At this point by measuring the external pressure indirectly get arterial blood pressure. In continuous blood pressure measurement today, volume compensation is the most mature, it can achieve changes in arterial blood pressure in real time tracking. However, this method has a great effect on venous congestion when measured over a long period of time. The part to be tested has to maintain a certain pressure for a long time, and the comfort is poor. At the same time, the testing equipment is more complicated.

At present, many scholars at home and abroad to study and improve the volume compensation law, in 2009, Heilongjiang University, College of Electrical and Mechanical Engineering Gao Shumin, Song Yilin and Japan Kanazawa University Engineering Department of Tanaka, Shinsei Yamamoto proposed to volume compensation method for continuous monitoring of wrist blood pressure Module, the module to the radial artery at the wrist as the test site, using a partial pressure cuff and a new electro-pneumatic converter [11]. In 2011, Shinobu Tanaka, IEEE member Kanazawa University in Japan, proposed a blood pressure monitoring module with a padded cuff to locally pressurize the radial artery. The principle of application is that volumetric compensation measures blood pressure [12].

C.Pulsewavevelocity (PWV)

Pulse wave is formed by the vibration of the heart spread out along the artery and blood vessels. The pulse wave velocity can reflect many cardiovascular pathological information. The waveform and amplitude of the pulse wave can infer the human body's blood pressure and other related human physiology Information [13]. In 1966, Schimmler calculated the relationship between pulse wave velocity and blood

pressure statistically. In 1976, a large number of experimental results by Gribbin and Steptoe and Sleight showed that the pulse wave speed reliably followed the blood pressure changes. The accurate arterial blood pressure value was deduced for the first time by Tanka, but the precision needs to be improved.

The pulse wave velocity method has to be compared with a standard measurement to establish a mathematical model between the pulse wave and the blood pressure value. Measurement, the required parameters into the blood pressure equation can be systolic and diastolic blood pressure. The pulse wave velocity method makes it easy to measure without the need for pressure. This method can accurately measure the average pressure and systolic blood pressure, but for the diastolic blood pressure there is a certain discrete type, the need to further improve its accuracy [14]. In 2008, Petr Zurek et al. At Hitler Technical University in Czech Republic proposed a comparison of blood pressure measurements using near-infrared CCD camera and pulse transit time, and established a mathematical model for statistical analysis. The diastolic blood pressure And systolic blood pressure [15].

One of the key problems in accurately measuring blood pressure lies in the effective extraction of the characteristics of blood pressure signals, and scholars at home and abroad have made improvements in this respect. The combination of wavelet transform and fuzzy recognition technology can effectively detect the peak point of pulse wave signal, accurately calculate the pulse wave conduction time and effectively extract the feature of the useful signal to accurately determine the value of the human body's high blood pressure. In 2008, Li Dingli and others from Zhejiang University Institute of Biomedical Engineering and Instrument Science put forward a method based on pulse wave velocity method, using wavelet transform to detect the peak point of pulse wave signal and accurately calculate the pulse wave conduction time, and on this basis, Human arterial blood pressure principles and methods. It solves the problems of ECG and pulse wave signal synchronization in other blood pressure acquisition system based on pulse wave velocity method and low calculation accuracy. Instrument error <8mmHg, mean square deviation <8mmHg, in line with the United States Institute for the Advancement of Medical Devices (AAMI) standard deviation of not more than 8mmHg [16].

In 2016, Gu Ya-xiong et al (School of Mechatronics Engineering, Southwest Petroleum University, Chongqing Cancer Hospital, Gu Ya-xiong, et al.) In order to overcome the difficulty of modeling BP model and low accuracy of model in noninvasive blood pressure measurement by pulse wave velocity method, (1 / TPTT) 2 modulus to establish a multi-modal blood pressure calculation model. The experimental results are in line with the requirements of the American Medical Device Promotion Society SP10-199 that the difference value of the electronic sphygmomanometer does not exceed 8 mmHg, demonstrating the validity of the multi-mode blood pressure calculation model for non-invasive blood pressure measurement [17].

D. Pulse wave characteristic parameter determination method

The pulse wave parameter determination method extracts characteristic points that can fully reflect blood pressure through the pulse wave, and establishes the relationship between the blood pressure and the pulse wave characteristic parameters according to the pulse wave principle and arterial elastic cavity theory. Pulse wave characteristic parameters commonly used are the main wave height, wave rise time, heavy pulse wave height, the relative height of the heavy pulse wave, the height of the descending midline, the relative height of the mid-fall, pulsation period [18].

In 1996, Luo et al. Proposed a new extraction method of pulse waveform characteristic value K based on the change of pulse wave area, which is proved by theoretical analysis and a large number of experiments. Peripheral vascular resistance, wall elasticity and blood viscosity and other physiological factors, they are important physiological indicators of clinical examination of cardiovascular disease [19]. In 2002, Jiaoxue Jun and Fang Xingye proposed the selection of multiple pulse wave parameters related to blood pressure by studying the relationship between blood pressure and pulse wave parameters, and established a characteristic equation suitable for different populations by stepwise regression analysis to achieve continuous measurement of blood pressure [20].

In 2014, Xiaochuan He et al at Carleton University studied a non-invasive method to estimate blood pressure. The main idea is to measure the pulse transit time (PTT), the delay between the peak of the ECG signal and the subsequent peak of the finger photoplethysmography (PPG) signal and to design three quadratic peak detection methods The secondary peak of the original PPG signal is revealed to overcome the problem that the position and amplitude of the main peak of the PPG signal will change when the dicrotic notch of the PPG signal is unobservable. The actual ECG, PPG and blood pressure measurements taken from the intensive care II multi-parameter smart monitoring database containing data reflecting the actual measured clinical signals were used. The results demonstrate that adjusted PTT can be used as an indicator of arterial blood pressure by eliminating the effect of the doubly-fed notch on PPG signaling [21].

E. Ultrasonic manometry

Ultrasonic Manometry The Doppler effect of ultrasound on blood flow and vessel wall motion can be used to detect blood pressure. It is characterized by a wide range of applications, such as accurate measurement of blood pressure in infants and shock patients. In addition, arterial waves can be completely reproduced. The measurement method is to place two sensors at the crotch strap distal to the caudal end of the cuff with a bandwidth of 1/3 sleeve, one for sending ultrasound waves to the artery, and one for receiving

reflected waves. During deflation of the cuff, when the brachial artery pressure is equal to the cuff pressure, the arterial wall starts to vibrate and cause Doppler shift, and the frequency of the cuff pressure detected at the first time is the systolic pressure and the frequency shift The cuff pressure at a significant reduction is diastolic. The accuracy of the method depends on the location of the sensor, so that when the body is in motion it causes changes in the ultrasound path between the sensor and the blood vessel, causing measurement errors [22].

Ⅳ. CONCLUSION

Continuous blood pressure measurement has very important clinical value, and with the improvement of equipment accuracy and cost reduction, non-invasive blood pressure measurement technology has become a common development direction at home and abroad. In the era of big data, the combination of blood pressure measurement with wireless network technology and cloud technology has also become a necessary trend.
In the non-invasive continuous blood pressure measurement method, the pulse wave velocity-based technique has broad prospects for development. Although the pulse wave and its parameters are very sensitive to various factors such as individual differences, affecting the measurement accuracy, and there is no unified standard of pulse wave conduction and arterial pressure. If combined with a variety of detection methods to find out the relationship between changes in blood pressure and pulse wave, blood pressure measurement accuracy will be further improved, the development is different from the traditional measurement methods based on pulse wave characteristics, with the application of new measurement techniques, noninvasive Continuous blood pressure measurement will have good applications and prospects.

References

[1] WEI An-hai, YIN Jun, CHANG Fei-ba, et al. Research Progress in Non-Invasive Continuous Blood Pressure Measure [J]. China Medical Devices, 2015, 30(11):68-70.

[2] ZHENG Li-hua, DOU Jian-hong, HE Xing-hua,et al. Improvement and development of non-invasive blood pres sure measurement techniques [J]. China Medical Equipment, 2013, 10(3):49-52.

[3] YU Xiao, LIN Jun, LI Su-yi. Development of Non-Invasive Blood Pressure Measurement Technology. [J]. Guangdong Medical Journal, 2012, 33(15):2356-2359.

[4] YUAN Yuan, XUE Lei, HE Jin-sheng. A New Automated Biood Pressure System Based on Auscultatory Identify Method[J]. Electronic Measurement Technology,2012,35(2): 76-79.

[5] WANG Wei-wei, PU Bao-ming, LI Jin-sheng,et al. Algorithm Improvement of Blood Pressure Measurement Based on Oscillography[J]. Computer Systems & Applications, 2012, 21(2): 196-199.

[6] Bai Rong-qing, Wei Jing-feng, Sha Xian-zheng. Study on Measurement Accuracy of Electronic Sphygmomanometer and Improvement Method [J]. Seek Medical And Ask The Medicine, 2013(4):166-167.

[7] Mafi M, RaJan S, Bolic M, Groza ZV, DaJani RH. Blood Pressure Estimation using Oscilometric Pulse Morphology. 33rd Annual International Conference of the IEEE EMBS [C], Boston Massachusetts USA, August 30-Seotember 3,2011.

[8] Xu Ke, Zhou Qi, Wei Yun-long.Noninvasive Measurement of Blood Pressure[J]. Journal of Chongqing University of Technology(Natural Science), 2008, 22(1): 164-167.

[9] Lee B, Jeong J, Cho C, et al. Cantilever Arrayed Blood Pressure Sensor for Arterial Applanation Tonometry. IEEE NEMS2013[C]. Suzhou China, 2013.

[10] Tanaka S, Nogawa M, Yamakoshi T, Yamakoshi K. Accuracy Assessment of a Noninvasive Device for Monitoring Beat-by-Beat Blood Pressure in the Radial Artery Using the Volume-Compensation Method[J]. IEEE TRANSACTIONS ON BIOMEDICAL ENGINEERING, 2007, 54(10): 1892-1895.

[11] GAO Shu-mei, SONG Yi-lin, TANAKA Shinobu,et al. An Instantaneous Blood Pressure Measuring System at Wrist Based on the Volume-Compensation Method[J]. Chinese Journal of Medical Instrumentation, 2009, 33(5): 323-327.

[12] D'Angelo LT, Lohmann.M, Lueth TC. A new device for motion-aware ambulatory blood pressure measurement. 2011 5th International Conference on Pervasive Computing Technologies for Healthcare(PervasiveHealth) and Workshops[C], Dublin, Ireland,2011

[13] Ma T, Zhang YT. A Correlation Study on the Variabilities in Pulse Transit Time, Blood Pressure, and Heart Rate Recorded Simultaneously from Healthy SubJects. Proceedings of the 2005 IEEE Engineering in Medicine and Biology 27th Annual Conference[C]. Shanghai China, 2005

[14] Wang Q, Wang YP, Mei Z, Liu ZW. An Inproved Algorithm for Noninvasive Blood Pressure Measurement. Bioelectronics and Bioinformatics (ISBB), 2011 International Symposium on[C]. Suzhou,China:2011

[15] ZHANG Jun-li, LIN Chang-yan, YANG Lin. Detection Of Waveform Characteristic of Pulse Wave and Analysis of Its Related Partial Hemodynamic Change[J]. Biomedical Engineering and Clinical Medicine, 2008,12(2): 104-107.

[16] LI Ding-li, CHEN Yu-quan, XING Lei,et al. Non-Invasive Blood Pressure Measure Based on Wavelet Transform[J]. Journal of Zhejiang University(Engineering Science), 2008, 42(9): 1648-1652.

[17] GUY Ya-wei, YANG Tao, BAO Ke,et al. Study on Multi-Mode Calculation Model in Non-Invasive Blood Pressure Measurement by Pulse Wave Velocity Method [J]. Chinese Journal of Biomedical Engineering, 2016, 35(6):691-698.

[18] Martina J R, Westerhof B E, Van G J, et al. Noninvasive continuous arterial blood pressure monitoring with Nexfin®.[J]. Anesthesiology, 2012, 116(5):1092-1103.

[19] Lou Zhi-chang, Zhang Song, Yang Wen-ming,et al. A Research on Characteristic Information of Pulse Wave [J]. Journal of Beijing University of Technology, 1996, 22(1):71-79.

[20] JIAO Xue-jun, FANG Ying-ye. Research on Continuous Measurement of Blood Pressure via Characteristic Parameters of Pulse Wave [J]. Journal of Biomedical Engineering, 2002, 9(2): 21-220.

[21] He X, Goubran R A, Liu X P. Signal enhancement of wearable ECG monitoring sensors based on Ensemble Empirical Mode Decomposition[C]// IEEE International Workshop on Medical Measurements and Applications Proceedings. IEEE, 2011:433-436.

[22] REN Zhao-hui, ZHAO Fu-qiang. Morden Blood Pressure Measurement [J]. Computer Engineering and Applications,2003,22(9):54-56.

Design of Plane Module Integrated Automatic Parking Device

Sun Huichao , Guo Jinyu, Zhang Yi, Yang Zikang
（School of Mechanical Science and Engineering , jilin University）

***Abstract*-With the rapid growth of vehicle ownership and parking demand, automatic mechanical parking lot has a fast development in recent years,but most related products having on the market are the space parking lot, due to the security risk of space structure itself and vehicle access time is longer, energy consumption and maintenance costs are higher and many other defects,they not been widely applied. The plane module integrated automatic parking device in this paper,with the design of the plane structure,and the integrated module, multi access port structure, solves the existing products. The defects are safe and fast access to vehicles while saving space.**

***Key words*-Mechanical design ; Automatic parking device； application research**

Ⅰ.INTRODUCE

THE 30-years-old mechanical parking system has been applied extensively in Japan, Korea and Germany. Japan, Korea and Taiwan province of China are the earliest area where started to use this parking system in Asia. Parking in the cities could occupy considerable space and land[1]. Furthermore, the distribution and concentration of parking area are consistent with the differential earnings from urban land, which means the area with the highest land values also has the biggest demand for parking. Therefore, the extension of parking space is difficult and requires a high price. However, mechanical three-dimensional parking system could solve this problem. China has been working on the study of this system since 1980s. Currently there have been various types of parking system with multiple structure on the market, such as lifting and transferring parking, aisle-stack parking, vertical lifting parking etc[2-3]. Many factors like complex structure, safety performance, high risk and cost etc. have limited the extensive usage of this system, which made the mechanical parking industry do not enter the period of rapid development, even though it has a great potential on the market[4].

This paper designed and developed and integrated type of automatic parking device which adopted planar model, in view of urgent market demand and defect of three-dimensional parking device. This device enjoys many advantages, such as simple structure, strong adaptability of space and short access time to the vehicles, which provides a new solution to the parking difficulty in the city area.

Ⅱ.THE DESIGN REQUIREMENTS AND OVERALL PLAN

A. The Design Requirements of the Flat Module Integrated Automatic Parking Device

Combining with flaws of three-dimensional parking device on the market and the functional conception of flat module integrated automatic parking device, we have listed the design requirements of this device as follow:

1. This device should have split joint which would be adaptive to different sizes of parking lot and different numbers of parking vehicles.

2. This device needs to access multiple vehicles at the same time in order to save owner’s time. Therefore, the device should be equipped with multiple access ports to meet the requirement of quick access of vehicles.

3. As the design of automatic parking technology, this device should fulfill the requirement of automatic control, which makes the whole parking system more convenient and efficient.

B. The Overall Plan of the Flat Module Integrated Automatic Parking Device

Based on the design requirement, we have finished the mechanical structure of this parking device as shown in Fig.1. The structure features maintain the following ones: 1. Carrying Platform; 2. Platform Chuck; 3. Elevation Meniscus; 4. Balanced Optical Lever; 5. Elevation Turn-screw A; 6. Mobile Platform (with thread engagement); 7. Mobile Wheels; 8. Mobile Turn-screw B; 9. Screw Bracket; 10. Splicing Track. Furthermore, it also includes two types of stepper motor, coupling, synchronous belt and wheel.

The operating principle of vehicle deposit is as follows. First of all, an additional track and screw are added in the outermost end of each column device. This position can be set as Position One. When the vehicle starts to drive in, the elevation meniscus will clamp the carrying platform in the ready-parking position. The stepper motors which is on the end of elevation turn-screw A can work simultaneously on both sides of track, in which way the two screws run synchronously and move the meniscus and the carrying platform up along the vertical direction. At this point, the stepper motor which is on the end of mobile turn-screw B starts running. Synchronous belt could guarantee the two screws run synchronously, so that the mobile platform and wheels could move along the splicing track longitudinally. As they reach the Position One, the elevation turn-screw A will put down the meniscus and the carrying platform, in order to let the vehicle drive in. Lastly, the elevation turn-screw A lift the meniscus and carrying platform up, while the mobile turn-screw B drives the mobile platform and wheels to the original position along the splicing track. It is when the vehicle and platform descend and the meniscus release the

clamping of carrying platform that the parking procedure is complete.

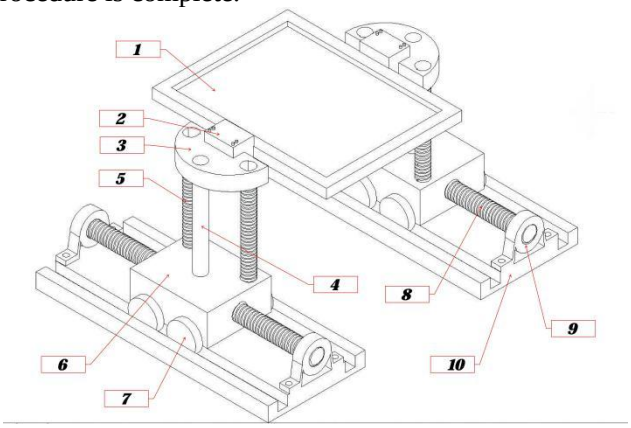

Fig.1 Isometric drawing of structure

III. THE STRUCTURAL DESIGN

Based on the overall design plan of this device, which can be shown in the Fig 1, here are the specific design description for each part of this device.

Structure 1 carrying platform is equipped in each section of the track, which is used to load and park vehicles. The border and clamping slot can be set on the platform to prevent the vehicle from sliding or falling during the course of transportation. These could also be used as the extended safety device which could protect vehicles against theft or burglars.

Structure 2 platform chuck is installed on both sides of platform, which is used for clamping the carrying platform and connecting the meniscus. The platform chuck and the meniscus is bolted (symmetrical around the front and back) together. It is connected to the carrying platform through controller, which could ensure the platform's movement after clamping and parking in a fixed position after the clamp is released.

Structure 3 elevation meniscus is applied to connect platform chuck with balanced optical lever and elevation turn-screw A. The connection of elevation turn-screw have adopted the thread engagement. The rotation of screw can transform into the elevation of meniscus. The meniscus and balanced optical lever are assembled together by clearance fit to prevent large friction which would increase power and bring damage to these two components.

Structure 4 balanced optical lever is used to connect elevation meniscus and mobile platform. The non-linear arrangement of optical lever and elevation turn-screw could increase the stability during the course of transportation, avoiding the sway of vehicle and carrying platform. The optical lever must have enough cross-sectional area and material with certain rigidity, in order to avoid the deformation caused by the end toque affecting the operation of device.

Structure 5 elevation turn-screw A could drive the carrying platform, platform chuck, elevation meniscus and vehicles, making them move upward smoothly along the vertical direction. The ball screw drive is applied in this device to ensure the flexibility of transmission and reduce the friction loss. Synchronous belt and wheel are installed separately beneath the two turn-screws in order to ensure synchronized operation. Stepper motor could be installed above the screw to connect with elevation turn-screw A through coupling. The motor is connected to the driver, and the driver is connected to the control panel, controlling the positive and negative rotation of stepper motor and the number of turns. It also could control the carrying platform, platform chuck, meniscus and vehicle go up and down according to the actual need.

Structure 6 mobile platform and Structure 7 mobile wheels could transport vehicles along the splicing track vertically. The screw thread of the mobile platform could connect to the mobile turn-screw B, then the rotation of mobile turn screw B drive the mobile platform to move longitudinally. The moderate cross-sectional area of the mobile platform could save space without affecting the space distribution of balanced optical lever, elevation turn-screw A and synchronous wheels. There should be more than 2 mobile wheels installed on each side to ensure the stability of the mobile platform.

Structure 8 mobile turn-screw B drives the mobile platform and wheels to move longitudinally. The ball screw drive is applied in this device to ensure the flexibility of transmission and reduce the friction loss. Synchronous belt and wheel are installed separately beneath the two turn-screws B in order to ensure synchronized operation. Stepper motor could be installed above screw to connect with mobile turn-screw B through coupling. The motor is connected to the driver, and the driver is connected to the control panel, controlling the positive and negative rotation of stepper motor and the number of turns. It also could control the longitudinal shift of mobile platform and wheels. Meanwhile, the stepper motors which are on the opposite side and same side could initiate synchronously. Mobile turn-screw should have split joint to meet the requirement of device's longitudinal length in different sizes of space. The two longitudinally adjacent screw respectively process a certain length of external thread and certain depth of internal thread in the binding ends. They are screwed together to realize the splicing ability so that the module can be integrated.

Structure 9 screw bracket and splicing track lift screws on the two ends to make sure the operation of mobile platform and wheels. The splicing track should have split joint to meet the requirement of device's longitudinal length in different sizes of space. The adjacent screws are connected by screw thread to realize the splicing ability so that the module can be integrated.

As shown in the Fig.2 the integration of splicing modules could be extensively applied in different size of parking lot. Each segment of turn-screw and track could split together through thread screw so that the former and latter sections or two screws can split together or separate[5]. In this condition, different

numbers of turn-screw and tracks can be applied according to different sizes of parking lots. As for the aspect of transmission, ball screw could avoid the interference of factors such as tooth profile and resilience. In addition, the synchronous wheels and belt which installed on the end of screw could make sure the synchronized operation. Multiple rows of devices are set horizontally for the requirement of quick access of vehicles, in which way independent operation of each device and various ports enable fast access to vehicles saving parking time.

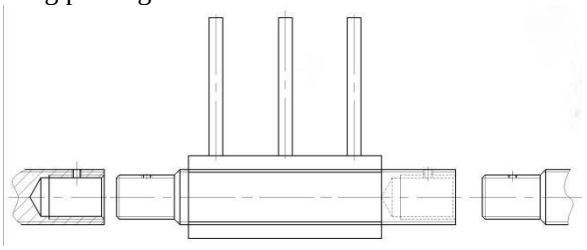

Fig.2 Schematic diagram of screw connection

Ⅳ. Instruction of System Control

The system control of this device can be divided into two parts. Part One is the control of turn-screw on the track to stop and initiate the platform to corresponding position, which is set to be Program A. Part Two is the control of turn-screw on mobile platform to ascend and descend the carrying platform when the mobile platform stops running, which is set to be Program B. These two parts are all controlled by single chip microcomputer, recording the program into the control panel which is connected to the driver. The driver is connected to the stepper motor in order to further control turn-screw that is coupled with motor[6-7]. The motor is driven by the driver that is connected to the control panel of Part One. Since the two screws on both sides of track are connected by synchronous wheels and belt, the rotation could be under simultaneous control. Program A Setting: stepper motor stops and backward rotates N circles after the N circles of positive rotation; then the screw is back to its original position; Program B still operates during this interval. As for the aspect of Part Two, the carrying platform is between two screws, so it is not convenient to install synchronous wheels and belt. In such case, two stepper motors are driven by two drivers which are connected to one control panel so that the synchronized rotation of these two screws can be under better control. Program B Setting: Two stepper motors (x, y) stop after M circles of positive or negative rotation, which could ascend and descend the vehicles and carrying platform.

Ⅴ.Interpretation of Result

The sample of automatic parking device which is based on the design plan could respond to the control requirement quickly. It also has the straightforward operation mode and perfect control system, which makes the parking procedure convenient and orderly. The whole system is reliable and secure with the stable operation. The adoption of mechanical automation parking could benefit the precise track of vehicle. Meanwhile, the mechanical parking method has tightened up the carport improving the space utilization. The whole system could operate in short distance along with multiple access ports, which saves the time for the uses. In addition, this device is characterized by low energy consumption and failure rate with smaller size and lower power, reducing the security risk and maintenance cost. It could be applied in high-traffic neighborhood or parking lot to fulfill the need of automatic parking.

Ⅵ. Conclusion

The flat module integrated automatic parking device has adopted planar design with a safe structure, which is different from the common three-dimensional parking device on the market. It also meets the requirement of module splicing and multiple automatic parking ports, solving the problems of three-dimensional parking device on the market. It provides a new solution for the society to deal with the problems such as shortage of parking space, long-time consuming, low efficiency, potential risk of parking chaos and vehicle damage.

References

[1] ZHANG Xiao-juan.The design of the stereo garage based on PLC control[J].Electronic Design Engineering,2014,(12)

[2] LI Dong-yang,SONG Xiao-fang .Overview and development prospects of stereo parking lot.Value Engineering.2016（12）

[3] ZHANG Qiu-jie.The development status and challenges of stereo garaage.Sciences & Wealth.2015（09）

[4] FANG Chao-lin.Review of stereo garage mechanic design.China Hi-tech Enterprises.2013（09）

[5] XIANG Qian-feng.Precision assurance and technical measurement of long lead screw machining technology.China Science and Technology Review.2015（24）

[6] SANG Yun-xiao.Research on stepping Motor Control system based on single Chip Microcomputer.China Science and Technology Review

[7] XU Bo.The application of SCM principle and application of automatic control scheme.Digital Technology and Application.2017（05）